

Analysis and stability of fatty acid esterified xanthophylls from microalgae

Yannick Weese poel

Thesis committee

Promotor

Prof. Dr H. Gruppen
Professor of Food Chemistry
Wageningen University

Co-promotor

Dr J.-P. Vincken
Assistant professor, Laboratory of Food Chemistry
Wageningen University

Other members

Prof. V. Fogliano, Wageningen University
Prof. C. Socaciu, UASVM, Cluj-Napoca, Romania
Prof. L. de Cooman, KU Leuven, Belgium
Prof. Dr H. Zuilhof, Wageningen University

This research was conducted under the auspices of the Graduate School VLAG (Advanced studies in Food Technology, Agrobiotechnology, Nutrition and Health Sciences).

Analysis and stability of fatty acid esterified xanthophylls from microalgae

Yannick Weesepoel

Thesis

submitted in fulfilment of the requirements for the degree of doctor
at Wageningen University
by the authority of the Rector Magnificus
Prof. Dr M.J. Kropff,
in the presence of the
Thesis Committee appointed by the Academic Board
to be defended in public
on Friday 12 September 2014
at 4 p.m. in the Aula.

Yannick Weesepeel

Analysis and stability of fatty acid esterified xanthophylls from microalgae,
182 pages.

PhD thesis, Wageningen University, Wageningen, NL (2014)

With references, with summaries in English and Dutch

ISBN: 978-94-6257-045-0

ABSTRACT

Fatty acid esterified xanthophylls (*e.g.* astaxanthin) produced by microalgae are regarded as a natural alternative for food colourants, but little is known on the stability of these compounds in foods. The aims of this research were (i) to develop protocols to analyze esterified xanthophylls, and their degradation products, from microalgae by UHPLC-PDA-ESI-MS and MALDI-TOF-MS, and (ii) to assess whether esterification influences xanthophyll stability.

Both analytical methods were successfully tested on complex palmitoyl astaxanthin mixtures of *Haematococcus pluvialis*. MALDI-TOF-MS analysis showed that sodiated $[M+Na]^+$ palmitoyl astaxanthin parents had higher ionization efficiency compared to the radical/protonated parents $[M]^{+•}/[M+H]^+$. Furthermore, TOF/TOF fragmentation of $[M+Na]^+$ parents yielded more diagnostic daughter ions than for $[M]^{+•}/[M+H]^+$ parents.

UHPLC-PDA-ESI-MS was applied to investigate xanthophyll biosynthesis in *Chlorella zofingiensis*. Upon nitrogen depletion, *C. zofingiensis* produced, amongst other pigments, ketolutein and its fatty acid ester. Ketolutein production was independent of the production of secondary β,β -carotene derivatives. Furthermore, UHPLC-PDA-ESI-MS was used to assess the oxidation products of palmitoyl astaxanthins and the influence of the fatty acid ester on colour stability. Mild light-accelerated autoxidation led to formation of free apo-astaxanthins and a new class of palmitoyl apo-astaxanthins. Harsh hypochlorite bleaching revealed (palmitoyl) epoxide-apo-9- and 13-astaxanthinones. Similarly, the methine bridges in the tetrapyrrole biliverdin were found to be susceptible to autoxidation.

An increase in palmitate esterification enhanced stability of all-*trans*-astaxanthin upon light-accelerated autoxidation in hexane. Esterification appeared to modulate the *cis-trans* equilibrium of astaxanthin, which seems to play a key role in its stability.

TABLE OF CONTENTS

Abstract

Chapter 1. General introduction	1
Chapter 2. Sodiation as a tool for enhancing the diagnostic value of MALDI-TOF/TOF-MS spectra of complex astaxanthin ester mixtures from <i>Haematococcus pluvialis</i>	29
Chapter 3. Nitrogen-depleted <i>Chlorella zofingiensis</i> produces astaxanthin, ketolutein and their fatty acid esters: a carotenoid metabolism study	53
Chapter 4. Analysis of palmitoyl apo-astaxanthinals, apo-astaxanthinones, and their epoxides by UHPLC-PDA-ESI-MS	83
Chapter 5. Preliminary UHPLC-PDA-ESI-MS screening of light-accelerated autoxidation products of the tetrapyrrole biliverdin	111
Chapter 6. Fatty acids attached to all- <i>trans</i> -astaxanthin alter its <i>cis-trans</i> equilibrium, and consequently its stability, upon light-accelerated autoxidation	123
Chapter 7. General discussion	145
Summary	157
Samenvatting	161
Acknowledgements	167
The author	169

Chapter 1

General introduction

PROJECT BACKGROUND

Among the last trends in food, a shift can be seen within consumer preferences from 'fast and easy' to 'wholesome, natural and honest'. In general, consumers wish more transparency, more focus on health and show more interest in the origin and composition of their food. One of the groups most at interest are children: artificial food additives have been associated with induction of behavioural changes such as attention deficit hyperactivity disorder (ADHD) (1, 2). An interesting new source of natural food colourants are algae (3, 4). Apart from biofuel, algal biomass also contains high value ingredients for food products, for instance omega-3 fatty acids, anti-oxidants and a wide spectrum of colourants, like carotenoids (*e.g.* β,β -carotene), xanthophylls or oxygenated carotenoids (*e.g.* astaxanthin) phycobiliproteins (*e.g.* C-phycocyanin) and chlorophylls (*e.g.* chlorophyll *a*) (5-7) (**Figure 1**).

Algae are fast growing, and can be cultivated where land is not suitable for conventional crops. Also, a constant production of algal biomass can be obtained, thereby bypassing seasonal production. Furthermore, compared to edible crops, carotenoid overproducing algae may contain pigment concentrations exceeding those found in higher plants. Astaxanthin is of special interest, because it can be overproduced by microalgae upon growth stress as will be discussed later. Furthermore, it is a better antioxidant than β,β -carotene (8). In order to be commercially interesting, the algae used for the production of carotenoids need to be mass cultured and should preferably produce a set of carotenoids in which the one of interest is prevalent. In most cases, microalgae are primarily cultivated for bio-fuel applications, but the pigments, proteins and carbohydrates in 'side-streams' of the biorefining process are increasingly recovered in order to make the production economically feasible (7, 9, 10). In the class of the marine green algae, species like *Dunaliella salina* and *Haematococcus pluvialis* are already well-known for their large biomass production and overproduction of β,β -carotene and astaxanthin, respectively (11, 12). Based on a biomass production for pigments of 175 million tons, and a pigment content of 3% for β,β -carotene and astaxanthin, 0.5% for lutein and 30% for phycobilins, global pigment production in 2013 was estimated to be 525 Kt (kilotons) β,β -carotene, 525 Kt astaxanthin, 87.5 Kt lutein and 2625 Kt phycobilins (13).

Nowadays, there is only a limited amount of algal strains known that produce colourants in sufficient amounts (6). Apart from β,β -carotene, there is little knowledge on the stability of, and degradation products from, algal carotenoids, in general and in food products. Hence, this thesis focuses on application of novel analytical techniques for determining the diversity of algal carotenoids, as well as on the stability and degradation products of algal carotenoids in model systems.

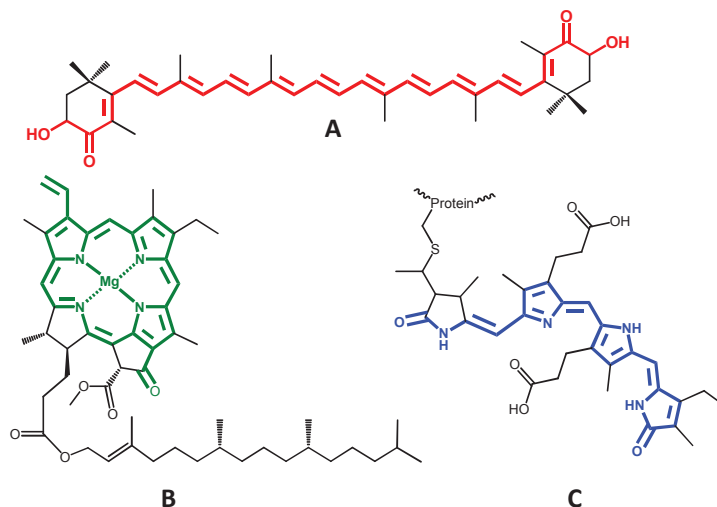


Figure 1. Representative examples of the main classes of pigments found in microalgae. **A** xanthophylls (astaxanthin) **B** chlorophylls (chlorophyll *a*), **C** phycobiliproteins (C-phycoerythrin). Chromophores were accentuated with the colour, in which they appear. Structures adapted from (14-16).

CAROTENOIDS

Carotenoids are a group of secondary metabolites that are considered to be among one of the most important groups of natural pigments in the plant and animal kingdoms (17). The name ‘carotene’ is literally derived from the orange roots of the carrot (*Daucus carota*). The most well-known examples of carotenoids might be represented by the bright yellow-orange colours of flowers (like sunflowers or marigold) or orange-red coloured fruits and vegetables (like tomatoes, oranges and paprika). However, the main portion of the carotenoid production occurs in the photosynthetic systems of plants and algae (18). Animals are generally believed to be incapable of synthesizing carotenoids by themselves, and obtain their coloured appearance from dietary carotenoids. Well-known examples are astaxanthin in goldfish, salmon and the feathers of flamingo. Besides, carotenoid-protein complexes (carotenoproteins) are found in for example lobsters. This astaxanthin-protein complex provides the lobster with its characteristic blue colour, which becomes red upon cooking due to denaturation of the carotenoprotein complex (18).

Carbon skeleton and end groups

The carotenoids described are all derived from the same basic C_{40} isoprenoid skeleton (Figure 2). Subsequent isoprenoid skeleton modifications (including carbon skeleton

shortening) yields the over 700 different naturally occurring carotenoids known so far, according to the latest reference work (14). Two cyclizations at both ends of the isoprenoid skeleton of ψ,ψ -carotene (lycopene) (**1**) leads to β,β -carotene (**2**). The International Union of Pure and Applied Chemistry (IUPAC) has introduced a numbering scheme for the position of the carbons in the carotenoid, which is used throughout carotenoid literature (19). Often, the systematic IUPAC carotenoid nomenclature is omitted and trivial names are used, as is also done in this work. Besides the β and ψ end groups, the IUPAC distinguishes five other types of end groups with their Greek letter prefixes as shown in **Figure 2** (19). Throughout this work, only carotenoids with β - and ϵ - cyclohexene end groups (and their epoxides) will be considered. Changing one of the β,β -carotene's β end groups into an ϵ end group results in β,ϵ -carotene, better known as α -carotene (**3**). Naturally, also two ϵ end groups can be present, resulting in ϵ,ϵ -carotene (**4**). The chromophore or 'polyene chain' is the system of conjugated double bonds to which the carotenoids owe their colour. It is most common for C_{40} carotenoids to contain 7 to 11 conjugated double bonds (19).

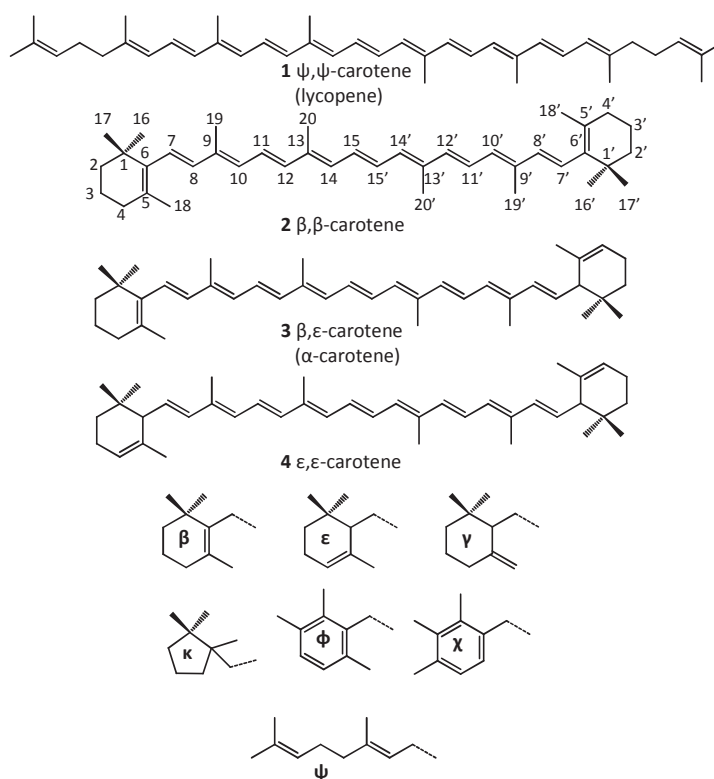


Figure 2. Basic carotenoid structures and end groups, adapted from (14).

Apocarotenoids

Apocarotenoids are carotenoids in which the carbon skeleton has been shortened by removal of fragments from one end or both ends (18). In **Figure 3**, a number of apocarotenoids resulting from β,β -carotene degradation is illustrated. Oxidative cleavage of the intact polyene chain is generally believed to result in two apocarotenoids (20). The oxidative cleavage of the C7-C8 conjugated double bond (CDB) results in the aldehydes β -cyclocitral (**5**) and β -apo-8'-carotenal (**6**). In a similar way, all CDBs in the polyene chain can be cleaved. Cleavage of the C9-C10 and C13-C14 CDB results in apocarotene ketones, because these sites are adjacent to the C19 and C20 methyl group, respectively. This results for the C9-C10 CDB cleavage in β -ionone (**7**) and for the C13-C14 CDB in β -apo-13-carotenone (**11**) and their respective aldehydes **8** and **12**. Cleavage of the C11-C12 results in β -ionylidene acetaldehyde (**9**) and β -apo-12'-carotenal (**10**). Finally, the cleavage of the middle C15-C15' bond results in two identical apo-carotenals, retinal (**13**). Besides aldehyde and ketone

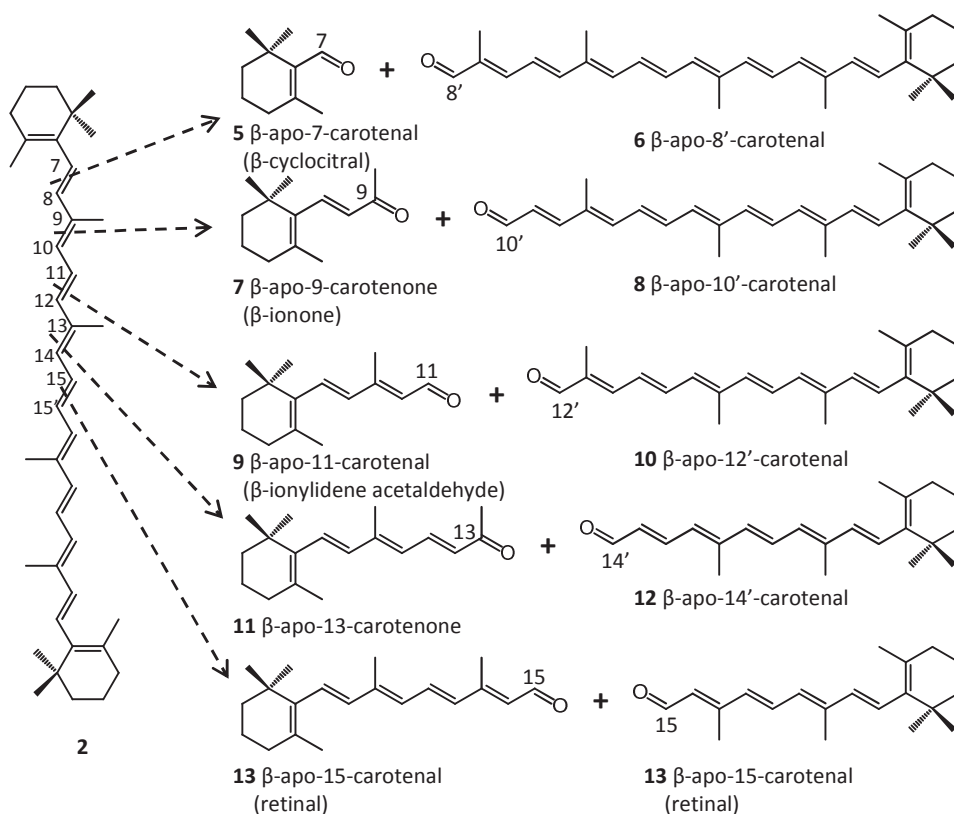


Figure 3. β -Apo-carotenoids formed from β,β -carotene. Structures adapted from (14, 20, 23).

degradation products, also products containing for example hydroxyl groups (apocarotenols) or carboxylic acid groups (apocarotenoic acids) have been described (14). Apocarotenoids have biological functions, the most well-known of which is vitamin A (*e.g.* immune system, vision), which is represented by a group of β -apo-15-carotene derivatives (21). The carboxylic acid derivative of retinol, retinoic acid, is used in the *all-trans* form (Tretinoin) as a drug for the treatment of acne. The 9-*cis* (Alitretinoin) and 13-*cis* (Isotretinoin) isomers of retinoic acid are also used to treat skin-related diseases (22). Every carotenoid can form apocarotenoids, which indicates that a plethora of apocarotenoids can be formed. Potentially every conjugated double bond in apocarotenoids can be oxidized, which results in dialdehydes and a smaller apocarotenoid (23). When occurring in foods, oxidative cleavage of carotenoids might result in loss of product quality and bioactivity (24), as will be elaborated later.

Xanthophylls

The vast majority of carotenoids contains one or more oxygen functions, like hydroxyl, keto or epoxide. They are commonly referred to as xanthophylls (19). In **Figure 4** a short overview of xanthophylls resulting from one to four oxygenation steps of the 'basic' carotenoids **2** - **4** is presented. As a second criterion, structures were selected on their presence in microalgae, with some exceptions to complete the overview (15).

The presence of hydroxyl groups is common, especially on the C3 position. Monohydroxyl substitution of the C3 positions gives the xanthophylls (β -)cryptoxanthin (the β prefix is often omitted) (**14**), zeinoxanthin (**16**) and α -cryptoxanthin (**17**). Evidently, positioning of the hydroxyl functionality on either the β or ϵ end group, yields the two different structures **16** and **17**. Substitution of the second C3 position yields zeaxanthin (**18**), lutein (**22**) and lactucaxanthin (**23**). Besides C3 hydroxyl substitution, also other positions on the cyclohexene ring can be hydroxylated (not shown). Additional substitution yields for example caloxanthin (**25**), hydroxylutein (**31**) and nostoxanthin (**32**).

Keto substitution of xanthophylls is often observed at the C4 position of a β end group. Echinenone (**15**) has one C4 occupied with a keto group and canthaxanthin also has the C4' position occupied. The combination of hydroxyl functions with keto functions yields for example 3-hydroxy-echinenone (**20**), 3'-hydroxy-echinenone (**21**), adonirubin (**28**), adonixanthin (**29**), fritschiellaxanthin (**30**) and astaxanthin (the 3*S*,3'*S* isomer) (**35**). More rare is the keto functionalization of an ϵ end group in for example 3-dehydrolactucaxanthin (**24**), which is at the C3 position.

Many xanthophylls possess an epoxy group, which is usually found at the C5-C6 position. Also the C5-C8 can have such a functionality, but these epoxides are often referred to as furanoids or furanoid oxides (19). Combining epoxidation with hydroxylation functionalization results in for example antheraxanthin (5,6-epoxide)

(26), mutatoxanthin (5,8-furanoid) (27), violaxanthin (5,6-5',6'-diepoxide) (33) and auroxanthin (5,8-5',8'-difuranoid) (34).

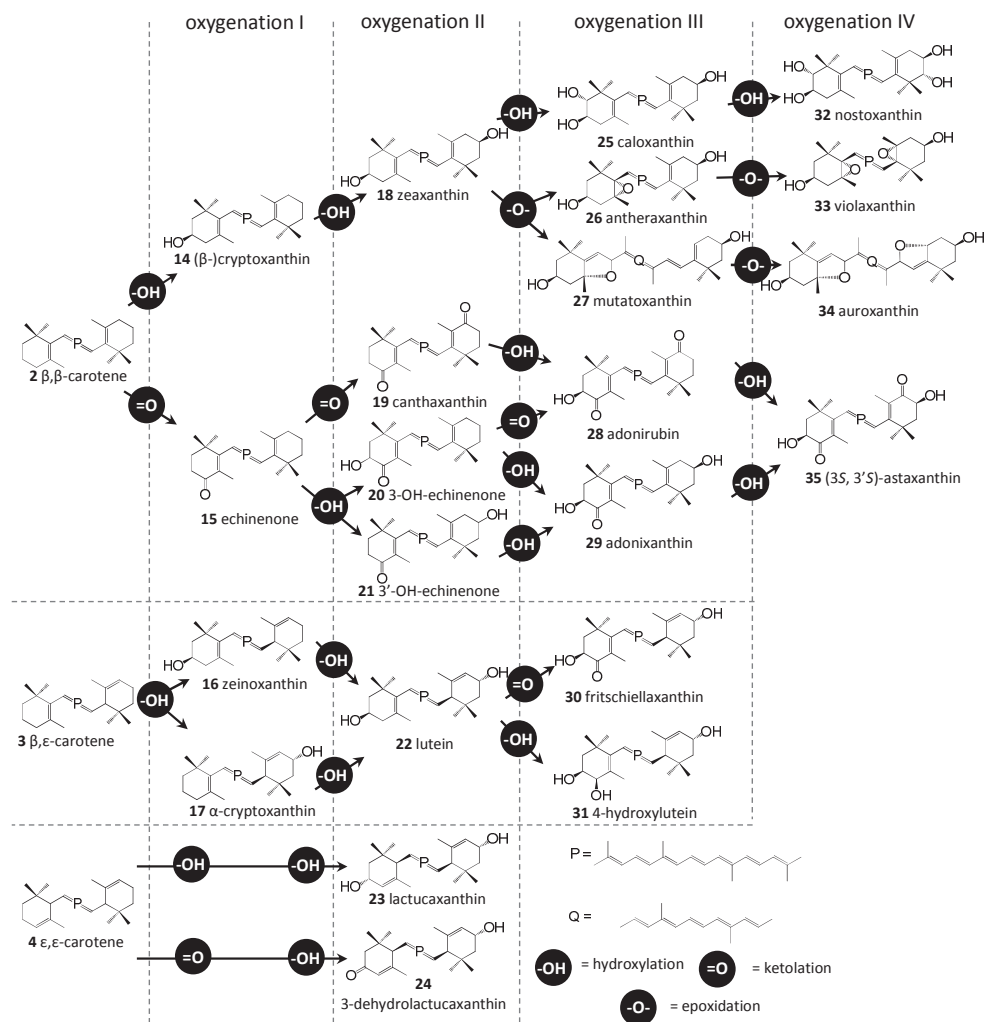


Figure 4. Multiple stages of hydroxyl, keto and epoxide functionalization of xanthophylls derived from carotenoids 2, 3 and 4. The ketolation and hydroxylation of 24 was drawn in a random order. Structures adapted from (14) (15).

Geometrical and optical isomerism

Carotenoids often have several kinds of geometrical and optical *R/S* isomers and derivatives. The most commonly encountered geometrical isomers within a single carotenoid structure are *cis/trans* (or *E/Z*) isomers. The naturally occurring carotenoids are mainly in the all-*trans* configuration (25). Isomerization of *trans*-

carotenoids to *cis*-isomers is induced by acids, heat and exposure to light (26). Although some of the isomers naturally exist, usually they are present as common isolation artefacts (27). Not all *cis*-isomers are energetically favourable to form. The formation of 9-, 9'-, 13- and 13'-*cis*-isomers is usually favourable because less steric hindrance is caused by the methyl groups at the 19, 19', 20 and 20' position. Furthermore, formation of 15-15'-*cis* isomers is also preferred because no flanking methyl groups are present. For astaxanthin, the formation of 9- (36) and 13-*cis* (37) isomers was reported to be favourable (**Figure 5A**) (28). Because astaxanthin is symmetrical, 9'- and 13'-*cis* isomers cannot be distinguished. Besides, multiple variations of *dicis* isomers were reported to exist (29, 30).

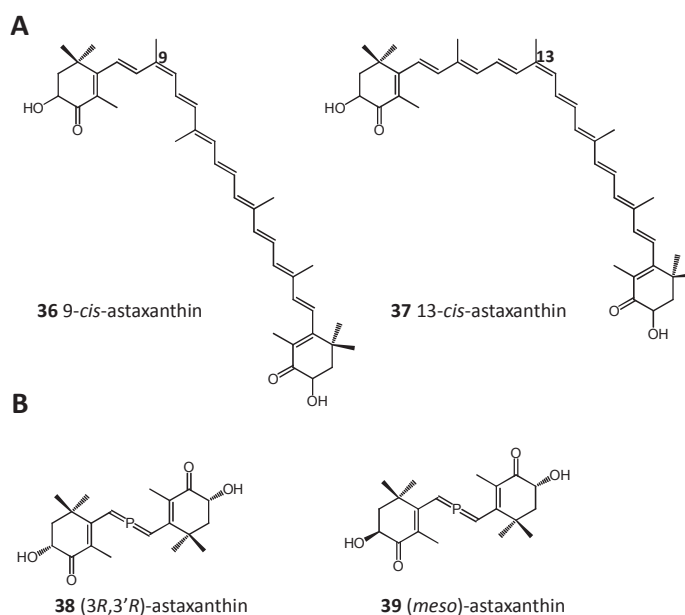


Figure 5. Structures of astaxanthin isomers. **A** geometrical isomers and

B *R/S* isomers. Structures adapted from (14, 29). P =

Optical *R/S* isomerism at the C3, and for ϵ end groups at the C6 position is commonly observed. The hydroxyl group or a polyene tail, respectively, can be positioned axial or equatorial on the cyclohexene chair (19). Astaxanthin derived from natural sources mostly consists of the configurational (3*S*,3'*S*)-isomers and (3*R*,3'*R*)-astaxanthin (35, **Figure 4** and 38, **Figure 5B**), whereas for astaxanthin derived from synthetic sources the *meso* form is most abundant (39, **Figure 5B**) (31). In *H. pluvialis* the (3*S*,3'*S*)-astaxanthin is predominant (32). The presence of an ϵ end group expands the possibilities for optical isomerism. For lutein (22) three configurational isomers were reported (C3', C6' and C3'-C6' epilutein) and for lactucaxanthin (23), nine

different configurational isomers were found in natural sources (tunaxanthin A – E and G - J) (14). Note that also with optical isomers, the (trivial) nomenclature is often not systematic.

Xanthophyll fatty acid esters

Hydroxylated xanthophylls can occur as fatty acid esters in algae, fruits and animals. The most well-known example for microalgae is the high degree of fatty acid esterification of astaxanthin in the microalgae *H. pluvialis* which is predominantly esterified with C18:3, C18:2, C18:1 and C16:0 fatty acids (e.g. astaxanthin diester (with saturated fatty acids) **40**, **Figure 6**) (29, 33, 34). When these microalgae are consumed by animals like e.g. shrimps (*Pandalus borealis*), the astaxanthin fatty acid esters can accumulate in the animal (33). Fucoxanthin (**41**) is an example of an acetylated

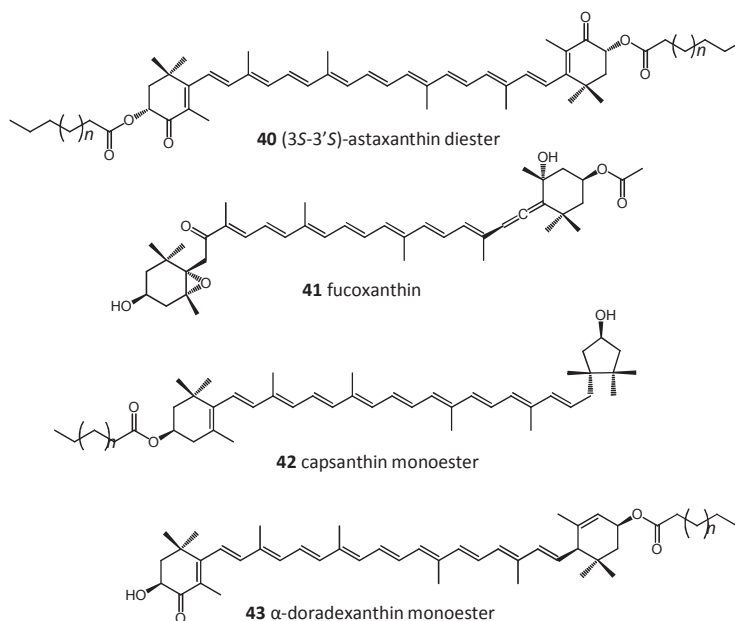


Figure 6. Examples of fatty acid esterified xanthophylls found in nature. Structures adapted from (14).

xanthophyll ester found in the microalga *Isochrysis galbana* (35, 36) and brown sea weeds (e.g. *Fucus serratus*) (37). In the microalga *Euglena sanguinea*, adonixanthin (29) fatty acid esters were found (34). In plants and fruits, also a wide array of examples can be found. In sea buckthorn berries (*Hippophae rhamnoides* L.) lutein (22), zeaxanthin (18) and cryptoxanthin (14) fatty acid esters are found (38-40), whereas red pepper pods (*Capsicum annuum* L.) contain capsanthin (42) fatty acid

esters (41). Remarkable examples of xanthophyll optical isomers in nature are found in the crab *Sesarma haematocheir*, which contains the (3*S*,3'*R*,6'*R*)-ketolutein fatty acid ester of fritschiellaxanthin (**30**) (42), whereas the goldfish (*Carassius auratus*) the (3*S*,3'*S*,6'*R*)-ketolutein fatty acid ester variant α -doradexanthin (**43**) (43).

MICROALGAE THAT OVERPRODUCE CAROTENOIDS

Haematococcus pluvialis

H. pluvialis is an unicellular green alga which is able to accumulate large quantities of astaxanthin under stress conditions, exceeding any other known algal source (5, 13). With an astaxanthin yield of 1.5 – 3% dry weight, *H. pluvialis* is regarded as one of the highest producers of this carotenoid (44). In *H. pluvialis* astaxanthin is most commonly found in esterified forms coupled with one (monoester, 70-90% (w/w)) or two (diesters, 5-25% (w/w)) fatty acids. The unmodified astaxanthin constitutes the remaining 5-10% (w/w) part (33, 45). Esterification of astaxanthin with fatty acids increases its hydrophobicity and limits its solubility range compared to artificial food colourants. This can be overcome in aqueous solutions by nanoencapsulation of the astaxanthin (46). Another possibility is that the algal biomass itself can be used as a colouring agent (47). Other pigments found are lutein, canthaxanthin, β,β -carotene, echinenone, neoxanthin, chlorophyll *a* and chlorophyll *b* (34). Astaxanthin from *H. pluvialis* is already applied in cosmetics and foods, and feed industries, where it serves as colouring agent and potent antioxidant (48). The algal extract is used as a food colourant in aquaculture feed in order to augment muscle pigments in salmonoids and crustaceans (49).

Chlorella zofingiensis

C. zofingiensis is an unicellular green alga belonging to the carotenogenic (carotenoid-overproducing) group of the Chlorophyta and is regarded as most important for this purpose besides *H. pluvialis* and *D. salina* (50). *C. zofingiensis* is proposed as an alternative for the mass production of astaxanthin because of its strong resistance to environmental stress conditions compared to *H. pluvialis* (51). Although the astaxanthin levels are lower compared to *H. pluvialis* (0.6-0.7% w/w, of which approximately 50% is esterified with one fatty acid ester) (52, 53), growth rates and maximum cell culture density are reported to be higher (54). Furthermore, *C. zofingiensis* is able to accumulate multiple xanthophylls in higher concentrations, in addition to astaxanthin. Lutein is found as high as 0.4% (w/w) during normal growth (54). When adverse growth conditions were applied canthaxanthin and adonixanthin accumulate besides the fatty acid esterified form of astaxanthin (52, 53). Recently, it was observed that accumulation of ketolutein in *C. zofingiensis* under adverse growth conditions might be possible (55). Little is reported on commercial activities for the

exploitation of *C. zofingiensis* pigments so far. Scaled-up growth experiments have been reported, but mainly focus on the optimization of the lipid accumulation for biodiesel applications (56-58).

DEGRADATION OF THE CAROTENOID CHROMOPHORE

Carotenoids are susceptible to isomerisation and oxidative degradation because of their characteristic polyene moiety (24). Upon tampering with the carotenoids' all-*trans* chromophore, the colour hue and colour intensity is often negatively affected. As an example, β,β -carotene is employed as illustration. Geometrical *cis-trans* isomerisation often does not affect the wavelength of maximum absorption to a large extent (2-6 nm hypsochromic shift) (Figure 7A and B). An increasing hypochromic

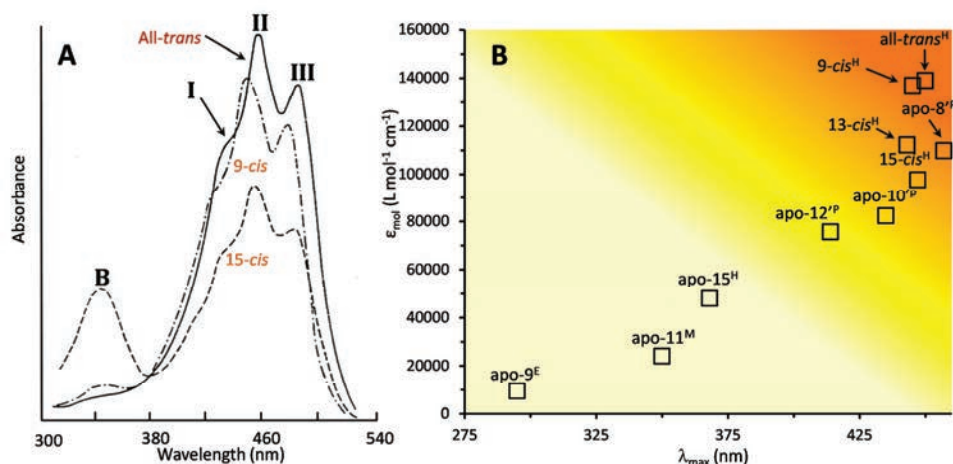


Figure 7. Effect of modifications of the chromophore of β,β -carotene resulting in hypsochromic or hypochromic shifts. **A** Comparison of the absorption spectra of geometrical isomers of β,β -carotene in hexane. Absorption maxima are annotated with I, II and III. The *cis*-peak is annotated with B. Adapted from (59). **B** Comparison between the absorption maxima (λ_{max}) and their respective molar extinction coefficients (ϵ_{mol}) for all-*trans*, several *cis*- β,β -carotenes and several β -apocarotenoids. Note that not all ϵ_{mol} values were obtained in the same solvent. ^Hhexane; ^Ppetroleum ether (b.p. 40-60 °C); ^Eethanol; ^M0.01 M alkaline methanol (radical anion of apo-9). Values obtained from (59-62).

shift is observed when the *cis*-CDB is positioned closer to the middle of the chromophore. The 15-*cis*- β,β -carotene has therefore the largest hypochromic shift of the mono-*cis* geometrical isomers and therefore also the lowest molar extinction coefficient. When the number of CDBs is reduced, as is the case with apocarotenoids, both hypsochromic and hypochromic shifts can occur (Figure 7B). The β -apo-8-astaxanthinal, which still has 10 CDBs, has approximately similar absorption maxima and molar extinction coefficient as the all-*trans* and *cis*- β,β -carotenes. When the

number of CDBs is reduced further, dramatic hypsochromic and hypochromic shifts are observed. For example, β -apo-15-carotenal has a 65% lower molar extinction coefficient and a 82 nm hypsochromic shift compared to all-*trans*- β,β -carotene. This indicates that maintaining the original carotenoid chromophore for colour stability is of the utmost importance for implementation as food colourants.

It has been suggested that food matrices enriched with algal pigments contain a variety of carotenoids and their fatty acid esters, and could result in a plethora of potential bioactive or toxic carotenoid products upon oxidative degradation (24, 63, 64). So far, mainly β,β -carotene has been used as a model carotenoid in degradation studies. In this thesis, spontaneous oxidation (autoxidation) and oxidative bleaching (hypochlorite bleaching) were studied, not of β,β -carotene, but of the xanthophyll astaxanthin.

β,β -Carotene and autoxidation

Autoxidation refers to the reaction of atmospheric oxygen with carotenoids and can occur easily for example during food processing and storage (24). It was proposed that autoxidation involved free radicals (**Figure 8A**) (65). Reaction rates increased when a free radical reaction initiator (*e.g.* 2,2'-azo-bis-isobutyronitrile) was added. Free radical scavengers like butylated hydroxytoluene or α -tocopherol decreased the reaction rate. Initiation of the autoxidation process involves the formation of a *singlet* biradical (**44**), stabilized by delocalization of the two unpaired electrons over the conjugated system. Therefore, all-*trans*- β,β -carotene (**2**) can easily isomerize to for example the 15,15'-*cis*- β,β -carotene (**45**). The twisting of the backbone will result in accumulation of unpaired spin density which will develop in each half of the molecule. This unpaired spin can be 'captured' by oxygen, resulting in carbon-peroxyl *triplet* biradicals (CarOO \cdot , for example **46** and **47**). Subsequent addition to a second neutral molecule of β,β -carotene following an intramolecular homolytic substitution (S_{Hi}) results in the 5,6- or 15,15'-epoxide (**48** and **49**) and a carotene alkoxy radical (CarO \cdot). A possible pathway for the formation of apocarotenals and apocarotenones is also proposed via addition of peroxy radicals to the β,β -carotene conjugated system (**Figure 8B**). The resulting peroxy- β -carotene adduct (**50**) undergoes a S_{Hi} reaction to produce the dioxetane **52** and the carotenyl radical **51**. The dioxetane is very unstable and decomposes to two apocarotenals or an apocarotenal and apocarotenone.

Autoxidation is accelerated by increased temperatures and exposure to light. These experiments involve oxidation with atmospheric (or controlled supply of) oxygen and therefore mostly result in similar oxidation products (24). Reaction temperatures up to 210 °C were used in this type of experiments (66). Amongst others, solvents used were toluene (67, 68), benzene (65), water (69, 70), glycerol (66) and corn/water suspensions (71).

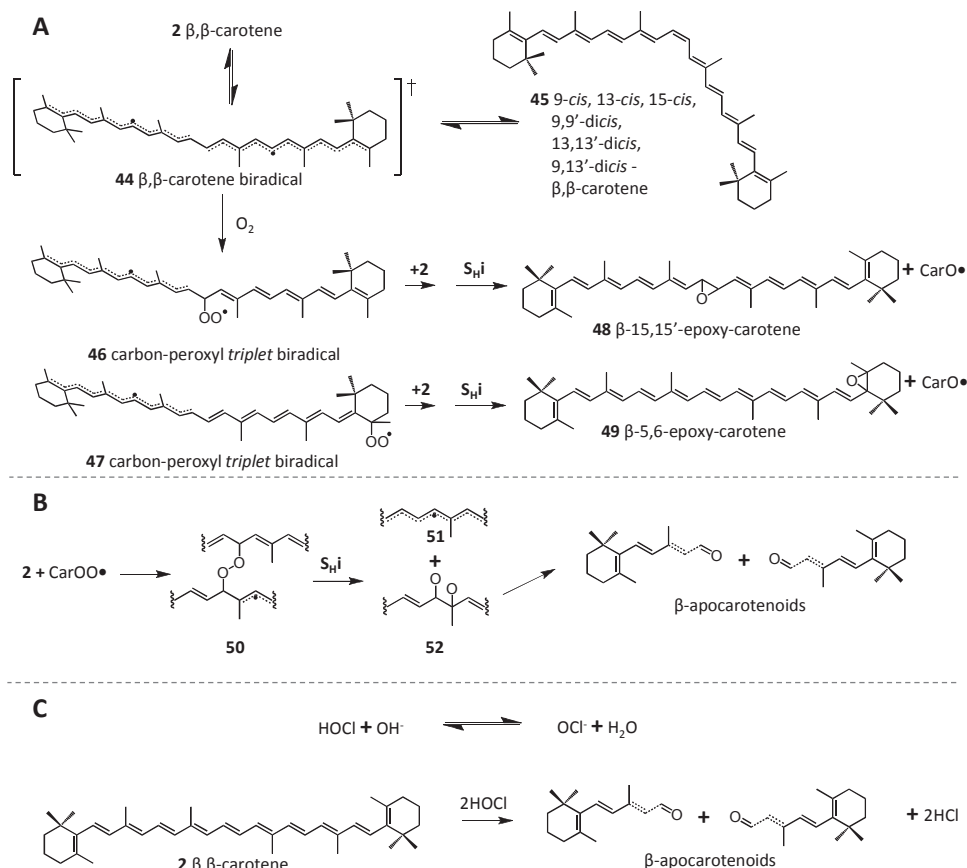


Figure 8. **A** Initiation of the autoxidation of β,β -carotene and formation of *cis*-carotenoids and epoxides, adapted from (24, 65). **B** Formation of apocarotenoids by autoxidation, adapted from (65). **C** Formation of apocarotenoids by oxidative hypochlorite bleaching, adapted from (77). CarO^\bullet = carotene alkoxy radical, CarOO^\bullet = carotene peroxy biradical.

β,β -Carotene and oxidative hypochlorite bleaching

The ability of β,β -carotene to scavenge peroxy radicals as described above, makes it a powerful antioxidant, also in membranes and cell organelles (72, 73). A particular strong oxidizing agent formed upon inflammatory reactions is hypochlorous acid (HOCl). HOCl is primarily produced to eliminate harmful bacteria or toxins, but it is also known to damage surrounding tissue (74). Unwanted side reactions are for example the oxidative cleavage of the conjugated system of carotenoids (67, 75, 76). Hypochlorous acid occurs together with its conjugated base hypochlorite (OCl^-) (**Figure 8C**). HOCl is the strongest oxidizing agent of this couple and is therefore the most reactive towards the carotenoids CDBs, which results in apocarotenoids. The

exact mechanism of degradation of polyene moieties by HOCl/OCl⁻ is not explicitly described in current literature. Furthermore, HOCl can be a molecular precursor for free radicals ([•]OH) and potentially also result in the formation of Car[•], CarO[•] and CarOO[•] radicals which can propagate the carotenoid oxidation (77). It was found that xanthophylls (**14**, **17**, **18** and anhydrolutein) were degraded faster than non-oxygenated carotenoids (**1**, **2** and **3**) (76). Degradation reactions in model systems were mostly performed in either buffered aqueous solutions to mimic blood conditions, or in methanol or ethanol to ensure good solubility of the carotenoids (67, 75, 76, 78).

Carotenoid oxidation products

For β,β-carotene, the type of oxidizing agent highly influences the degradation products formed. After initiation of the degradation process, the (apo)carotenoids formed react further with themselves or other molecules in the environment to a complex mixture of products (24). In **Figure 9** the most abundant stable degradation products for β,β-carotene for both oxidation reactions are summarized. Reaction products were characterized by gas chromatography combined with mass spectrometry, liquid chromatography or thin layer chromatography.

For autoxidation, besides the *cis*-isomers **45** and epoxides **48** and **49** (**Figure 8A**), the main stable products were found to be other epoxy- or furanoid-β-carotenes (**53** - **55**) and echinenone (**15**). Furthermore, all possible β-apocarotenals and β-apocarotenones (**6** - **13**), low molecular weight volatiles (**56** - **62**) and carbon dioxide were found (24, 65). Besides, also unidentified higher molecular weight compounds were formed (65). The 5,8-furanoids **54** and **55** can be directly formed similarly as the 5,6-epoxides, although this could also proceed via an acid-catalyzed furanoid rearrangement (79). In general, first the epoxides are produced, followed by apocarotenoids from which finally smaller volatiles are formed. The apocarotenones (*e.g.* **7**, **56**, **58**) were found to accumulate over the apocarotenals, because the aldehyde group is more susceptible to subsequent autoxidation than a ketone group (65). Recently, autoxidation products of astaxanthin (apo-astaxanthins) were revealed (80). Very little is known about the degradation of esterified xanthophylls and their degradation products.

For hypochlorite bleaching, reaction products identified were β-apo-13-carotenone (**11**) and β-apo-15- and 14'-carotenal (**12** and **13**). Volatiles were mainly structures **5**, **7** and **56** - **59**. For the reaction of hypochlorite and xanthophyll (esters) no reports are available, although some reports have been published on the degradation of xanthophylls by other strong oxidizing agents. The formation of apocantaxanthins upon canthaxanthin oxidation by nickel peroxide also resulted in a limited set of CDB cleavage products (81). A similar trend was observed for oxidation of astaxanthin with peroxyxynitrite, although also nitroastaxanthins were found (82).

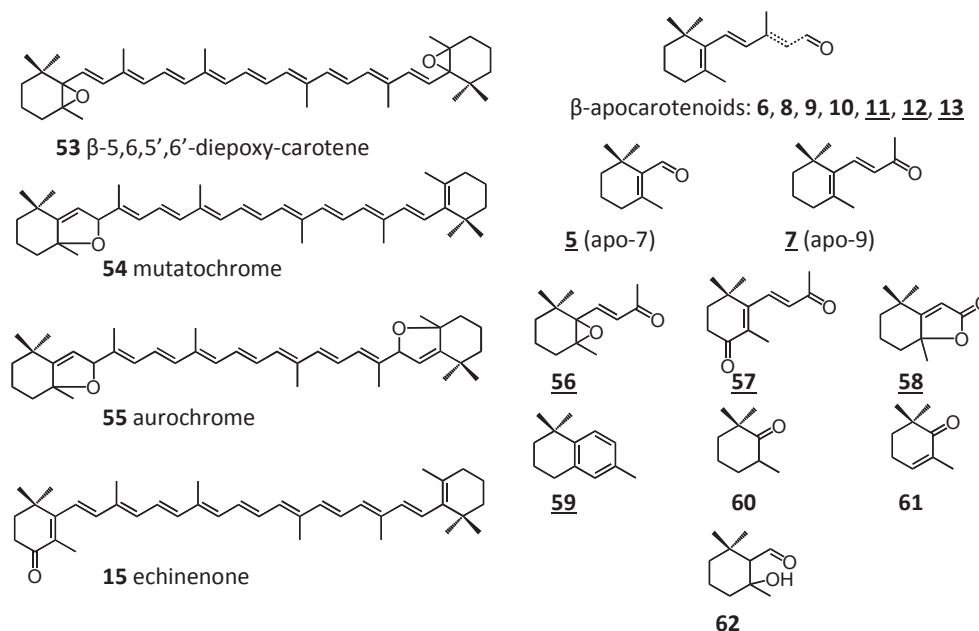


Figure 9. Oxidation products formed upon autoxidation and hypochlorite bleaching (underlined numbers) of β,β -carotene. Underlined numbers were also found upon autoxidation. **5** β -cyclocitral, **7** β -ionone, **56** 5,6-epoxy- β -ionone, **57** 4-oxo- β -ionone, **58** dihydroactinidiolide, **59** 1,1,6-trimethyltetrahydronaphthalene, **60** 2,2,6-trimethylcyclohexanone, **61** 2,6,6-trimethyl-2-cyclohexen-1-one, **62** 2-hydroxy-2,6,6-trimethylcyclohexa-1-carboxaldehyde. Structures adapted from (24, 65, 67, 69-71).

STABILITY OF XANTHOPHYLL FATTY ACID ESTERS

In this thesis, we focus on the use of algal xanthophylls with a special interest for astaxanthin from *H. pluvialis*. Studies performed in the past on assessing the stability of astaxanthin, or stabilizing astaxanthin, are numerous, and all differ in astaxanthin source, purity, matrix, exposure and measuring methods. Astaxanthin sources reported were crawfish (*P. clarkii*) (83), krill (*E. superba*) (84), salmon (*S. salar*) (85), *H. pluvialis* (44, 86), shrimp (*L. setiferus* and *L. vannamei*) (83, 87-90), or from a chemical source (46, 89, 91, 92). The natural astaxanthin was either purified (84), extracted using oils or solvents (83) or contained within the model food (85, 87). Furthermore, astaxanthin was often stabilized by encapsulation (46, 86), mixed with a solid matrix (89, 91, 92) or mixed with oils (44). Subsequently the samples were exposed to either heat, irradiation with light or headspace (oxygen) exposure, while the astaxanthin content was followed over time by spectrophotometry or LC. From data obtained by spectrophotometry, kinetic information on the degradation (either

colour loss or astaxanthin degradation) was obtained, expressed as an apparent k -value (k_{app}) or Arrhenius related activation energy (E_a) for colour loss or astaxanthin degradation. With LC, the decrease of astaxanthin could be expressed more precisely as k_{ast} . Mostly first order degradation kinetics were found, with E_a values for the degradation of astaxanthin between 88 and 97 kJ mol⁻¹ in lipid containing systems (83, 87).

Given the diversity of these experiments and complexity of the matrices, it is not possible to compare results with each other. Besides, there are hardly any studies taking into account the effect of fatty acid esterification on the stability of astaxanthin, which is important as natural astaxanthin extracts, rich in esterified astaxanthin, are increasingly used in food formulations. Few studies elaborate on the influence of esterification with fatty acids for xanthophylls other than astaxanthin (**Table 1**). The most extended study on this topic concerned a comparative study on capsanthin and capsanthin diester in cyclohexane, ethanol and aqueous emulsions (93). The stability of the free capsanthin increased in aqueous medium (*e.g.* the E_a increased), but in all cases capsanthin diester had a higher E_a . Interestingly, zero order kinetics were observed for degradation in cyclohexane and ethanol, whereas first order kinetics was found for that in water. Activation energies were always lower when the degradation was performed in light conditions compared to dark conditions (93). In contrast, it was found that fatty acid esterification was of no influence on the stability of capsanthin (94). For astaxanthin and its esters in benzene and hexane, diester showed higher stability, followed by monoester and free astaxanthin (84). However, in acetone and ethanol differences in stability started to fade. Subagio *et al.* (1999) found that the degradation rate k_{app} was dependent on the start concentration of lutein. Upon heating in benzene again lutein diesters showed the highest stability. When irradiated with UV light at 10 °C diesters and monoesters had similar stability, whereas free lutein was degraded at a relatively high rate (95). Similar behaviour was observed for cryptoxanthin in tetrahydrofuran, hexane and lecithin, where the monoester was always more stable than the free molecule (96, 97).

Concluding from **Table 1**, it is unclear what the real influence of the fatty acid ester is on (colour) stability of the xanthophyll backbone. Furthermore also the solvent employed seems to play a substantial role in the xanthophyll stability. In general, it is not known why esterification influences the stability of xanthophylls. Assuming that the degradation of xanthophylls implies the loss of conjugation, it is rather surprising that fatty acid esters influence this while they do not directly affect the chromophore. Evidently, the degradation of a xanthophyll involves multiple reactions which can occur simultaneously as explained earlier.

Table 1. Overview on literature reports comparing the stability of xanthophylls with identical backbone with various degree of fatty acid esterification.

Xanthophyll	DE	Solvent	Stability conclusion	Method	Ref
capsanthin	F	cyclohexane	D > F	UV-Vis	(93)
	D				
	F	ethanol	D > F		
	D				
capsanthin	F	water/tween	D > F	LC	(94)
	D	(emulsion)			
	F	ethanol/powder	ethanol(dark/light): F = D powder: F = M = D		
astaxanthin	F	benzene	D > M > F	UV-Vis	(84)
	M				
	D				
	F	hexane	D > M > F		
	M				
	D				
	F	acetone	-20 °C: D > M > F, other temperatures: D = M = F		
	M				
	D				
	lutein	F	ethanol		
M					
D					
cryptoxanthin	F	tetrahydrofuran	M > F	LC	(96)
	M		type of fatty acid (C12:0, C14:0, C16:0) no influence		
cryptoxanthin	F	hexane	M _{C16:0} = M _{acetate} > F	UV-Vis	(97)
	M _{acetate}				
	M _{C16:0}				
	F	lecithin (liposome)	M _{C16:0} > M _{acetate} > F		
	M _{acetate}				
	M _{C16:0}				

DE: degree of esterification, F: free astaxanthin, M: astaxanthin monoester, D: astaxanthin diester.

In addition to that, it was not clear if UV-Vis or LC measurements were comparable and in which way both methods influenced the conclusion drawn (**Table 1**). Following colour loss by spectroscopy at a single wavelength will result in an E_a representing the sum of all reactions taking place (*e.g.* the E_a of colour loss). Furthermore, as shown in **Figure 7**, geometrical *cis* isomers and apocarotenoids with still a large number of CDBs remaining can also contribute to the total colour of the

liquid. Therefore, monitoring the decrease of the individual *all-trans* xanthophyll by LC will result in more specific information on the kinetics of degradation.

SEPARATION, IDENTIFICATION AND QUANTIFICATION OF CAROTENOIDS

Liquid chromatography

Reversed-phase liquid chromatography (RP-LC) has become the method of choice for separation, identification and quantification of carotenoids. Numerous reports have been compiled, summarizing combinations of column, mobile phases, and mobile phase modifiers with specific carotenoid separations (most recent (98, 99)). Recently, the performance of the 'Golden Standard' HPLC C30 column was compared with numerous UHPLC column chemistries (100). Overall, the HPLC C30 was found to perform better in separations, albeit with up to four times longer analysis time. Carotenoid separations are therefore expected to be most efficient using a combination of UHPLC and a C30 stationary phase, but this C30 stationary phase for UHPLC is not available yet. Throughout this work, UHPLC in combination with an Acquity UPLC BEH Shield RP C18 column was used. This stationary C18 phase is endcapped and is functionalized with hydrophilic carbamate groups (-N-(C=O)-O-).

Identification by LC and PDA-MS/MS detection

The use of LC coupled to a photo diode array (PDA) detector and *in-line* to a mass spectrometric interface is a powerful tool for the annotation of (apo)carotenoids in complex mixtures (98, 101). Identification is normally performed by matching chemical standards (if available), UV-Vis absorption spectra, parent masses and fragmentation patterns. The indisputable determination of chirality and *cis-trans* geometrical isomers generally requires the use of circular dichroism or nuclear magnetic resonance spectroscopy.

The UV-Vis spectrum of a carotenoid is usually first examined because it can provide information on the number of conjugated double bonds, geometrical *cis-trans* isomers and the type of end group (**Figure 7A**). Furthermore modifications of the cyclic end group can be addressed like allenic (not discussed here), carbonyl, epoxide and hydroxyl groups. The position of the absorption maxima (I, II, III), the spectral fine structure (% III/II) and the possible presence of a *cis*-peak (B) are very specific for the type of carotenoid and are described in detail elsewhere (59). Examples of UV-Vis spectra can be found throughout this thesis.

Application of only UV-Vis spectra for identification has limitations, because carotenoids can have identical UV-Vis spectra or co-elution can occur. Coupling to an *in-line* mass detector has the advantage that additional information on the mass of the carotenoid and molecular structure can be gained. Typically, ionization techniques like atmospheric pressure chemical ionization (APCI) (102) and electrospray

ionization (ESI) (103) in positive mode are used (98). In positive mode, carotenoids ionize into their radical species $[M]^{\bullet+}$ or protonated species $[M+H]^+$ depending on the type of carotenoid, type of spray interface and mobile phase (modifier) used (98, 104-106). Furthermore, in ESI, xanthophylls are known to form salt adducts like $[M+Na]^+$, probably due to the presence of an oxygen moiety on their cyclohexene end groups (34, 107, 108). Tandem MS/MS fragmentation provides the diagnostic fragment ions characteristic for the carotenoid. Neutral losses of 92 and 106 Da (*e.g.* found as $[M-92]^{\bullet+}$, $[M+H-92]^+$ and $[M+Na-92]^+$) represent the elimination of toluene and xylene and are specific for the presence of a polyene backbone (109, 110). The presence of hydroxyl groups on xanthophylls is characterized by losses of water $[M-17]^{\bullet+}$ or $[M-18]^+$ (98). Xanthophylls with fatty acid esters have characteristic losses of $[M+H-FA]^+$ or $[M+Na-FA]^+$. The sodiated xanthophyll esters eject the diagnostic toluene and xylene neutral losses, while the protonated species are reluctant to do so (34).

MALDI-TOF-MS

Direct MS analysis, without prior separation, increases sample throughput tremendously. Matrix assisted laser desorption time of flight mass spectrometry (MALDI-TOF-MS) is a technique in which a rapid mass spectrometric fingerprint of a sample can be acquired. Prerequisite is the formation of diagnostic fragments generated by post source decay (PSD) or TOF/TOF fragmentation, which leads to unambiguous annotation. Only a handful of reports is known until now dealing with this matter and carotenoids. MALDI-TOF-MS was used as a tool for the analysis of a group model carotenoids, xanthophylls and fatty acid esterified xanthophylls (111). Furthermore, identification and quantification of plant carotenoids (*e.g.* lycopene, β , β -carotene, lutein) (112), carotenoids, xanthophylls and xanthophyll fatty acids in fruit juices (113) and carotenoids in metabolically engineered *Bacillus subtilis* (114) represent the only studies done with MALDI-TOF-MS to our knowledge. A drawback of MALDI-TOF-MS is that no spectral data can be acquired and that it is difficult to distinguish between isomers.

Quantification by LC

Carotenoids obey the Lambert-Beer law. Therefore the response of the PDA at a designated wavelength will have a linear relation with the concentration of a chemically pure carotenoid standard within certain limits. For numerous (apo)carotenoids the molar extinction coefficients ϵ_{mol} ($\text{L mol}^{-1} \text{ cm}^{-1}$) and specific absorption coefficients $A_{1\text{cm}}^{1\%}$ ($\text{L g}^{-1} \text{ cm}^{-1}$) are reported (15, 59). The two values are related as:

$$\epsilon_{\text{mol}} = (A_{1\text{cm}}^{1\%} * \text{molecular mass carotenoid}) / 10$$

Quantitative analysis of carotenoids can be done by spectrophotometric methods or LC peak areas, provided that their accurate absorption coefficients in the desired solvent are available. For calculation of the concentration of carotenoids which have not been calibrated by a chemically pure standard, peak areas can be corrected using their corresponding ϵ_{mol} or $A_{1\text{cm}}^{1\%}$. When using the $A_{1\text{cm}}^{1\%}$, the concentration of target colourant analyte can be calculated as:

$$C(\mu\text{g/mL})_{\text{analyte}} = \text{peak area}_{\text{analyte}} * (A_{1\text{cm}}^{1\%} \text{ analyte} / A_{1\text{cm}}^{1\%} \text{ standard})$$

It should be noted that the effect of solvents and wavelengths (at which the absorption of colourants is measured) on absorption may be substantial. For instance, $A_{1\text{cm}}^{1\%}$ values of fucoxanthin in acetone and carbon disulphide are 1060 and 2036 L g⁻¹ cm⁻¹, respectively (59).

THESIS OUTLINE

As stated above, only a limited number of studies has been performed on (i) the influence of the fatty acid esterification on the colour stability of astaxanthin, (ii) the application of novel analytical techniques for determination of the carotenoids in *H. pluvialis* and *C. zoofingiensis* and the degradation products of astaxanthin with different degree of fatty acid esterification in model systems. To accomplish these goals, in this thesis, hyphenated (UHPLC-PDA-ESI-MS) and *off-line* (MALDI-TOF-MS) analysis techniques are employed to understand the effect of fatty acid esterification on astaxanthin stability.

In **Chapter 2**, the development of a MALDI-TOF-MS screening method is described that allows direct profiling of complex mixtures of fatty acid mono- and diesterified astaxanthins. First, astaxanthin monopalmitate and dipalmitate standards were used to describe the TOF/TOF fragmentation patterns for $[M]^{+}/[M+H]^{+}$ and $[M+Na]^{+}$ parents. The method was subsequently validated using two complex mixtures of astaxanthin monoesters and diesters obtained from the hexane extract of *H. pluvialis*. In **Chapter 3**, a new UHPLC-PDA-ESI-MS method is developed to gain new insights in the regulation of overproduction of carotenoids in *C. zoofingiensis* upon nitrogen depletion. Combining the quantitative LC analysis and diphenylamine-inhibited growth, new insights into the carotenoid biosynthetic pathways of the alga are revealed. In **Chapter 4**, free astaxanthin, astaxanthin monopalmitate and dipalmitate were subjected to light-accelerated autoxidation and hypochlorite bleaching in a model system. A new UHPLC-PDA-ESI-MS application was developed to properly assess the degradation products. The treatments differed in severity, and were expected to yield different sets of apo-astaxanthins. Furthermore, we expected that the relatively stable fatty acid ester bond of astaxanthin would result in a new

class of esterified apo-astaxanthins. Similarly, in **Chapter 5**, UHPLC-PDA-ESI-MS was used to identify light-accelerated autoxidation products from (free) biliverdin. Biliverdin was used as a model for the covalently attached tetrapyrroles in phycobiliproteins. In **Chapter 6**, the influence of the fatty acid ester on the colour stability and degradation of free astaxanthin, astaxanthin monopalmitate and dipalmitate by light-accelerated autoxidation are further examined, as literature is contradicting on this topic. Further insight on the influence of the fatty acid ester on colour stability is provided by monitoring the isomerization and degradation products over time by UHPLC-PDA-MS/MS. The results of these chapters are discussed in **Chapter 7**. The implications of this research on mass spectrometry of xanthophylls are elaborated, and stability of astaxanthin fatty acid esters in different solvents is addressed.

REFERENCES

- Schab, D. W.; Trinh, N. H., Do artificial food colors promote hyperactivity in children with hyperactive syndromes? A meta-analysis of double-blind placebo-controlled trials. *Journal of developmental and behavioral pediatrics* **2004**, *25*, 423-434.
- Kobylewski, S. J., MF, Food dyes: a rainbow of risks. <http://cspinet.org/new/pdf/food-dyes-rainbow-of-risks.pdf> Last accessed **19 may 2014**.
- Guedes, A. C.; Amaro, H. M.; Malcata, F. X., Microalgae as sources of carotenoids. *Marine drugs* **2011**, *9*, 625-644.
- Dufossé, L., Chapter 5.4 Pigments from microalgae and micro-organisms: sources of food colorants. In: *Food colorants, chemical and functional properties*, Edited by: Socaciu, C., CRC Press, Taylor & Francis Group, Boca Raton, FL, USA **2007**, pp. 400-422.
- Plaza, M.; Herrero, M.; Cifuentes, A.; Ibanez, E., Innovative natural functional ingredients from microalgae. *Journal of agricultural and food chemistry* **2009**, *57*, 7159-7170.
- Mulders, K. J. M.; Lamers, P. P.; Martens, D. E.; Wijffels, R. H., Phototrophic pigment production with microalgae: biological constraints and opportunities. *Journal of phycology* **2014**, 229-242.
- Wijffels, R. H.; Barbosa, M. J.; Eppink, M. H. M., Microalgae for the production of bulk chemicals and biofuels. *Biofuels bioproducts and biorefining* **2010**, *4*, 287-295.
- Pérez-Gálvez, A.; Mínguez-Mosquera, M. I., Esterification of xanthophylls and its effect on chemical behavior and bioavailability of carotenoids in the human. *Nutrition research* **2005**, *25*, 631-640.
- Milledge, J. J., Commercial application of microalgae other than as biofuels: a brief review. *reviews in environmental science and bio-technology* **2011**, *10*, 31-41.
- Borowitzka, M., High-value products from microalgae-their development and commercialisation. *Journal of applied phycology* **2013**, *25*, 743-756.
- Lamers, P. P.; Janssen, M.; De Vos, R. C. H.; Bino, R. J.; Wijffels, R. H., Exploring and exploiting carotenoid accumulation in *Dunaliella salina* for cell-factory applications. *Trends in biotechnology* **2008**, *26*, 631-638.
- Jeffrey, S. W.; Wright, S. W.; Zapata, M., Chapter 1: Microalgal classes and their signature pigments. *Phytoplankton pigments: characterization, chemotaxonomy, and applications in oceanography*. Edited by: Roy, S., Llewellyn C.A., Egeland, E.S., Johnsen, G. Cambridge University Press, New York, NY, USA **2011**, pp. 3-77.

13. Markou, G.; Nerantzis, E., Microalgae for high-value compounds and biofuels production: a review with focus on cultivation under stress conditions. *Biotechnology advances* **2013**, *31*, 1532-1542.
14. Britton, G.; Liaaen-Jensen, S.; Pfander, S., Carotenoids Handbook. Birkhäuser Verlag, Basel, Switzerland **2004**.
15. Egeland, E. S., Part VII: Data sheets aiding identification of phytoplankton carotenoids and chlorophylls. In: *Phytoplankton pigments: characterization, chemotaxonomy, and applications in oceanography*. Roy, S., Llewellyn C.A., Egeland, E.S., Johnsen, G. Cambridge University Press, New York, NY, USA **2011**, pp. 665-822.
16. Blot, N.; Wu, X. J.; Thomas, J. C.; Zhang, J.; Garczarek, L.; Bohm, S.; Tu, J. M.; Zhou, M.; Ploscher, M.; Eichacker, L.; Partensky, F.; Scheer, H.; Zhao, K. H., Phycourobilin in trichromatic phycocyanin from oceanic cyanobacteria is formed post-translationally by a phycoerythrobilin lyase-isomerase. *The Journal of biological chemistry* **2009**, *284*, 9290- 9298.
17. Isler, O., Introduction. In: *Carotenoids Vol. 1A Isolation and analysis*, Edited by Britton G., Liaaen-Jensen S., Pfander H., Birkhäuser Verlag, Basel, Switzerland **1995**, pp. XXVII-XXVIII.
18. Britton, G.; Liaaen-Jensen, S.; Pfander, S., Chapter 2: Carotenoids today and challenges for the future. In: *Carotenoids Vol. 1A Isolation and analysis*, Edited by Britton G., Liaaen-Jensen S., Pfander H., Birkhäuser Verlag, Basel, Switzerland **1995**, pp. 13-26.
19. Weedon, B. C. L.; Moss, G. P., Chapter 3: Structure and nomenclature. In: *Carotenoids Vol. 1A Isolation and analysis*, Edited by Britton G., Liaaen-Jensen S., Pfander H., Birkhäuser Verlag, Basel, Switzerland **1995**, pp. 27-70.
20. Mordt, R. C.; Walton, J. C.; Burton, G. W.; Hughes, L.; Ingold, K. U.; Lindsay, D. A., Exploratory study of beta-carotene autoxidation. *Tetrahedron letters* **1991**, *32*, 4203-4206.
21. Gregory III, J. F., Chapter 7: Vitamins, In: *Fennema's Food Chemistry, 4th edition*, Edited by: Damodaran, S; Parkin, K.L., Fennema, O.R. CRC Press, Taylor & Francis Group, New York, NY, USA **2008**, pp. 441-521.
22. Amann, P. M.; Merk, H. F.; Baron, J. M., Retinoids in dermatopharmacology. *Hautarzt* **2014**, *65*, 98-105.
23. Alder, A.; Holdermann, I.; Beyer, P.; Al-Babili, S., Carotenoid oxygenases involved in plant branching catalyse a highly specific conserved apocarotenoid cleavage reaction. *Biochemical journal* **2008**, *416*, 289-296.
24. Boon, C. S.; McClements, D. J.; Weiss, J.; Decker, E. A., Factors Influencing the chemical stability of carotenoids in foods. *Critical reviews in food science and nutrition* **2010**, *50*, 515-532.
25. Chandler, L.; Schwartz, S., HPLC Separation of *cis-trans* carotene isomers in fresh and processed fruits and vegetables. *Journal of food science* **1987**, *52*, 669-672.
26. van den Berg, H.; Faulks, R.; Granado, H. F.; Hirschberg, J.; Olmedilla, B.; Sandmann, G.; Southon, S.; Stahl, W., The potential for the improvement of carotenoid levels in foods and the likely systemic effects. *Journal of the science of food and agriculture* **2000**, *80*, 880-912.
27. Schiedt, K.; Liaaen-Jensen, S., Chapter 5: Isolation and analysis. In: *Carotenoids Vol. 1A Spectroscopy*, Edited by Britton G., Liaaen-Jensen S., Pfander H., Birkhäuser Verlag, Basel, Switzerland **1995**, pp. 81-108.
28. Yuan, J.-P.; Chen, F., Isomerization of *trans*-astaxanthin to *cis*-isomers in organic solvents. *Journal of agricultural and food chemistry* **1999**, *47*, 3656-3660.
29. Holtin, K.; Kuehnle, M.; Rehbein, J.; Schuler, P.; Nicholson, G.; Albert, K., Determination of astaxanthin and astaxanthin esters in the microalgae *Haematococcus pluvialis* by LC- (APCI)MS and characterization of predominant carotenoid isomers by NMR spectroscopy. *Analytical and bioanalytical chemistry* **2009**, *395*, 1613-1622.

30. Euglert, G.; Vecchi, M., *trans/cis* Isomerization of astaxanthin diacetate/isolation by HPLC. and identification by ¹H-NMR. Spectroscopy of three mono-*cis*- and six di-*cis*-isomers. *Helvetica chimica acta* **1980**, *63*, 1711-1718.
31. Krinsky, N.; Mathews-Roth, M.; Taylor, R.; Bernhard, K., Synthetic astaxanthin. The route of a carotenoid from research to commercialisation. In *Carotenoids*, Springer, New York, NY, USA **1989**, pp. 337-363.
32. Renstrom, B.; Borch, G.; Skulberg, O. M.; Liaaen-Jensen, S., Natural occurrence of enantiometric and *meso*-astaxanthin. 3. Optical purity of (3S,3'S)-astaxanthin from *Haematococcus pluvialis*. *Phytochemistry* **1981**, *20*, 2561-2564.
33. Breithaupt, D. E., Identification and quantification of astaxanthin esters in shrimp (*Pandalus borealis*) and in a microalga (*Haematococcus pluvialis*) by liquid chromatography mass spectrometry using negative ion atmospheric pressure chemical ionization. *Journal of agricultural and food chemistry* **2004**, *52*, 3870-3875.
34. Frassanito, R.; Cantonati, M.; Flaim, G.; Mancini, I.; Guella, G., A new method for the identification and the structural characterisation of carotenoid esters in freshwater microorganisms by liquid chromatography/electrospray ionisation tandem mass spectrometry. *Rapid communications in mass spectrometry* **2008**, *22*, 3531-3539.
35. Mulders, K. M.; Weesepeel, Y.; Lamers, P.; Vincken, J.-P.; Martens, D.; Wijffels, R., Growth and pigment accumulation in nutrient-depleted *Isochrysis* aff. *galbana* T-ISO. *Journal of applied phycology* **2013**, 1-10.
36. Airs, R. L.; Llewellyn, C. A., Improved detection and characterization of fucoxanthin-type carotenoids: novel pigments in *Emiliana Huxleyi* (Prymnesiophyceae). *Journal of phycology* **2006**, *42*, 391-399.
37. Haugan, J. A.; Liaaen-Jensen, S., Algal carotenoids. 54. Carotenoids of brown-algae (Phaeophyceae). *biochemical systematics and ecology* **1994**, *22*, 31-41.
38. Pop, R. M.; Weesepeel, Y.; Socaciu, C.; Pintea, A.; Vincken, J. P.; Gruppen, H., Carotenoid composition of berries and leaves from six Romanian sea buckthorn (*Hippophae rhamnoides* L.) varieties. *Food chemistry* **2014**, *147*, 1-9.
39. Weller, P.; Breithaupt, D. E., Identification and quantification of zeaxanthin esters in plants using liquid chromatography-mass spectrometry. *Journal of agriculture and food chemistry* **2003**, *51*, 7044-7049.
40. Giuffrida, D.; Pintea, A.; Dugo, P.; Torre, G.; Pop, R. M.; Mondello, L., Determination of carotenoids and their esters in fruits of sea buckthorn (*Hippophae rhamnoides* L.) by HPLC-DAD-APCI-MS. *Phytochemical analysis* **2012**, *23*, 267-273.
41. Schweiggert, U.; Kammerer, D. R.; Carle, R.; Schieber, A., Characterization of carotenoids and carotenoid esters in red pepper pods (*Capsicum annuum* L.) by high-performance liquid chromatography/atmospheric pressure chemical ionization mass spectrometry. *Rapid communications in mass spectrometry* **2005**, *19*, 2617-2628.
42. Matsuno, T.; Ookubo, M., Carotenoid-pigments of crustacea. 4. The 1st isolation and identification of fritschiellaxanthin from a crab *Sesarma haematocheir* (Akategani in Japanese). *Bulletin of the japanese society of scientific fisheries* **1982**, *48*, 653-659.
43. Buchecker, R.; Eugster, C. H.; Weber, A., Absolute configuration of alpha-doradexanthin - new carotenoid from *Fritschiella tuberosa* IYeng. *Helvetica chimica acta* **1978**, *61*, 1962- 1968.
44. Rao, A. R.; Sarada, R.; Ravishankar, G. A., Stabilization of astaxanthin in edible oils and its use as an antioxidant. *Journal of the science of food and agriculture* **2007**, *87*, 957-965.
45. Orosa, M.; Franqueira, D.; Cid, A.; Abalde, J., Analysis and enhancement of astaxanthin accumulation in *Haematococcus pluvialis*. *Bioresource technology* **2005**, *96*, 373-378.

46. Tachaprutinun, A.; Udomsup, T.; Luadthong, C.; Wanichwecharungruang, S., Preventing the thermal degradation of astaxanthin through nanoencapsulation. *International journal of pharmaceutics* **2009**, *374*, 119-124.
47. Gouveia, L.; Raymundo, A.; Batista, A. P.; Sousa, I.; Empis, J., *Chlorella vulgaris* and *Haematococcus pluvialis* biomass as colouring and antioxidant in food emulsions. *European food research and technology* **2005**, *222*, 362-367.
48. Guerin, M.; Huntley, M. E.; Olaizola, M., *Haematococcus* astaxanthin: applications for human health and nutrition. *Trends in biotechnology* **2003**, *21*, 210-216.
49. Lorenz, R. T.; Cysewski, G. R., Commercial potential for *Haematococcus* microalgae as a natural source of astaxanthin. *Trends in biotechnology* **2000**, *18*, 160-167.
50. Solovchenko, A. E., Physiology and adaptive significance of secondary carotenogenesis in green microalgae. *Russian journal of plant physiology* **2013**, *60*, 1-13.
51. Orosa, M.; Torres, E.; Fidalgo, P.; Abalde, J., Production and analysis of secondary carotenoids in green algae. *Journal of applied phycology* **2000**, *12*, 553-556.
52. Orosa, M.; Valero, J. F.; Herrero, C.; Abalde, J., Comparison of the accumulation of astaxanthin in *Haematococcus pluvialis* and other green microalgae under N-starvation and high light conditions. *Biotechnology letters* **2001**, *23*, 1079-1085.
53. Bar, E.; Rise, M.; Vishkautsan, M.; Arad, S., Pigment and Structural Changes in *Chlorella zofingiensis* upon Light and Nitrogen Stress. *Journal of Plant Physiology* **1995**, *146*, 527-534.
54. Del Campo, J. A.; Rodriguez, H.; Moreno, J.; Vargas, M. A.; Rivas, J.; Guerrero, M. G., Accumulation of astaxanthin and lutein in *Chlorella zofingiensis* (Chlorophyta). *Applied microbiology and biotechnology* **2004**, *64*, 848-854.
55. Bauch, M. E. Identifizierung und Quantifizierung der Ketocarotinoide in Dauerstadien von Grünalgen und Ketocarotinoidbiosynthese im Modellorganismus *Chlamydomonas reinhardtii*. Johannes Gutenberg-Universität, Mainz, Germany, **2011**.
56. Yuan, Z.; Wang, Z.; Takala, J.; Hiltunen, E.; Qin, L.; Xu, Z.; Qin, X.; Zhu, L., Scale-up potential of cultivating *Chlorella zofingiensis* in piggery wastewater for biodiesel production. *Bioresource technology* **2013**, *137*, 318-325.
57. Huo, S. H.; Wang, Z. M.; Zhu, S. N.; Zhou, W. Z.; Dong, R. J.; Yuan, Z. H., Cultivation of *Chlorella zofingiensis* in bench-scale outdoor ponds by regulation of pH using dairy wastewater in winter, South China. *Bioresource technology* **2012**, *121*, 76-82.
58. Feng, P. Z.; Deng, Z. Y.; Hu, Z. Y.; Fan, L., Lipid accumulation and growth of *Chlorella zofingiensis* in flat plate photobioreactors outdoors. *Bioresource technology* **2011**, *102*, 10577-10584.
59. Britton, G., Chapter 2: UV/Visible spectroscopy. In: *Carotenoids Vol. 1B Spectroscopy*, Edited by Britton G., Liaaen-Jensen S., Pfander H., Birkhäuser Verlag, Basel, Switzerland **1995**, pp. 13-62.
60. Barua, A.B.; Olson, J.A.; Furr, H.C.; van Breemen, R.B., Chapter 1: Vitamin A and carotenoids. In: *Modern chromatographic analysis of vitamins*. Edited by: Leenheer, A. P. d.; Lambert, W. E.; Van Bocxlaer, J. F., 3rd ed.; Marcel Dekker, New York, NY, USA **2000**, pp 13- 86.
61. Schierle, J.; Härdi, W.; Faccin, N.; Bühler, I.; Schüep, W., Example 8: Geometrical isomers of β , β -carotene. In: *Carotenoids Vol. 1A Isolation and analysis*, Edited by Britton G., Liaaen-Jensen S., Pfander H., Birkhäuser Verlag, Basel, Switzerland **1995**, pp 265-272.
62. Raynaud, C.; Poteau, R.; Maron, L.; Jolibois, F., *Ab initio* molecular dynamics simulation of the UV absorption spectrum of β -ionone. *Journal of molecular structure* **2006**, *771*, 43-50.
63. Siems, W.; Salerno, C.; Crifo, C.; Sommerburg, O.; Wiswedel, I., beta-Carotene degradation products - formation, toxicity and prevention of toxicity. In *Food factors for health promotion*, Edited by: Yoshikawa, T., Ed. Karger: Basel, Switzerland **2009**, Vol. 61, pp. 75-86.
64. Hurst, J. S.; Saini, M. K.; Jin, G. F.; Awasthi, Y. C.; van Kuijk, F., Toxicity of oxidized beta-carotene to cultured human cells. *Experimental eye research* **2005**, *81*, 239-243.

65. Mordi, R. C.; Walton, J. C.; Burton, G. W.; Hughes, L.; Ingold, K. U.; Lindsay, D. A.; Moffatt, D. J., Oxidative-degradation of beta-carotene and beta-apo-8'-carotenal. *Tetrahedron* **1993**, *49*, 911-928.
66. Onyewu, P. N.; Ho, C. T.; Daun, H., Characterization of β -carotene thermal degradation products in a model food system. *Journal of the American oil chemists' society* **1986**, *63*, 1437-1441.
67. Handelman, G. J.; Vankuijk, F. J. G. M.; Chatterjee, A.; Krinsky, N. I., Characterization of products formed during the autoxidation of beta-carotene. *Free radical biology and medicine* **1991**, *10*, 427-437.
68. El-Tinay, A. H.; Chichester, C. O., Oxidation of β -carotene. Site of initial attack. *Journal of organic chemistry* **1970**, *35*, 2290-2293.
69. Kanasawud, P.; Crouzet, J. C., Mechanism of formation of volatile compounds by thermal degradation of carotenoids in aqueous medium. 1. beta-Carotene degradation. *Journal of agricultural and food chemistry* **1990**, *38*, 237-243.
70. Henry, L. K.; Puspitasari-Nienaber, N. L.; Jaren-Galan, M.; van Breemen, R. B.; Catignani, G. L.; Schwartz, S. J., Effects of ozone and oxygen on the degradation of carotenoids in an aqueous model system. *Journal of agricultural and food chemistry* **2000**, *48*, 5008-5013.
71. Marty, C.; Berset, C., Degradation Products of *trans*-beta-carotene produced during extrusion cooking. *Journal of food science* **1988**, *53*, 1880-1886.
72. Palozza, P.; Krinsky, N. I.; Lester, P., 38. Antioxidant effects of carotenoids *in vivo* and *in vitro*: an overview. *Methods in enzymology*, **1992**, Vol. 213, pp, 403-420.
73. Burton, G. W.; Ingold, K. U., β -Carotene: an unusual type of lipid antioxidant. *Science* **1984**, *224*, 569-573.
74. Hazen, S. L.; Hsu, F. F.; Gaut, J. P.; Crowley, J. R.; Heinecke, J. W.; Lester, P., 12. Modification of proteins and lipids by myeloperoxidase. *Methods in enzymology*, **1999**, Vol. 300, pp. 88-105.
75. Sommerburg, O.; Langhans, C. D.; Arnhold, J.; Leichsenring, M.; Salerno, C.; Crifò, C.; Hoffmann, G. F.; Debatin, K. M.; Siems, W. G., beta-Carotene cleavage products after oxidation mediated by hypochlorous acid - a model for neutrophil-derived degradation. *Free radical biology and medicine* **2003**, *35*, 1480-1490.
76. Panasenکو, O. M.; Panasenکو, O. O.; Briviba, K.; Sies, H., Hypochlorite destroys carotenoids in low density lipoproteins thus decreasing their resistance to peroxidative modification. *Biochemistry - Moscow* **1997**, *62*, 1140-1145.
77. Panasenکو, O. M.; Gorudko, I. V.; Sokolov, A. V., Hypochlorous acid as a precursor of free radicals in living systems. *Biochemistry - Moscow* **2013**, *78*, 1466-1489.
78. Alija, A. J.; Bresgen, N.; Sommerburg, O.; Siems, W.; Eckl, P. M., Cytotoxic and genotoxic effects of beta-carotene breakdown products on primary rat hepatocytes. *Carcinogenesis* **2004**, *25*, 827-831.
79. Eugster, C. H., Chapter 4: Chemical derivatization: Microscale tests for the presence of common functional groups in carotenoids. In: *Carotenoids Vol. 1A Isolation and analysis*, Edited by Britton G., Liaen-Jensen S., Pfander H., Birkhäuser Verlag, Basel, Switzerland **1995**, 71-80.
80. Etoh, H.; Suhara, M.; Tokuyama, S.; Kato, H.; Nakahigashi, R.; Maejima, Y.; Ishikura, M.; Terada, Y.; Maoka, T., Auto-oxidation products of astaxanthin. *Journal of oleo science* **2012**, *61*, 17-21.
81. Lutz-Roder, A.; Jezussek, M.; Winterhalter, P., Nickel peroxide induced oxidation of canthaxanthin. *Journal of agricultural and food chemistry* **1999**, *47*, 1887-1891.
82. Hayakawa, T.; Kulkarni, A.; Terada, Y.; Maoka, T.; Etoh, H., Reaction of astaxanthin with peroxynitrite. *Bioscience biotechnology and biochemistry* **2008**, *72*, 2716-2722.
83. Pu, J. N.; Sathivel, S., Kinetics of lipid oxidation and degradation of flaxseed oil containing crawfish (*Procambarus clarkii*) astaxanthin. *Journal of the American oil chemists' society* **2011**, *88*, 595-601.

84. Miki W.; Kondo Y.; Murakami M.; Yamaguchi K.; Konosu S.; Satake M.; Fujita T., The stability of carotenoids pigments in the antarctic krill *Euphausia superba*. *Bulletin of Japanese society of scientific fisheries* **1983**, *49*, 1417-1420.
85. Sheehan, E. M.; O'Connor, T. P.; Sheehy, P. J. A.; Buckley, D. J.; Fitz-Gerald, R., Stability of astaxanthin and canthaxanthin in raw and smoked Atlantic salmon (*Salmo salar*) during frozen storage. *Food chemistry* **1998**, *63*, 313-317.
86. Kittikaiwan, P.; Powthongsook, S.; Pavasant, P.; Shotipruk, A., Encapsulation of *Haematococcus pluvialis* using chitosan for astaxanthin stability enhancement. *Carbohydrate polymers* **2007**, *70*, 378-385.
87. Niamnuy, C.; Devahastin, S.; Soponronnarit, S.; Raghavan, G. S. V., Kinetics of astaxanthin degradation and color changes of dried shrimp during storage. *Journal of food engineering* **2008**, *87*, 591-600.
88. Franco-Zavaleta, M. E.; Jimenez-Pichardo, R.; Tomasini-Campocosio, A.; Guerrero-Legarreta, I., Astaxanthin extraction from shrimp wastes and its stability in 2 model Systems. *Journal of food science* **2010**, *75*, C394-C399.
89. Armenta, R. E.; Guerrero-Legarreta, I., Stability studies on astaxanthin extracted from fermented shrimp byproducts. *Journal of agricultural and food chemistry* **2009**, *57*, 6095-60100.
90. Chen, X. L.; Chen, R.; Guo, Z. Y.; Li, C. P.; Li, P. C., The preparation and stability of the inclusion complex of astaxanthin with beta-cyclodextrin. *Food chemistry* **2007**, *101*, 1580-1584.
91. Yuan, C.; Jin, Z. Y.; Xu, X. M.; Zhuang, H. N.; Shen, W. Y., Preparation and stability of the inclusion complex of astaxanthin with hydroxypropyl-beta-cyclodextrin. *Food chemistry* **2008**, *109*, 264-268.
92. Kim, S.; Cho, E.; Yoo, J.; Cho, E.; Choi, S. J.; Son, S. M.; Lee, J. M.; In, M. J.; Kim, D. C.; Kim, J. H.; Chae, H. J., beta-CD-mediated encapsulation enhanced stability and solubility of astaxanthin. *Journal of the Korean society for applied biological chemistry* **2010**, *53*, 559-565.
93. Minguez-Mosquera, M. I.; Jaren-Galan, M., Kinetics of the decolouring of carotenoid-pigments. *Journal of the science of food and agriculture* **1995**, *67*, 153-161.
94. Goda, Y.; Nakamura, H.; Sakamoto, S. S.; Ishikawa, K.; Maitani, T.; Yamada, T., Photo-stability of coloring constituents in paprika color. *Journal of the food hygienic society of Japan* **1997**, *38*, 240-247.
95. Subagio, A.; Wakaki, H.; Morita, N., Stability of lutein and its myristate esters. *Bioscience biotechnology and biochemistry* **1999**, *63*, 1784-1786.
96. Fu, H.; Xie, B.; Fan, G.; Ma, S.; Zhu, X.; Pan, S., Effect of esterification with fatty acid of β -cryptoxanthin on its thermal stability and antioxidant activity by chemiluminescence method. *Food chemistry* **2010**, *122*, 602-609.
97. Arita, S.; Otsuki, K.; Osaki, K.; Murata, Y.; Shimoishi, Y.; Tada, M., Reduction in photostability by the esterification of beta-cryptoxanthin. *Bioscience biotechnology and biochemistry* **2004**, *68*, 451-453.
98. Rivera, S. M.; Canela-Garayoa, R., Analytical tools for the analysis of carotenoids in diverse materials. *Journal of chromatography A* **2012**, *1224*, 1-10.
99. Rezanka, T.; Olsovska, J.; Sobotka, M.; Sigler, K., The use of APCI-MS with HPLC and other separation techniques for identification of carotenoids and related compounds. *Current analytical chemistry* **2009**, *5*, 1-25.
100. Bijttebier, S.; D'Hondt, E.; Noten, B.; Hermans, N.; Apers, S.; Voorspoels, S., Ultra high performance liquid chromatography versus high performance liquid chromatography: stationary phase selectivity for generic carotenoid screening. *Journal of chromatography A* **2014**, *1332*, 46-56.
101. van Breemen, R. B., Liquid chromatography mass spectrometry of carotenoids. *Pure and applied chemistry* **1997**, *69*, 2061-2066.

102. van Breemen, R. B.; Huang, C. R.; Tan, Y. C.; Sander, L. C.; Schilling, A. B., Liquid chromatography mass spectrometry of carotenoids using atmospheric pressure chemical ionization. *Journal of mass spectrometry* **1996**, *31*, 975-981.
103. van Breemen, R. B., Electrospray liquid-chromatography mass-spectrometry of carotenoids. *Analytical chemistry* **1995**, *67*, 2004-2009.
104. Bijttebier, S. K. A.; D'Hondt, E.; Hermans, N.; Apers, S.; Voorspoels, S., Unravelling ionization and fragmentation pathways of carotenoids using orbitrap technology: a first step towards identification of unknowns. *Journal of mass spectrometry* **2013**, *48*, 740-754.
105. Guaratini, T.; Vessecchi, R.; Pinto, E.; Colepicolo, P.; Lopes, N. P., Balance of xanthophylls molecular and protonated molecular ions in electrospray ionization. *Journal of mass spectrometry* **2005**, *40*, 963-968.
106. Guaratini, T.; Vessecchi, R. L.; Lavarda, F. C.; Maia Campos, P. M.; Naal, Z.; Gates, P. J.; Lopes, N. P., New chemical evidence for the ability to generate radical molecular ions of polyenes from ESI and HR-MALDI mass spectrometry. *The analyst* **2004**, *129*, 1223-1226.
107. Krue, A.; Kaupmees, K.; Liigand, J.; Oss, M.; Leito, I., Sodium adduct formation efficiency in ESI source. *Journal of mass spectrometry* **2013**, *48*, 695-702.
108. Li, H.; Tyndale, S. T.; Heath, D. D.; Letcher, R. J., Determination of carotenoids and all-*trans*-retinol in fish eggs by liquid chromatography-electrospray ionization-tandem mass spectrometry. *Journal of chromatography B* **2005**, *816*, 49-56.
109. Enzell, C. R.; Back, S., Chapter 7: Mass spectrometry. In: *Carotenoids Vol. 1B Spectroscopy*, Edited by Britton G., Liaaen-Jensen S., Pfander H., Birkhäuser Verlag, Basel, Switzerland **1995**, pp. 261-320.
110. Guaratini, T.; Lopes, N. P.; Pinto, E.; Colepicolo, P.; Gates, P. J., Mechanism for the elimination of aromatic molecules from polyenes in tandem mass spectrometry. *Chemical communications* **2006**, 4110-4112.
111. Kaufmann, R.; Wingerath, T.; Kirsch, D.; Stahl, W.; Sies, H., Analysis of carotenoids and carotenol fatty acid esters by matrix-assisted laser desorption ionization (MALDI) and MALDI-post-source-decay mass spectrometry. *Analytical biochemistry* **1996**, *238*, 117-128.
112. Fraser, P. D.; Enfissi, E. M.; Goodfellow, M.; Eguchi, T.; Bramley, P. M., Metabolite profiling of plant carotenoids using the matrix-assisted laser desorption ionization time-of-flight mass spectrometry. *The plant journal* **2007**, *49*, 552-564.
113. Wingerath, T.; Kirsch, D.; Kaufmann, R.; Stahl, W.; Sies, H., Fruit juice carotenol fatty acid esters and carotenoids as identified by matrix assisted laser desorption ionization (MALDI) mass spectrometry. *Journal of agriculture and food chemistry* **1996**, *44*, 2006-2013.
114. Yoshida, K.; Ueda, S.; Maeda, I., Carotenoid production in *Bacillus subtilis* achieved by metabolic engineering. *Biotechnology letters* **2009**, *31*, 1789-1793.

Chapter 2

Sodiation as a tool for enhancing the diagnostic value of MALDI-TOF/TOF-MS spectra of complex astaxanthin ester mixtures from *Haematococcus pluvialis*

The microalga *Haematococcus pluvialis* produces the pigment astaxanthin mainly in esterified form with a multitude of fatty acids, which results in a complex mixture of carotenol mono- and diesters. For rapid fingerprinting of these esters, matrix assisted laser desorption ionization time of flight mass spectrometry (MALDI-TOF/TOF-MS) might be an alternative to traditional chromatographic separation combined with MS. Investigation of ionization and fragmentation of astaxanthin mono- and diester palmitate standards in MALDI-TOF/TOF-MS showed that sodium adduct parent masses $[M+Na]^+$ gave much simpler MS^2 spectra than radical / protonated $[M]^{\bullet+}/[M+H]^+$ parents. $[M+Na]^+$ fragments yielded diagnostic polyene-specific eliminations and fatty acid neutral losses, whereas $[M]^{\bullet+}/[M+H]^+$ fragmentation resulted in a multitude of non-diagnostic daughters. For diesters, a benzonium fragment, formed by polyene elimination, was required for identification of the second fatty acid attached to the astaxanthin backbone. Parents were forced into $[M+Na]^+$ ionization by addition of sodium acetate and best signal to noise ratios were obtained in the 0.1 to 1.0 mM range. This method was applied to fingerprinting astaxanthin esters in a crude *H. pluvialis* extract. Prior to MALDI-TOF/TOF-MS, the extract was fractionated by normal phase Flash chromatography to obtain fractions enriched in mono- and diesters and to remove pheophytin *a*, which compromised monoester signals. All 12 types of all-*trans* esterified esters found in LC were identified with MALDI-TOF/TOF-MS, with the exception of two minor monoesters.

Based on: Weesepeel, Y.; Vincken, J.-P.; Pop, R.M.; Liu, K.; Gruppen, H., Sodiation as a tool for enhancing the diagnostic value of MALDI-TOF/TOF-MS spectra of complex astaxanthin ester mixtures from *Haematococcus pluvialis*, *Journal of mass spectrometry*, **2013**, 48, 862-874

INTRODUCTION

The microalga *Haematococcus pluvialis* produces the red xanthophyll (oxygenated carotenoid) astaxanthin (3,3'-dihydroxy- β - β '-carotene-4,4'-dione) in high quantities (2 - 3% (w/w) dry weight) (1). The 3-hydroxyl groups on the β -rings can be free (unmodified astaxanthin), or esterified with fatty acids resulting in monoesters or diesters. Predominantly esterified with C16 and C18 fatty acids, monoesters are the most abundant (70-90% (w/w)) of the astaxanthin derivatives. Diesters (5-25% (w/w)) and unmodified form (5-10% (w/w)) constitute the remaining part, depending on growth conditions and harvest time (2). Astaxanthin ester accumulation by *H. pluvialis* is of interest nowadays due to their superior antioxidant properties (3), application as potential pigment in foods (4, 5) and improved bioavailability compared to free astaxanthin (6).

In order to study the compatibility of esterified astaxanthins with food matrices, fractions enriched in natural astaxanthin esters are required. Preparative Flash chromatography is the method of choice to obtain such fractions (7). For correct pooling of the esters desired, characterization of the fractions obtained is necessary. Because individual astaxanthin esters have identical chromophores (8), analytical separation is required for correct identification. Reversed phase liquid chromatography (RP-LC) has been the most favoured technique for analysis of xanthophylls in the last decades (9, 10). In combination with soft ionization mass spectrometry, like atmospheric pressure chemical ionization (APCI) or electrospray ionization (ESI), fatty acids esterified to the xanthophyll can be characterized by parent mass fragmentation (11). Even though LC analysis time can be greatly reduced by ultra-high performance liquid chromatography (UHPLC), separation of a complex xanthophyll ester mixture is still laborious (12).

Using matrix-assisted laser desorption ionization time of flight mass spectrometry (MALDI-TOF-MS), LC can be omitted, thereby offering the opportunity for high sample throughput and rapid fingerprinting of xanthophyll esters. Although used in the analysis of carotenoids in plant tissues (13), bacterial samples (14) and liquid food matrices (15) research on xanthophyll ester analysis using MALDI-TOF/TOF-MS is scarce.

Upon ionization in MALDI-TOF-MS, xanthophyll (esters) form a combination of radical $[M]^{\bullet+}$, protonated $[M+H]^+$, and sodiated $[M+Na]^+$ parent ions. Generation of diagnostic ions for identification of carotenoids using MALDI-TOF-MS is traditionally done by post-source-decay (PSD), although nowadays this is mostly referred to as TOF/TOF fragmentation (16). Generally, unambiguous proof for the presence of carotenoids is obtained by mass spectrometric detection of the in-polyene chain fragment toluene (neutral loss (NL) 92 Da) (17). Additionally, xylene (NL 106 Da) can be observed as co-fragment. The simultaneous occurrence of multiple parent ions not

only dilutes the signal intensity of each, but also complicates the interpretation of the PSD fragmentation spectra in particular. Unfortunately, there is an incomplete picture with respect to fragmentation pathways of the three kinds of parent ions upon PSD fragmentation. For instance, radical $[M]^{\bullet+}$ parent ions of xanthophyll esters show a clear toluene loss in PSD fragmentation (16). In contrast, $[M+H]^+$ parent ions do not form toluene or xylene fragments, at least not with ESI ion trap MS (7). When $[M+Na]^+$ adducts of xanthophyll esters were ion trap fragmented, loss of toluene and xylene was more pronounced and fragmentation patterns showed less non-diagnostic fragments than with $[M+H]^+$ adducts (7). Similar observations have been obtained for astaxanthin and canthaxanthin in ESI tandem quadrupole (18) and for fucoxanthin-type carotenoids in APCI ion trap (19). Overall, it is unclear if the ionization and fragmentation behaviour described for $[M+H]^+$ and $[M+Na]^+$ ions with APCI or ESI ion trap are also applicable to MALDI-TOF/TOF-MS. This is particularly relevant, as it has been suggested that xanthophylls prefer to form $[M+Na]^+$ adducts over $[M]^{\bullet+}$ / $[M+H]^+$ ions (18).

Hence, in the present study a new MALDI-TOF/TOF-MS application was developed enabling the rapid analysis of astaxanthin esters. Ionization behaviour and fragmentation using TOF reacceleration of different type of parent ions were evaluated. The effect of sodium content on signal to noise ratios of two astaxanthin ester standards was demonstrated. Validation of the MALDI-TOF/TOF-MS method was done by characterization of astaxanthin esters in a *H. pluvialis* extract and pools enriched therein.

MATERIALS AND METHODS

Materials

Haematococcus pluvialis dried flakes were obtained from Ingrepro B.V. (August 2009, Borculo, The Netherlands), (3*RS*,3'*RS*)-astaxanthin (97%), (3*RS*,3'*RS*)-astaxanthin monopalmitate (97%) and astaxanthin dipalmitate (98%) were purchased from Carotenature (Lupsingen, Switzerland). Methanol (99.8%), acetonitrile (99.97%) and ethyl acetate (99.9%) (all w/w) were obtained from Biosolve (Valkenswaard, The Netherlands). Sodium acetate (99.0% w/w) and potassium acetate (99.0% w/w) were purchased from Merck (Darmstadt, Germany). Dichloromethane (99.8%), hexane (98%) and formic acid (98.0%) were obtained from Sigma-Aldrich (St. Louis, MO, USA). MALDI-TOF-MS grade 2,5-dihydroxybenzoic acid (DHB) was obtained from Bruker Daltonics (Bremen, Germany), Dowex AG 50W-X8 resin was purchased from Bio-Rad Laboratories (Hercules, CA, USA), Maltodextrin DP 6 was purchased from AVEBE (Veendam, The Netherlands). Fat-free quartz sand was obtained from Büchi (Flawil, Switzerland).

Sample preparation

A *H. pluvialis* hexane extract was obtained via pressurized solvent extraction. A stainless steel extraction tube (40 mL) contained 0.5 g of dried *H. pluvialis* flakes ground with 55 g of fat-free quartz sand and was applied to an E-916 Speed Extractor (Büchi, Flawil, Switzerland). Extraction was carried out using four subsequent 15 min cycles with *n*-hexane at 40 °C and 100 bar. Each extraction receptacle was protected from heat and light during the extraction to prevent light-induced isomerization and oxidation of carotenoids. Extracts were dried in reduced light using a rotary evaporator at 40 °C. Subsequently, samples were re-dissolved in ethyl acetate, then supplemented with acetonitrile to reach a ratio of ethyl acetate:acetonitrile 1:3 (v/v). Prior to UHPLC or Flash chromatography, samples were centrifuged (5 min; 21,380 $\times g$; 5 °C).

MALDI-TOF/TOF-MS

A solution of 5 mg mL⁻¹ DHB in 50% (v/v) methanol was used as matrix (13, 15). Sodium acetate was either omitted or added to the matrix in several concentrations to a maximum of 100 mM. Desalting was done by addition of a spatula (19.5 \pm 1.9 mg) of Dowex 50W-X8 resin to 400 μ L matrix and sample, stirring for 10 min, and subsequent centrifugation (5 min; 21,380 $\times g$; 5 °C). Approximately 1 mg of crystalline astaxanthin monopalmitate (Ast C16:0) and dipalmitate (Ast C16:0/C16:0) were separately dissolved in dichloromethane. Standards were diluted using *n*-hexane to concentrations of 19.5 \pm 0.3 μ g mL⁻¹ for Ast C16:0 and 21.8 \pm 0.3 μ g mL⁻¹ for Ast C16:0/C16:0. The concentrations were determined in hexane:dichloromethane 98:2 (v/v) at 470 nm using the free astaxanthin molar extinction coefficient ϵ_{mol} of 125,100 L mol⁻¹ cm⁻¹ (20). The concentrations determined were subsequently corrected for the difference in molecular weight assuming that the fatty acid moiety had no influence on the ϵ_{mol} . Flash fractions were contained in the original solvent at the time of elution (acetonitrile/ethyl acetate) and concentrated under a stream of nitrogen in reduced light if the concentration was too low. In order to avoid phase separation in sample spots, the sandwich method was used: one μ L DHB solution was applied onto a stainless steel sample plate (Bruker Daltonics), air dried and subsequently a layer of 1 μ L standard was applied, which was also air dried. This was covered with 1 μ L DHB solution and air dried. For the *H. pluvialis* extract and Flash fractions, samples were mixed with DHB solution in a 1:1 (v/v) ratio on the sample plate and air dried.

MALDI-TOF/TOF-MS spectra were recorded using an Ultraflexextreme workstation controlled by FlexControl 3.3 software (Bruker Daltonics) equipped with a N₂ laser of 337 nm and operated in positive mode. Calibration was performed using maltodextrin DP6 and a mass scan range from 550 to 1,500 Da was used. Spectra were recorded by automatic operation. For full MS spectra, the reflector mode was used with 26.40 and 13.70 kV. For TOF/TOF fragmentation, parent and fragment ions were

reaccelerated using a LIFT device located in the flight tube with reflector voltages of 29.50 and 13.95 kV. The precursor ion selector was set at 0.45% of the desired parent mass, the LIFT voltages were set at 19.00 and 3.15 kV, and the LIFT metastable suppressor was disabled. FlexAnalysis 3.3 (Bruker Daltonics) was used for data reprocessing. A successful measurement was defined as an astaxanthin ester signal to noise (S/N) ratio with a minimum value of 3 units. The S/N was defined as the ratio of the astaxanthin parent signal to the standard deviation of the instruments background noise. Both values were calculated for every individual sample spot. The Sophisticated Numerical Annotation Procedure (SNAP, Bruker Daltonics) algorithm was used for isotope ratio determinations. MassFrontier 7.0 (Thermo Scientific) was used for prediction of fragmentation pathways.

RP-UHPLC analysis

Separation and identification of xanthophylls and porphyrins in the *H. pluvialis* extract and the Flash fractions were carried out using an Accela UHPLC system (Thermo Scientific, San Jose, CA, USA) equipped with pump, degasser, auto sampler, photo diode array (PDA) detector and coupled *in-line* to a LTQ-Velos double ion trap mass spectrometer equipped with a heated ESI probe (Thermo Scientific). Samples were injected into an Aquity UHPLC Shield C18 BEH column (2.1 × 150 mm, 1.7 µm particle size; Waters, Milford, MA, USA) fitted to a Vanguard pre-column (2.1 × 5 mm, 1.7 µm particle size; Waters). The eluents were the following: 50% (v/v) acetonitrile in demineralized water (A), acetonitrile (B) and ethyl acetate (C), all containing 0.1% (v/v) formic acid as mobile phase modifier. The flow rate was 300 µL/min and the sample injection volume was 3.0 µL. The elution program was started from 25% (v/v) A, 75% (v/v) B and followed by: 0 - 7 min – linear gradient to 100% (v/v) B; 7 - 15 min – isocratic at 100% (v/v) B; 15 - 22.5 min – linear gradient to 87.5% (v/v) B, 12.5% (v/v) C; 22.5 - 24 min – linear gradient to 70% (v/v) B, 30% (v/v) C; 24 - 34 min – linear gradient to 100% (v/v) C; 34 - 35 min – isocratic at 100% (v/v) C. The eluent was adjusted to its initial composition in 5 min, followed by equilibration for 10 min. Detection wavelengths for UV-Vis were set at 470 ± 0.5 nm (astaxanthin) and 660 ± 0.5 nm (porphyrins). Data were recorded at 10 Hz.

Electrospray ionisation ion trap mass spectrometry (ESI-IT-MS)

Mass spectrometric data were recorded in positive ion mode. Nitrogen was used as both sheath gas (5 arbitrary units) and auxiliary gas (2 arbitrary units). Most settings were optimized via automatic tuning using 'Tune Plus' (Xcalibur 2.10, Thermo Scientific). The system was tuned with 5 µL/min direct injection of 1 µg/mL (3*RS*,3'*RS*)-astaxanthin in acetonitrile : ethyl acetate : hexane (73.5 : 24.5 : 2.0 (v/v)) containing 0.1% (v/v) formic acid, the ion transfer tube was 400 °C and the source voltage 3.5 kV. Data were recorded over the *m/z* range 550-1,000 (0-7.5 min), 650-

1,000 (7.5-22 min) and 1,000-1,250 (22-35 min). Dynamic data-dependent MS² fragmentation was performed on the most intense parent ion ($x = 1$) and subsequently on the second most intense parent ($x = 2$). A repeat count of two MS² spectra per parent ion and a maximum of $x = 25$ or within a time frame of 5.0 s were used as settings. The collision induced dissociation (CID) was set to 35%. Dynamic exclusion was used for fragmentation of astaxanthin [M+H]⁺, [M+Na]⁺ and [M+K]⁺ parent ions within a single chromatographic peak. Data acquisition and reprocessing were done with Xcalibur 2.10 (Thermo Scientific).

NP-Flash chromatography

A Reveleris Flash chromatography system (Grace, Deerfield, IL, USA) was used to obtain pools of astaxanthin monoesters and diesters. Two-hundred and fifty milligrams of *H. pluvialis* extract in *n*-hexane were applied to a Reveleris 40 g silica column (45 mL column volume, particle size 40 μ m, Grace). The flow rate was maintained at 40 mL/min, *n*-hexane (A) and ethyl acetate (B) were used as eluents. The elution program was started at 100% (v/v) A and then a block gradient as follows: 0 - 3 min – isocratic at 100% (v/v) A; 3 - 6 min – isocratic at 5% (v/v) B; 6 - 9 min – isocratic at 10% (v/v) B; 9 - 12 min – isocratic at 20% (v/v) B. Separation was stopped after 12 min and fractions were pooled visually by colour. Pools were concentrated under N₂ flow in reduced light for UHPLC-ESI-MS or MALDI-TOF/TOF-MS analysis.

RESULTS AND DISCUSSION

RP-UHPLC-ESI-MS characterization of pigments in *H. pluvialis* extract

Fifty-eight carotenoids and porphyrins were identified in the *H. pluvialis* hexane extract by RP-UHPLC separation (**Figure 1A**). PDA visible absorption, full MS and MS² spectra were used for peak assignment of free carotenoids and porphyrins (**Table 1**) and astaxanthin esters (**Table 2**) (7, 21). Astaxanthin in all-*trans* (peak 2) and its geometrical *cis* isomers (peaks 3 and 4) were in the free (non-esterified) form (**Figure 1B**). Besides, 9'-*cis*-neoxanthin, lutein, and canthaxanthin were found with absorption spectra and MS data matching those of the all-*trans* forms (22, 23). Porphyrins were detected at 660 nm (**Figure 1A**). The absorption spectrum of peak 56 showed a hypsochromic shift compared to the chlorophyll *a* spectrum (no further data shown) and was, therefore, annotated as pheophytin *a*. Pheophytin *a* had a parent mass of m/z 871 and MS² fragmentation showed the loss of the phytol tail [M-278]⁺• and the loss of acetic acid [M-278-60]⁺•. Besides the epimer of pheophytin *a* (peak 58), also hydroxylated allomer forms were found (peaks 55 and 57) (24). Peak 53 was identified as chlorophyll *b* by absorption spectrum, parent mass and fragmentation ions of phytol and acetic acid (22).

Esterified astaxanthins exhibited a 1-2 nm hypsochromic shift compared to free astaxanthin as reported earlier (7). For identification of fatty acids esterified to astaxanthin, MS² data were required. Astaxanthin monoesters (**Figure 1A**, peaks 8-29) represented the major part of the xanthophylls present in the extract. The final part of the chromatogram consisted of astaxanthin diesters (**Figure 1C**, peaks 30-52), emphasizing the diversity of differently esterified carotenoids in *H. pluvialis*. Besides the main esterified all-*trans*-astaxanthin isomers, also *cis* isomers were found, which eluted after the respective all-*trans* form. Astaxanthin *cis* isomers had a hypsochromic shift in the absorption maximum (10-15 nm) and an extra peak emerging at 370 nm (so-called '*cis* peak'), which was not always detected, and which is known to be more prominent when the position of the *cis* bond was closer to the centre of the polyene chain (**Figure 1D**) (8, 22). Up to 4 *cis* forms were identified and putatively annotated as reported previously.

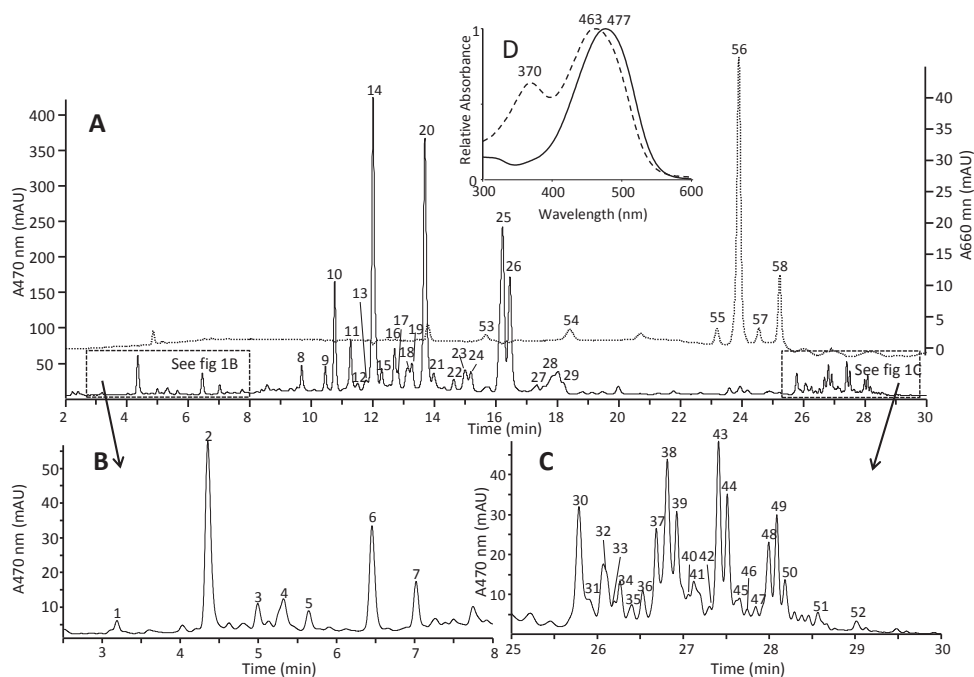


Figure 1. RP-UHPLC profile of crude *H. pluvialis* extract. **A** Chromatogram of carotenoids (450 nm, continuous line) and chlorophylls (660 nm, dotted line). **B** Excerpt profile of free xanthophylls. **C** Excerpt profile of astaxanthin diesters. **D** Visible spectra of all-*trans* astaxanthin C18:3 (continuous line) and *cis*-astaxanthin C18:3 (dotted line).

Table 1. Non-esterified carotenoids and chlorophylls tentatively assigned by RP-UHPLC-ESI-MS in the hexane extract of *H. pluvialis*.

Peak no.	Rt. (min)	Compound	Vis _{max} (nm)	Isomer	Parent ion (m/z)	MS ² product ions in m/z (relative intensity)	Ref.
1	3.19	9'-cis-neoxanthin	413, 438, 466	9'-cis	601.7	N.D.	(22)
2	4.35	astaxanthin	478	all-trans	597.7	579.6(100), 561.6(20), 505.5(25), 487.6(10), 523.5(10)	(22)
3	4.99	astaxanthin	467	cis	597.7	579.5(40), 561.6(10), 505.5(10), 349.4(90), 293.4(100)	(21)
4	5.32	astaxanthin	376, 467	cis	597.7	579.5(100), 561.5(20), 505.5(20), 491.5(10), 379.5(10), 349.5(10), 293.4(10)	(21)
5	5.64	hydroxy-carotenoid-like	329, 467	cis	581.6	563.5(100), 545.5(10), 475.5(10), 361.5(20), 203.2(15)	
6	6.46	lutein	426, 446, 475	all-trans	568.7	550.6(20), 476.5(100), 458.6(10), 430.5(15), 338.5(60)	(22)
7	7.02	canthaxanthin	475	all-trans	565.7	547.5(100), 509.5(20), 491.5(40), 473.5(40), 459.5(20), 363.4(70), 335.4(50), 309.5(50), 281.4(60), 203.2(50)	(22)
53	15.73	chlorophyll b	456, 645	N.A.	908.0	879.8(15), 815.9(10), 637.7(40), 629.4(100), 611.7(50), 569.3(20), 541.3(15)	(22)
54	18.40	porphyrin like	416, 432, 660	N.A.	N.D.	N.D.	(22)
55	23.19	hydroxy-pheophytin a	408, 666	N.A.	888.0	869.8(30), 609.4(30), 591.4(100)S, 531.4(20)	(22, 24)
56	23.90	pheophytin a	409, 503, 535, 607, 664	N.A.	872.0	593.4(100), 533.4(60)	(22)
57	24.55	hydroxy-pheophytin a'	410, 667	N.A.	887.9	609.5(100), 591.5(30), 531.4(10)	(22, 24)
58	25.23	pheophytin a'	409, 501, 535, 611, 666	N.A.	871.9	593.6(100), 533.5(10)	(22)

N.D.: not determined. N.A.: not applicable

All esterified astaxanthin esters showed three types of ionization in ESI-IT-MS; $[M+H]^+$, $[M+Na]^+$ and $[M+K]^+$. Radical ions were not observed when using this type of mass spectrometry. Identification of astaxanthin esters was always done using the following diagnostic fragments: (i) in-polyene chain elimination of toluene (NL 92 Da) and xylene (NL 106 Da), and (ii) neutral losses of one or two esterified fatty acid(s). The fragment representing the free astaxanthin molecule can be used as confirmation of the type of carotenoid, together with the absorption spectrum of the chromatographic peak. Fragment ions were calculated and are depicted in **Figure 2**, the fragmentation data are provided in **Table 2**. Fragment structures for $[M+K]^+$ ions were similar to those for $[M+Na]^+$ and, therefore, neither annotated in **Table 2** nor depicted in **Figure 2B**.

For in-polyene chain elimination, the toluene fragment intensity (**I**) was low for $[M+H]^+$ fragment ions (average relative intensity 10%), whereas it was the main fragment ion of $[M+Na]^+$ and $[M+K]^+$. Elimination of xylene (**II**) was observed for $[M+Na]^+$ and $[M+K]^+$ ions (average relative intensity 15%), while it was absent for $[M+H]^+$ ions. Three main fragments of the release of the esterified fatty acid could be identified for $[M+H]^+$ ions: (i) Sequential loss of the fatty acid after β -ring hydroxyl group loss (**III** and **IV**), (ii) loss of the fatty acid (**V**), and (iii) loss of the fatty acid in the ketene form (**VI**), which was in most cases not pronounced. Fragment **VI** represented also the mass of the free astaxanthin (proton inclusive). The water loss exhibited by $[M+H]^+$ ions (**III**) gave the most abundant fragment. This is undesirable, because it did not contribute to structure elucidation and suppressed the diagnostic ions. Additionally, more minor fragments, which could be associated to fatty acid losses, were found (data not shown). These fragments had no particular contribution in the elucidation of the astaxanthin ester structure. This was in contrast to $[M+Na]^+$ and $[M+K]^+$ ions, for which only fragments **V** was found and where the salt ions acted as suppressors of water loss, thereby elevating the signal of the diagnostic ions (**I**, **II** and **V**). For the astaxanthin diesters, similar fragmentation patterns for $[M+H]^+$ (except for water loss **III**) and $[M+Na]^+$ / $[M+K]^+$ ions were observed. Due to the low abundance of diesters and more extensive degradation (for example **III** and **IX**) during fragmentation, suitable $[M+H]^+$ spectra were scarcely observed. The $[M+Na]^+$ and $[M+K]^+$ ions showed again more diagnostic and simpler fragmentation spectra by single losses of fatty acids (**III** fragments) than the $[M+H]^+$. Fragments of $[M+H]^+$ and $[M+Na]^+$ ions were in accordance with previously reported data (7).

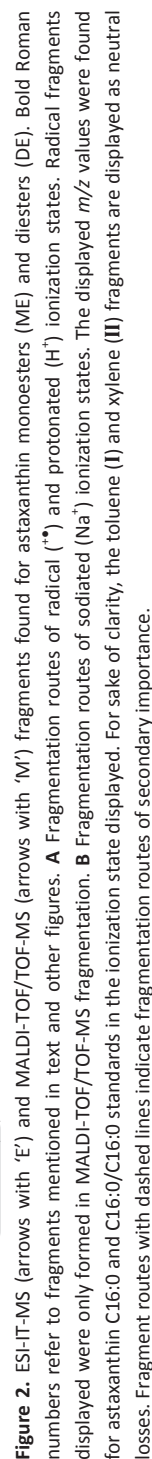


Table 2. Esterified astaxanthins tentatively assigned by RP-UHPLC-ESI-MS in the hexane extract of *H. pluvialis*. Roman numbers refer to fragment ions in **Figure 2**.

Peak no ^a	Rt (min)	Compound	λ_{\max} (nm)	Ionization type	MS ² product ions assigned in Figure 2 in <i>m/z</i> (relative intensity)					
					Parent ion	I	II	III	V	III-2 nd (DE only) ^b
8	9.69	all- <i>trans</i> -ast C16:4	474	[M+H] ⁺	827.9	N.D.	N.D.	609.7(50)	579.5(100)	N.A.
				[M+Na] ⁺	849.9	759.8(100)	745.7(30)	N.D.	601.6(35)	N.A.
9	10.46	all- <i>trans</i> -ast C16:3	474	[M+H] ⁺	829.9	737.8(10)	727.8(10)	811.8(100)	579.5(40)	N.A.
				[M+Na] ⁺	851.9	759.8(100)	745.8(30)	N.D.	601.6(40)	N.A.
10	10.76	all- <i>trans</i> -ast C18:4	477	[M+H] ⁺	856.0	763.7(10)	749.8(5)	837.8(100)	579.5(30)	N.A.
				[M+Na] ⁺	878.0	785.8(100)	771.7(30)	N.D.	601.5(30)	N.A.
11	11.28	<i>cis</i> -ast C20:5	470	[M+H] ⁺	882.0	789.7(50)	775.8(15)	863.9(100)	579.5(30)	N.A.
				[M+Na] ⁺	904.0	811.9(100)	797.9(30)	886.0(5)	601.6(25)	N.A.
12	11.51	<i>cis</i> -ast C18:4	380, 454	[M+H] ⁺	855.9	N.D.	N.D.	N.D.	N.D.	N.A.
				[M+Na] ⁺	878.0	785.8(100)	771.8(30)	859.9(10)	601.6(30)	N.A.
12	11.51	<i>cis</i> -ast C22:3	380, 454	[M+H] ⁺	N.D.	N.D.	N.D.	N.D.	N.D.	N.A.
				[M+Na] ⁺	932.8	839.9(10)	825.9(25)	913.9(80)	601.6(15)	N.A.
13	11.79	<i>cis</i> -ast C18:4	378, 460	[M+H] ⁺	856.0	N.D.	N.D.	N.D.	N.D.	N.A.
				[M+Na] ⁺	878.0	785.8(100)	771.8(25)	859.9(10)	601.6(30)	N.A.
14	12.01	all- <i>trans</i> -ast C18:3	477	[M+H] ⁺	858.0	765.9 (3)	751.8(5)	839.8(100)	579.6(40)	N.A.
				[M+Na] ⁺	880.0	787.8(100)	771.8(30)	859.9(10)	601.6(30)	N.A.
15	12.29	<i>cis</i> -ast C18:3	469	[M+H] ⁺	857.9	N.D.	N.D.	N.D.	N.D.	N.A.
				[M+Na] ⁺	880.0	787.8(100)	773.8(25)	859.9(5)	601.6(50)	N.A.
16	12.71	<i>cis</i> -ast C20:4	472	[M+H] ⁺	884.0	791.8(10)	777.8(5)	866.0 (40)	579.5(10)	N.A.
				[M+Na] ⁺	906.0	813.8(100)	799.8(30)	887.9(5)	601.6(40)	N.A.
17	12.82	<i>cis</i> -ast C18:3	463	[M+H] ⁺	858.0	765.8(5)	751.24(5)	839.9(100)	579.5(30)	N.A.
				[M+Na] ⁺	878.0	787.8(100)	773.8(30)	N.D.	601.6(70)	N.A.
18	13.12	<i>cis</i> -ast C18:3	370, 462	[M+H] ⁺	858.0	765.8(3)	751.7(5)	839.9(100)	579.6(80)	N.A.
				[M+Na] ⁺	880.0	787.8(100)	773.8(30)	N.D.	601.6(30)	N.A.
19	13.27	<i>cis</i> -ast C18:3	370, 462	[M+H] ⁺	858.0	N.D.	N.D.	839.9(40)	579.6(100)	N.A.
				[M+Na] ⁺	880.0	787.8(100)	773.8(30)	N.D.	601.6(35)	N.A.
20	13.69	all- <i>trans</i> -ast C18:2	475	[M+H] ⁺	860.0	N.D.	753.9(5)	841.9(100)	579.5(50)	N.A.
				[M+Na] ⁺	882.1	789.8(100)	775.8(25)	N.D.	601.6(40)	N.A.
21	13.98	<i>cis</i> -ast C18:2	469	[M+H] ⁺	860.0	N.D.	N.D.	N.D.	N.D.	N.A.
				[M+Na] ⁺	882.0	789.9(100)	775.8(20)	N.D.	601.6(40)	N.A.
21	13.98	<i>cis</i> -ast C20:3	469	[M+H] ⁺	886.0	N.D.	N.D.	N.D.	N.D.	N.A.
				[M+Na] ⁺	908.0	815.8(100)	801.8(30)	N.D.	601.6(30)	N.A.
22	14.63	<i>cis</i> -ast C18:2	464	[M+H] ⁺	860.0	N.D.	N.D.	N.D.	N.D.	N.A.
				[M+Na] ⁺	882.0	789.8(100)	775.8(30)	N.D.	601.6(50)	N.A.

Chapter 2

Table 2. Continued

Peak no ^a	Rt (min)	Compound	λ_{\max} (nm)	Ionization type	MS ² product ions assigned in Figure 2 in <i>m/z</i> (relative intensity)					
					Parent ion	I	II	III	V	III-2 nd (DE only) ^b
23	15.00	<i>cis</i> -ast C18:2	374, 464	[M+H] ⁺	860.0	N.D.	N.D.	N.D.	N.D.	N.A.
				[M+Na] ⁺	882.0	789.8(100)	775.8(30)	N.D.	601.6(40)	N.A.
24	15.19	<i>cis</i> -ast C18:2	370, 464	[M+H] ⁺	860.0	N.D.	N.D.	841.9(30)	579.5(20)	N.A.
				[M+Na] ⁺	882.0	789.9(100)	775.8(30)	N.D.	601.6(40)	N.A.
25	16.22	all- <i>trans</i> - ast C18:1	477	[M+H] ⁺	862.0	N.D.	N.D.	843.9(50)	579.6(30)	N.A.
				[M+Na] ⁺	884.0	791.8(100)	777.8(30)	853.8(5)	601.6(40)	N.A.
26	16.46	all- <i>trans</i> - ast C16:0	476	[M+H] ⁺	835.0	N.D.	729.8(10)	817.9(100)	579.6(60)	N.A.
				[M+Na] ⁺	858.0	765.8(100)	751.8(25)	840.0(10)	601.6(40)	N.A.
27	17.33	<i>cis</i> -ast C18:1	465	[M+H] ⁺	862.0	N.D.	N.D.	844.0(60)	579.5(10)	N.A.
				[M+Na] ⁺	884.0	791.9(100)	777.8(20)	853.8(5)	579.6(25)	N.A.
28	18.02	<i>cis</i> -ast C18:1	370, 465	[M+H] ⁺	862.0	N.D.	N.D.	N.D.	N.D.	N.A.
				[M+Na] ⁺	884.0	791.8(100)	777.8(25)	N.D.	601.5(35)	N.A.
29	18.19	<i>cis</i> -ast C16:0	374, 462	[M+H] ⁺	836.0	N.D.	N.D.	817.9(100)	579.6(70)	N.A.
				[M+Na] ⁺	858.0	765.8(100)	751.8(25)	839.9(100)	601.6(40)	N.A.
30	25.79	all- <i>trans</i> - ast C18:2/C18:3	477	[M+H] ⁺	1120.2	1028.1(10)	1014.1(5)	842.0(50)	N.A.	839.9(40)
				[M+Na] ⁺	1142.3	1050.1(100)	1036.2(20)	861.9(20)	N.A.	864.0(40)
31	25.90	all- <i>trans</i> - ast C16:3/C18:1	476	[M+H] ⁺	N.D.	N.D.	N.D.	N.D.	N.A.	N.D.
				[M+Na] ⁺	1116.2	1024.1(100)	1010.1(30)	866.0(30)	N.A.	834.0(30)
32	26.07	<i>cis</i> -ast C18:2/C18:3	475	[M+H] ⁺	1120.2	1028.1(10)	N.D.	841.9(60)	N.A.	839.9(50)
				[M+Na] ⁺	1142.2	1050.2(100)	1036.1(15)	862.0(30)	N.A.	863.9(25)
33	26.20	<i>cis</i> -ast diester	473	[M+H] ⁺	N.D.	N.D.	N.D.	N.D.	N.A.	N.D.
				[M+Na] ⁺	N.D.	N.D.	N.D.	N.D.	N.A.	N.D.
34	26.27	<i>cis</i> -ast C18:2/C18:3	473	[M+H] ⁺	1120.2	1028.1(15)	1014.1(5)	841.8(45)	N.A.	840.0(40)
				[M+Na] ⁺	1142.3	1050.2(100)	1036.2(15)	864.0(35)	N.A.	861.9(30)
35	26.40	<i>cis</i> -ast C18:1/C20:5	380, 468	[M+H] ⁺	1146.2	1054.1(10)	1040.1(5)	843.9(30)	N.A.	864.0(50)
				[M+Na] ⁺	1167.3	1076.2(100)	1061.3(20)	866.0(15)	N.A.	885.9(20)
36	26.53	<i>cis</i> -ast C18:2/C18:3	380, 466	[M+H] ⁺	1120.2	1028.1(5)	N.D.	841.9(25)	N.A.	840.0(20)
				[M+Na] ⁺	1142.3	1050.2(100)	1036.2(20)	863.9(20)	N.A.	862.0(30)
37	26.69	all- <i>trans</i> - ast C18:2/C18:2	476	[M+H] ⁺	1122.2	N.D.	1016.2(5)	841.9(50)	N.A.	N.A.
				[M+Na] ⁺	1144.2	1052.2(100)	1038.3(25)	863.9(45)	N.A.	N.A.
38	26.82	all- <i>trans</i> - ast C18:1/C18:3	476	[M+H] ⁺	1122.2	1030.1(10)	1016.0(5)	844.0(60)	N.A.	839.8(45)
				[M+Na] ⁺	1144.3	1052.2(100)	1038.3(25)	865.9(10)	N.A.	862.0(20)
39	26.93	all- <i>trans</i> - ast C16:0/C18:3	477	[M+H] ⁺	1096.1	1004.1(10)	N.D.	839.8(25)	N.A.	818.0(25)
				[M+Na] ⁺	1118.2	1026.2(100)	1012.1(15)	861.8(15)	N.A.	840.1(25)
40	27.06	<i>cis</i> -ast C18:1/C18:3	471	[M+H] ⁺	1122.1	1030.0(15)	1016.0(5)	844.1(40)	N.A.	840.0(30)
				[M+Na] ⁺	1144.2	1052.1(100)	1036.1(25)	866.0(25)	N.A.	861.9(35)
41	27.12	<i>cis</i> -ast C18:1/C18:3	470	[M+H] ⁺	1122.2	1029.9(10)	1015.9(5)	839.9(35)	N.A.	840.1(50)
				[M+Na] ⁺	1144.3	1052.0(100)	N.D.	861.9(30)	N.A.	862.0(30)

Table 2. Continued

Peak no ^a	Rt (min)	Compound	λ_{max} (nm)	Ionization type	MS ² product ions assigned in Figure 2 in <i>m/z</i> (relative intensity)					
					Parent ion	I	II	III	V	III-2 nd (DE only) ^b
42	27.30	<i>cis</i> -ast C16:0/C18:3	380, 461	[M+H] ⁺	1096.2	N.D.	N.D.	N.D.	N.A.	N.D.
				[M+Na] ⁺	1118.2	1026.1(100)	1012.2(30)	861.9(30)	N.A.	839.9(60)
43	27.41	<i>all-trans</i> -ast C18:1/C18:2	477	[M+H] ⁺	1124.2	1032.1(15)	1018.0(5)	844.0(40)	N.A.	842.0(40)
				[M+Na] ⁺	1146.3	1054.2(100)	1040.3(20)	866.1(20)	N.A.	864.0(40)
44	27.51	<i>all-trans</i> -ast C16:0/C18:2	476	[M+H] ⁺	1098.1	1006.1(10)	N.D.	842.0(45)	N.A.	817.9(25)
				[M+Na] ⁺	1120.2	1028.2(100)	1014.2(20)	864.0(35)	N.A.	840.0(20)
45	27.65	<i>cis</i> -ast C18:1/C18:2	380, 469	[M+H] ⁺	1124.2	1032.0(20)	1018.0(5)	844.0(40)	N.A.	841.9(20)
				[M+Na] ⁺	1146.1	1054.1(100)	1039.9(40)	865.9(15)	N.A.	864.0(35)
46	27.74	<i>cis</i> -ast C16:0/C18:2	380, 467	[M+H] ⁺	1098.1	N.D.	N.D.	842.0(40)	N.A.	819.9(35)
				[M+Na] ⁺	1120.0	1028.0(100)	1013.1(15)	864.0(20)	N.A.	839.9(15)
47	27.84	<i>cis</i> -ast C18:2/C18:1	380, 467	[M+H] ⁺	1124.3	N.D.	N.D.	N.D.	N.A.	N.D.
				[M+Na] ⁺	1146.2	1054.1(100)	1040.1(25)	865.9(40)	N.A.	863.9(30)
48	28.00	<i>all-trans</i> -ast C18:1/C18:1	478	[M+H] ⁺	1126.2	N.D.	1020.0(5)	843.8(45)	N.A.	N.A.
				[M+Na] ⁺	1148.2	1056.2(100)	1042.2(20)	866.0 (50)	N.A.	N.A.
49	28.09	<i>all-trans</i> -ast C16:0/C18:1	478	[M+H] ⁺	1100.1	1008.2(15)	994.1(5)	844.0(55)	N.A.	817.8(40)
				[M+Na] ⁺	1122.3	1030.2(100)	1016.2(15)	865.9(20)	N.A.	840.0(30)
50	28.18	<i>all-trans</i> -ast C16:0/C16:0	476	[M+H] ⁺	1074.2	982.1(15)	968.0(5)	817.9(40)	N.A.	N.A.
				[M+Na] ⁺	1096.3	1004.2(100)	990.2(15)	840.0(35)	N.A.	N.A.
51	28.57	<i>cis</i> -ast diester	380, 473	[M+H] ⁺	1146.2	N.D.	N.D.	N.D.	N.A.	N.D.
				[M+Na] ⁺	1168.2	N.D.	N.D.	N.D.	N.A.	N.D.
52	29.02	<i>cis</i> -ast diester	380, 470	[M+H] ⁺	1120.1	N.D.	N.D.	N.D.	N.A.	N.D.
				[M+Na] ⁺	1142.2	N.D.	N.D.	N.D.	N.A.	N.D.

^aDouble assigned peaks numbers were co-eluting astaxanthins. ^bDiesters have a second **III** fragment, because they can contain two different fatty acids. N.D.: Not detected. N.A.: Fragment **V** is not applicable for diesters. Monoesters do not have two esterified fatty acids, so fragment **III** – 2nd is not applicable.

From this data, it was clear that astaxanthin ester salt adducts showed less extensive degradation upon fragmentation than the protonated form. Ionization of salt adducts leads to fragment ions with an increased diagnostic value, and more straight forward interpretation of spectra. Therefore, also for MALDI-TOF/TOF-MS analysis, salt adducts were hypothesized to be the most suitable ions for mass spectrometric identification of astaxanthins.

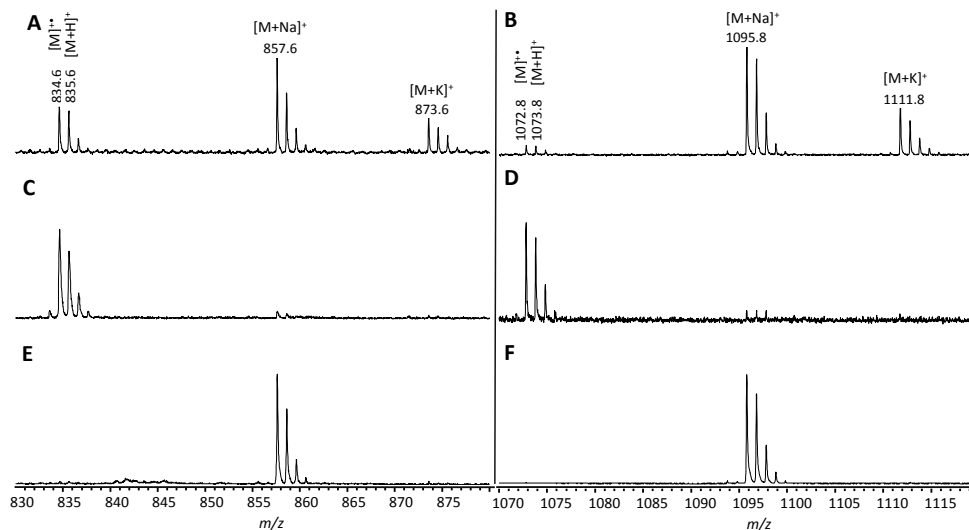


Figure 3. MALDI-TOF-MS spectra of Ast C16:0 and Ast C16:0/C16:0. **A** and **B** untreated, **C** and **D** desalted, **E** and **F** in the presence of 10 mM NaOAc.

MALDI-TOF-MS ionization, desalting and salting of astaxanthin esters

Two standards, astaxanthin monopalmitate (Ast C16:0) and astaxanthin dipalmitate (Ast C16:0/C16:0) were used to compare the ionization behaviour and fragmentation patterns of different astaxanthin ionization states. MALDI-TOF-MS spectra of untreated Ast C16:0 and Ast C16:0/C16:0 spots showed four types of ionization: radical ion $[M]^{\bullet+}$, protonated $[M+H]^+$, sodiated $[M+Na]^+$ and potassiated $[M+K]^+$ ions (**Figures 3A** and **B**). The distribution of the total signal over four different ionization types was unfavourable, because fewer ions per type were available for fragmentation and more complex spectra were obtained. Especially for Ast C16:0/C16:0, the $[M]^{\bullet+}/[M+H]^+$ signal was low compared to that of the salted ionization states.

In order to enhance the limit of detection, different strategies might be employed. First, $[M+Na]^+$ and $[M+K]^+$ ions might be suppressed at the ion gate of the MALDI (15), but in the case of astaxanthin esters this would lead to a major signal loss because of the prevalence to form $[M+Na]^+$ and $[M+K]^+$ ions. Physical removal of salt ions using an ion-exchange resin, like Dowex, was a second option (**Figures 3C** and **D**) and prevented the formation of $[M+Na]^+$ and $[M+K]^+$ ions. The disadvantage of these approaches is that they favoured the $[M]^{\bullet+}$ and $[M+H]^+$ ions, which might lead to complicated MS² spectra. The third option was to convert all astaxanthin ions to a single salt adduct by addition of sodium acetate (NaOAc) to the DHB matrix (**Figures 3E** and **F**), with the possible advantage of obtaining less complex parent mass and MS² spectra.

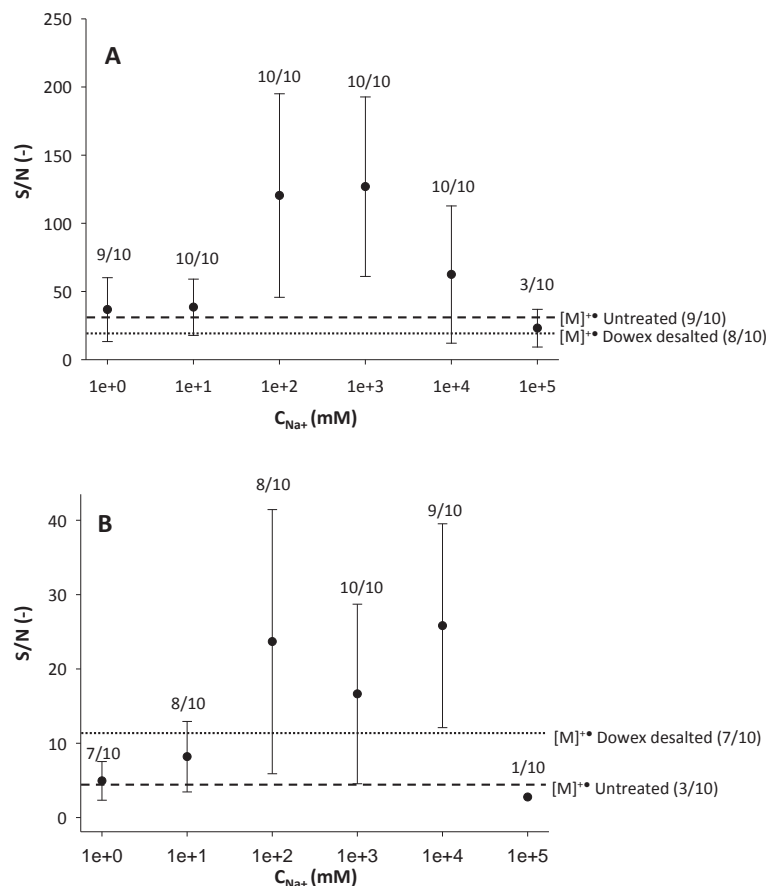


Figure 4. Effect of increasing NaOAc concentrations on signal to noise (S/N) ratios of $[M+Na]^+$ adducts ($n = 10$ per salt concentration) for **A** Ast C16:0 and **B** Ast C16:0/C16:0. Numbers above the data points express the success rate of finding a measurement with signal threshold $S/N > 3$. The horizontal dashed lines represent the average S/N ($n = 10$) of untreated $[M]^+$ ions and (Dowex) desalted $[M]^+$ ions.

To make a quantitative decision on which of the approaches described above would give highest signal to noise (S/N) ratios, series of ten spots of either desalted samples or samples to which different amounts of NaOAc were added, were compared to each other (**Figure 4**). For the desalted Ast C16:0 spots, the overall $[M]^+$ signal to noise (S/N) ratio decreased compared to the untreated $[M]^+$ S/N (**Figure 4A**) and 8 out of 10 spots gave signals above the minimum threshold ($S/N = 3$). For $[M+Na]^+$ ions, the S/N ratios were drastically increased with an optimum between 0.1 – 1.0 mM sodium ions and all spots were above the minimum threshold value. Higher concentrations of sodium resulted in a collapse of S/N ratios and for 100 mM sodium

only 3 out of 10 spots were above the minimum threshold. Although addition of sodium increased S/N ratios, the standard deviation between measurements also increased. This might be explained by the formation of hot spots in the crystallized matrix due to the presence of salt. Therefore, one should be cautious with using this approach when quantification is important.

For the Ast C16:0/C16:0 standard, a similar trend was observed, although less clear and with lower S/N ratios (**Figure 4B**) than for the Ast C16:0 standard. Although the $[M]^+\bullet$ S/N and success rate of Ast C16:0/C16:0 improved after desalting, the use of the ion-exchange resin in dichloromethane/hexane resulted in several interfering peaks in the m/z 550-800 region (results not shown), which was undesirable.

MALDI-TOF/TOF-MS fragmentation of $[M]^+\bullet$ / $[M+H]^+$ and $[M+Na]^+$

As described above, sodiated astaxanthin ester ions gave more simple fragmentation patterns in ESI-IT-MS than their respective protonated ions. To investigate if this was also the case for MALDI-TOF/TOF-MS and whether unambiguous identification of the astaxanthin ester structure using only TOF fragmentation was possible, full fragmentation spectra of Ast C16:0 $[M]^+\bullet$ / $[M+H]^+$ and $[M+Na]^+$ ions were recorded (**Figure 5**) and fragment structures were assigned (**Figure 2**).

The fragmentation pattern of the sodiated adduct of Ast C16:0 upon TOF fragmentation showed similar behaviour compared to ESI-IT-MS fragmentation and showed less extensive degradation compared to the MALDI $[M]^+\bullet$ / $[M+H]^+$ parents (**Figure 2B**). Toluene $[M+Na-92]^+$ (**I**) and xylene $[M+Na-106]^+$ (**II**) losses found at m/z 765.5 and 751.4 were most abundant. The signal intensity of xylene eliminations were around 10 to 20% of that of the toluene loss. Fragment **V** (m/z 601.3) indicated the loss of C16:0 and showed the molecular mass of astaxanthin without the β -ring hydroxyl group. Based on literature data (25) on fragmentation of diosphenol acetate endgroups in carotenoids, the formation of fragment **VIII** (m/z 465.2) could be explained by the rearrangement of electrons from the C5-C6 and C18 double bond in the β end group to form a stabilized benzonium ion, closing at C18 to C9 (inset **Figure 5B**). The remainder of the carotenoid was eliminated at the C9-C10 position. The esterified fatty acid was still attached to the β end group of the benzonium ion (similar as with an acetate group (26)). A similar fragmentation principle was observed with Ast C16:0/C16:0 $[M+Na]^+$. As expected, a fragment of astaxanthin with one of the two C16:0 fatty acids still esterified was found at m/z 839.5 (**III**). Remarkably, the loss of both fatty acids (in ESI-IT-MS this fragment had an average m/z of 583.6) was not observed. Instead, similar to Ast C16:0, fragment **VIII** at m/z 465.2 was found. Although other fragmentation pathways might be proposed, most probably a tandem fragmentation of the first C16:0 resulting in m/z 839.5 and subsequent formation of the benzonium ion and elimination at C9-C10 position occurred.

For Ast C16:0 $[M]^+\bullet$ and $[M+H]^+$, fragmentation was carried out on a mixed population, because attempts to individually fragment both ionization states resulted in loss of parent ion signal. The $[M]^+\bullet/[M+H]^+$ fragmentation pattern (**Figure 5A**) showed a multitude of daughter ions, which could be assigned to structures originating from both ionization types. Furthermore, only a small part of these fragments had diagnostic value. The $[M-92]^+\bullet$ (**I**) was relatively low in intensity and could be assigned to fragmentation of the $[M]^+\bullet$ ion. The $[M-106]^+\bullet$ was not observed and, therefore, assignment of a polyene moiety was not conclusive. Fragmentation of single fatty acid losses with m/z 579.3 could be assigned for both $[M-C16:0]^+\bullet$ and $[M+H-C16:0]^+$ (**V**). Furthermore, the fatty acid loss of C16:0 in the ketene form at m/z 597.3 could also be assigned to both $[M]^+\bullet$ and $[M+H]^+$ ionization states (**VI**). The main peak at m/z 550.3 could be assigned to fragment **VII**, formed from fragment **V** by ring-opening, similar to the previously reported β -ring opening of free carotenoids (26). The proposed fragments might have been observed earlier, but were not annotated for TOF or ESI-IT-MS fragmentation (7, 15). In the lower m/z 100 to 400 region, a multitude of fragments possibly originating from polyene tail fragmentations and fatty acids were found. Except for fragment m/z 201.1 (inset **Figure 5A**), the main fragments at m/z

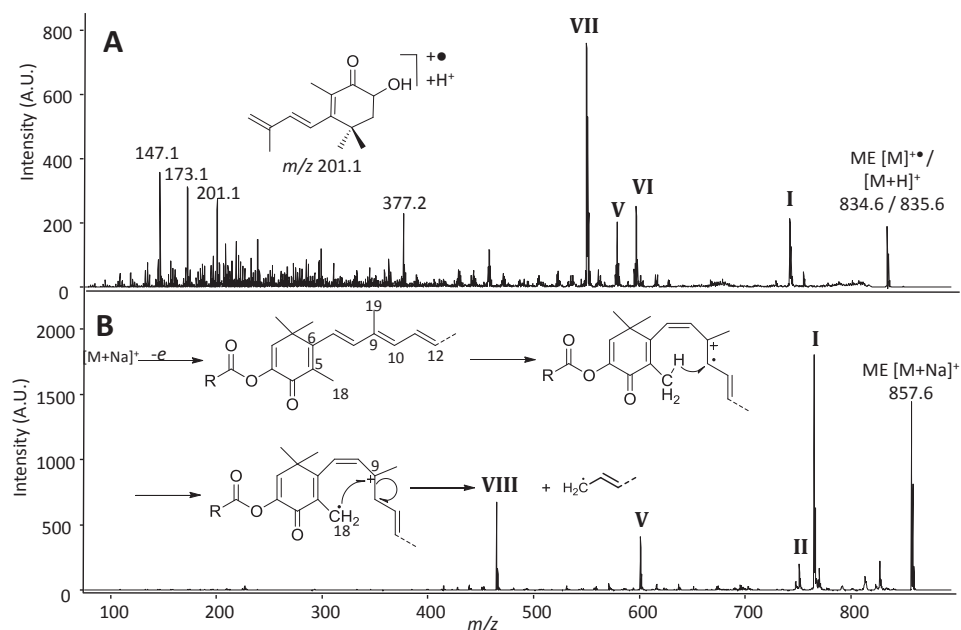


Figure 5. MALDI-TOF/TOF-MS fragmentation spectra of Ast C16:0 for **A** $[M]^+\bullet/[M+H]^+$ and **B** $[M+Na]^+$. Roman numbers refer to structures in **Figure 2**.

377.2, 173.1 and 147.1 could not be related to Ast C16:0 in a logical way without considering major rearrangements as was proposed above for the benzonium fragment **VIII** upon fragmentation of $[M+Na]^+$.

For Ast C16:0/C16:0 $[M]^{\bullet}$ and $[M+H]^+$ (**Figure 2A**), a similar fragmentation pattern was found with neutral loss of toluene (**I**), fatty acid loss (**III**) and fatty acid loss in the ketene form (**IX**). Also in this case, the main fragment (m/z 788.5) was formed by β -ring opening (**X**). This fragment was probably formed in a similar way as fragment **VII**. In the lower m/z region, again a fragment with m/z 201.1 was found, as well as other lower fragments with m/z values identical as found for Ast C16:0.

Overall, sodiated fragmentation patterns were similar for TOF and ESI-IT-MS fragmentation and were less complex compared to $[M]^{\bullet}$ / $[M+H]^+$ fragmentation. This might be due to the freedom of movement of the radical or proton in the polyene chain. The latter resulted in numerous intra-molecular rearrangements. Although one might argue that these small fragments have diagnostic value for the presence of a polyene moiety, it is evident that correct annotation of peaks in mass spectra will be difficult when analysing complex mixtures of xanthophyll esters. Similar types of rearrangements might also be proposed when fragmenting $[M+Na]^+$ ions in TOF fragmentation, but apparently the number of sites for sodium attachment are limited. This makes $[M+Na]^+$ TOF fragmentation a very useful tool for unambiguous determination of astaxanthin esters. Along with restricted fragmentation, the second advantage of sodiated fragmentation is the higher sensitivity (higher S/N ratios), which was observed previously in LC-MS experiments (11, 19).

Sodiated MALDI-TOF/TOF-MS characterization of *H. pluvialis* astaxanthin esters

To verify that addition of NaOAc and the fragmentation of sodium adducts was also effective in analysis of complex astaxanthin ester mixtures found in nature, MALDI-TOF/TOF-MS analysis of a crude *H. pluvialis* extract, as well as of pools enriched in astaxanthin monoesters and diesters, was performed.

Crude *H. pluvialis* extract analysis

Assuming that all astaxanthin esters are in the sodiated state with 1 mM NaOAc, analysis windows were chosen from m/z 830 to 950 (C16:0 to C20:*n*) for monoesters and from m/z 1080 to 1200 (C16:0/C16:0 to C20:*n*/C20:*n*) for diesters, in accordance with fatty acid esterified carotenoids found during LC-MS analysis (**Table 2**). Both monoesters (**Figure 6A**) and diesters (not shown) could be visualized by the sodiated parent masses. However, the main ion found in the monoester m/z region was identified as pheophytin *a* as confirmed with TOF fragmentation (**Figure 6A**). Pheophytin *a* was not ionized in the $[M+Na]^+$ from, but remained in $[M]^{\bullet}$ / $[M+H]^+$ form as also was observed in ESI-MS (**Figure 1** and **Table 1**). Unambiguous

identification of astaxanthin monoesters by TOF fragmentation was challenging, because the monoesters were present in the regions flanking m/z 871 (m/z 857 to 885). Even at the smallest possible mass gate range, fragment ions of pheophytin *a* overruled astaxanthin ester signals. For astaxanthin diesters, the measurement was particularly difficult, because of their low abundance and diversity in the extract.

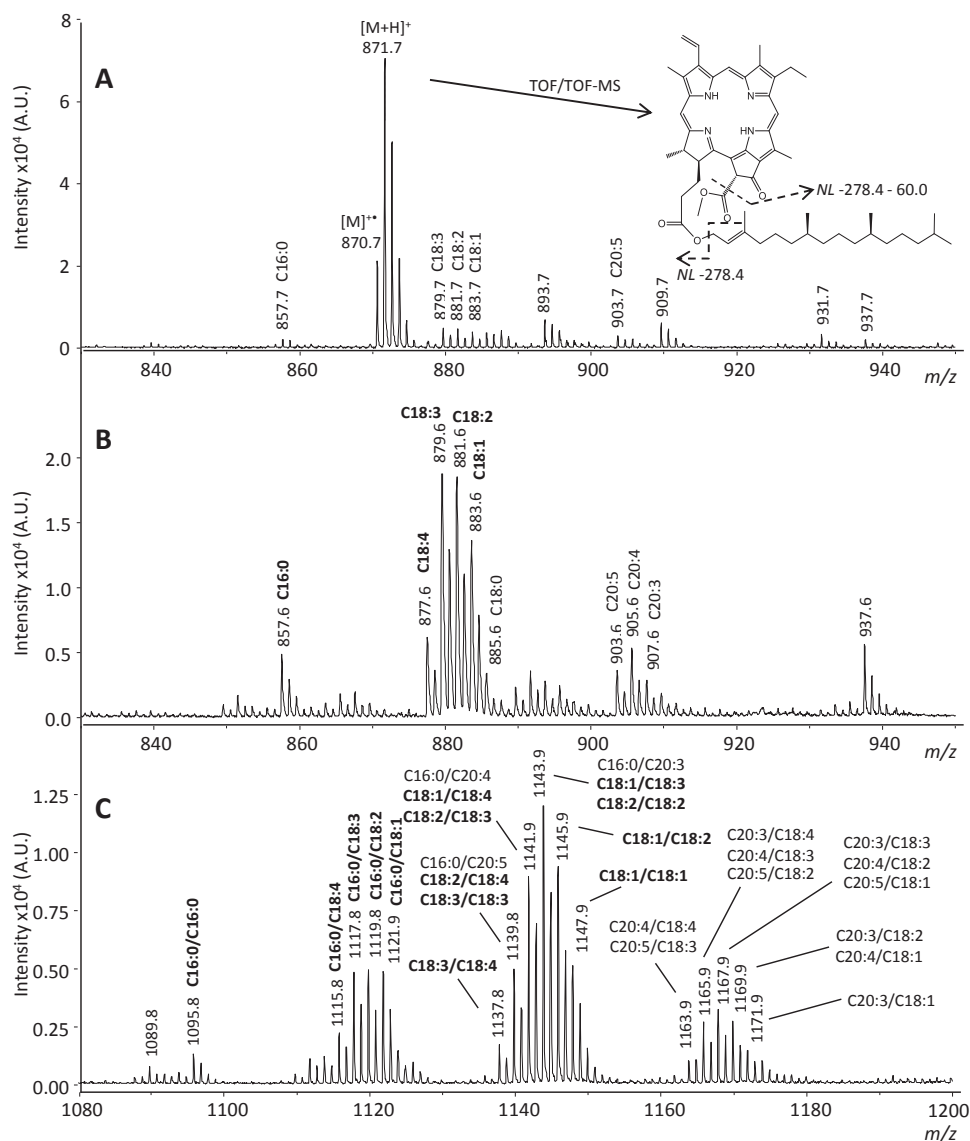


Figure 6. Description see pp. 48.

Figure 6 (pp. 47). MALDI-TOF-MS spectra using 1 mM NaOAc. **A** Monoester region of crude *H. pluvialis* extract with schematic pheophytin *a* fragmentation. **B** NP-Flash enriched astaxanthin monoester pool. **C** NP-Flash enriched astaxanthin diester pool. Astaxanthin esters are annotated with the (combination of) fatty acids concerned. Annotations displayed in bold were unambiguously identified by fragmentation of the respective parent masses.

Monoester analysis

To facilitate recording TOF fragmentation spectra, NP-Flash chromatography was used for removal of pheophytin *a* in the monoester region and for enrichment of the diesters. In **Figure 6B** an astaxanthin monoester pool, consisting of chromatographic peaks 8 to 29 (**Figure 1**), was analysed. Clearly, removal of pheophytin *a* was effective for amplification of the astaxanthin ester signal. Considering the fatty acids to be esterified to astaxanthin, as measured by ESI-MS, the main parent masses that were expected were astaxanthin esterified to C16:0, C18:1 to C18:4 and C20:3 to C20:5, along with their respective isotopes. These main parent masses were indeed found as sodiated parent masses. Also, other possible higher fatty acids (for example m/z 937.6) were observed, but these were not elaborated further.

To unambiguously prove the structure of the esters, a quartet of C18:4 to C18:1 $[M+Na]^+$ ions were simultaneously TOF fragmented (**Figure 7A**). Fragments still containing fatty acids were observed as signals with similar intensities as observed with the $[M+Na]^+$ parent group. Similar to sodiated C16:0 monoester fragmentation, the loss of toluene (**I**) and xylene (**II**) was observed. Since no other singlet peaks were observed than the one at m/z 601.3 (**V**), the latter unambiguously proved the presence of astaxanthin as the only carotenoid. The quartet of peaks at m/z 485.2 to 491.3, were assigned to fragment **VIII**. The peak at m/z 698.9 could not be explained and was not observed with astaxanthin C16:0 standard fragmentation. Indications for the presence of a C18:0 monoester were found by two small diagnostic peaks at m/z 793.9 (**I**) and 779.7 (**II**), although no clear parent mass was observed. The monoester C16:0 was annotated similarly as described in **Figure 5B**. Similarly, the other monoester groups in **Figure 6B** were fragmented. Astaxanthin monoesters with a C20:*n* fatty acid had a TOF fragmentation spectrum containing **I** and **II**, but fragments **V** and **VIII** were not detected. This was due to interfering fragments in the m/z 878.0 to 883.0 region, which might be caused by a contaminating compound (results not shown).

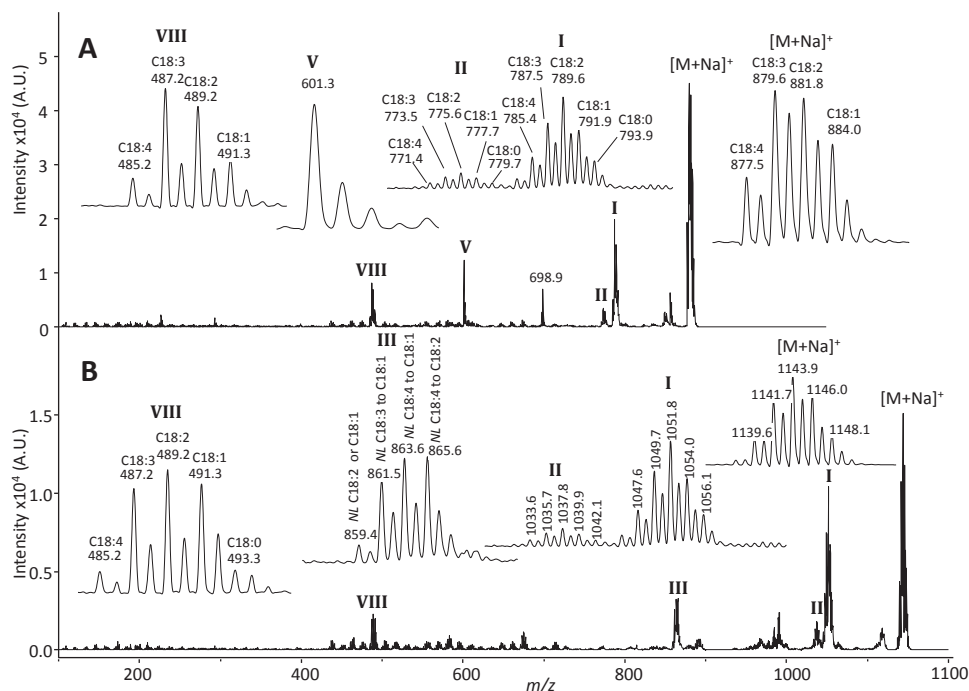


Figure 7. MALDI-TOF/TOF-MS fragmentation of groups of astaxanthin esters using 1 mM NaOAc. **A** Fragmentation spectrum of astaxanthin C18:1, C18:2, C18:3 and C18:4. **B** Fragmentation spectrum of astaxanthin C18:n/C18:n group. Roman character-annotated peaks refer to structures in **Figure 2**.

Diester analysis

Identification of the fatty acids attached to diesters was possible in a similar way, but more complicated, as numerous assignments could be given to individual parent masses (**Figure 6C**). Assuming that the fatty acids attached to diesters are similar as to those present in the monoesters, a theoretical number of 6 groups of peaks should be observed: C16:0/C16:0, C16:0/C18:n, C16:0/C20:n, C18:n/C18:n, C18:n/C20:n and C20:n/C20:n (C18:n, $n = 1$ to 4; C20:n, $n = 3$ to 5). In the MALDI-TOF-MS spectrum shown, four distinct groups were observed, the C16:0/C20:n and C18:n/C18:n group were overlapping. Furthermore, the C20:n/C20:n group in the m/z 1187 to 1195 region was present, but in negligible quantities compared to the other diesters as expected from LC-MS analysis.

Similar to fragmentation of monoesters, a quintet of C18:n/C18:n and C16:0/C20:n parents was TOF fragmented and resulted in four diagnostic fragment groups for identification (**Figure 7B**). The presence of a polyene tail was shown by fragment groups **I** and **II** and could be related to the parent masses directly. The group representing structure **III** was important to demonstrate which fatty acids were split

from the quintet of parent masses. In this case strong proof was found for losses of C18:1 to C18:4 fatty acids. Negligible signals were found for losses of C16:0 and C20:*n* fatty acids in the flanking regions of group **III**. As could be expected from our LC analysis, the amounts of astaxanthin decorated with a combination of C16:0 and C20:*n* fatty acids were low.

Although it was clear that fragment group **III** represented several daughter ions which underwent C18:*n* fatty acid fragmentation, it was unclear to which parent these daughters belonged. For the sake of clarity, the annotation of parent mass *m/z* 1141.7 is illustrated in Figure 8 as an example. Three combinations of C18 fatty acids were possible in order to obtain *m/z* 1141.7. Both fatty acids attached to astaxanthin should have a corresponding fragment ion in group **III**, where the neutral loss is represented by one of the fatty acids. No neutral losses corresponding to C18:5 and C18:0 were observed, ruling out the option of Ast C18:5/C18:0. Fatty acid losses of C18:1 to C18:4 were found, showing that the other two options displayed in Figure 8 indeed occurred. In order to confirm the other fatty acids of the Ast C18:3/C18:2 and Ast C18:4/C18:1, the benzonium fragments (**VIII**) were required. In the case of diesters, group **VIII** always had a neutral loss of 375 Da compared to group **III**. This neutral loss was 17 Da less than for monoester **VIII** fragments and could be explained by the loss of one OH group upon fragmentation of the first fatty acid of the diester. For both Ast C18:3/C18:2 and Ast C18:4/C18:1, the fragments in group **III** had a corresponding fragment in group **VIII**, confirming that both compounds were present. Similarly, groups of C16:0/C16:0 and C16:0/C18:*n* diesters were successfully identified.

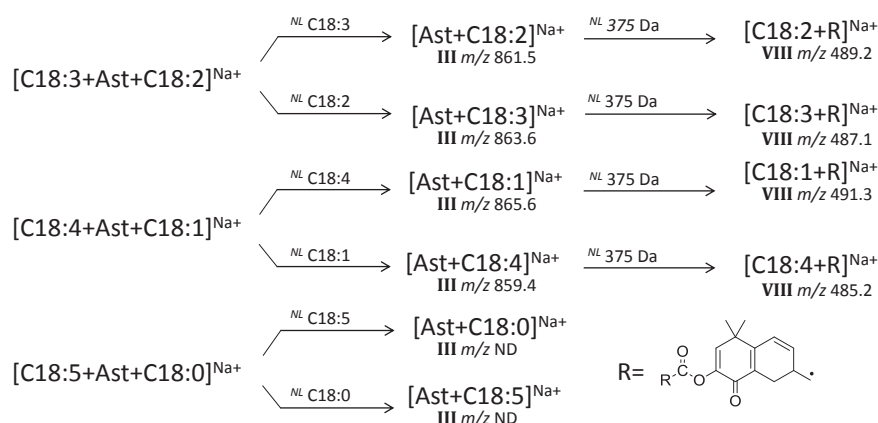


Figure 8. Example of step-by-step identification of astaxanthin diesters, associated to parent mass *m/z* 1141.7 from **Figure 7B**. Roman numbers refer to **Figure 2**.

CONCLUDING REMARKS

MALDI-TOF/TOF-MS was superior in rapid fingerprinting of complex astaxanthin ester mixtures over LC-MS and showed excellent accuracy in mass spectrometric data. Only few minor monoesters, which were found in LC analysis (C16:4 and C16:2), were not found upon MALDI-TOF/TOF-MS analysis. The advantage of simultaneous fragmentation of groups of similar astaxanthins in the sodiated form gave clearly grouped fragments, which were diagnostic for the structure of the astaxanthin esters.

ACKNOWLEDGEMENTS

This work was supported by FeyeCon D&I and by grants from NL Agency and the Ministry of Education, Culture and Science (Project no.FND09014).

REFERENCES

1. Rao, A. R.; Sarada, R.; Ravishankar, G. A., Stabilization of astaxanthin in edible oils and its use as an antioxidant. *Journal of the science of food and agriculture* **2007**, *87*, 957-965.
2. Miao, F.; Lu, D.; Li, Y.; Zeng, M., Characterization of astaxanthin esters in *Haematococcus pluvialis* by liquid chromatography-atmospheric pressure chemical ionization mass spectrometry. *Analytical biochemistry* **2006**, *352*, 176-181.
3. Plaza, M.; Herrero, M.; Cifuentes, A.; Ibanez, E., Innovative natural functional ingredients from microalgae. *Journal of agricultural and food chemistry* **2009**, *57*, 7159-7170.
4. Cysewski, R. T. L. G. R., Commercial potential for *Haematococcus* microalgae as a natural source of astaxanthin. *Trends in biotechnology* **2000**, *18*, 160-167.
5. Chandi, G. K.; Gill, B. S., Production and characterization of microbial carotenoids as an alternative to synthetic colors: a review. *International journal of food properties* **2011**, *14*, 503-513.
6. Pérez-Gálvez, A.; Mínguez-Mosquera, M. I., Esterification of xanthophylls and its effect on chemical behavior and bioavailability of carotenoids in the human. *Nutrition research* **2005**, *25*, 631-640.
7. Frassanito, R.; Cantonati, M.; Flaim, G.; Mancini, I.; Guella, G., A new method for the identification and the structural characterisation of carotenoid esters in freshwater microorganisms by liquid chromatography/electrospray ionisation tandem mass spectrometry. *Rapid communications in mass spectrometry* **2008**, *22*, 3531-3539.
8. Britton, G., Chapter 2: UV/Visible spectroscopy. In: *Carotenoids Vol. 1B Spectroscopy*, Edited by Britton G., Liaaen-Jensen S., Pfander H., Birkhäuser Verlag, Basel, Switzerland **1995**, pp. 13-62.
9. Rezanka, T.; Olsovska, J.; Sobotka, M.; Sigler, K., The use of APCI-MS with HPLC and other separation techniques for identification of carotenoids and related compounds. *Current analytical chemistry* **2009**, *5*, 1-25.
10. Rivera, S. M.; Canela-Garayoa, R., Analytical tools for the analysis of carotenoids in diverse materials. *Journal of chromatography A* **2012**, *1224*, 1-10.
11. Weller, P.; Breithaupt, D. E., Identification and quantification of zeaxanthin esters in plants using liquid chromatography-mass spectrometry. *Journal of agriculture and food chemistry* **2003**, *51*, 7044-7049.

12. Chauveau-Duriot, B.; Doreau, M.; Noziere, P.; Graulet, B., Simultaneous quantification of carotenoids, retinol, and tocopherols in forages, bovine plasma, and milk: validation of a novel UPLC method. *Analytical and bioanalytical chemistry* **2010**, *397*, 777-790.
13. Fraser, P. D.; Enfissi, E. M.; Goodfellow, M.; Eguchi, T.; Bramley, P. M., Metabolite profiling of plant carotenoids using the matrix-assisted laser desorption ionization time-of-flight mass spectrometry. *The plant journal* **2007**, *49*, 552-564.
14. Yoshida, K.; Ueda, S.; Maeda, I., Carotenoid production in *Bacillus subtilis* achieved by metabolic engineering. *Biotechnology letters* **2009**, *31*, 1789-1793.
15. Wingerath, T.; Kirsch, D.; Kaufmann, R.; Stahl, W.; Sies, H., Fruit juice carotenol fatty acid esters and carotenoids as identified by matrix assisted laser desorption ionization (MALDI) mass spectrometry. *Journal of agriculture and food chemistry* **1996**, *44*, 2006-2013.
16. Kaufmann, R.; Wingerath, T.; Kirsch, D.; Stahl, W.; Sies, H., Analysis of carotenoids and carotenol fatty acid esters by matrix-assisted laser desorption ionization (MALDI) and MALDI-post-source-decay mass spectrometry. *Analytical biochemistry* **1996**, *238*, 117-128.
17. Guaratini, T.; Lopes, N. P.; Pinto, E.; Colepiccolo, P.; Gates, P. J., Mechanism for the elimination of aromatic molecules from polyenes in tandem mass spectrometry. *Chemical communications* **2006**, 4110-4112.
18. Li, H.; Tyndale, S. T.; Heath, D. D.; Letcher, R. J., Determination of carotenoids and all-*trans*-retinol in fish eggs by liquid chromatography-electrospray ionization-tandem mass spectrometry. *Journal of chromatography B* **2005**, *816*, 49-56.
19. Airs, R. L.; Llewellyn, C. A., Improved detection and characterization of fucoxanthin-type carotenoids: novel pigments in *Emiliana huxleyi* (Prymnesiophyceae). *Journal of phycology* **2006**, *42*, 391-399.
20. Schüep, W.; Schierle, J., Example 9: Determination of stabilized, added astaxanthin in fish feeds and pre-mixes. In: *Carotenoids Vol. 1A Isolation and analysis*, Edited by Britton G., Liaaen-Jensen S., Pfander H., Birkhäuser Verlag, Basel, Switzerland **1995**, pp. 273-276.
21. Holtin, K.; Kuehnle, M.; Rehbein, J.; Schuler, P.; Nicholson, G.; Albert, K., Determination of astaxanthin and astaxanthin esters in the microalgae *Haematococcus pluvialis* by LC-(APCI)MS and characterization of predominant carotenoid isomers by NMR spectroscopy. *Analytical and bioanalytical chemistry* **2009**, *395*, 1613-1622.
22. Egeland, E. S., Part VII: Data sheets aiding identification of phytoplankton carotenoids and chlorophylls. In: *Phytoplankton pigments: characterization, chemotaxonomy, and applications in oceanography*. Roy, S., Llewellyn C.A., Egeland, E.S., Johnsen, G. Cambridge University Press, New York, NY, USA **2011**, pp. 665-822
23. Britton, G.; Liaaen-Jensen, S.; Pfander, S., Carotenoids Handbook. Birkhäuser Verlag, Basel, Switzerland **2004**.
24. Walker, J. S.; Jie, C.; Keely, B. J., Identification of diastereomeric chlorophyll allomers by atmospheric pressure chemical ionisation liquid chromatography/tandem mass spectrometry. *Rapid communications in mass spectrometry* **2003**, *17*, 1125-1131.
25. Baldas, J.; Porter, Q. N.; Leftwick, A. P.; Holzel, R.; Weedon, B. C. L.; Szabolcs, J., Mass spectrometry of carotenoid ketones. *Journal of the chemical Society D* **1969**, 415-416.
26. Enzell, C. R.; Back, S., Chapter 7: Mass spectrometry. In: *Carotenoids Vol. 1B Spectroscopy*, Edited by Britton G., Liaaen-Jensen S., Pfander H., Birkhäuser Verlag, Basel, Switzerland **1995**, pp. 261-320.

Nitrogen-depleted *Chlorella zofingiensis* produces astaxanthin, ketolutein and their fatty acid esters: a carotenoid metabolism study

Natural carotenoids such as astaxanthin, β,β -carotene and lutein are pigments with a high market value. We studied the effects of nitrogen depletion on the carotenoid metabolism of *Chlorella zofingiensis* (Chlorophyta) and the subsequent treatment with diphenylamine (DPA), an inhibitor of the biosynthesis of secondary ketocarotenoids. Pigments were identified and quantified based on reversed phase ultra-high performance liquid chromatography photo diode array tandem mass spectrometry (RP-UHPLC-PDA-MSⁿ). Nitrogen depletion (without DPA) resulted in a degradation of chlorophylls and primary carotenoids and an accumulation of astaxanthin, ketolutein, canthaxanthin, adonixanthin, and β,β -carotene. The DPA treatment decreased the overall production of β,β -carotene derivatives (sum of astaxanthin, canthaxanthin, echinenone and adonixanthin), however, the production of ketolutein and degradation of primary carotenoids were not modified. This suggests that the regulatory mechanisms controlling the flux towards ketolutein and primary carotenoids were not affected by the decreased levels of β,β -carotene derivatives. In addition, DPA increased production of the individual carotenoids adonixanthin and echinenone. Insight into the regulation of microalgal carotenoid biosynthesis as demonstrated in this paper is essential when a large-scale carotenoid production process is to be optimized or a recombinant *C. zofingiensis* strain is to be designed with the intention of excessively producing primary or secondary carotenoids.

Based on: Mulders, K.J.M., Weesepeel, Y., Bodenes, P., Lamers, P.P., Vincken, J.-P., Martens, D.E., Gruppen, H., Wijffels, R.H., Nitrogen-depleted *Chlorella zofingiensis* produces astaxanthin, ketolutein and their fatty acid esters: a carotenoid metabolism study. *Accepted for publication in Journal of applied phycology*, DOI 10.1007/s10811-014-0333-3

INTRODUCTION

Natural carotenoids such as astaxanthin, β,β -carotene and lutein are pigments with a high market value. It has been claimed that these carotenoids beneficially affect health due to their anti-oxidative activity (1). Possible production organisms of naturally derived carotenoids that have gained significant attention are microalgae, because they contain an extensive number of various carotenoids, part of which can be produced in concentrations exceeding those ascertained in higher plants by one or more orders of magnitude. Nevertheless, economically feasible microalgal carotenoid production will require process and/or strain optimization (2).

Microalgal carotenoids can be categorized into primary and secondary carotenoids. Primary carotenoids are functionally bound to the photosystems inside the chloroplast, whereas secondary carotenoids are not bound to the photosystems. An even more significant difference is their concentration under various growth conditions. Under prolonged limited-light growth conditions, secondary carotenoids are generally absent or present only in extremely low concentrations, and primary carotenoids are generally present in their maximal concentration (typically, below 0.5 % $dw(w/w)$) (2). Under adverse growth conditions (referred to as 'stress' conditions), primary carotenoids are generally degraded and, in certain green algae, secondary carotenoids are produced in excessive amounts (up to 10 % $dw(w/w)$) (3). As a consequence of these different responses, overproduction of the primary and secondary carotenoids requires different approaches. Secondary carotenoid overproduction necessitates optimization of the process (stress) conditions, which may be enhanced by additional genetic engineering. Although subsaturating light conditions result in minor increases in primary pigment concentrations, actual overproduction of primary carotenoids requires modification of the carotenoid biosynthesis routes, *i.e.* with genetic engineering (2). Both approaches share that insight into pigment metabolic regulation is crucial.

Chlorella zofingiensis is one of the most important carotenogenic green algae in relationship to biotechnological applications (4). In this species, lycopene, which can be converted into β,ϵ -carotene (α -carotene) or β,β -carotene (**Figure 1**), is the precursor of all primary and secondary carotenoids. Hydroxylation of α -carotene yields lutein, the most abundant primary carotenoid of *C. zofingiensis* (5). Hydroxylation of β,β -carotene provides zeaxanthin, which can be epoxidised twice, resulting in violaxanthin which can then be isomerised, leading to neoxanthin. Under adverse growth conditions, *C. zofingiensis* can accumulate multiple secondary carotenoids including astaxanthin, canthaxanthin, and adonixanthin (6, 7). Presumably, β,β -carotene is transferred first to the cytosol where it is subsequently converted into astaxanthin (**Figure 1**). This conversion requires two oxygenation and two hydroxylation reactions. Oxygenations are catalysed by β,β -carotene ketolase

(BKT), and hydroxylations are catalysed by a β,β -carotene hydroxylase (CHYb). Esterification of astaxanthin results in monoesters and diesters which appear to accumulate in triacylglyceride (TAG) oil bodies (**Figure 1**) (4). It has been postulated that, in *C. zoofingensis*, zeaxanthin can also be a precursor of astaxanthin through conversion into adonixanthin (**Figure 1**). However, this pathway has not yet been fully resolved (8, 9). Furthermore, the accumulation of canthaxanthin in a relatively high concentration has led to the speculation that this carotenoid is an end product rather than a precursor of astaxanthin (8). This speculation requires further confirmation. Finally, it was recently reported that BKT converts the primary carotenoid lutein into the secondary carotenoid ketolutein under adverse growth conditions (10). As this ascertainment is contradictory with all other available literature, this requires confirmation. Thus, whereas primary carotenoid biosynthesis pathways in *C. zoofingensis* are thoroughly investigated, those for secondary carotenoids require further elucidation. Furthermore, the metabolic regulation of primary and secondary carotenoid biosynthesis is extensively under-investigated which is, as stated, of utmost importance when designing a metabolically engineered carotenoid production strain or optimizing a large-scale carotenoid production process. The aim of this paper was to obtain additional insight into the pathways and regulation of carotenoid metabolism of *C. zoofingensis*.

This was accomplished by depleting *C. zoofingensis* of nitrogen, which effectively induces secondary carotenogenesis, and subsequently adding diphenylamine (DPA), an inhibitor of BKT (9, 11, 12). Since BKT catalyses multiple secondary carotenoid conversions (**Figure 1**), inhibition was expected to lead to insight into the pathway of astaxanthin biosynthesis as it did, for example, in the green alga *Haematococcus pluvialis* (11-14). Additionally, as primary and secondary carotenoids of *C. zoofingensis* possess a common metabolic precursor, and BKT catalyses the first step of secondary carotenogenesis, inhibition with DPA was expected to alter the primary pigment metabolism (*e.g.* lutein biosynthesis) and reveal insights in carotenoid metabolic regulation. To ensure that the entire collection of carotenoids of *C. zoofingensis* would be revealed, carotenoids were identified employing reversed phase liquid chromatography and additional mass spectrometry.

MATERIALS AND METHODS

Materials

(3*RS*)-Adonirubin (95%), (3*S*,3'*R*)-adonixanthin (99%), (3*RS*,3'*RS*)-astaxanthin (97%), (3*RS*,3'*RS*)-astaxanthin monopalmitate (97%), (3*RS*,3'*RS*)-astaxanthin dipalmitate (98%), canthaxanthin (98%), echinenone (98%), (*rac.*)-3-hydroxyechinenone (97%), lutein (96%) and (3*R*,3'*R*)-zeaxanthin (97%) (all *w/w*) were purchased from CaroteNature (Lupsingen, Switzerland). Violaxanthin (98%), lycopene (92%),

cryptoxanthin (β -cryptoxanthin) (98%), antheraxanthin (97%), α -cryptoxanthin (98%), and β,ϵ -carotene (α -carotene) (88%) (all w/w) were purchased in approximately 1 mg mL⁻¹ ethanol or acetone solutions from DHI laboratory products (Hørsholm, Denmark). Chlorophyll *a* (90.0% w/w) was purchased from Wako Pure Chemical Industries (Osaka, Japan). Methanol (99.8%), acetonitrile (99.97%), ethyl acetate (99.9%) and chloroform (stabilized with 0.5-1.5% (w/v) ethanol, purity after correction for stabilizer 99.9%) were obtained from Biosolve (Valkenswaard, the Netherlands). Dichloromethane (99.8%), acetone (99.8%), n-hexane (98%), formic acid (98.0%), sodium chloride (99.0% w/w), β,β -carotene (97% w/w) and butylated hydroxytoluene (BHT) (99% w/w) were obtained from Sigma-Aldrich (St. Louis, MO, USA). Demineralized water was prepared using a Milli-Q water purification system (Millipore, Billerica, MA, USA).

Cultivation

Chlorella zofingiensis UTEX B32, recently suggested to be renamed to *Chromochloris zofingiensis* (Fucíková and Lewis, 2012), was obtained from the University of Texas Culture Collection of Algae (UTEX) and cultivated in (replete) modified M-8 medium (**Table 1**) (modified from Mandalam and Palsson 1998). Nitrogen-depleted medium was similarly prepared with the exception that KNO₃ was substituted with KCl (at a concentration of 29.67 mM) to retain a total osmolarity of 0.323 Osm. It was assumed that the organic pH buffer Hepes, which contains two nitrogen atoms, was not consumed by *C. zofingiensis*.

Cultures were pre-cultivated in 250-mL shake flasks containing 100 mL (replete) medium that were situated in a culture chamber at 28 °C in continuous light emanating from white fluorescent tubes with a light intensity of 231-255 $\mu\text{mol photons m}^{-2} \text{s}^{-1}$ and continuously shaken at 100 rpm with a head space containing an air/CO₂ ratio of 95/5% (v/v).

To achieve nitrogen starvation, cells were washed with a nitrogen-depleted medium. Washing was performed by centrifugation of cells at 700 rpm (94×g) for 10 min and subsequent resuspension of cell pellet in 25 mL of nitrogen-depleted medium. Following two washing occurrences, cells were inoculated in 250-mL shake flasks containing 150 mL of nitrogen-depleted medium at a dry weight cell concentration of 1.7 g L⁻¹. Cells were placed into a culture chamber in the same conditions as described for the pre-cultivation. Every two days, beginning at day zero, a sample was taken for cell dry weight measurements and pigment extraction and quantification. Due to increasing biomass concentrations, sample volumes decreased over time. The extracted sample volumes were: 16 mL, 10 mL, 10 mL, 7 mL, 5.5 mL, 5.5 mL, 5.5 mL, 5.5 mL (at day 0, 2, 4, 6, 8, 10, 12 and 14, respectively). A 10 mM DPA stock solution (in DMSO) was prepared and retained in the dark to prevent DPA degradation. Beginning in day two, 1 mL DPA stock solution was added to each culture

immediately following sampling. This resulted in concentration increases of 60 μM DPA for the DPA treated cultures. To the control cultures, only 1 mL of DMSO (without DPA) was added.

To obtain nitrogen-replete and nitrogen-depleted *C. zofingiensis* cells for Freeze Fracture Scanning Electron Micrographs, *C. zofingiensis* cells were pre-cultured in a shake flask under a low incident light intensity ($20 \mu\text{mol photons m}^{-2} \text{s}^{-1}$) and diluted 10 times in nitrogen-depleted medium to achieve a concentration of $\sim 0.3 \text{ g/L}$. This shake flask, containing a volume of 110 mL, was incubated under a low incident light intensity ($20 \mu\text{mol photons m}^{-2} \text{s}^{-1}$). Cells achieved nitrogen depletion after approximately one week. Two weeks later, samples were taken from the nitrogen-replete pre-culture and from the nitrogen depleted culture for Freeze Fracture Scanning Electron Microscopy and dry weight, pigment, and triacylglyceride (TAG) analysis.

Table 1. Composition of (replete) modified M-8 medium.

Compound	Concentration ($\mu\text{mol L}^{-1}$)	Compound	Concentration ($\mu\text{mol L}^{-1}$)
Hepes	$100.00 \cdot 10^3$	$\text{MnCl}_2 \cdot 4\text{H}_2\text{O}$	65.59
KNO_3	$29.67 \cdot 10^3$	$\text{ZnSO}_4 \cdot 7\text{H}_2\text{O}$	11.13
NaHCO_3	$10.00 \cdot 10^3$	$\text{CuSO}_4 \cdot 5\text{H}_2\text{O}$	7.33
$\text{Na}_2\text{HPO}_4 \cdot 2\text{H}_2\text{O}$	$6.90 \cdot 10^3$	H_3BO_3	1.00
$\text{MgSO}_4 \cdot 7\text{H}_2\text{O}$	$1.62 \cdot 10^3$	Vitamins ($\mu\text{g L}^{-1}$)	
$\text{Na}_2\text{EDTA} \cdot 2\text{H}_2\text{O}$	447.94		
NaFeEDTA	277.85		
$\text{CaCl}_2 \cdot 2\text{H}_2\text{O}$	90.00		
		Thiamine	200.00
		Biotine	1.00

Biomass determination

Cell dry weight measurements were performed in duplicate by filtering and drying the biomass as described by (19).

Freeze fracture scanning electron microscopy

A small droplet containing nitrogen-replete or nitrogen-depleted *C. zofingiensis* cells was placed on copper hollow rivets and promptly frozen in liquid ethane. The rivets were situated in a cryo-sample holder in liquid nitrogen and thereafter transferred to the cryo-preparation system (MED 020/ VCT 100, Leica, Vienna, Austria) onto the sample stage at -93°C and at 1.3×10^{-6} Torr. Thereafter, the samples were fractured and freeze dried for 5 min and subsequently sputter coated with a layer of 10 nm Tungsten at -93°C . The samples were cryo-shielded and transferred into the field emission scanning microscope (Magellan 400, FEI, Eindhoven, The Netherlands) onto the sample stage at -120°C at 1.6×10^{-6} Torr. The analysis was performed at a working

distance of 4-4.5 mm with SE detection at 2 kV and 6.3 pA. Contrast and sharpness of digital images were optimized with Photoshop CS5.

TAG extraction, identification and quantification

All lipophilic components were obtained by a sequence of mechanical cell disruption and solvent based (methanol/chloroform) lipid extraction as described by (20). The TAG fraction was obtained using a solid phase extraction (SPE) column as described by (21) with 10 mL 7:1 (v/v) hexane:diethylether as eluent. Solvents were evaporated and fatty acids of TAG were transesterified to fatty acid methyl esters (FAMES). FAMES were identified and quantified utilizing GC-FID as described by (21).

Pigment extraction

Pigment extracts were obtained by a sequence of mechanical cell disruption and solvent based (methanol/chloroform) pigment extraction as described by (22) with the exception that, after sampling, the cells were centrifuged for 5 min at 2500 rpm (1204×g). The cell pellet was transferred to a bead beating tube and centrifuged again for 5 min at 2500 rpm (1204×g). Supernatant was discarded, and cells were stored at -80 °C. The cells were subsequently freeze dried. One mL of methanol/chloroform was added to the bead beating tube where after the cells were physically disrupted by employing a Precellys® 24 bead beater (Bertin Technology, Montigny-le Bretonneux, France). To inhibit cell heating, 60 s of disruption at 2500 rpm (1204×g) was followed by 5 min of cooling on ice. For each sample, three series of disruption/cooling cycles were performed. After extraction, the dried chloroform fraction was resolved in acetone : methanol 7 : 3 (v/v) containing 0.10% (w/v) BHT and supplemented to 75% (v/v) acetonitrile for LC analysis.

Separation, identification and quantification of pigments

Separation and identification of carotenoids and porphyrins were performed on an Accela UHPLC system (Thermo Scientific, San Jose, CA, USA) equipped with a pump, degasser, auto sampler, and photo diode array (PDA) detector, coupled *in-line* to a LTQ-VelosPro dual-pressure ion trap mass spectrometer equipped with a H-ESI probe (Thermo Scientific). Samples (5.0 µL) were quantitatively injected on an Aquity UPLC Shield C18 BEH column (2.1 × 150 mm, 1.7 µm particle size; Waters, Milford, MA, USA) fitted to a Vanguard pre-column (2.1 × 5 mm, 1.7 µm particle size; Waters). The eluents were (A) 50% (v/v) acetonitrile in demineralized water, (B) acetonitrile and (C) ethyl acetate which all contained 0.10% (v/v) formic acid. The flow rate was maintained at 300 µL min⁻¹. The program was initiated from 25% A / 75% B and then as follows: to 15 min – linear gradient to 100% B; to 22.5 min – isocratic at 100% B; to 29.5 min – linear gradient to 87.5% B/ 12.5% C; to 31.5 min – linear gradient to 70% B / 30% C; to 41.5 min – linear gradient to 100% C; to 42.5 min - isocratic at 100% C.

After 42.5 min, the eluent composition reverted to its initial composition in 7.5 min followed by an equilibration phase of 2.5 min. Detection wavelengths for UV-Vis were adjusted to 450 nm (carotenoids) and 660 nm (porphyrins) with a 1 nm wavelength step and 9 nm filter bandwidth.

All mass spectrometric data was recorded as described by Mulders *et al.* (2013) with the exception that data was recorded over the m/z range 500 - 620 (0.0 - 17.0 min), 500 - 900 (17.0 - 30.0 min) and 1000 - 1250 (30.0 - 42.5 min). Data acquisition and reprocessing were performed with Xcalibur 2.10 (Thermo Scientific). The standards employed for identification of carotenoids and their corresponding absorption coefficients are depicted in **Table 2**. The criteria for compound identification included identical retention time, UV-Vis absorption and spectral fine structure, and parent mass as well as MS² fragmentation pattern with one of the standards. Compounds without a matching standard were identified with comparison to literature data (23, 24). Unknown compounds were not annotated in **Figure 2** and **Table 3** for the sake of clarity. Chlorophyll *b*, in high concentrations, exhibited fronting in this LC system.

For quantification, lutein, canthaxanthin, and chlorophyll *a* were exploited. Approximately 1 mg of lutein and canthaxanthin were initially dissolved in dichloromethane and subsequently diluted with 4 volumes of ethanol (lutein) or *n*-hexane (canthaxanthin). Further dilution in ethanol or *n*-hexane respectively was performed in order to measure within the linear range of the spectrophotometer. Therefore, the content of dichloromethane was lower than 0.5% (v/v) upon determination of the concentrations of lutein and canthaxanthin. Chlorophyll *a* was first dissolved in ethyl acetate and subsequently diluted with 3 volumes of 90% (v/v) aqueous acetone. Standard concentrations were measured prior to UHPLC analysis, employing their respective absorption coefficients ($A_{1\text{cm}}^{1\%}$): 2550 L g⁻¹ cm⁻¹ (445 nm, 100% ethanol) for lutein; 2200 L g⁻¹ cm⁻¹ (469 nm 100% cyclohexane) for canthaxanthin; and 887 L g⁻¹ cm⁻¹ (664 nm, 90% (v/v) aqueous acetone) for chlorophyll *a* (24). PDA calibration was performed utilizing five different concentrations of the standards injected in duplicate. For this calibration, the response of the all-*trans* and *cis* structure of the carotenoid standards was considered equal for quantification. The detector was ascertained as linear for lutein and canthaxanthin between 0.07 and 8.20 µg mL⁻¹ with a minimum R² of 0.998. For chlorophyll *a*, the detector was linear between 0.23 and 23.38 µg mL⁻¹ with an R² of 0.978.

Carotenoids were quantified as lutein equivalents employing the lutein calibration curve. The responses were corrected using the $A_{1\text{cm}}^{1\%}$ illustrated in **Table 2** with the exception of canthaxanthin. An absorption coefficient of 2500 L g⁻¹ cm⁻¹ was utilized for unknown carotenoids (*e.g.* lutein-like components) and carotenoids of

which the absorption coefficient was not documented (*e.g.* ketolutein). Fatty acid esterified astaxanthin and ketolutein were assumed to possess similar molar extinction coefficients as their non-esterified analogues, and were expressed as equivalents of their respective non-esterified analogues in mole L⁻¹ culture volume or % g/g dw. Chlorophyll *b* ($A_{1\text{cm}}^{1\%}$ 514 L g⁻¹ cm⁻¹, 647 nm, 90% (v/v) aqueous acetone) and derivatives were expressed via chlorophyll *a* using the chlorophyll *a* calibration curve. The detector response was corrected for chlorophyll *b* using the ratio of the absorption coefficients of chlorophyll *a* and *b*.

Table 2. Absorption coefficients used for quantification of carotenoids found in *C. zofingiensis*.

Compound	$A_{1\text{cm}}^{1\%}$ (L g ⁻¹ cm ⁻¹)	Ref.	Compound	$A_{1\text{cm}}^{1\%}$ (L g ⁻¹ cm ⁻¹)	Ref.
9'- <i>cis</i> -Neoxanthin	2330	(24)	Lutein	2550	(24)
Violaxanthin	2450	(24)	Lutein-like carotenoid	2500	(23)
Neochrome	2270	(24)	Canthaxanthin	2200	(24)
Astaxanthin (free, monoester and diester)	2060	(24)	Echinenone	2160	(24)
Ketolutein (free, monoester and diester)	2500	(23)	β,β-Carotene	2590	(24)
Adonixanthin	2500	(23)			

RESULTS AND DISCUSSION

To obtain additional insight into the pathways and regulation of the carotenoid metabolism of *C. zofingiensis*, cells were nitrogen depleted to induce secondary carotenogenesis and subsequently DPA-treated to inhibit ketocarotenoids biosynthesis. 60 μM DPA was introduced to nitrogen-depleted cultures every two days beginning on day two. Every two days, cell dry weights and pigment compositions were analysed. Below, chlorophylls and carotenoids ascertained in nitrogen-replete and nitrogen-depleted *C. zofingiensis* cells are identified and the degradation and accumulation kinetics of the overall biomass and the annotated pigments upon nitrogen depletion and DPA treatment are discussed (**Figures 2 – 7**) and **Figure S1**). To properly represent net accumulation/degradation of pigments, pigment kinetics are depicted in moles per litre culture volume. For a reference, pigment contents on a dry weight basis are depicted in **Figure S2**. Conclusions concerning the carotenoid metabolism are summarized graphically in **Figure 8**. Finally, oil droplet formation in nitrogen-depleted *C. zofingiensis* cells is elaborated to support the presumed location of carotenoid accumulation.

Pigment identification

A profound variation in the carotenoid profile of extracts between the nitrogen-replete and nitrogen-depleted *C. zoefingiensis* cells was observed (**Figure 2**). The key findings were the emergence of ketolutein and ketolutein esters upon nitrogen depletion, confirming the finding by Bauch (2011). For both chromatograms, peaks are annotated in **Table 3**.

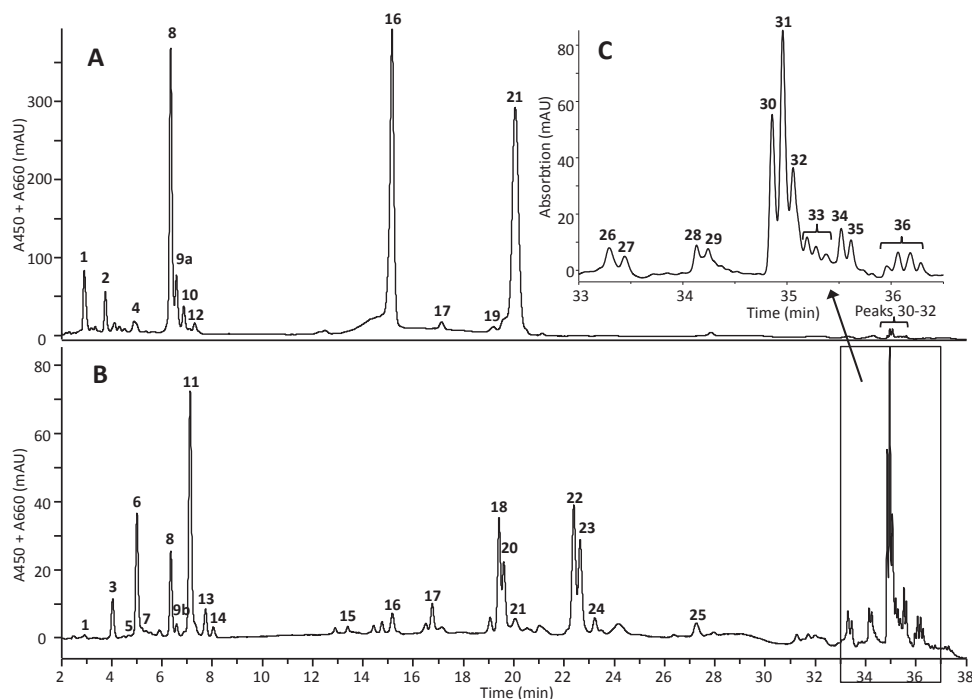


Figure 2. Representative RP-UHPLC chromatograms (450 and 660 nm summed) of *C. zoefingiensis* extract. **A** Nitrogen-replete cells, **B** nitrogen-depleted cells and **C** enlargement of chromatogram of nitrogen-depleted cells RT 33.0 to 36.5 min.

The annotation of ketolutein (β,ϵ -end groups) was performed by comparison with adonixanthin (β,β -end groups). Although the molecular weight of both carotenoids is comparable, pronounced differences in visible absorption spectra and MS² spectra were found (**Figures 3A - C**). The spectral fine structure of ketolutein had two absorption maxima, where adonixanthin had one maximum. Furthermore, the spectral fine structure of ketolutein excluded the possibilities of having a carotenoid epoxide or a carotenoid with an allenic group, or both (*e.g.* diadinoxanthin). The 8 nm hypsochromic shift of ketolutein, compared to adonixanthin, indicated the presence of a smaller conjugated system. This hypsochromic shift can be attributed to the

presence of an ε -end group. A similar hypsochromic shift has also been documented for zeaxanthin (β,β -end groups, λ_{\max} (II) = 450 nm in hexane) and lutein (β,ε -end groups, λ_{\max} (II) = 445 nm in hexane) (24). Similar observations were made when comparing this for the group of the ketoluteins, (comprising of four reported stereoisomers fritschiellaxanthin, 4-ketolutein F, α -doradexanthin and 4-ketolutein D) to adonixanthin (25).

Additional evidence for an ε -end group was ascertained in the MS² fragmentation spectra of ketolutein and adonixanthin. It has been reported that the C6-C7 bond adjacent to a hydroxylated ε -end group is more prone to fragmentation than that adjacent to a hydroxylated β -end group in the case of electron impact mass spectrometry (26). Extrapolating this for ketolutein in combination with the milder CID fragmentation, observation of at least one fragment with a neutral loss of 138 Da was expected. In the MS² spectrum of ketolutein, two such neutral losses were found as the two primary fragments: one direct loss at m/z 444.3 and a loss combined with an in-chain polyene elimination of toluene (92 Da) at m/z 352.3 (**Figure 3B**). For adonixanthin, the neutral loss of 138 was not found, and only (combinations of) water and toluene losses were ascertained (**Figure 3C**). Similar observations were made with fragmentation of lutein and zeaxanthin (24, 26, 27). From a biological point of view, it seems likely that the ketolutein found represents fritschiellaxanthin, one of the four reported stereoisomers of ketolutein. However, the exact *R/S* configuration was not determined by CD / NMR. Furthermore, no chemical standards were at our disposal to confirm this stereochemistry. Therefore, throughout this work, the generic annotation ketolutein is employed.

The visible absorption spectra of ketolutein and peaks 22, 23, 25 and 36 were identical, indicating that ketolutein was also evident in its esterified form to one or two fatty acids (**Figure 3A**). Sodiated $[M+Na]^+$ fragment spectra of the carotenoid esters were employed to confirm this as they exhibited more efficient ionization and less complex mass spectra (28, 29). In **Figure 3D**, the MS² fragment spectrum of ketolutein ME C18:1 $[M+Na]^+$ is depicted. The identification of this ester was performed similar to astaxanthin monoesters and diesters. In the case of monoesters, the fragment at m/z 587.5 was used to identify the attached fatty acid and to also confirm the molecular mass of ketolutein (*e.g.* 587.5 + H₂O – Na = 582.5 Da). The visible spectra of peak group 36 exhibited similar spectral fine structures, indicating that the backbone was ketolutein. Identification of the fatty acids in these ketolutein diesters could not be performed due to lack of fragmentation data. Still, because astaxanthin mono- and diesters were predominantly esterified with C16:0 and C81:1 fatty acids, the assumption could be made that this was also the case for ketolutein diesters. The fatty acid esterification was not exclusively with C16:0 and C18:1; lower abundances were also discovered for the C18:0, C18:2 and C18:3 fatty acid esters for astaxanthin mono- and diesters.

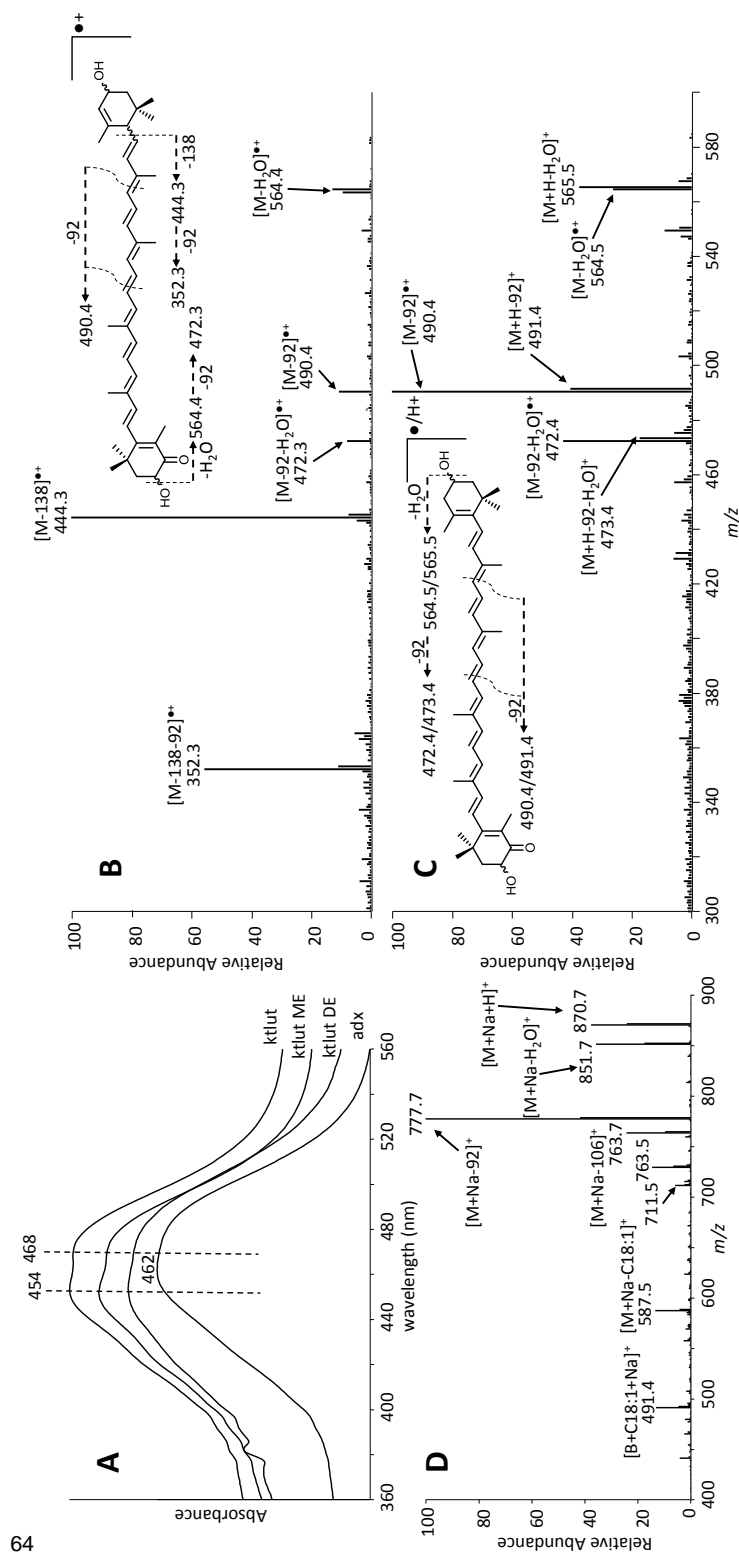


Figure 3. **A** Visible absorption spectra of the three different forms of ketolutein and adonixanthin. **B** Comparison and fragment annotation of the MS² fragmentation of ketolutein [M]^{••+} parent (peak 6) and **C** adonixanthin [M]^{••+}/[M+H]^{••+} (peak 7). **D** Annotation of the C18:1 esterified fatty acid from ketolutein ME C18:1 (peak 22) by MS² fragmentation of its [M+Na]^{••+} parent. Ktlut = ketolutein, Ktlut ME = ketolutein monoester, Ktlut DE = ketolutein diester, adx = adonixanthin; other abbreviations, see footnote **Table 3**.

Identification of the other primary and secondary pigments, *e.g.* canthaxanthin, adonixanthin, β,β -carotene, lutein, violaxanthin, and chlorophyll *a* and *b* were in accordance with previous reports of *C. zofingiensis* (5, 6, 9, 30). 9'-*cis*-Neoxanthin, *cis*-neochrome-like, and the *cis*-lutein-like compounds were not previously documented in *C. zofingiensis* which were identified empirically by comparison to reference data. From **Figure 1** also adonirubin, 3-hydroxyechinenone, lycopene, cryptoxanthin, α -cryptoxanthin, and β,ϵ -carotene were expected to be present. However, upon comparison with standards, they were not ascertained in our analysis. The presence of zeaxanthin could not be determining with certainty, although Wang and co-workers (2008) detected a substantial amount of this carotenoid. Zeaxanthin standards has similar retention time as peaks 9a/9b, but the UV-Vis and MS² spectra did not match. This might be explained by coelution.

Optimizing DPA concentration and addition frequency

Although DPA is exploited in multiple studies to obtain insight into microalgae carotenoid accumulation (9, 11, 12), numbers regarding DPA degradation kinetics are minimal. To gain insight in the DPA degradation rate under the experimental conditions described in this work and to locate the most optimal DPA concentration with respect to the inhibition of carotenogenesis, a range of DPA concentrations was added to nitrogen-depleted *C. zofingiensis*, and the effect on pigment accumulation (carotenoids and chlorophylls) was examined. In individual experiments, DPA was added once after two days of nitrogen starvation in the following concentrations: 0 (control), 10, 20, 30, 60, 100 or 200 μ M. The most significant variation in pigment concentrations between the control and the DPA-treated culture was ascertained in the culture to which 60 μ M DPA was added. In addition, the results suggested that DPA was inactivated after approximately three days following the addition (results not shown). Therefore, in the experiment described in the current paper, DPA was added every two days, resulting each time in a concentration increase of 60 μ M, in order to maintain an effective DPA concentration for two weeks.

Table 3. Compounds tentatively assigned in the extracts of *C. zofingiensis* by UHPLC-PDAESI-MSⁿ.

Peak No.	Compound	Rt. (min)	λ_{\max} (nm)	Band ratio (% III:I) ^a	Ionization type	Parent ion (m/z)	MS ⁿ product ions (assignment, % rel. intensity) ^b	Ref ^c
1	9'- <i>cis</i> -Neoxanthin	2.91	416, <u>438</u> , 467	82	[M] ⁺⁺ /[M+H] ⁺	600.5/601.4	582.5(100), 567.4(30), 508.4(M-92, 30), 507.4(M-92, 30), 383.4(50), 255.3(50), 221.2(50) ^c	(24)
2	Violaxanthin	3.75	418, <u>440</u> , 470	82	[M] ⁺⁺ /[M+H] ⁺	600.5/601.4	583.4(100), 565.5(20), 508.4(M-92, 30), 491.4(M-18-92, 15), 415.3(30), 319.3(20), 265.3(40), 221.2(20) ^c	Std, (24)
3	Astaxanthin	4.05	<u>474</u>	0	[M+H] ⁺	597.5	579.5(100), 561.5(40), 503.4(M-92,30), 491.4(M-106, 20), 379.3(35), 277.3(20), 287.2(25)	Std, (24)
4	(<i>cis</i>)-Neochrome-like	4.51	404, <u>421</u> , 447	58-65	[M] ⁺⁺	600.4	582.4(100), 568.5(60), 520.4(40), 508.4(M-92,70), 507.4(90), 476.4(50), 415.3(50), 221.1(65)	(24)
5	Antheraxanthin	5.00	N.D.	N.D.	[M] ⁺⁺	584.5	N.D.	(24)
6	Ketolutein	5.00	<u>454</u> , 468	0	[M] ⁺⁺	582.5	564.4(20), 563.5(15), 490.4(M-92, 20), 472.3(M-92-18, 15), 444.3(M-138, 100), 352.3(M-92-138, 60)	(25) ^d
7	Adonixanthin	5.20	<u>460</u>	0	[M] ⁺⁺ /[M+H] ⁺	582.5/583.5	565.5(40), 564.5(30), 549.5(10), 491.4(M-92, 40), 490.4(M-92, 100), 473.4(20), 472.4(40) ^c	Std, (25)
8	Lutein	6.36	424, <u>447</u> , 473	47	[M] ⁺⁺	568.5	550.4(5), 519.1(10), 476.3(M-92, 100), 338.2(75)	Std, (24)
9a	<i>cis</i> -Lutein-like	6.58	422, <u>442</u> , 469	29	[M] ⁺⁺	568.5	550.4(10), 476.4(100), 430.4(10), 338.3(50)	(23, 24)
9b	<i>cis</i> -Lutein-like or zeaxanthin-like	6.58	(443), <u>450</u> , 468	N.D.	[M] ⁺⁺	568.5	476.4(100), 338.30(20)	(23, 24)
10	<i>cis</i> -Lutein	6.87	422, <u>441</u> , 469	50	[M] ⁺⁺	568.5	550.5(5), 476.4(100), 458.3(M-18-92, 10), 430.4(5), 338.3(40)	(23, 24)
11	Canthaxanthin	7.13	<u>473</u>	0	[M+H] ⁺	565.5	547.4(60), 473.4(M-92, 20), 459.4(M-106, 20), 427.3(M-138, 15), 413.4(20), 363.3(100), 361.3(30), 349.2(20), 269.3(20), 203.1(70)	Std, (24)
12	<i>Cis</i> -Lutein-like	7.31	332, 419, <u>441</u> , 468	30	[M] ⁺⁺	568.5	550.5(20), 476.4(100), 458.3(M-18-92, 10), 430.3(15), 338.3(70)	(23, 24)
13	<i>cis</i> -Canthaxanthin	7.74	<u>466</u>	0	[M+H] ⁺	565.5	N.D.	(24)
14	<i>cis</i> -Canthaxanthin	8.05	370, <u>464</u>	0	[M+H] ⁺	565.5	N.D.	(24)
15	Echinenone	13.39	<u>459</u>	0	[M] ⁺⁺	550.7	550.7(100), 494.5(5), 458.4(M-92, 30), 427.4(10), 402.4(10), 335.3(10)	Std, (24)
16	Chlorophyll <i>b</i>	15.15	456, 595, 645	N.A.	N.D.	N.D.	N.D.	(24)
17	Chlorophyll <i>b</i> -like	17.13	432, 457, 647	N.A.	N.D.	N.D.	N.D.	(24)
18	Astaxanthin ME C18:1	19.42	<u>473</u>	0	[M+Na] ⁺	883.8	839.7(M-H ₂ O, 20), 791.7(M-92, 100), 777.7(M-106, 30), 601.4(M-FA, 40), 491.4(B+FA, 15)	(28, 29)
19	β , β -Carotene	19.19	475 ^e	N.D.	[M] ⁺⁺	536.5	444.4(M-92, 100)	Std, (24)

Table 3. Continued

20	Astaxanthin ME C16:0	19.60	<u>473</u>	0		[M+Na] ⁺	857.8	813.6(M-H ₂ O, 20), 765.5(M-92, 100), 751.5(M-106, 30), 601.3(M-FA, 40), 465.3(M+FA, 10)	Std, (28, 29)
21	Chlorophyll <i>a</i>	20.06	382, 413, 429, 580, 616, 661	N.A.		[M-Mg+2H] ⁺	871.7	593.4(M-Phytol, 100), 533.4(M-Phytol-60, 60)	Std, (24)
22	Ketolutein ME C18:1	22.39	<u>451</u> , 468	0		[M+Na] ⁺	869.7	851.7(M-H ₂ O, 35), 777.7(M-92, 100), 763.7(M-106, 30), 587.5(M-FA, 15), 491.4(B+FA, 15)	(28, 29)
23	Ketolutein ME C16:0	22.64	<u>451</u> , 468	0		[M+Na] ⁺	843.7	825.7(M-H ₂ O, 40), 751.6(M-92, 100), 737.6(M-92, 30), 587.4(M-FA, 20), 465.4(B+FA, 10)	(28, 29)
24	Astaxanthin ME C18:0	23.23	334, <u>468</u>	0		[M+Na] ⁺	885.8	867.7(10), 841.7(30), 793.7(100), 779.6(30), 601.4(30), 493.4(15)	(28, 29)
25	Ketolutein ME	27.26	455, <u>468</u>	0		N.D.	N.D.	N.D.	(28, 29)
26	Astaxanthin DE C18:1/C18:3	33.29	<u>475</u>	0		[M+Na] ⁺	1143.9	1051.8(M-92, 100), 1037.9(M-106, 30), 865.7(M-FA, 40), 861.6(M-FA, 40)	(28, 29)
27	Astaxanthin DE C16:0/C18:3	33.44	<u>473</u>	0		[M+Na] ⁺	1117.9	1025.8(M-92, 100), 1011.8(M-92, 30), 861.6(M-FA, 40), 839.7(M-FA, 35)	(28, 29)
28	Astaxanthin DE C18:1/C18:2	34.13	<u>470</u>	0		[M+Na] ⁺	1146.0	1053.9(M-92, 100), 1039.9(M-106, 30), 865.7(M-FA, 40), 863.7(M-FA, 50)	(28, 29)
29	Astaxanthin DE C16:0/C18:2	34.24	<u>468</u>	0		[M+Na] ⁺	1120.0	1027.9(M-92, 100), 1013.9(M-106, 30), 863.7(M-FA, 50), 839.7(M-FA, 35)	(28, 29)
30	Astaxanthin DE C18:1/C18:1	34.86	<u>475</u>	0		[M+Na] ⁺	1148.0	1055.9(M-92, 100), 1041.9(M-106, 30), 865.7(M-FA, 80)	(28, 29)
31	Astaxanthin DE C16:0/C18:1	34.96	<u>476</u>	0		[M+Na] ⁺	1122.1	1029.9(M-92, 100), 1015.9(M-106, 30), 865.7(M-FA, 50), 839.7(M-FA, 50)	(28, 29)
32	Astaxanthin DE C16:0/C16:0	35.06	<u>474</u>	0		[M+Na] ⁺	1096.1	1033.9(M-92, 100), 989.9(M-106, 30), 839.8(M-FA, 80)	(28, 29)
33	<i>cis</i> of peak 30 - 32	35.19-35.38	<u>462</u>	0		[M+Na] ⁺	Idem	Idem	(28, 29)
34	Astaxanthin C18:0/C18:1	35.52	<u>474</u>	0		[M+Na] ⁺	1150.1	1057.9(M-92, 100), 1043.9(M-106, 30), 867.8(M-FA, 50), 865.8(M-FA, 40)	(28, 29)
35	Astaxanthin C16:0/C18:0	35.62	<u>474</u>	0		[M+Na] ⁺	1124.1	1031.9(M-92, 100), 1017.9(M-106, 30), 867.7(M-FA, 40), 839.7(M-FA, 40)	(28, 29)
36	Ketolutein DE's	35.96-36.28	<u>454</u>	0		N.D.	N.D.	N.D.	(25)

N.D.: not determined. N.A.: not applicable. ^aWhen no fine structure, no peak heights II and III nor a minimum between them can be defined, the band ratio was annotated as 0 %. ^bM-92 in-polyene toluene elimination, M-106 in-polyene xylene elimination, M-FA neutral loss of fatty acid, B+FA benzonium fragment with fatty acid. ^cFragments of both [M]⁺ and [M+H]⁺ occurred in the MS² spectrum due to the isolation width of the ion trap. ^dThe MS² spectrum of α -doradexanthin was closest to our finding of the ketolutes reported in this reference ^eIncomplete spectrum due to overlap with chlorophyll *a*.

Biomass production

During the entire cultivation period, the control and the DPA-treated cultures exhibited no significant variation in biomass production. Following a steep initial increase, biomass production levelled off around day eight for all cultures. Both the treated and the control cultures increased from 1.7 to 4.6 L g⁻¹ in biomass concentration (**Figure 4**). As the medium was nitrogen-depleted from the beginning of cultivation, no additional nitrogen-containing cell material such as DNA and protein could be formed. Photosynthesis and carbon fixation still continued in the absence of nitrate. Therefore, it appears plausible that the ascertained biomass increase is due to carbon-rich storage compounds such as TAG. This has been described for nitrogen-depleted *C. zofingiensis* by (21) who observed a biomass increase of 580 % *dw* and TAG accumulation of up to 40 % (w/w) *dw*. The absence of a significant variation in biomass production between the control and the treated cultures demonstrated that DPA did not affect the overall production of secondary storage compounds or carbon fixation.

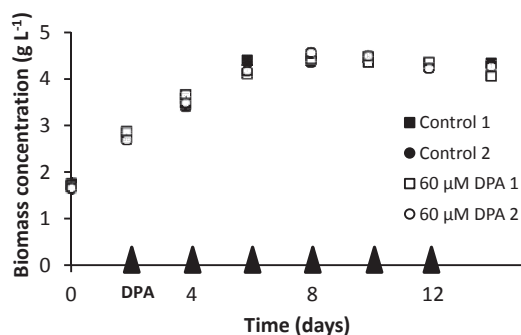


Figure 4. Time courses of dry weight biomass concentration of nitrogen-depleted *C. zofingiensis* exposed to no DPA (control) or exposed to repeated additions of DPA resulting each time in a concentration increase of 60 μM. *Triangles* indicate DPA additions. Absolute deviations from the mean of duplicate dry weight measurements were all less than 4%.

Degradation of chlorophylls and primary carotenoids

The chlorophylls and primary carotenoids found in the treated culture were identical to those ascertained in the control, specifically, chlorophyll *a* and *b*, lutein, 9'*cis*-neoxanthin, and violaxanthin. The cellular contents of these pigments all decreased over time with no significant difference between the control and the treated culture

(Figure 5). This demonstrates that DPA did not affect the overall degradation of primary pigments.

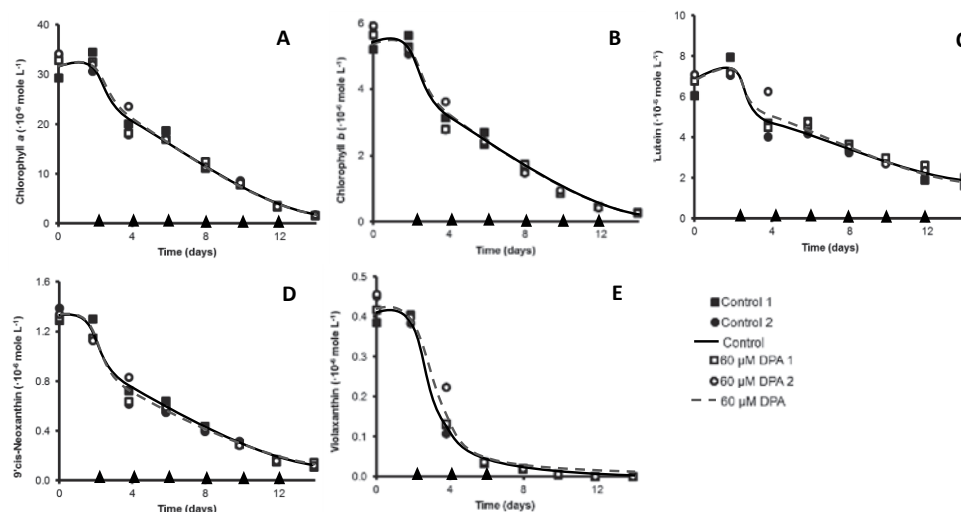


Figure 5. Time courses of **A** chlorophyll *a*, **B** chlorophyll *b*, **C** lutein, **D** 9'-cis-neoxanthin and **E** violaxanthin in moles per litre culture volume of nitrogen-depleted *C. zofingiensis* exposed to no DPA (control) or exposed to repeated additions of DPA resulting each time in a concentration increase of 60 μM . Triangles indicate DPA additions. Lines are for visual guidance.

Under nitrogen-replete conditions, the primary pigments comprised more than 99.9 % of the total pigment content of *C. zofingiensis* (Figures 5 and 6, t_0). These pigments are located in the photosystems of the chloroplast, and all are capable of harvesting light energy (2, 31-33) which is converted into chemical energy. Active degradation of these individual pigments may be a strategy of the cell to manage the oversaturating light conditions that resulted from the nitrogen depletion, as was, for example, observed in *Isochrysis galbana* (34). However, the equiproportional decrease of chlorophyll *a*, *b*, and 9'-cis-neoxanthin lends support to the assumption that entire photosystems were degraded rather than specific light harvesting pigments.

Remarkably, in both the control and the treated culture, violaxanthin was degraded at a significantly higher rate than the other primary pigments (Figure 5). Violaxanthin is a component of the violaxanthin cycle and can be converted into zeaxanthin under oversaturating light conditions via antheraxanthin, which is part of a photoprotective mechanism (35, 36). However, as no additional zeaxanthin or antheraxanthin was discovered in either the control or the treated culture, it is questionable whether this degradation cycle was genuinely operational in our experiments. It may be that violaxanthin, antheraxanthin and zeaxanthin were all

degraded. In addition, it is remarkable that, in both the control and in the treated culture, lutein was degraded at a lower rate compared to the other primary pigments.

Accumulation of secondary carotenoids

The secondary carotenoids ascertained in the treated culture were also the same as those discovered in the control, specifically, astaxanthin, ketolutein, canthaxanthin, adonixanthin, echinenone, and β,β -carotene. For the majority of these carotenoids, the cellular content was significantly different between the control and the treated culture (**Figure 6**), indicating that under nitrogen-deplete conditions DPA had a significant effect on the formation of secondary carotenoids.

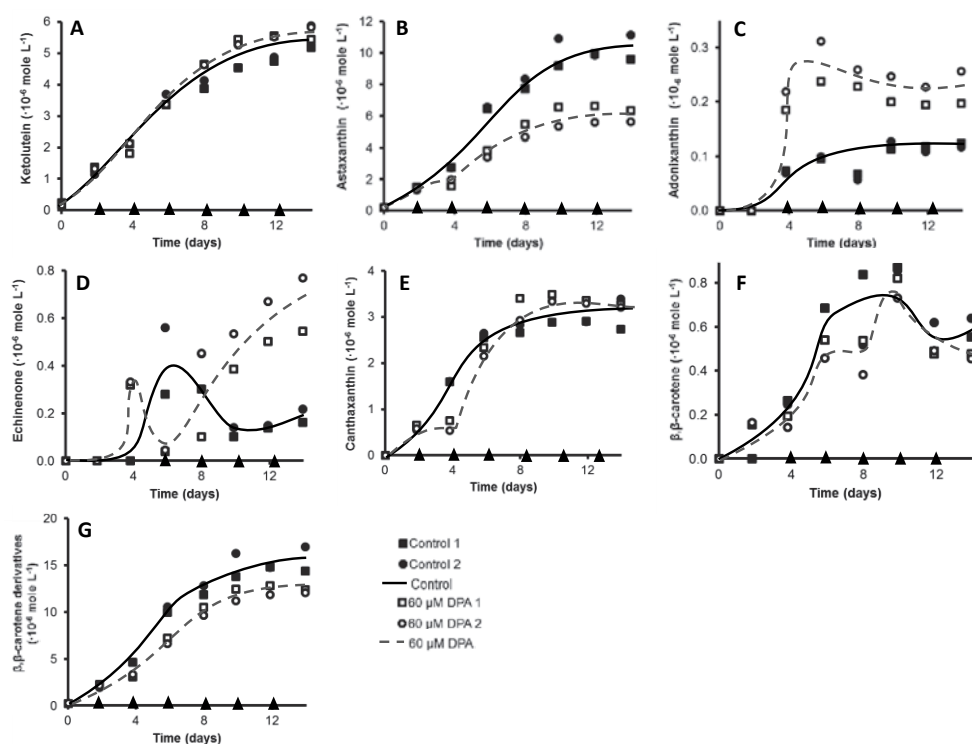


Figure 6. A Concentrations of total ketolutein (sum of free, mono- and diesters), B total astaxanthin (sum of free, mono- and diesters), C adonixanthin, D echinenone, E canthaxanthin, F β,β -carotene and G all β,β -carotene derivatives (sum of total astaxanthin, adonixanthin, echinenone and canthaxanthin) in moles per litre culture volume in nitrogen-depleted *C. zoefingiensis* exposed to no DPA (control) or exposed to repeated additions of DPA resulting each time in a concentration increase of 60 μM . Triangles indicate DPA additions. Lines are for visual guidance.

Ketolutein. Ketolutein was the second most abundant secondary carotenoid in nitrogen-depleted *C. zofingiensis*. The cellular content increased gradually from zero to the final content with no significant variations between the control and the treated culture (**Figure 6A**). In all cultures, ketolutein was ascertained primarily as monoester, to a more moderate extent in the free form (unesterified), and to a very minimal extent as diester (esterified with C16:0 and C18:1 fatty acids).

The absence of a significant difference in ketolutein concentration between the control and the treated culture indicated that DPA did not affect the overall formation of ketolutein. Ketolutein most plausibly resulted from lutein oxygenation which requires one enzymatic conversion catalysed by a ketolase. Expression of the BKT gene (from *H. pluvialis*) in *Chlamydomonas reinhardtii* which naturally synthesises β,β -carotene, zeaxanthin, and lutein but no β -end group ketocarotenoids such as echinenone and adonixanthin, resulted in synthesis of ketolutein, whereas no β -end group ketocarotenoids were synthesised (37). This supports the premise that ketolutein emerged from lutein via oxidation by BKT. It is remarkable that the lutein to ketolutein conversion by BKT was not affected by DPA. This may be explained by assuming that the enzyme that catalysed ketolutein biosynthesis was insensitive to DPA, either because it was a completely different ketolase (encoded by a different yet-unidentified gene), or because BKT may have been embedded in a multiprotein complex causing its insensitivity to DPA.

Ketolutein was found esterified with similar fatty acids as astaxanthin. Surprisingly, ketolutein was found mainly as monoester, whereas astaxanthin was detected primarily as diester, despite the fact that they both possess two hydroxyl groups. This might suggest that either the β -end group is more easily acylated than the ϵ -end group or that the adjacent carbonyl is a prerequisite for acylation.

Astaxanthin. Astaxanthin was the most abundant secondary carotenoid in nitrogen-depleted *C. zofingiensis*. In both the control and the treated cultures, its content increased gradually. From the moment that DPA was added, the increase in the treated culture was half as high as in the control culture (**Figure 6B**), indicating that DPA significantly inhibited production of astaxanthin.

Theoretically, adonixanthin and adonirubin may both be precursors of astaxanthin (**Figure 1**). Since adonixanthin was detected, the pathway to this carotenoid must have been present. Because adonixanthin was found in a very low concentration and only in the free form, it may be speculated that the pathway from adonixanthin to astaxanthin was existing as well. It remains ambiguous whether adonirubin was a precursor of astaxanthin as well since this carotenoid was lacking in nitrogen depleted *C. zofingiensis*.

Adonixanthin. In both the control and the treated cultures, the cellular content of adonixanthin increased gradually. From the moment that DPA was added, the increase in the treated culture was approximately twice as high as in the control

culture (**Figure 6C**). This finding supports the speculation that, in nitrogen depleted *C. zofingiensis*, adonixanthin was converted into astaxanthin.

Adonixanthin may be formed from echinenone via 3-hydroxyechinenone or 3'-hydroxyechinenone, as in *H. pluvialis* (17), or from zeaxanthin, as proposed by (8, 9). This latter hypothesis was based on reduced zeaxanthin degradation in carotenogenic cultures exposed to DPA. As mentioned previously, no substantial amounts of zeaxanthin could be detected in any of the cultures. Additionally, we did not discover reduced degradation of zeaxanthin precursors (*i.e.* all other primary carotenoids) in the DPA-treated cultures. Therefore, our results do not support the hypothesis that, in nitrogen depleted *C. zofingiensis*, adonixanthin is formed from zeaxanthin. In contrast, echinenone attained a cellular content that was approximately seven times as high in the treated cultures as in the control (**Figure 6D**). This supports the hypothesis that echinenone is a possible precursor of adonixanthin.

Canthaxanthin. In both the control and the treated cultures, canthaxanthin was ascertained in relatively high cellular contents (comparable to esterified ketolutein contents). In both cultures, the cellular content increased gradually. In the treated cultures, canthaxanthin was detected only on day four in significantly lesser amounts compared to the control culture (**Figure 6E**). This indicates that canthaxanthin formation was inhibited for only two days which was compensated with increased canthaxanthin production the two days thereafter. It remains unclear what mechanism caused the recovery from DPA inhibition.

Huang *et al.* (2006) also discovered relatively high contents of canthaxanthin and, as stated, speculated that canthaxanthin is an end product rather than a precursor of astaxanthin. Our data do not provide further insights with regard to this speculation.

β,β -carotene. In both the control and the treated cultures, β,β -carotene was ascertained at low cellular contents (comparable to echinenone, adonixanthin, and free astaxanthin contents), with no significant variation between the control and the treated culture (**Figure 6F**). The low cellular β,β -carotene content indicates that this carotenoid was promptly converted into echinenone and, moreover, that a high β,β -carotene content was not required for induction of secondary carotenogenesis.

Novel insights in the regulation of carotenogenesis in *C. zofingiensis*

In both the DPA-treated culture and the control, accumulation of secondary carotenoids occurred simultaneously with a decrease in primary carotenoids (grey lines, **Figure 7**). This lends support to the supposition that, under nitrogen-deplete conditions, secondary carotenoids were formed from primary carotenoids. However, the overall carotenoid content increased (black lines, **Figure 7**), which indicates that, in the DPA-treated culture and in the control, at least part of the secondary carotenoids were synthesized *de novo*. Since the consumed quantity of lutein equalled

approximately the produced amount of ketolutein, it may be assumed that, instead of degrading into other products, lutein was completely converted into ketolutein. Since lutein constituted the major fraction of primary carotenoids (>80%), this implies that the remaining secondary carotenoids (echinenone, canthaxanthin, adonixanthin and astaxanthin) must have been almost completely formed *de novo* in both the control and the DPA-treated cultures.

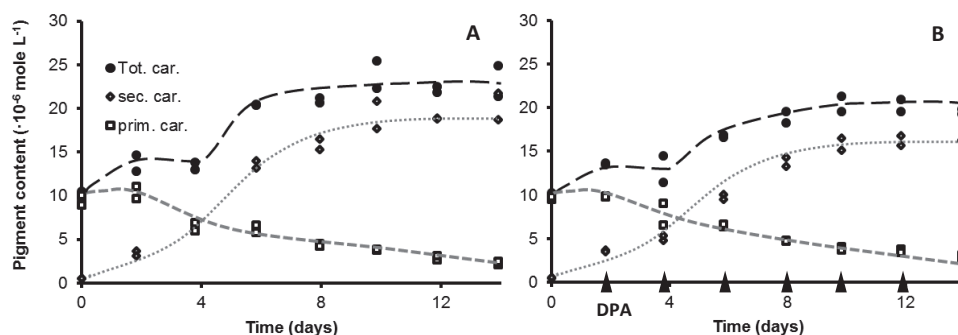
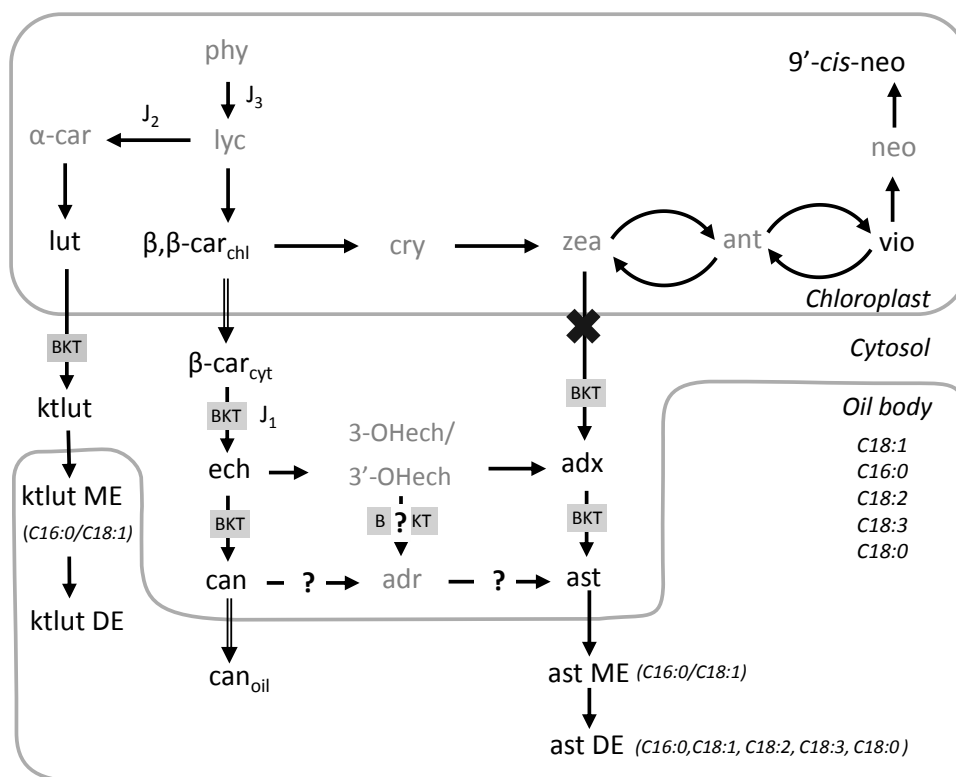


Figure 7. Primary, secondary and total carotenoid contents of nitrogen-depleted *C. zofingiensis* exposed to **A** no DPA or exposed to **B** repeated additions of DPA. *Primary carotenoids* include lutein, neoxanthin and violaxanthin. *Secondary carotenoids* include astaxanthin (sum of free, mono- and diesters), ketolutein (sum of free and mono- and diesters), canthaxanthin, adonixanthin, echinenone and β , β -carotene. *Total carotenoids* include both primary and secondary carotenoids. *Lines* are for visual guidance.

The overall cellular content of echinenone, canthaxanthin, adonixanthin, and astaxanthin was significantly different between the DPA-treated cultures and the controls. The overall content was reduced particularly during the first four days after the initial DPA addition (between day 2 and 6; **Figure 6G**), indicating that, during this time, the flux through J_1 was significantly diminished (**Figure 8**). In contrast, the overall cellular contents of lutein and ketolutein were not significantly affected (**Figures 5C and 6A**) nor were the contents of other primary carotenoids (**Figures 5D-E**) which resulted in an overall decrease of carotenoid production (**Figures 7A versus 7B**). Thus, although DPA reduced the flux through J_1 , the flux through J_2 and the degradation of primary pigments remained unaffected, which implies a decreased flux through J_3 (**Figure 8**). The decreased flux through J_3 can be explained by assuming that a regulatory mechanism was present which prevented increased production of ketolutein or primary carotenoids. It remains unclear what mechanism caused the recovery from DPA inhibition after day six.

In this work, BKT activity was inhibited employing an enzyme inhibitor which mimicked downregulation of BKT by genetic engineering. Our findings suggest that downregulation of the BKT enzyme of *C. zofingiensis* through genetic engineering and



74

Oil body formation

Secondary carotenoids and their esters are generally assumed to accumulate in TAG oil bodies (4). To gain insight into oil body formation in nitrogen-depleted *C. zofingiensis*, freeze fracture scanning electron micrographs were created, and TAG and secondary carotenoid compositions of nitrogen-replete and nitrogen-depleted *C. zofingiensis* cells were analysed (no DPA added) (**Figure 9**). The nitrogen-replete cells contained virtually no secondary carotenoids (less than 0.001% (g/g dw)), whereas this concentration in the nitrogen-depleted cells was 0.1% (g/g dw) (comparable with the nitrogen-depleted cells on day five of the control culture).

In the nitrogen-depleted culture, the TAG fatty acids C18:1, C16:0, C18:2, C18:3 and C18:0 were detected in the highest concentrations (**Figure 9H**). The replete and depleted cells contained 1% and 12% (g/g dw) TAG fatty acids, respectively (**Figure 9F**). In the replete cells, a moderate number of tiny oil bodies were ascertained (less than 100 nm in diameter) (**Figure 9C**) whereas, in the depleted cells, multiple larger oil bodies were discovered throughout the cell in various sizes (up to 600 nm in length). These oil bodies remained separate despite their close proximity (**Figures 9D-E**). The existence of multiple separate oil bodies suggests that these oil bodies were formed independently. In both the replete and depleted culture, oil bodies were found exclusively in the cytosol and, therefore, not in the chloroplasts (**Figures 9A - E**). If oil bodies had been apparent in the chloroplast, they would have been visible as demonstrated in *Dunaliella salina* (22) on similarly obtained micrographs.

Since the fatty acids detected most abundantly in TAG were identical to those discovered esterified to astaxanthin and ketolutein, these fatty acids may have been cleaved by lipases from *de novo* synthesised TAG, as was speculated for the astaxanthin esterified fatty acids in *H. pluvialis* (4). Otherwise, newly formed fatty acids may have been directly esterified to secondary carotenoids before forming TAG, as speculated by (17).

Similar as in *C. zofingiensis*, in *H. pluvialis* oil bodies are located in the cytosol (17, 38). In this species, astaxanthin as well as β,β -carotene was ascertained in oil bodies located in the cytosol (13), indicating that the conversion from β,β -carotene to astaxanthin occurs in the cytosol. Evidence was found of BKT in *H. pluvialis* in the chloroplast as well as in the oil bodies, however, BKT appeared to be active only on the surface of the oil bodies (38). Considering the many similarities between *C. zofingiensis* and *H. pluvialis* (i.e. TAG oil bodies location, the fatty acids present in TAG and esterified to secondary carotenoids, and enzymes involved in secondary carotenogenesis), it may be speculated that, in *C. zofingiensis*, the secondary carotenoids were also synthesised on the surface of the oil bodies and subsequently accumulated in the oil bodies. However, ketolutein may be synthesised in the chloroplast as well after which it may be transferred, esterified, and accumulated in oil

bodies located in the cytosol. Both speculations need to be confirmed with more in-depth research on enzyme activity location of BKT and esterases.

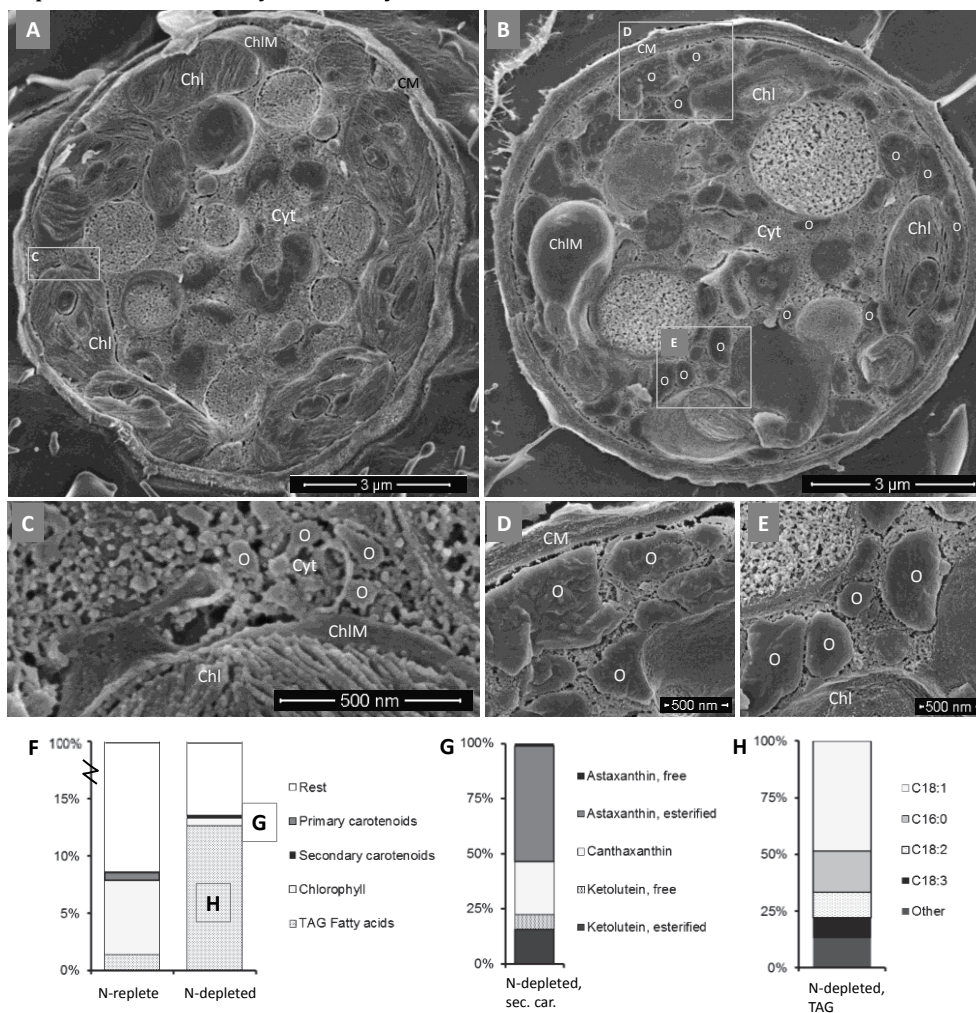


Figure 9. Freeze fracture scanning electron micrographs and pigment and triacylglyceride (TAG) composition of nitrogen-replete and nitrogen-depleted *C. zofingiensis* cells. **A** whole nitrogen-replete cell. **B** whole nitrogen-depleted cell **C** enlargement of cytoplasm located oil droplets in nitrogen-replete cell. **D** and **E** enlargement of cytoplasm located oil droplets in nitrogen-depleted cells. **F** cell composition (mass percentages of dw), including pigments and TAG fatty acids, of the nitrogen-replete and nitrogen-depleted cells. **G** abundance of individual secondary carotenoids as percentage of total secondary carotenoids in the depleted cells. **H** abundance of individual TAG fatty acids as percentage of total TAG fatty acids in the depleted cells. Percentages expressed as % g/g dw. *Other* includes C12:0, C14:0, C16:1, C16:2, C16:3, C16:4, C18:0, C18:4 and C20:1. Cyt = cytosol, Chl = chloroplast, ChlM = chloroplast membrane, CM = cell membrane, O = oil body.

CONCLUSIONS

In conclusion, besides esterified and free astaxanthin, canthaxanthin echinenone and adonixanthin, *C. zofingiensis* overproduces the secondary carotenoid ketolutein and its fatty acid esters. Whereas ketolutein must have been synthesised from pre-formed lutein, other secondary carotenoids were almost completely synthesised *de novo*. Moreover, although DPA inhibited the overall production of all other ketocarotenoids, it did not affect the production of ketolutein and its fatty acid esters or the metabolism of primary carotenoids such as lutein.

ACKNOWLEDGEMENTS

We gratefully thank Tiny Franssen-Verheijen of Wageningen Electron Microscopy Centre for her help with the Cryo-SEM. This work was supported by FeyeCon D&I and by grants from NL Agency and the Ministry of Education, Culture and Science (Project no. FND09014).

REFERENCES

1. Spolaore, P.; Joannis-Cassan, C.; Duran, E.; Isambert, A., Commercial applications of microalgae. *Journal of bioscience and bioengineering* **2006**, *101*, 87-96.
2. Mulders, K. J. M.; Lamers, P. P.; Martens, D. E.; Wijffels, R. H., Phototrophic pigment production with microalgae: biological constraints and opportunities. *Journal of phycology* **2014**, *50*, 229-242.
3. Lamers, P. P.; Janssen, M.; De Vos, R. C. H.; Bino, R. J.; Wijffels, R. H., Exploring and exploiting carotenoid accumulation in *Dunaliella salina* for cell-factory applications. *Trends in biotechnology* **2008**, *26*, 631-638.
4. Solovchenko, A. E., Physiology and adaptive significance of secondary carotenogenesis in green microalgae. *Russian journal of plant physiology* **2013**, *60*, 1-13.
5. Del Campo, J. A.; Rodriguez, H.; Moreno, J.; Vargas, M. A.; Rivas, J.; Guerrero, M. G., Accumulation of astaxanthin and lutein in *Chlorella zofingiensis* (Chlorophyta). *Applied microbiology and biotechnology* **2004**, *64*, 848-854.
6. Bar, E.; Rise, M.; Vishkautsan, M.; Arad, S., Pigment and structural changes in *Chlorella zofingiensis* upon light and nitrogen stress. *Journal of plant physiology* **1995**, *146*, 527-534.
7. Orosa, M.; Torres, E.; Fidalgo, P.; Abalde, J., Production and analysis of secondary carotenoids in green algae. *Journal of applied phycology* **2000**, *12*, 553-556.
8. Huang, J. C.; Wang, Y.; Sandmann, G.; Chen, F., Isolation and characterization of a carotenoid oxygenase gene from *Chlorella zofingiensis* (Chlorophyta). *Applied microbiology and biotechnology* **2006**, *71*, 473-479.
9. Wang, Y.; Chen, T., The biosynthetic pathway of carotenoids in the astaxanthin-producing green alga *Chlorella zofingiensis*. *World Journal of microbiology and biotechnology* **2008**, *24*, 2927-2932.

10. Bauch, M. E. Identifizierung und Quantifizierung der Ketocarotinoide in Dauerstadien von Grünalgen und Ketocarotinoidbiosynthese im Modellorganismus *Chlamydomonas reinhardtii*. Johannes Gutenberg-Universität, Mainz, Germany **2011**.
11. Harker, M.; Young, A. J., Inhibition of astaxanthin synthesis in the green-alga, *Haematococcus pluvialis*. *European Journal of Phycology* **1995**, *30*, 179-187.
12. Fan, L.; Vonshak, A.; Gabbay, R.; Hirshberg, J.; Cohen, Z.; Boussiba, S., The biosynthetic pathway of astaxanthin in a green alga *Haematococcus pluvialis* as indicated by inhibition with diphenylamine. *Plant and cell physiology* **1995**, *36*, 1519-1524.
13. Collins, A. M.; Jones, H. D. T.; Han, D.; Hu, Q.; Beechem, T. E.; Timlin, J. A., Carotenoid distribution in living cells of *Haematococcus pluvialis* (Chlorophyceae). *PLoS ONE* **2011**, *6*(9), e24302.
14. Zhekisheva, M.; Zarka, A.; Khozin-Goldberg, I.; Cohen, Z.; Boussiba, S., Inhibition of astaxanthin synthesis under high irradiance does not abolish triacylglycerol accumulation in the green alga *Haematococcus pluvialis* (Chlorophyceae). *Journal of phycology* **2005**, *41*, 819-826.
15. Jin, E.; Lee, C. G.; Polle, J. E. W., Secondary carotenoid accumulation in *Haematococcus* (Chlorophyceae): Biosynthesis, regulation, and biotechnology. *Journal of microbiology and biotechnology* **2006**, *16*, 821-831.
16. Kanehisa Laboratories, Kegg pathway database. <http://www.genome.jp/kegg/pathway.html>. Last accessed **25 Jul 2013**.
17. Lemoine, Y.; Schoefs, B., Secondary ketocarotenoid astaxanthin biosynthesis in algae: a multifunctional response to stress. **2010**, *106*, 155-177.
18. Vidhyavathi, R.; Venkatachalam, L.; Sarada, R.; Ravishankar, G. A., Regulation of carotenoid biosynthetic genes expression and carotenoid accumulation in the green alga *Haematococcus pluvialis* under nutrient stress conditions. *Journal of experimental botany* **2008**, *59*, 1409-1418.
19. Kliphuis, A. M. J.; Janssen, M.; van den End, E. J.; Martens, D. E.; Wijffels, R. H., Light respiration in *Chlorella sorokiniana*. *Journal of applied phycology* **2011**, *23*, 935-947.
20. Breuer, G.; Evers, W. A. C.; de Vree, J. H.; Kleinegris, D. M. M.; Martens, D. E.; Wijffels, R.; H; Lamers, P. P., Analysis of fatty acid content and composition in microalgae. *Journal of visualized experiments* **2013**, e50628.
21. Breuer, G.; Lamers, P. P.; Martens, D. E.; Draaisma, R. B.; Wijffels, R. H., The impact of nitrogen starvation on the dynamics of triacylglycerol accumulation in nine microalgae strains. *Bioresource technology* **2012**, *124*, 217-226.
22. Lamers, P. P.; van de Laak, C. C. W.; Kaasenbrood, P. S.; Lorier, J.; Janssen, M.; De Vos, R. C. H.; Bino, R. J.; Wijffels, R. H., Carotenoid and fatty acid metabolism in light-stressed *Dunaliella salina*. *Biotechnology and bioengineering* **2010**, *106*, 638-648.
23. Britton, G., Chapter 2: UV/Visible spectroscopy. In: *Carotenoids Vol. 1B Spectroscopy*, Edited by: Britton G., Liaaen-Jensen S., Pfander H., Birkhäuser Verlag, Basel, Switzerland **1995**, pp. 13-62.
24. Egeland, E. S., Part VII: Data sheets aiding identification of phytoplankton carotenoids and chlorophylls. In: *Phytoplankton pigments: characterization, chemotaxonomy, and applications in oceanography*. Roy, S., Llewellyn C.A., Egeland, E.S., Johnsen, G. Cambridge University Press, New York, NY, USA **2011**, pp. 665-822.
25. Britton, G.; Liaaen-Jensen, S.; Pfander, S., *Carotenoids Handbook*. Birkhäuser Verlag, Basel, Switzerland **2004**.
26. Enzell, C. R.; Francis, G. W.; Liaaen-Jensen, S., Mass spectrometric studies of carotenoids. 2. A survey of fragmentation reactions. *Acta chemica Scandinavia* **1969**, *23*, 727-750.
27. Enzell, C. R.; Back, S., Chapter 7: Mass spectrometry. In: *Carotenoids Vol. 1B Spectroscopy*, Edited by Britton G., Liaaen-Jensen S., Pfander H., Birkhäuser Verlag, Basel, Switzerland **1995**, pp. 261-320.

28. Frassanito, R.; Cantonati, M.; Flaim, G.; Mancini, I.; Guella, G., A new method for the identification and the structural characterisation of carotenoid esters in freshwater microorganisms by liquid chromatography/electrospray ionisation tandem mass spectrometry. *Rapid communications in mass spectrometry* **2008**, *22*, 3531-3539.
29. Weesepoel, Y.; Vincken, J.-P.; Pop, R. M.; Liu, K.; Gruppen, H., Sodiation as a tool for enhancing the diagnostic value of MALDI-TOF/TOF-MS spectra of complex astaxanthin ester mixtures from *Haematococcus pluvialis*. *Journal of mass spectrometry* **2013**, *48*, 862-874.
30. Orosa, M.; Valero, J. F.; Herrero, C.; Abalde, J., Comparison of the accumulation of astaxanthin in *Haematococcus pluvialis* and other green microalgae under N-starvation and high light conditions. *Biotechnology letters* **2001**, *23*, 1079-1085.
31. Dall'Osto, L.; Lico, C.; Alric, J.; Giuliano, G.; Havaux, M.; Bassi, R., Lutein is needed for efficient chlorophyll triplet quenching in the major LHCII antenna complex of higher plants and effective photoprotection in vivo under strong light. *BMC plant biology*. **2006**, *6*:32.
32. Falkowski, P. G.; Raven, J. A., *Aquatic photosynthesis*, 2nd edition. Princeton University Press, Princeton, New Jersey, United Kingdom, **2007**, 484 pp.
33. Sukenik, A.; Livne, A.; Neori, A.; Yacobi, Y. Z.; Katcoff, D., Purification and characterization of a light-harvesting chlorophyll-protein complex from the marine Eustigmatophyte *Nannochloropsis* sp. *Plant cell physiology* **1992**, *33*, 1041-1048.
34. Mulders, K. M.; Weesepoel, Y.; Lamers, P.; Vincken, J.-P.; Martens, D.; Wijffels, R., Growth and pigment accumulation in nutrient-depleted *Isochrysis* aff. *galbana* T-ISO. *Journal of applied phycology* **2013**, 1-10.
35. Goss, R.; Jakob, T., Regulation and function of xanthophyll cycle-dependent photoprotection in algae. *Photosynthesis research* **2010**, *106*, 103-122.
36. Jahns, P.; Holzwarth, A. R., The role of the xanthophyll cycle and of lutein in photoprotection of photosystem II. *Biochimica et biophysica acta - bioenergetics* **2012**, *1817*, 182-193.
37. Vila, M.; Galvan, A.; Fernandez, E.; Leon, R., Ketocarotenoid biosynthesis in transgenic microalgae expressing a foreign beta-C-4-carotene oxygenase gene. *Methods in molecular biology* **2012**, *892*, 283-95.
38. Grunewald, K.; Hirschberg, J.; Hagen, C., Ketocarotenoid biosynthesis outside of plastids in the unicellular green alga *Haematococcus pluvialis*. *Journal of biological chemistry* **2001**, *276*, 6023-6029.

SUPPLEMENTARY INFORMATION

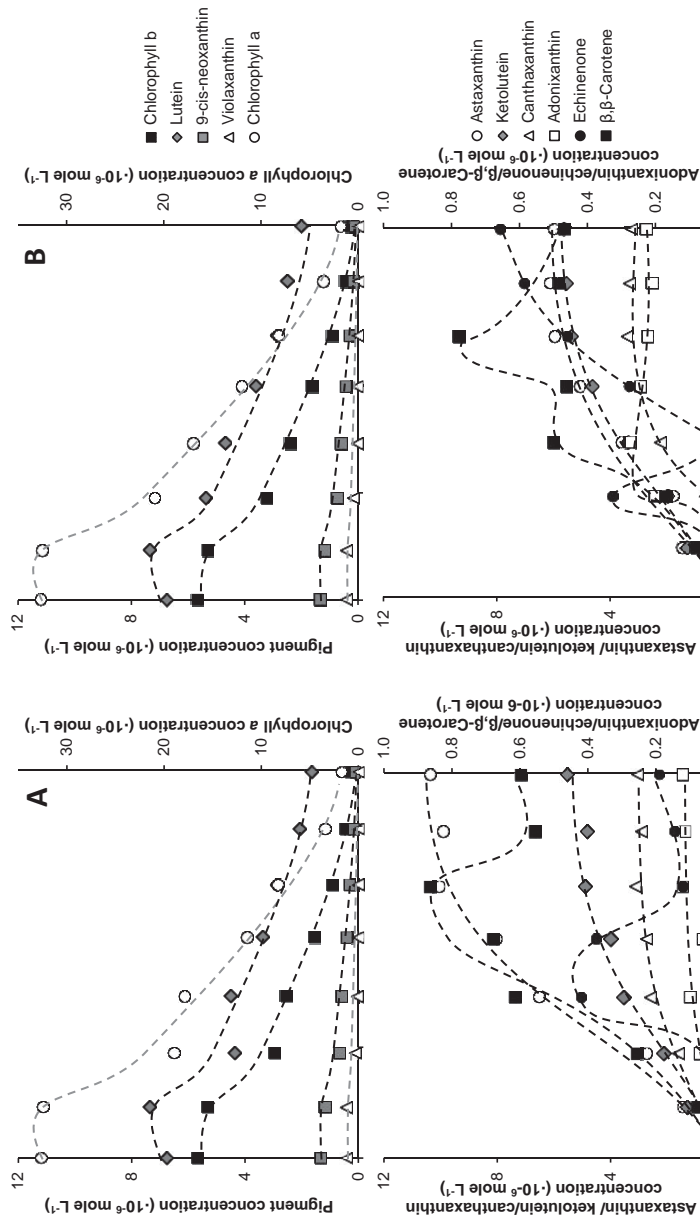


Figure S1. Time courses of chlorophyll a, chlorophyll b, lutein, 9'-cis-neoxanthin, violaxanthin, total astaxanthin (sum of free, mono- and diesters), total ketolutein (sum of free, mono- and diesters), canthaxanthin, adonixanthin, echinenone and β - β -carotene in moles per litre culture volume of nitrogen-depleted *C. zoefingensis* exposed to A no DPA (control) and exposed to B repeated additions of DPA resulting each time in a concentration increase of 60 μM . Data points represent averages of biological duplicates. For separate data points see Fig. 5 and 6. Solid triangles in B indicate DPA additions. Lines are for visual guidance.

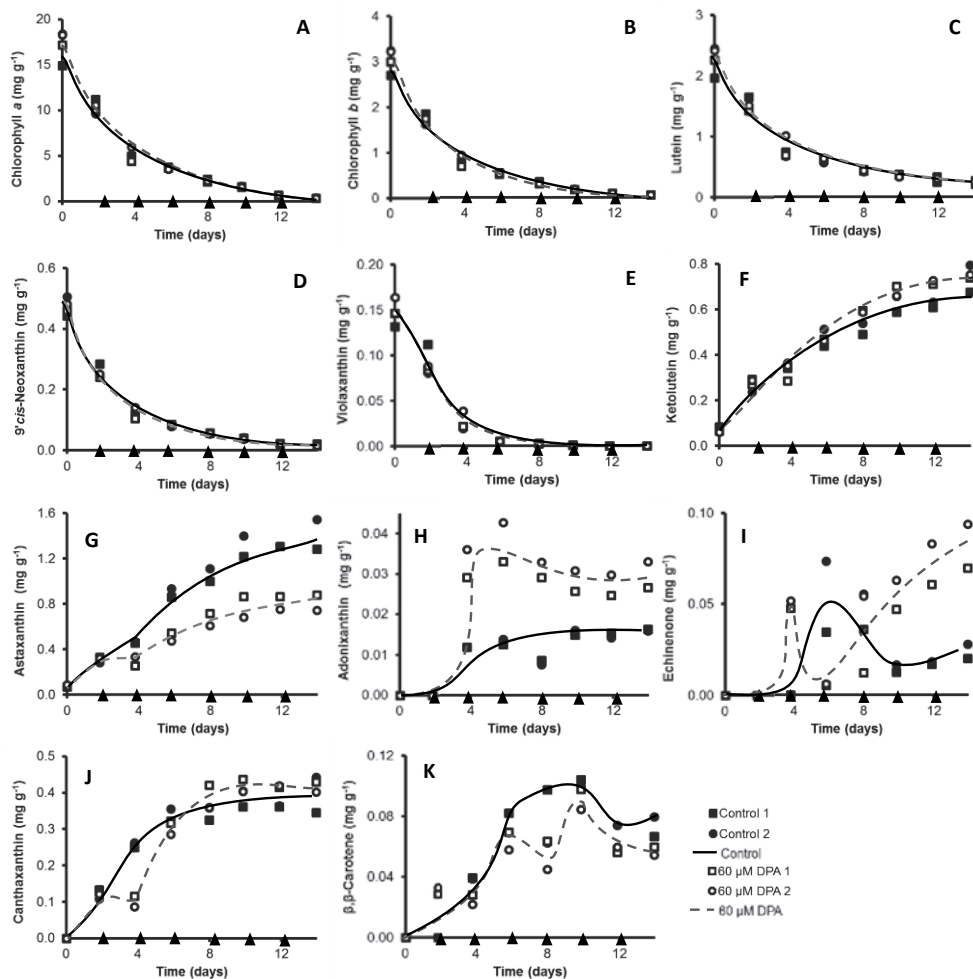


Figure S2. Contents (in mg/g DW) of **A** chlorophyll *a*, **B** chlorophyll *b*, **C** lutein, **D** 9'*cis*-neoxanthin, **E** violaxanthin, **F** total ketolutein (sum of free, mono- and diesters), **G** total astaxanthin (sum of free, mono- and diesters), **H** adonixanthin, **I** echinenone, **J** canthaxanthin and **K** β,β-carotene of nitrogen-depleted *C. zofingiensis* exposed to no DPA (control) and exposed to repeated additions of DPA resulting each time in a concentration increase of 60 μM. Triangles indicate DPA additions. Lines are for visual guidance.

Chapter 4

Analysis of palmitoyl apo-astaxanthinals, apo-astaxanthinones, and their epoxides by UHPLC-PDA-ESI-MS

A new reversed phase ultra-high performance liquid chromatography (RP-UHPLC) with photo diode array (PDA) and positive mode *in-line* electrospray ionization mass spectrometric (ESI-MS) detection was developed for simultaneous identification of apo-astaxanthins and fatty acid-esterified apo-astaxanthins. To obtain representative astaxanthin degradation products, free astaxanthin, as well as astaxanthin with one or two palmitate esters, were subjected to two different degradation processes in a methanolic model system: (i) Light-accelerated autoxidation, representing processing and storage conditions of products, and (ii) hypochlorous acid/hypochlorite (HOCL/OCl⁻) bleaching, which occurs in the blood circulation upon inflammatory reactions. Apo-astaxanthinals and -ones containing 3 (apo-9) to 10 (apo-8') conjugated double bonds were found upon light-accelerated autoxidation for all three types of astaxanthin (with exception of free apo-8-astaxanthinal). Fragmentation of the [M+H]⁺ and [M+Na]⁺ parent masses of the apo-astaxanthins from the dipalmitate astaxanthin indicated that they were all esterified with palmitate. Astaxanthin monopalmitate light-accelerated autoxidation resulted in a mixture of free and esterified apo-astaxanthinals and -ones. The ester bond attaching the fatty acid was hardly affected by autoxidation. HOCL/OCl⁻ bleaching rapidly converted the astaxanthin into a mixture of epoxy-apo-9- and epoxy-apo-13-astaxanthinones. Blue-shifts compared to their non-epoxidized apo-astaxanthinone forms indicated that for the apo-13-astaxanthinone, the epoxide group was in the 5,6-epoxide configuration. Furthermore, apo-11-, 15-, 14'- and 12'-astaxanthinals were traced. With HOCL/OCl⁻ bleaching, the ester bond of the apo-astaxanthin palmitoyl esters was degraded as was observed for the diesters. In conclusion, RP-UHPLC-PDA-ESI-MS was found to be a powerful tool for assessing astaxanthin degradation products, even when formed in trace amounts.

Based on: Weesepeel, Y., Gruppen, H., de Bruijn, W., Vincken, J.-P., Analysis of palmitoyl apo-astaxanthinals, apo-astaxanthinones, and their epoxides by UHPLC-PDA-ESI-MS, *Submitted to Journal of agricultural and food chemistry*.

INTRODUCTION

For many years, addition of artificially produced carotenoids to food products has been common practice in the food industry. Recent market demands towards natural substitutes have stimulated research on obtaining and utilising carotenoids of natural origin. Algae, like *Haematococcus pluvialis*, can be used for producing these natural carotenoids (1). *H. pluvialis* produces the red carotenoid astaxanthin (3,3'-dihydroxy- β,β -carotene-4,4'-dione, **Figure 1**) in 2 to 3% (w/w) dry weight (dw) quantities. Different from its chemically synthesized astaxanthin analogue, *H. pluvialis*' astaxanthin predominantly exists of mono- and diesterified fatty acid forms, 70-90% and 5-25% (w/w) dw, respectively (2, 3).

Carotenoids are regarded as powerful antioxidants, which degrade during processing and dietary uptake of foods. This process has been investigated especially for β,β -carotene. Various types of degradation reactions are associated with food processing and dietary uptake and evidently result in many degradation products (4). In **Figure 1**, three reactions, generally known to occur upon carotenoid degradation, are putatively projected on astaxanthin (esters). Cleavage of conjugated double bonds (CDBs) results in a series of apo-astaxanthin (astaxanthins with a shortened carbon skeleton) aldehydes and ketones (Reaction 1, R1a and b, respectively). Depending on which CDB is disrupted, a pair of aldehydes (R1a) or a ketone and an aldehyde (R1b) is formed. Epoxidation of the 5-6 CDB of astaxanthin can result in 5,6-epoxy-astaxanthins (Reaction 2a, R2a). This process can also yield 5,8-furanoid-astaxanthins, which can be formed directly, or via acidic rearrangement from the 5,6-epoxide form (R2b). Furthermore, the cleavage of the fatty acid ester might result in free astaxanthin or astaxanthin monoester (Reaction 3, R3). Finally, the degradation products resulting from R1, R2 and R3 can undergo additional degradation via reactions R1 and/or R2, until they end up as structures with little resemblance to the original carotenoid (4-8). Also *cis-trans* isomerisation might be regarded as a degradation reaction, but is not further considered here (4).

A common carotenoid degradation reaction that results in R1 and R2 degradation products is oxidation. A relatively mild form of oxidation, occurring during product processing and storage, is autoxidation. This reaction can occur spontaneously and is accelerated by light sensitization, oxygen and/or elevated temperatures. During autoxidation the CDBs of the carotenoid chromophore are reduced or cleaved, resulting in numerous products. Autoxidation is generally believed to proceed via carbon-peroxyl *triplet* radicals, which propagate the reaction via intramolecular homolytic substitution (9). In contrast, a relatively aggressive oxidative agent is hypochlorous acid (HOCl). In the human body, HOCl can be formed upon inflammatory reactions by the enzyme myeloperoxidase in polymorphonuclear leukocytes (10). There, HOCl is primarily produced to eliminate harmful bacteria

and/or toxins, but it is also known to damage surrounding tissue (11, 12). Also, the dietary carotenoids present in the bloodstream (13, 14) can be converted by HOCl into oxidation products that might be toxic (15, 16). HOCl occurs in equilibrium with its corresponding base OCl⁻ and together they are referred to as HOCl/OCl⁻ or hypochlorite. The reaction products formed from β,β -carotene by hypochlorite bleaching were β -apo-13-carotenone, β -apo-15-carotenal and β -apo-14'-carotenal. Furthermore, smaller volatiles derived from C7-C8 (*e.g.* β -cyclocitral) and C9-10 (*e.g.* β -ionone, dihydroactinidiolide) cleavages were found (17, 18).

Unlike β,β -carotene, xanthophylls (oxygenated carotenoids), comprising amongst others astaxanthin, canthaxanthin, lutein, and zeaxanthin, have neither gained much attention with respect to autoxidation nor hypochlorite bleaching. Furthermore, the fate of the fatty acid ester has not been assessed. For hypochlorite bleaching, it has been reported that the xanthophylls lutein, zeaxanthin, α -cryptoxanthin, β -cryptoxanthin and anhydrolutein were degraded, but no reaction products were described (19). Upon oxidation of canthaxanthin by nickel peroxide mainly apo-canthaxanthinals and -ones were found (20). It was also shown that upon autoxidation of free astaxanthin a series of apo-astaxanthinals and -ones were found with apo-13-astaxanthinone as the main reaction product (21). Treatment by peroxyxynitrite resulted in a mixture of apo-astaxanthins and nitro-astaxanthins (22). The stability of the ester bond, connecting astaxanthin and a fatty acid, has never been assessed using light-accelerated autoxidation or hypochlorite bleaching, although the deliberate removal of the fatty acid by means of methanolic saponification and lipases has been reported (23, 24).

As a consequence of esterification with fatty acids, the number of potential xanthophyll oxidative degradation products is expected to be larger than that for non-esterified xanthophylls. Therefore, this study reports on the analysis of apo-astaxanthin mixtures by a new method comprising reversed phase ultra-high performance liquid chromatography (RP-UHPLC) in combination with *in-line* electrospray ionization mass spectrometry (ESI-MS). For triggering the formation of reaction products through the various routes R1a and b, R2a and b and R3, light-accelerated autoxidation and hypochlorite bleaching was performed on astaxanthin, astaxanthin monopalmitate ester, and astaxanthin dipalmitate ester. The experiments were performed in pure solvent to minimize matrix effects.

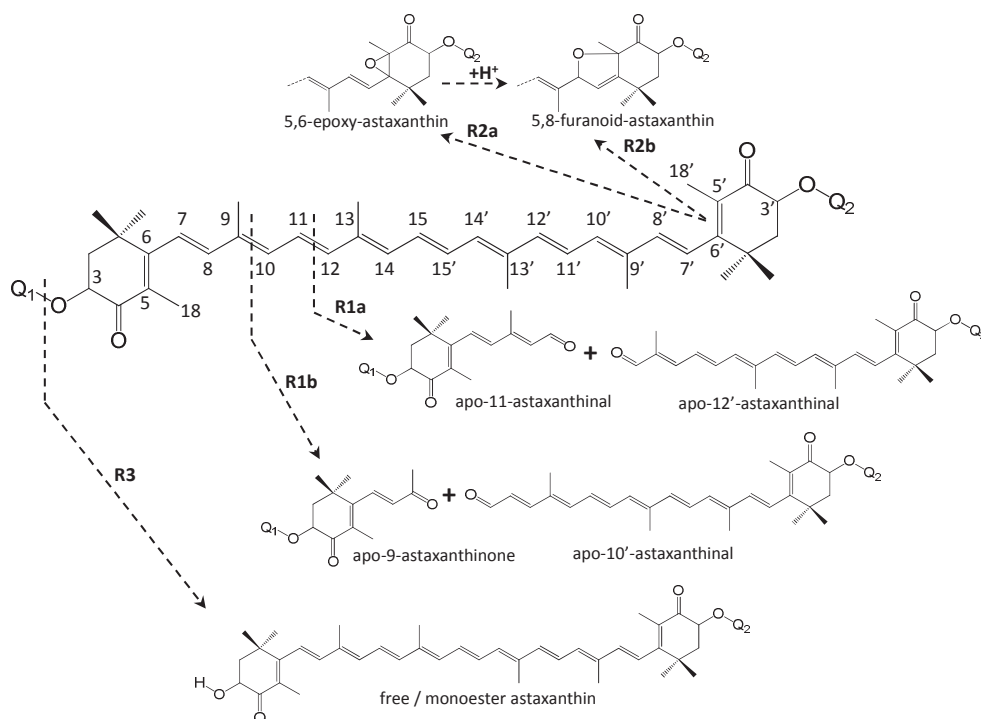


Figure 1. Chemical structure astaxanthin and examples of degradation reactions and products. Reaction 1 (**R1a** and **b**) CDB cleavage, Reaction 2 (**R2a** and **b**) 5,6-epoxide and 5,8-furanoid formation, Reaction 3 (**R3**) de-esterification. Free astaxanthin: $Q_1 = Q_2 = H$, astaxanthin monopalmitate: $Q_1 = (C=O)-C_{15}H_{31}$ and $Q_2 = H$, astaxanthin dipalmitate: $Q_1 = Q_2 = (C=O)-C_{15}H_{31}$.

MATERIALS AND METHODS

Materials

(3*RS*)-Apo-12'-astaxanthinal (>98% w/w), (3*RS*,3'*RS*)-astaxanthin (97% w/w), (3*RS*,3'*RS*)-astaxanthin monopalmitate (97% w/w), and (3*RS*,3'*RS*)-astaxanthin dipalmitate (98% w/w) were purchased from Carotenature (Lupsingen, Switzerland). ULC/MS grade methanol absolute ($\geq 99.9\%$ w/w), acetonitrile ($\geq 99.9\%$ w/w), water and formic acid (99% w/w), AR grade ethyl acetate (99.8% w/w), and HPLC grade chloroform ($\geq 99.9\%$ v/v, corrected for stabilizer, stabilized by 0.5-1.5% (w/v) ethanol) were purchased from Biosolve (Valkenswaard, The Netherlands). Sodium hypochlorite solution (active Cl 12.3% - 14.9% w/v) in H_2O was purchased from Carl Roth (Karlsruhe, Germany).

Preparation of carotenoid stock solutions

Apo-12'-astaxanthinal, free astaxanthin, astaxanthin monopalmitate and astaxanthin dipalmitate were separately dissolved in chloroform. All stock solution concentrations were determined spectrophotometrically in hexane:chloroform (minimum 98% v/v *n*-hexane). Astaxanthin concentrations were determined at 470 nm using the absorption coefficient $A_{1\text{cm}}^{1\%}$ of 2100 L g⁻¹ cm⁻¹ (25). For astaxanthin monopalmitate and dipalmitate concentrations were subsequently corrected for the difference in molecular weight, assuming that the fatty acid moiety did not contribute to absorption, yielding values of $A_{1\text{cm}}^{1\%}$ 1501 and 1167 L g⁻¹ cm⁻¹, respectively. For apo-12'-astaxanthinal concentrations were determined at 421 nm using the $A_{1\text{cm}}^{1\%}$ of 2276 (26).

Light-accelerated autoxidation

Free astaxanthin, astaxanthin monopalmitate, and astaxanthin dipalmitate were separately diluted in methanol to concentrations of 18.0, 19.6 and 24.0 μM respectively. Aliquots (1.5 mL) were transferred to quartz cuvettes (type 114-QS, Hellma Analytics, Müllheim, Germany) closed with stoppers. A headspace of approximately 50 μL was left, filled with atmospheric air. Three cuvettes for each type of astaxanthin were irradiated for 3 h in a Suntest XLS+ (Atlas MTS, Chicago, IL, USA) equipped with a 1700 W Xenon Arc lamp and window glass filter. Irradiation energy was set to 30 W m⁻² and black standard temperature was maintained at 79 °C, which corresponded to a methanol sample temperature of 55 °C. The triplicates were pooled per type of astaxanthin and evaporated to dryness under a stream of nitrogen. Next, samples were re-dissolved in ethyl acetate and subsequently supplemented with acetonitrile to reach a ratio of ethyl acetate:acetonitrile 1:3 (v/v). Prior to UHPLC injection, samples were filtered using Whatman Rezist 13 0.45 μm PTFE syringe filters (GE Life Sciences, Fairfield, CT, USA).

Hypochlorite bleaching

Bleaching of astaxanthin with hypochlorite was adapted from (15). Free astaxanthin, astaxanthin monopalmitate, and astaxanthin dipalmitate were diluted in 900 μL methanol to concentrations of 30.3, 32.9 and 40.4 μM respectively. Subsequently, degradation was carried out by addition of 65 μL of approximately 12% (w/v) NaOCl solution and incubating for 10 min at room temperature in daylight. Estimation of the decrease in absorbance at 470 nm in time was made by comparison with a methanol/hypochlorite blank. Subsequently, the methanol layer was extracted three times using 900 μL *n*-hexane each time. The *n*-hexane layers were pooled and evaporated to dryness under a stream of nitrogen in the dark. Rearrangement of 5,6-epoxides into 5,8-furanoids was performed by dissolving the evaporated hexane layer in 2.0 mL of 100 % (v/v) ethanol. Eight hundred μL of the ethanol resolved

degradation products was acidified with 50 μL 0.1 M HCl (27, 28). Prior to UHPLC analysis, samples were prepared as for light-accelerated autoxidation.

RP-UHPLC-PDA-ESI-MS analysis of degradation products

Separation and identification of carotenoid degradation products was carried out using a Thermo Accela UHPLC system (Thermo Scientific, San Jose, CA, USA) equipped with pump, degasser, auto sampler and photo diode array (PDA) detector and coupled *in-line* to a LTQ-Velos double ion trap mass spectrometer equipped with a heated ESI probe (Thermo Scientific). Samples were injected onto an Acquity UPLC BEH Shield RP18 column (2.1 x 150 mm, 1.7 μm particle size; Waters, Milford, MA, USA) fitted to a Vanguard pre-column (2.1 x 5 mm, 1.7 μm particle size; Waters). The flow rate was 300 $\mu\text{L min}^{-1}$, operated at 23°C. The eluents used were the following: 1% (v/v) acetonitrile in millipore water (A), acetonitrile (B) and ethyl acetate (C), all containing 0.10% (v/v) formic acid as a mobile phase modifier. The elution program was started from 95% (v/v) A, 5% (v/v) B and followed by 0-20 min – linear gradient to 100% (v/v) B; 20-25 min – isocratic at 100% (v/v) B; 25-32 min – linear gradient to 100% (v/v) C; 32-35 min – isocratic at 100% (v/v) C. The eluent was adjusted to its initial composition in 10 min, followed by equilibration for 5 min. Detection wavelengths for UV-Vis were set at 280 ± 0.5 nm, 370 ± 0.5 nm and 450 ± 0.5 nm. Data were recorded at 10 Hz.

Mass spectrometric data were recorded in positive ion mode. Nitrogen was used as both sheath (30 arbitrary units) and auxiliary gas (10 arbitrary units). Settings of the mass spectrometer were tuned by 3 $\mu\text{L min}^{-1}$ direct injection of apo-12'-astaxanthinal in a mixture of ethyl acetate:acetonitrile 1:3 (v/v). Most settings were optimized via automatic tuning by using LTQ Tune Plus 2.7 (Thermo Scientific). Temperature of the ion transfer tube was 450 °C and the source voltage 3.5 kV. Data were recorded over the *m/z* segments 150-350 (0.50-10.00 min), 250-500 (10.00-15.40 min), 350-500 (15.40-19.00 min), 420-680 (19.00-23.00 min), 400-575 (23.00-24.40 min), 400-590 (24.40-24.95 min), 542-650 (24.95-26.80 min), 615-720 (26.80-29.30 min) and 615-1250 (29.30-37.00 min). Within these segments dynamic data-dependent MS² fragmentation was performed on the most intense parent ion ($x = 1$) and subsequently on the second most intense parent ($x = 2$). Dynamic exclusion was used to identify co-eluting apo-astaxanthins. Also it served the purpose of fragmenting both $[\text{M}+\text{H}]^+$ and $[\text{M}+\text{Na}]^+$ spectra within one chromatographic peak. A repeat count of two MS² spectra per parent ion and a maximum of $x = 25$ or within a time frame of 5.0 s were used as settings. The collision-induced dissociation was set to 35%. Data acquisition and reprocessing were done with Xcalibur 2.2 (Thermo Scientific).

RESULTS AND DISCUSSION

Time course of colour loss of various astaxanthins

The astaxanthin degradation was performed by light-accelerated autoxidation via exposure to high intensity light conditions and elevated temperatures. Conventional autoxidation in darkness at lower temperatures could take up to several weeks (29). Exposure of the parental all-*trans* forms of the three types of astaxanthin to light-accelerated autoxidation decreased the absorption at 470 nm (**Figure 2A**). After 180 min of exposure, a decrease of 13% for the free astaxanthin was observed, 30% of the monoester and 44% of the diester. Subsequently, UHPLC-PDA-ESI-MS was used to assess the degradation products formed. As it is known that β,β -carotene forms small volatile compounds upon extensive degradation (8, 9), our degradation experiments were terminated with a high proportion of residual parent material, so that an overview of intermediate degradation products would be obtained. After 45 min, the absorption of the free astaxanthin and monoester was not reduced (**Figure 2A**). Their absorption spectra only showed a hypsochromic shift of 3-5 nm (data not shown). In contrast, the diester already showed a decrease in A_{470} of 14% within 45 min. This indicated that esterification can influence colour stability, which has also been reported before (30, 31).

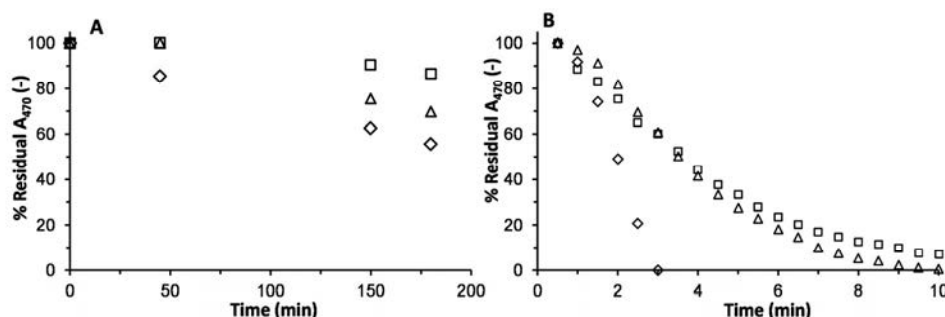


Figure 2. Decrease in visible absorption of various astaxanthins subjected to **A** light-accelerated autoxidation and **B** hypochlorite bleaching over time at 470 nm followed by spectrophotometry. Free astaxanthin (\square); astaxanthin monopalmitate (\triangle); astaxanthin dipalmitate (\diamond).

The three types of astaxanthin were also exposed to bleaching with astaxanthin : HOCl ratios in the range of 1 : 3.5 and 1 : 5.0 (*mol/mol*). These ratios were reported to occur (locally) in inflamed tissues in the body (18). The three types of astaxanthins all showed a ~100% decrease in A_{470} upon bleaching, within 10 min (**Figure 2B**). This indicated that the reaction approached the end-point. No noticeable differences in stability between the free and monopalmitate astaxanthin degradation were observed, whereas the dipalmitate astaxanthin showed a more rapid degradation, as was also observed with light-accelerated autoxidation. No plausible

explanation for this difference could be provided. Due to the different conditions applied for the light-accelerated autoxidation and hypochlorite bleaching, they resulted in different sets of degradation products to test the analysis method.

Free apo-astaxanthinals and apo-astaxanthinones (R1a-b)

The absorbance maxima of the various degradation products of astaxanthin (esters) were expected to be related to the number of CDBs present in the molecules. In order to detect the widest array of apo-astaxanthins possible by PDA, detection wavelengths were set at 450, 380 and 280 nm. Using these three wavelengths, upon light-accelerated autoxidation a plethora of peaks was found of which 44 could be tentatively annotated (**Figure 3** and **Table 1**). Free apo-astaxanthinals and -ones were found at different detection wavelengths and eluted between approximately 7.0 and 18.0 min. For the astaxanthin dipalmitate samples no PDA response was observed, indicating that no free apo-astaxanthinals and -ones were formed. A first ascertainment of the apo-astaxanthinals and -ones was done by locating their predicted m/z values with the full scan MS data accompanying a chromatographic peak (**Table 1**). Using this approach, the matching protonated parent masses ($[M+H]^+$) for apo-9- and apo-13-astaxanthinone, apo-11-, apo-15-, apo-14'-, apo-12'- and apo-10'-astaxanthinal were found upon treatment of both free and monopalmitate astaxanthin. The accompanying absorption spectra of these apo-astaxanthins had increasing λ_{\max} values from apo-9-astaxanthinone (260-270 nm) to apo-10'-astaxanthinal (452 nm). The smallest aldehyde, apo-7-astaxanthinal, was probably also formed. However, our approach will not visualize this compound due to its limited conjugated system and/or likely volatile properties. Nevertheless, the MS trace showed $[M+H]^+$ (m/z 183) values that could potentially be associated with apo-7-astaxanthinal, but no diagnostic MS^2 fragments could be obtained for a reliable annotation.

The identification was further verified by analysing MS^2 fragmentation of all $[M+H]^+$ parents annotated and comparison with the MS^2 spectrum of the apo-12'-astaxanthinal standard, which had similar retention time, parent mass and MS^2 fragmentation as the apo-12'-astaxanthinal formed (peak 12) in our degradation study. The MS^2 spectra of the apo-astaxanthinals and -ones all showed similar fragmentation behaviour upon CID fragmentation (**Table S1**). In **Figure 4A** fragmentation of apo-12'-astaxanthinal is displayed as an example. The most intense neutral loss in the MS^2 spectra of the free apo-astaxanthinals and -ones was 18 Da yielding the fragment m/z 363.2. The loss originates from the hydroxyl group at C3, analogous to water neutral loss with the (native) astaxanthin molecule (32). The second water loss, yielding the fragment with m/z 345.1, might have originated from the loss of the aldehyde group at C12'. Exception to this dominant water loss was found for apo-11-astaxanthinal, which showed a neutral loss of 42 Da (m/z 205) as

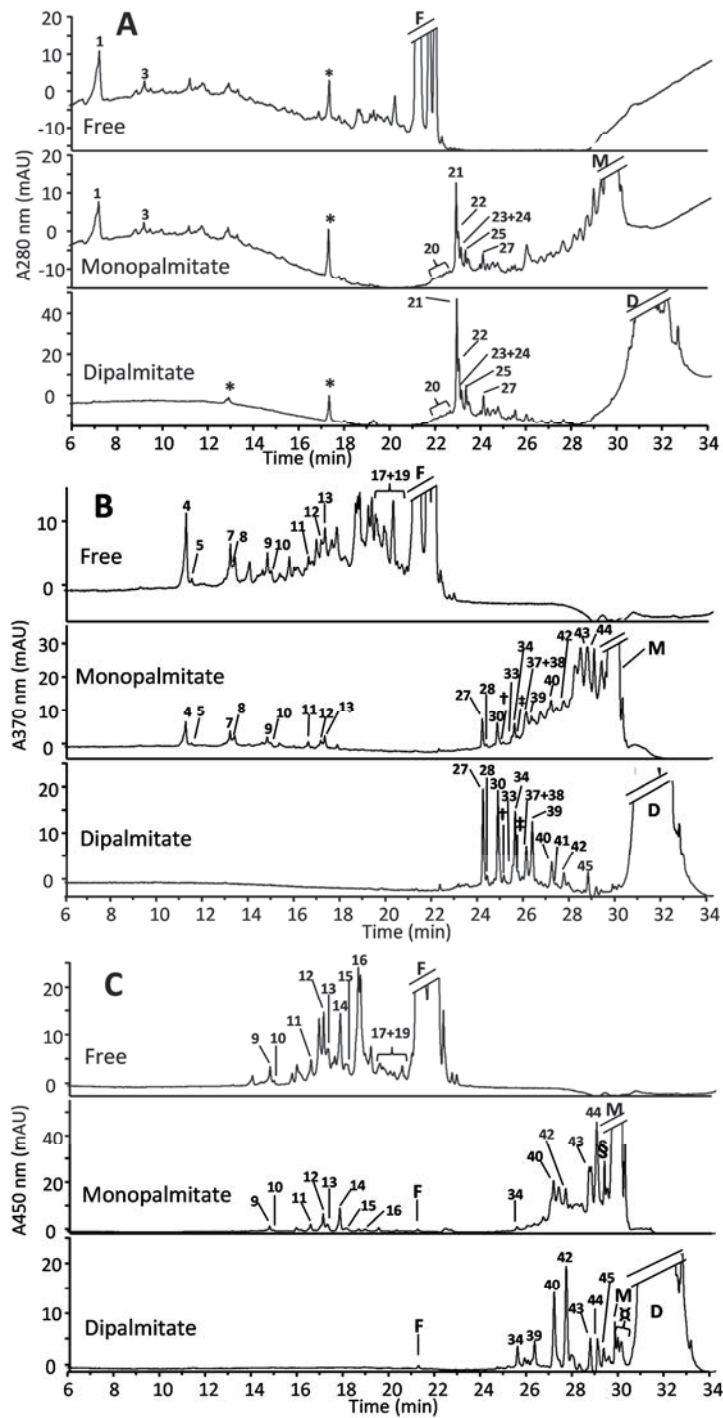


Figure 3. RP-UHPLC-UV chromatograms of free astaxanthin, its monoester and its diester in methanol after 3 h of light-accelerated degradation. **A** 280 nm; **B** 370 nm; **C** 450 nm. F = free all-*trans*- and *cis*-astaxanthin; M = all-*trans*- and *cis*-astaxanthin monoester palmitate; D = all-*trans*- and *cis*-astaxanthin diester palmitate; * = ghost peak; † = peak 29; ‡ = peak 34; § = peaks 46, 47, 48; ¶ = peaks 49, 50, 51.

Table 1. Apo-astaxanthins and epoxy-astaxanthins formed during light-accelerated autoxidation and hypochlorite degradation of free astaxanthin, astaxanthin monopalmitate and astaxanthin dipalmitate tentatively assigned by UHPLC-ESI-MS. Degradation products are divided into classes and sorted from smallest carotenoid backbone upwards. Underlined parent masses were in the $[M+Na]^+$ ionization state. Peak numbers refer to **Figure 2** and **4**. Additional MS² fragmentation data in **Table S1** and **S2**.

No.	Rt. (min)	Identification ^a	Method ^b	UV-Vis _{max} (nm)	$[M+H]^+$, $[M+Na]^+$ (m/z)	No.	Rt. (min)	Identification ^a	Method ^b	UV-Vis _{max} (nm)	$[M+H]^+$, $[M+Na]^+$ (m/z)
Apo-astaxanthin ketones											
1	7.30	Apo-9-astaxanthinone	L	260-270	223.1	2	8.71	Epoxy-apo-9-astaxanthinone	H	268-271	239.1
22	22.98	Apo-9-astaxanthinone PE	L	260-270 ^c	461.3, <u>483.3</u>	21	22.89	Epoxy-apo-9-astaxanthinone PE	L, H	260-270 ^c	477.2
23	23.10	Apo-9-astaxanthinone PE	L, H	260-270 ^c	461.3, <u>483.3</u>	26	23.37	Epoxy-apo-9-astaxanthinone PE	H	260-270 ^c	477.3
4	11.24	Apo-13-astaxanthinone	L, H	345	289.1	6	12.83	Epoxy-apo-13-astaxanthinone	H	336	305.1
5	11.49	Apo-13-astaxanthinone	L	345	289.2	29	24.67	Epoxy-apo-13-astaxanthinone PE	H	335	543.4, <u>565.3</u>
27	24.05	Apo-13-astaxanthinone PE	L, H	340	527.4, <u>549.4</u>	Epoxy-apo-astaxanthin aldehydes					
28	24.22	Apo-13-astaxanthinone PE	L	330	527.4, <u>549.4</u>	32	25.31	Epoxy-apo-15-astaxanthinal PE	H	393	569.4
Apo-astaxanthin aldehydes											
20	21.81- 22.39 ^d	Apo-7-astaxanthinal PE	L	<260	421.2, <u>443.1</u>	36	25.56	Epoxy-apo-15-astaxanthinal PE	L	401 ^c	569.4
3	9.27	Apo-11-astaxanthinal	L, H	300-305	249.1	38	25.91	Epoxy-apo-15-astaxanthinal PE	L	342 ^c	569.4
24	23.10	Apo-11-astaxanthinal PE	L, H	260-270 ^c	487.3, <u>509.3</u>	13	17.24	Epoxy-apo-12'-astaxanthinal	L	409	397.2
25	23.29	Apo-11-astaxanthinal PE	L, H	313	487.3, <u>509.3</u>	39	26.15	Epoxy-apo-12'-astaxanthinal PE	L	394	635.4
7	13.15	Apo-15-astaxanthinal	L, H	381	315.2	43	28.58	Epoxy-apo-12'-astaxanthinal PE	L	420	635.4, <u>657.4</u>
8	13.27	Apo-15-astaxanthinal	L, H	363	315.2	Epoxy-astaxanthins					
						17	18.00- 20.50 ^d	Epoxy-astaxanthin	L	N.D.	613.3

Table 1. Continued

30	24.69	Apo-15'-astaxanthinal PE	L, H	377	553.4, <u>575.4</u>	18.00-20.50 ^d	Diepoxy-astaxanthin	L	N.D.	629.3
31	24.94	Apo-15'-astaxanthinal PE	L, H	380-390 ^c	553.4, <u>575.4</u>	18.00-20.50 ^d	Triepoxy-astaxanthin	L	N.D.	645.3
9	14.75	Apo-14'-astaxanthinal	L, H	414	341.2	29.30-29.60 ^d	Epoxy-astaxanthin PE	L	400	851.6, <u>873.7</u>
10	14.92	Apo-14'-astaxanthinal	L, H	403	341.2	29.30-29.60 ^d	Diepoxy-astaxanthin PE	L	N.D.	<u>889.5</u>
34	25.43	Apo-14'-astaxanthinal PE	L, H	398 ^c	579.4, <u>601.4</u>	29.30-29.60 ^d	Triepoxy-astaxanthin PE	L	N.D.	<u>905.5</u>
35	25.54	Apo-14'-astaxanthinal PE	H	397	579.4, <u>601.4</u>	30.60-31.10 ^d	Epoxy-astaxanthin diPE	L	N.D.	1089.8
37	25.91	Apo-14'-astaxanthinal PE	L	342 ^c	579.4, <u>601.4</u>	30.60-31.10 ^d	Diepoxy-astaxanthin diPE	L	N.D.	1106.7
12	17.07	Apo-12'-astaxanthinal	L, H	429	381.2	30.60-31.10 ^d	Triepoxy-astaxanthin diPE	L	N.D.	<u>1143.8</u>
40	27.01	Apo-12'-astaxanthinal PE	L, H	430	619.4, <u>641.4</u>	Other apo-astaxanthins				
41	27.23	Apo-12'-astaxanthinal PE	H	412	619.4, <u>641.4</u>	25.34	Epoxy-apo-15'-astaxanthinoic acid PE	L	400 ^c	585.4, <u>607.4</u>
14	17.78	Apo-10'-astaxanthinal	L	452	407.2	16.53	Apo-12'-astaxanthinoic acid	L	414	397.2
15	18.05	Apo-10'-astaxanthinal	L	410	407.2	18.65	Apo-8'-astaxanthinol	L	425	449.2
42	27.54	Apo-10'-astaxanthinal PE	L	449	645.4, <u>667.5</u>					
44	28.88	Apo-8'-astaxanthinal PE	L	450	685.4					
45	29.15	Apo-8'-astaxanthinal PE	L	440	685.4					

N.D., not determined; PE, palmitate ester. ^aEpoxides can be either in the 5,6 or 5,8 configuration. ^bL, light-accelerated autooxidation; H, hypochlorite bleaching. ^cMixture of visible spectra due to co-elution. ^dNo accurate retention time could be determined.

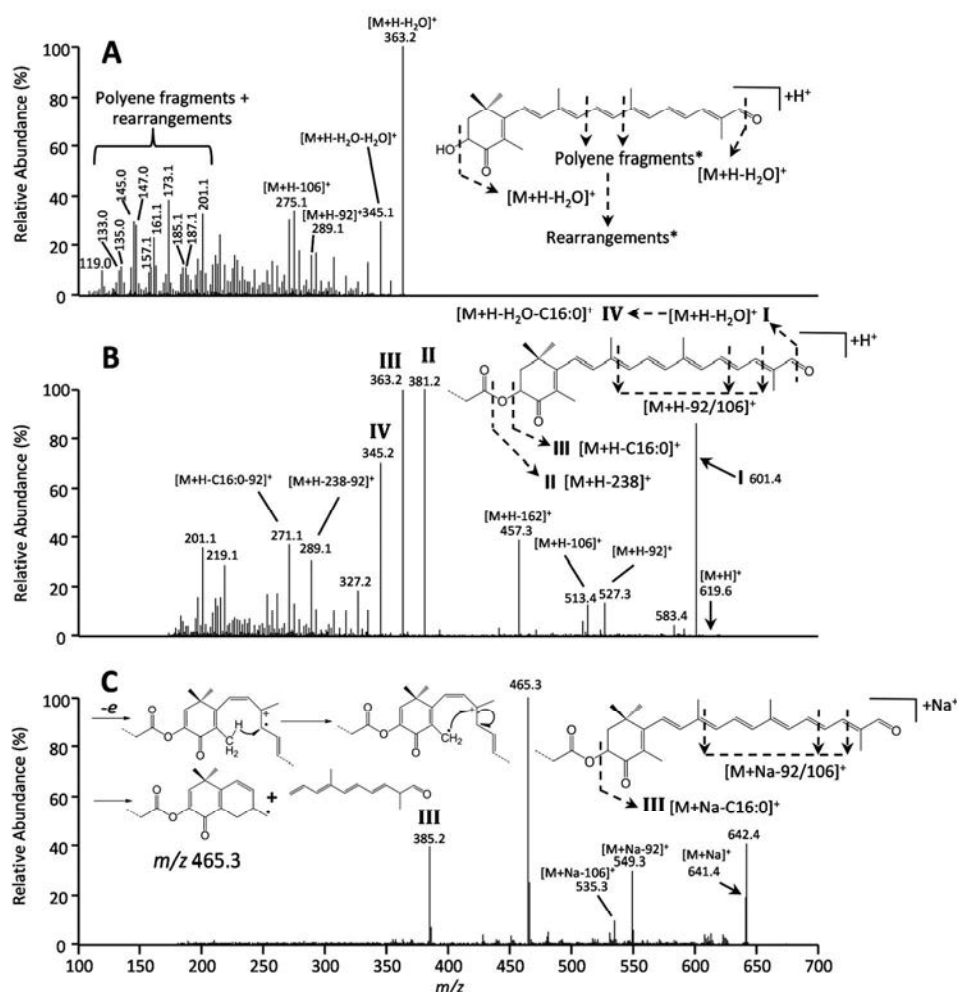


Figure 4. **A** MS² spectrum of [M+H]⁺ 12'-apo-astaxanthinal; **B** MS² spectrum of [M+H]⁺ 12'-apo-astaxanthin palmitate ester; **C** MS² spectrum of [M+Na]⁺ 12'-apo-astaxanthin palmitate ester. * = examples, fragmentation can occur at multiple C-C bonds in the polyene moiety. Roman numbers refer to MS² fragments in Table S2.

main fragment. This preference for ejecting 42 Da instead of 18 Da could not be explained. CID fragmentation of [M+H]⁺ apo-12-astaxanthinal, and all of the other free apo-astaxanthin aldehydes and ketones described, resulted in a multitude of smaller fragments, typical for carotenoids (7). In our study, these smaller fragments at *e.g.* *m/z* 201, 187, 185, 173, 161, 159, 147, 145, 135, 133 and 119 could be interpreted similarly as for apo-carotenals and -ones derived from β,β-carotene upon EI-MS, in which a saturated carbon-carbon bond is fragmented and the molecular ion is

rearranged. A series of polyene fragmentations and tandem rearrangements resulted in multiple ejections of CH_4 and CH_2 giving rise to this wide array of smaller MS^2 fragment ions (7). Fragments resulting from toluene and xylene polyene elimination products were low in abundance and could in the case of apo-12' astaxanthinal be annotated to m/z 289.1 and 275.1. Other fragment ions could not be rerouted to a fragmentation of the parent ion.

Apo-astaxanthinal and apo-astaxanthinone palmitate esters (R1a-b)

When astaxanthin monopalmitate and dipalmitate were subjected to light-accelerated autoxidation, additional peaks appeared in the hydrophobic region of the chromatogram (21.5 – 30 min) (**Figure 3**). Again, a first annotation was performed by tracing of their respective parent masses (**Table 1**). Upon assessment of the UV-vis absorption spectra of the peaks, a similar trend was observed as for the free apo-astaxanthinals and -ones (**Figure 5**). The absorption maxima were slightly deviating from previously reported λ_{max} values of purified free apo-astaxanthinals and -ones (1 – 14 nm), possibly due to the use of the different LC solvents and co-elution with other reaction products (21). This led to the conclusion that a series of apo-9- to apo-8'-astaxanthinals and -ones palmitate esters were formed.

Similar as for the astaxanthin esters, MS^2 spectra were used to identify the apo-astaxanthin backbone and the esterified fatty acid (**Table S2**) (32). As an example, the fragmentation of $[\text{M}+\text{H}]^+$ apo-12'-astaxanthinal palmitate (peak 38) is explained (**Figure 4B**). Again, water loss, yielding fragment m/z 601.4 (**I**) was observed, but this time resulting from the aldehyde or ketone group. Most abundant were the fragments at m/z 381.2 (**II**) representing the apo-12'-astaxanthinal backbone and m/z 363.2 (**III**), which represented the apo-astaxanthin that ejected C16:0. The typical polyene elimination products toluene (92 Da) and xylene (106 Da) were found at m/z 527.4 and 513.4 respectively, albeit in low intensities. Toluene and xylene neutral losses were only formed for apo-12'-astaxanthins and larger apo-astaxanthins and not for the smaller ones. Furthermore, tandem losses of water and palmitate yielded the fragment at m/z 345.2, (**IV**). Also tandem losses of palmitate ketene and toluene (yielding m/z 289.1), and palmitate and toluene (yielding m/z 271.1) were observed. Contrary to the free apo-7-astaxanthinal, molecular ions of the palmitate ester of apo-7-astaxanthinal (peak 20) could be detected between $R_t = 21.8 - 22.4$ min. Upon fragmentation of both the $[\text{M}+\text{H}]^+$ and $[\text{M}+\text{Na}]^+$ parents (m/z 421.2 and 443.1, respectively), diagnostic fragments **I**, **II** and **III** could be annotated.

As an additional confirmation of the apo-astaxanthinal and -none palmitoyl structures, esterified astaxanthin sodium adducts $[\text{M}+\text{Na}]^+$ were analysed. It has been shown that upon fragmentation, the MS^2 of sodiated ions strongly deviated from the protonated MS^2 fragmentation (32, 33). This was also the case for apo-astaxanthin palmitate esters as shown in **Figure 4C**. No fragments similar to **II** were found in this

case, only the palmitate loss **III** is visible at m/z 385.2 (for apo-7-astaxanthinal and apo-9-astaxanthinone a neutral loss of 238 Da was visible). The main fragment at m/z 465.3 represented a sodiated benzonium ion and could be explained, similarly as for astaxanthin esters, by ring closure at C18 to C9 after electron rearrangement at C5-C6 (**Inset Figure 4C**) (33, 34). Remarkably, the formation of this benzonium ion was dominant over the other fragments, and could already be observed with apo-9-astaxanthinone. As the sodiated parent mass of apo-9-astaxanthinone is m/z 483.3, one might argue that the m/z 465.4 fragment represents a simple water loss.

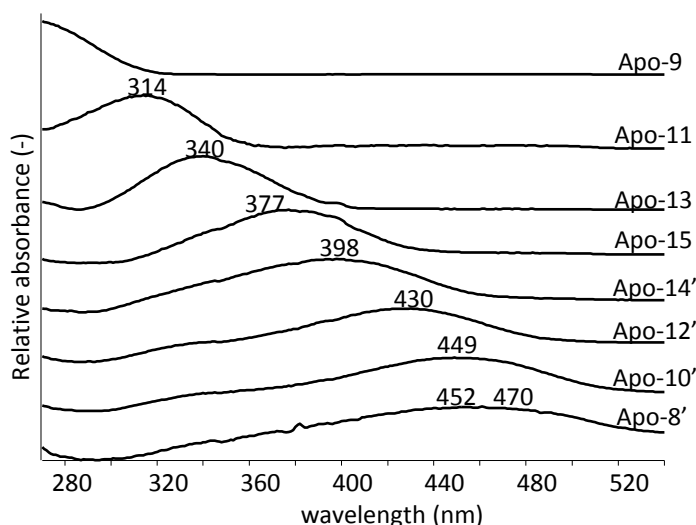


Figure 5. Overlay of UV-Vis absorbance spectra of several apo-astaxanthin palmitate ester ketones and aldehydes.

Other apo-astaxanthins and *cis*-apo-astaxanthins (R1a-b)

Besides aldehyde and keto functional groups, we also screened for apo-astaxanthinols and apo-astaxanthinoic acids. Only one apo-astaxanthinol could be annotated. Instead of the parent mass of apo-8'-astaxanthinal, an m/z of 449.2 was detected, suggestive for apo-8'-astaxanthinol (peak 16, **Table 1**, **Figure 3C**). The presence of a C7-C8 CDB apo-8'-degradation product indicated that probably the corresponding 7-apo-astaxanthin was also formed.

In **Table 1** it can be observed that multiple annotations for similar apo-astaxanthinal or -ones were made (*e.g.* peaks 5, 8, 10, 15, 39). Probably these represented different *cis*-apo-astaxanthin geometrical isomers. As also *cis*-isomers were formed from all-*trans* astaxanthin (results not shown), this conclusion seems plausible. Assignment of the geometrical isomers using blue shifts in λ_{\max} compared to the all-*trans* isomer is common practice. As these compounds were present in trace

amounts, and because it was not always possible to baseline separate degradation products in order to obtain a spectrum representing a single compound, *cis* and all-*trans* annotations were not pursued.

Epoxy-astaxanthins (R2a and b)

The formation of epoxides was observed for intact astaxanthin (esters) upon light-accelerated degradation (**Table 1**). For the free astaxanthin, parent masses associated with mono, di and tri-epoxides were found (peaks 17 – 19), eluting together with a plethora of other components just before the free astaxanthin peak F at 370 nm (**Figure 3B**). Presumably, the astaxanthin epoxides were also visible at 450 nm (**Figure 3C**), because epoxides normally show a small hypsochromic shift compared to astaxanthin as will be elaborated later. Fragmentation of the epoxides showed two consecutive water losses and again a multitude of smaller fragments, the most intense of which were annotated in **Tables S1** and **S2**. Most likely, the epoxide groups were in the 5,6-epoxide or the 5,8-furanoid position, reported predominant in autoxidation of β,β -carotene (5, 9). When the carotenoid's C5-C6 and C5'-C6' positions are occupied with epoxides, a third epoxide group might for example be located at the 15-15' position (9). Similarly, mono, di and tri-epoxides were found for astaxanthin monopalmitate (peaks 46 - 48) and dipalmitate (peaks 49 – 51) (**Table 1**, **Figure 3B-C**). Also for the monopalmitate, the formation of intact astaxanthin epoxides upon autoxidation was observed as a large hump, which made it difficult to pinpoint exact retention times.

Epoxy-apo-astaxanthinones and -astaxanthinals (R1a-b and R2 a-b)

Two abundant free apo-astaxanthins, that were found upon hypochlorite degradation of free astaxanthin, its monopalmitate and its dipalmitate, had parent masses of m/z 239.1 and 305.1. These corresponded to the mass of epoxy-apo-9-astaxanthinone (peak 2) and epoxy-apo-13-astaxanthinone (peak 6), respectively (**Table 1** and **Figure 6**). Furthermore, for the astaxanthin monopalmitate and dipalmitate, the esterified forms of the epoxy-apo-9-astaxanthinone with m/z 477.3 (peak 26) and epoxy-apo-13-astaxanthinone with m/z 543.4 (peak 29) were annotated. Following the identification strategy used throughout this study, the epoxy palmitate ester species were identified by fragments **II** and **III** (**Figure 4B**), similar as for apo-12'-astaxanthinal palmitate.

MS² fragmentation could not clarify the position of the epoxide groups, as both parent ions would result in similar fragment ions (5, 35). Therefore, further evidence for the identification of the apo-9 and apo-13 epoxide ketones was provided by the UV-Vis absorption spectra. First, the epoxy-apo-13-astaxanthinone (peak 6) and its palmitate ester (peak 29) showed a blue shift of approximately 5 nm in the

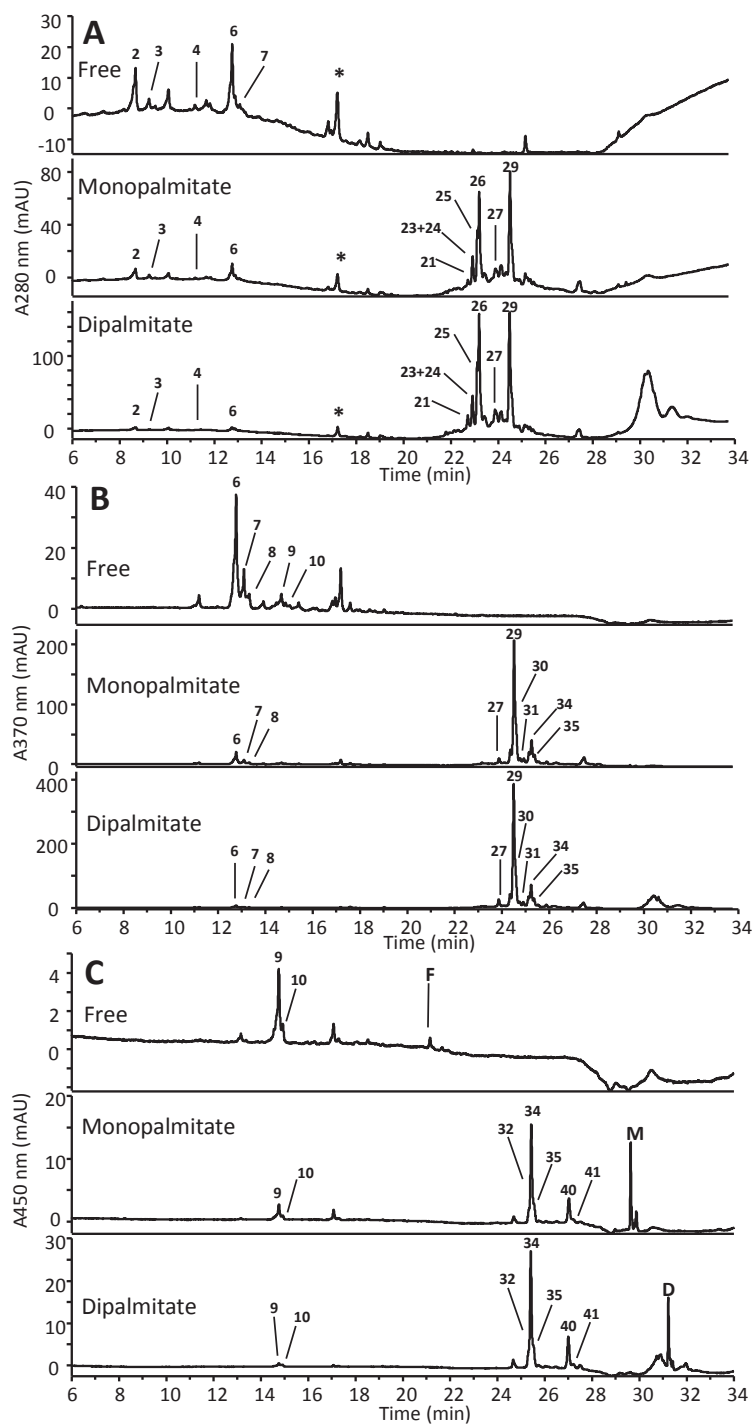


Figure 6. RP-UHPLC-UV profiles of hypochlorite degraded free, monoester and diester astaxanthin in methanol. **A** 280 nm; **B** 370 nm; **C** 450 nm. F = free all-*trans*- and *cis*-astaxanthin; M = all-*trans*- and *cis*-astaxanthin monoester palmitate; D = all-*trans*- and *cis*-astaxanthin diester palmitate; * = ghost peak.

UV-Vis absorption spectrum compared to apo-13-astaxanthinone (palmitate ester) (**Figure 7A**). This indicated that the conjugated system was only slightly shortened. The magnitude of the hypsochromic shift is dependent on the position of the epoxide group. Typically, a 5,6-epoxide group only shortens the conjugated system with a single double bond, whereas with a 5,8-furanoid group two double bonds are sacrificed. For intact carotenoids, epoxidation results in blue shifts of 4 – 13 nm for 5,6-epoxides (*e.g.* zeaxanthin – antheraxanthin) and 23 – 28 nm blue shifts for 5,8-furanoids (*e.g.* zeaxanthin – mutatoxanthin) (36). For the apo-9 epoxide ketones a blue-shift could not be detected due to the detection limits of the PDA detector. Although the influence of a shortened carbon skeleton of apo-astaxanthins on the magnitude of the hypsochromic shift has never been reported, the observed blue shift indicated the presence of a 5,6-epoxide rather than a 5,8-furanoid group for the apo-13 epoxide (peak 29).

Acidification of the apo-astaxanthin degradation products in ethanol with 0.1 M hydrochloric acid, followed by RP-UHPLC analysis did not lead to unambiguous annotation of the 5,6 or 5,8 configuration of the epoxide group (**Figure 7B**) (28). Peak 21 and 26 (apo-9) remained intact, hinting at a 5,8-configuration. Peak 29 (apo-13) only partially disappeared and no ketone-related new peaks appeared, hinting at either a 5,6-epoxide or a 5,8-furanoid configuration. However, for peak 29 the hypsochromic shift after acidification was only 9 nm, which might be attributed to the disappearance of apo-15-astaxanthinal palmitate (peak 30) (**Figure 7B**). This small hypsochromic shift would argue in favour of the 5,6-epoxide. The acidification protocol was originally designed for intact carotenoids, thus without the presence of reactive aldehyde and ketone groups as in apo-astaxanthins. All apo-astaxanthin aldehydes disappeared upon acidification, whereas the less reactive ketones partially remained. Therefore, acidification seems less suitable for distinguishing 5,6-epoxides and 5,8-furanoids in the more reactive apocarotenoids.

Epoxidation of carotenoids with HOCl might proceed as has been described for unsaturated fatty acids and cholesterol (37). In **Figure 7C** this reaction is visualized as follows: the electrophilic addition of HOCl to the 5-6 CDB resulted in intermediate **1**. The remaining OH[•] is added to either the C5 or C6, resulting in chlorohydrin carotenoids (**2**). The 5,6-epoxide (**3**) or 5,8-furanoid (**4**) is subsequently formed by dehydrochlorination of **2** (38). Additionally, the released HCl from **2** might trigger the conversion of **3** into **4**. Chlorohydrins might also be an end-point in this type of reactions (37), but this was not the case here, as indicated by the isotope ratio of parent mass m/z 305.1 (**Figure 7D**). The presence of a chlorohydrin structure would have resulted in a relative intensity of 32% for the third parent mass isotope (m/z 307.1), where only a relative intensity of 3.8% was found. This supported the formation of 5,6-epoxides or 5,8-furanoids and excluded the presence of a chlorohydrin structure.

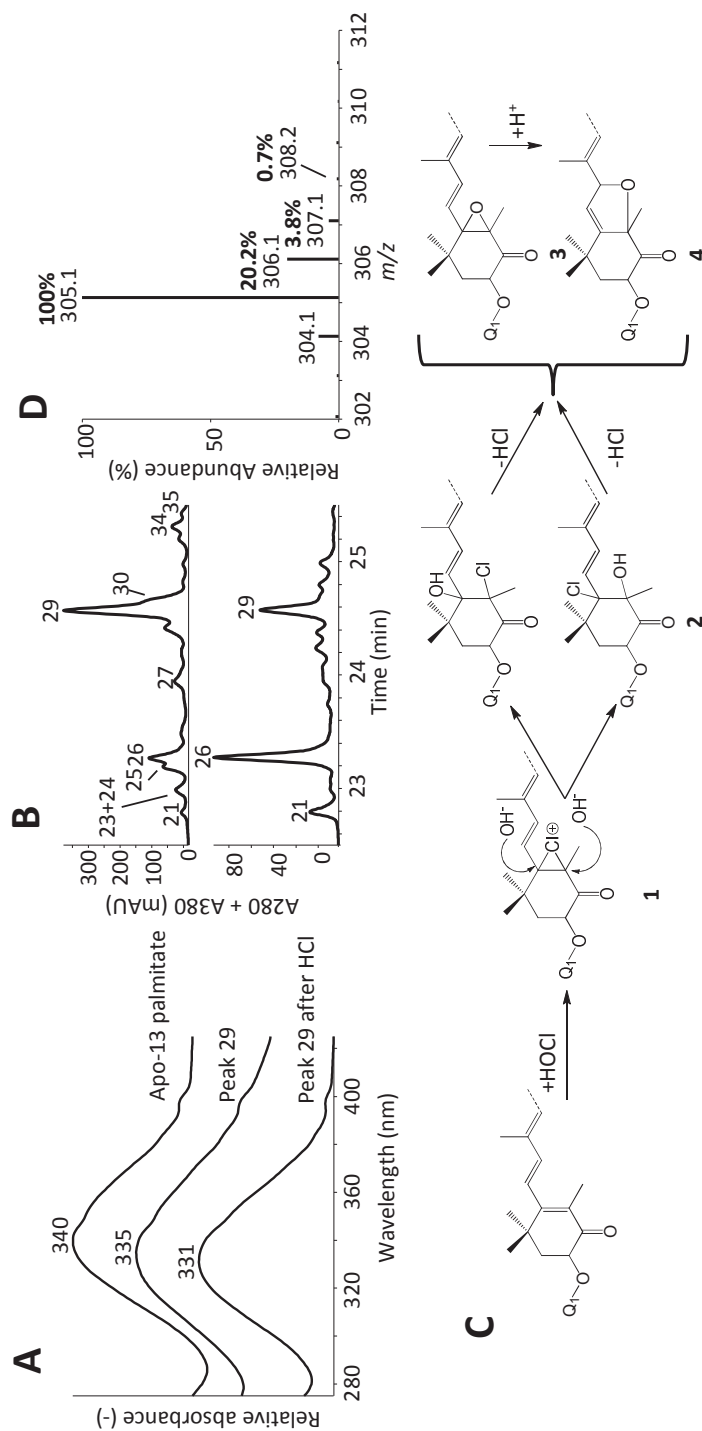


Figure 7. **A** Overlay of UV-Vis absorption spectra of apo-13-astaxanthinone palmitate ester (top), epoxy-apo-13-astaxanthinone palmitate ester (middle) and epoxy-apo-13-astaxanthinone palmitate ester after acidification with HCl (bottom); **B** RP-UHPLC-UV profiles (sum of detection wavelengths 280 and 370 nm) of hypochlorite degraded astaxanthin dipalmitate (top) and 0.1 M HCl acidified hypochlorite degraded astaxanthin dipalmitate (bottom) Numbers refer to **Table 1**. **C** Reaction scheme for the formation of chlorohydrins (**2**) via intermediate carbenium ion **1**, conversion to 5,6-epoxy-apo-astaxanthin (**3**) or 5,8-furanoid-apo-astaxanthin (**4**) by dehydrochlorination. Q₁ is either H or (C=O)-C₁₅H₃₁; **D** Full-MS spectrum of apo-13-astaxanthinone (peak 6), average of 31 spectra.

Epoxy-apo-astaxanthinals and -ones were also found in conjunction with Reaction 1 upon light-accelerated degradation. For free astaxanthin and astaxanthin monopalmitate, two isomers of epoxy-apo-12'-astaxanthinal (peak 11 and 13) were annotated (**Table 1**). The absorbance maximum of the epoxy-apo-12'-astaxanthinal had a hypsochromic shift of approximately 15 and 20 nm compared to apo-12'-astaxanthinal. The occurrence of multiple epoxides can be explained by either isomerisation of the polyene backbone (all-*trans* to *cis* conversion), or the variation in 5,6-epoxide or 5,8-furanoid, or a combination thereof. Besides apo-astaxanthins esterified with palmitate, also their epoxidized forms were found upon degradation of astaxanthin monopalmitate and dipalmitate. The palmitoyl esters of epoxy-apo-9-astaxanthinone (peak 22), epoxy-apo-15-astaxanthinal (peaks 32, 36 and 38), epoxy-apo-12'-astaxanthinal (peaks 39 and 43) and epoxy-apo-15-astaxanthinoic acid (peak 33) were all traced.

Degradation of the fatty acid ester (R3)

Upon examining of the diester chromatograms (**Figure 3C and 6C**), de-esterification was observed with especially the hypochlorite bleaching treatment, as free apo-astaxanthins (*e.g.* peaks 2-4, 6-10) were formed. The de-esterification did not lead to the annotation of any new compounds and proceeded in conjunction with Reaction 1, and occasionally Reaction 2. Most probably, the de-esterification proceeded via a base-induced hydrolysis with the apo-astaxanthin as the leaving group. The reactive nucleophile in this case is likely a hypochlorite anion (OCl^-) or a hydroxide (OH^-) resulting from the HOCl . As the degradation was performed in methanol, also a methoxide anion (MeO^-) might have served as nucleophile, resulting in a fatty acid methyl ester.

For light-accelerated autoxidation, trace amounts of free astaxanthin (Peak F) and astaxanthin monopalmitate (Peak M) were found (**Figure 3C**). When the degradation was continued to 7 h, also no accumulation of free astaxanthin and astaxanthin monopalmitate was observed (data not shown). Observation of the trace amounts of de-esterification products upon light-accelerated autoxidation (*e.g.* a system which does not favour de-esterification) underlines the sensitivity of the analysis method employed.

CONCLUSIONS

A plethora of degradation products of the xanthophyll astaxanthin with different degrees of fatty acid esterification were identified for the first time. The use of RP-UHPLC separation in combination with PDA and tandem MS fragmentation enabled us to identify a wide range of (fatty acid-esterified) apo-astaxanthins formed upon light-accelerated autoxidation and hypochlorite bleaching. In our approach, the separation

and identification of esterified and non-esterified apo-astaxanthins could be performed simultaneously.

ACKNOWLEDGEMENTS

This work was supported by FeyeCon D&I and by grants from NL Agency and the Ministry of Education, Culture and Science (Project no. FND09014).

REFERENCES

1. Guedes, A. C.; Amaro, H. M.; Malcata, F. X., Microalgae as sources of carotenoids. *Marine drugs* **2011**, *9*, 625-644.
2. Hussein, G.; Sankawa, U.; Goto, H.; Matsumoto, K.; Watanabe, H., Astaxanthin, a carotenoid with potential in human health and nutrition. *Journal of natural products* **2006**, *69*, 443-449.
3. Miao, F.; Lu, D.; Li, Y.; Zeng, M., Characterization of astaxanthin esters in *Haematococcus pluvialis* by liquid chromatography-atmospheric pressure chemical ionization mass spectrometry. *Analytical biochemistry* **2006**, *352*, 176-81.
4. Boon, C. S.; McClements, D. J.; Weiss, J.; Decker, E. A., Factors influencing the chemical stability of carotenoids in foods. *Critical reviews in food science and nutrition* **2010**, *50*, 515-532.
5. Rodriguez, E. B.; Rodriguez-Amaya, D. B., Formation of apocarotenals and epoxycarotenoids from β -carotene by chemical reactions and by autoxidation in model systems and processed foods. *Food chemistry* **2007**, *101*, 563-572.
6. Stratton, S. P.; Schaefer, W. H.; Liebler, D. C., Isolation and identification of singlet oxygen oxidation products of β -carotene. *Chemical research in toxicology* **1993**, *6*, 542-547.
7. Marty, C.; Berset, C., Degradation products of trans-beta-carotene produced during extrusion cooking. *Journal of food science* **1988**, *53*, 1880-1886.
8. Kanasawud, P.; Crouzet, J. C., Mechanism of formation of volatile compounds by thermal degradation of carotenoids in aqueous medium. 1. beta-Carotene degradation. *Journal of agricultural and food chemistry* **1990**, *38*, 237-243.
9. Mordi, R. C.; Walton, J. C.; Burton, G. W.; Hughes, L.; Ingold, K. U.; Lindsay, D. A.; Moffatt, D. J., Oxidative degradation of beta-carotene and beta-apo-8'-carotenal. *Tetrahedron* **1993**, *49*, 911-928.
10. Albrich, J. M.; McCarthy, C. A.; Hurst, J. K., Biological reactivity of hypochlorous acid: implications for microbicidal mechanisms of leukocyte myeloperoxidase. *Proceedings of the national academy of sciences of the United States of America* **1981**, *78*, 210-214.
11. Hazen, S. L.; Hsu, F. F.; Gaut, J. P.; Crowley, J. R.; Heinecke, J. W.; Lester, P., Modification of proteins and lipids by myeloperoxidase. In *Methods in enzymology*, Academic Press: 1999; Vol. 300, pp 88-105.
12. Panasenkov, O. M.; Gorudko, I. V.; Sokolov, A. V., Hypochlorous acid as a precursor of free radicals in living systems. *Biochemistry - Moscow* **2013**, *78*, 1466-1489.
13. Norkus, E. P.; Norkus, K. L.; Dharmarajan, T. S.; Schierle, J.; Schalch, W., Serum lutein response is greater from free lutein than from esterified lutein during 4 weeks of supplementation in healthy adults. *Journal of the American college of nutrition* **2010**, *29*, 575-585.
14. Granado, F.; Olmedilla, B.; Gil-Martinez, E.; Blanco, I., Lutein ester in serum after lutein supplementation in human subjects. *British journal of nutrition* **1998**, *80*, 445-449.

15. Alija, A. J.; Bresgen, N.; Sommerburg, O.; Siems, W.; Eckl, P. M., Cytotoxic and genotoxic effects of beta-carotene breakdown products on primary rat hepatocytes. *Carcinogenesis* **2004**, *25*, 827-831.
16. Siems, W.; Salerno, C.; Crifo, C.; Sommerburg, O.; Wiswedel, I., beta-Carotene degradation products - formation, toxicity and prevention of toxicity. In *Food factors for health promotion*, Edited by Yoshikawa, T., Edition Karger, Basel, Switzerland, **2009**, Vol. 61, pp 75-86.
17. Handelman, G. J.; Vankuijk, F. J. G. M.; Chatterjee, A.; Krinsky, N. I., characterization of products formed during the autoxidation of beta-carotene. *Free radical biology and medicine* **1991**, *10*, 427-437.
18. Sommerburg, O.; Langhans, C. D.; Arnhold, J.; Leichsenring, M.; Salerno, C.; Crifò, C.; Hoffmann, G. F.; Debatin, K. M.; Siems, W. G., beta-Carotene cleavage products after oxidation mediated by hypochlorous acid - a model for neutrophil-derived degradation. *Free radical biology and medicine* **2003**, *35*, 1480-1490.
19. Panasencko, O. M.; Panasencko, O. O.; Briviba, K.; Sies, H., Hypochlorite destroys carotenoids in low density lipoproteins thus decreasing their resistance to peroxidative modification. *Biochemistry - Moscow* **1997**, *62*, 1140-1145.
20. Lutz-Roder, A.; Jezussek, M.; Winterhalter, P., Nickel peroxide induced oxidation of canthaxanthin. *Journal of agricultural and food chemistry* **1999**, *47*, 1887-1891.
21. Etoh, H.; Suhara, M.; Tokuyama, S.; Kato, H.; Nakahigashi, R.; Maejima, Y.; Ishikura, M.; Terada, Y.; Maoka, T., Auto-oxidation products of astaxanthin. *Journal of oleo science* **2012**, *61*, 17-21.
22. Hayakawa, T.; Kulkarni, A.; Terada, Y.; Maoka, T.; Etoh, H., Reaction of astaxanthin with peroxynitrite. *Bioscience biotechnology and biochemistry* **2008**, *72*, 2716-2722.
23. Yuan, J. P.; Chen, F., Purification of *trans*-astaxanthin from a high-yielding astaxanthin ester-producing strain of the microalga *Haematococcus pluvialis*. *Food chemistry* **2000**, *68*, 443-448.
24. Halldorsson, A.; Haraldsson, G. G., Fatty acid selectivity of microbial lipase and lipolytic enzymes from salmonid fish intestines toward astaxanthin diesters. *Journal of the American oil chemists' society* **2004**, *81*, 347-353.
25. Britton, G., Chapter 2: UV/Visible spectroscopy. In: *Carotenoids Vol. 1B Spectroscopy*, Edited by Britton G., Liaaen-Jensen S., Pfander H., Birkhäuser Verlag, Basel, Switzerland **1995**, pp 13-62.
26. CaroteNature GmbH, Lupsingen, Switzerland, data sheet (*rac*.)-12'-apo-astaxanthinal.
27. Rivera, S. M.; Canela-Garayoa, R., Analytical tools for the analysis of carotenoids in diverse materials. *Journal of chromatography A* **2012**, *1224*, 1-10.
28. Eugster, C. H., Chapter 4: Chemical derivatization: Microscale tests for the presence of common functional groups in carotenoids. In: *Carotenoids Vol. 1A Isolation and analysis*, Edited by Britton G., Liaaen-Jensen S., Pfander H., Birkhäuser Verlag, Basel, Switzerland **1995**, pp 71-80.
29. Ghidouche, S.; Rey, B.; Michel, M.; Galaffu, N., A rapid tool for the stability assessment of natural food colours. *Food chemistry* **2013**, *139*, 978-985.
30. Minguez-Mosquera, M. I.; Jaren-Galan, M., Kinetics of the decolouring of carotenoid-pigments. *Journal of the science of food and agriculture* **1995**, *67*, 153-161.
31. Subagio, A.; Wakaki, H.; Morita, N., Stability of lutein and its myristate esters. *Bioscience biotechnology and biochemistry* **1999**, *63*, 1784-1786.
32. Frassanito, R.; Cantonati, M.; Flaim, G.; Mancini, I.; Guella, G., A new method for the identification and the structural characterisation of carotenoid esters in freshwater microorganisms by liquid chromatography/electrospray ionisation tandem mass spectrometry. *Rapid communications in mass spectrometry* **2008**, *22*, 3531-9.
33. Weesepoel, Y.; Vincken, J.-P.; Pop, R. M.; Liu, K.; Gruppen, H., Sodiation as a tool for enhancing the diagnostic value of MALDI-TOF/TOF-MS spectra of complex astaxanthin ester mixtures from *Haematococcus pluvialis*. *Journal of mass spectrometry* **2013**, *48*, 862-874.

34. Baldas, J.; Porter, Q. N.; Leftwick, A. P.; Holzel, R.; Weedon, B. C. L.; Szabolcs, J., Mass spectrometry of carotenoid ketones. *Journal of the chemical Society D* **1969**, 415-416.
35. Enzell, C. R.; Back, S., Chapter 7: Mass spectrometry. In: *Carotenoids Vol. 1B Spectroscopy*, Edited by Britton G., Liaaen-Jensen S., Pfander H., Birkhäuser Verlag, Basel, Switzerland **1995**, pp 261-320.
36. Egeland, E. S., Part VII: Data sheets aiding identification of phytoplankton carotenoids and chlorophylls. In: *Phytoplankton pigments: characterization, chemotaxonomy, and applications in oceanography*. Edited by Roy, S., Llewellyn C.A., Egeland, E.S., Johnsen, G. Cambridge University Press, New York, USA **2011**, pp 665-822.
37. Spickett, C. M.; Jerlich, A.; Panasenko, O. M.; Arnhold, J.; Pitt, A. R.; Stelmaszynska, T.; Schaur, R. J., The reactions of hypochlorous acid, the reactive oxygen species produced by myeloperoxidase, with lipids. *Acta biochimica Polonia* **2000**, 47, 889-899.
38. Panasenko, O. M., The mechanism of the hypochlorite-induced lipid peroxidation. *BioFactors* **1997**, 6, 181-190.

SUPPLEMENTARY INFORMATION

Table S1. MS² data of non-esterified apo-astaxanthins formed during light-accelerated autoxidation and hypochlorite degradation of free astaxanthin, astaxanthin monopalmitate and astaxanthin dipalmitate tentatively assigned by UHPLC-ESI-MS. Peak numbers refer to **Figures 3** and **6**.

No.	Rt. (min)	Identification ^a	[M+H] ⁺ (m/z)	MS ² product ions in m/z (relative abundance)
1	7.30	Apo-9-astaxanthinone	223.1	205.0(100), 187.1(20), 177.1(5), 163.1(10), 147.0(5), 147.0(10)
2	8.71	Epoxy-apo-9-astaxanthinone	239.1	221.0(50), 193.1(60), 189.0(70), 161.0(100), 142.0(50), 138.0(35)
3	9.27	Apo-11-astaxanthinal	249.1	231.1(100), 213.0(30), 203.1(20), 189.1(15), 185.1(10), 173.1(15), 147.0(10), 135.0(10)
4	11.24	Apo-13-astaxanthinone	289.1	271.1(100), 270.2(55), 253.1(15), 247.8(10), 229.1(20), 215.0(40), 189.1(10), 187.0(15), 173.1(15), 137.1(5), 135.1(5), 106.1(20)
5	11.49	Apo-13-astaxanthinone	289.2	Idem 4 ^c
6	12.83	Epoxy-apo-13-astaxanthinone	305.1	287.1(30), 286.1(15), 273.1(100), 255.1(60), 245.1(40), 227.1(80), 217.1(20), 213.1(10), 201.1(10), 199.1(10), 153.1(10), 121.0(10)
7	13.15	Apo-15-astaxanthinal	315.2	297.1(100), 283.1(35), 269.1(15), 241.1(15), 213.1(10), 201.1(5), 187.1(20), 173.1(10), 161.1(5), 159.1(5), 149.1(5), 147.0, (5)
8	13.27	Apo-15-astaxanthinal	315.2	Idem 6 ^c
9	14.75	Apo-14'-astaxanthinal	341.2	323.2(100), 305.2(20), 295.2(20), 283.2(30), 271.1(20), 253.1(15), 239.1(20), 201.1(25), 189.1(10), 187.1(10), 185.2(10), 173.1(25), 147.1(30)
10	14.92	Apo-14'-astaxanthinal	341.2	Idem 9 ^c
11	16.53	Apo-12'-astaxanthinoic acid	397.2	379.2(20), 361.2(10), 291.1(20), 271.1(100), 209.1(5), 173.1(5), 159.0(10), 147.1(5)
12	17.07	Apo-12'-astaxanthinal	381.2	363.2(100), 345.2(30), 275.1(40), 271.1(35), 215.1(25), 201.1(30), 173.1(35), 161.1(25), 147.0(25), 145.0(25)

Table S1. Continued.

13	17.24	Epoxy-apo-12'-astaxanthinal	397.2	379.2(30), 351.2(80), 333.2(30), 245.1(20), 227.2(20), 173.1(100), 147.0(35)
14	17.78	Apo-10'-astaxanthinal	407.2	389.2(100), 371.2(10), 361.2(20), 301.1(20), 253.1(15), 201.0(15), 189.1(10), 187.1(20), 147.0(10)
15	18.05	Apo-10'-astaxanthinal	407.2	Idem 14 ^c
16	18.65	Apo-8'-astaxanthinol	449.2	431.2(100), 413.2(20), 343.1(15), 295.1(15), 285.1(20), 236.9(50), 217.1(15), 177.0(15), 173.0(20)
17	18.00-20.50 ^d	Epoxy-astaxanthin	613.3	595.3(100), 577.3(40), 567.3(10), 559.3(10), 395.2(10), 377.2(15)
18	18.00-20.50 ^d	Diepoxy-astaxanthin	629.3	N.D.
19	18.00-20.50 ^d	Triepoxy-astaxanthin	645.3	627.3(100), 609.3(30), 340.1(25), 288.2(15)

N.D., not determined.

^aEpoxides can be either in the 5,6 or 5,8 configuration.^bTentatively identified based on MS data only.^cIdem: MS² spectrum, including relative intensities of the fragments, similar as peak number indicated.^dNo accurate retention time could be determined.

Table S2. MS² fragmentation data of fatty acid esterified apo-astaxanthins formed during light-accelerated autoxidation and hypochlorite degradation of free astaxanthin, astaxanthin monopalmitate and astaxanthin dipalmitate tentatively assigned by UHPLC-ESI-MS. Peak numbers refer to **Figures 3** and **6**, and roman numbers refer to **Figure 4**.

No.	Rt. (min)	Identification ^a	Ionization type	Parent ion (m/z)	MS ² product ions (relative abundance) ^b				
					I	II	III	IV	Other
20	21.81-	Apo-7-astaxanthinal	[M+H] ⁺	421.2	403.2(50)	183.0(25)	165.0(15)	N.D.	389.2(15), 374.2(100), 355.2(70), 352.7(40), 321.1(15), 239.1(55)
	22.39 ^c	palmitate ester	[M+Na] ⁺	443.1	425.2(70)	205.0(60)	187.0(40)	N.D.	411.2(100), 398.2(30), 387.1(40), 306.8(50), 301.1(40), 159.1(30)
21	22.89	Epoxy-apo-9-astaxanthinone palmitate ester	[M+H] ⁺	477.2	448.3(10)	239.1(100)	221.1(10)	N.D.	433.3(10), 405.2(60), 393.3(80), 192.1(15), 155.0(25)
			[M+Na] ⁺	N.D.	N.D.	N.D.	N.D.	N.D.	N.D.
22	22.98	Apo-9-astaxanthinone palmitate ester	[M+H] ⁺	461.3	443.3(10)	223.1(100)	205.1(40)	187.1(15)	418.4(5), 389.2(10), 239.2(5), 163.1(15), 159.1(10), 147.0(5)
			[M+Na] ⁺	483.3	465.4(40)	245.1(65)	227.0(100)	N.D.	455.4(10), 451.4(10), 439.3(25), 427.3(35), 203.1(15), 183.1(5)
23	23.10	Apo-9-astaxanthinone palmitate ester	[M+H] ⁺	461.3	443.4(10)	223.1(95)	205.1(100)	187.1(40)	172.1(5), 163.1(5), 159.1(10), 147.0(15)
			[M+Na] ⁺	483.3	465.4(30)	245.1(10)	227.0(100)	N.D.	455.4(10), 439.4(25), 183.1(5)
24	23.10	Apo-11-astaxanthinal palmitate ester	[M+H] ⁺	487.3	469.4(55)	249.1(100)	231.1(90)	213.1(20)	203.1(30), 189.1(10), 185.1(10), 175.0(15)
			[M+Na] ⁺	509.3	491.3(10)	271.1(10)	253.0(15)	N.D.	481.3(30), 465.3(100), 380.3(10), 339.2(5), 225.1(5), 185.1(10)
25	23.29	Apo-11-astaxanthinal palmitate ester	[M+H] ⁺	487.3	469.3(45)	249.1(100)	231.1(75)	213.1(15)	203.1(25), 189.1(5), 185.1(15), 175.0(10), 171.1(5)
			[M+Na] ⁺	509.3	491.4(5)	271.1(5)	253.2(25)	N.D.	481.3(25), 465.3(100), 185.1(5)
26	23.37	Epoxy-apo-9-astaxanthinone palmitate ester	[M+H] ⁺	477.3	N.D.	239.1(100)	221.0(10)	N.D.	193.1(10), 189.0(15), 161.0(20)
			[M+Na] ⁺	N.D.	N.D.	N.D.	N.D.	N.D.	N.D.
27	24.05	Apo-13-astaxanthinone palmitate ester	[M+H] ⁺	527.4	509.3(100)	289.1(20)	271.1(65)	253.1(10)	333.1(5), 187.0(5)
			[M+Na] ⁺	549.4	531.4(5)	311.1(10)	293.1(100)	N.D.	465.3(60), 453.3(25), 278.0(5), 271.1(10), 263.1(5), 229.1(5)
28	24.22	Apo-13-astaxanthinone palmitate ester	[M+H] ⁺	527.4	509.4(30)	289.1(100)	271.1(95)	253.1(25)	229.1(20), 215.0(35), 211.1(15), 173.0(15)
			[M+Na] ⁺	549.4	531.3(10)	311.1(10)	293.1(100)	275.1(5)	465.3(65), 271.1(10), 263.0(5), 250.1(5), 229.1(5), 173.1(5)
29	24.67	Epoxy-apo-13-astaxanthinone palmitate ester	[M+H] ⁺	543.4	N.D.	305.1(100)	287.1(5)	N.D.	511.3(60), 483.4(15), 273.1(25), 255.1(25), 245.1(10), 227.1(15)
			[M+Na] ⁺	565.3	547.4(10)	327.1(10)	309.1(80)	N.D.	465.3(100), 287.1(15)
30	24.69	Apo-15-astaxanthinal palmitate ester	[M+H] ⁺	553.4	535.4(15)	315.1(70)	297.1(100)	279.1(35)	269.1(25), 251.1(10), 241.1(35), 213.0(25), 185.1(10), 173.1(10)
			[M+Na] ⁺	575.4	N.D.	337.2(5)	319.1(100)	N.D.	467.3(45), 465.3(70), 297.1(5), 291.1(5), 253.2(5)

Table S2. Continued.

31	24.94	Apo-15'-astaxanthinal palmitate ester	[M+H] ⁺ [M+Na] ⁺	553.4 575.4	535.3(20) 557.4(25)	315.1(80) 337.1(10)	297.1(100) 319.1(80)	279.1(30) N.D.	521.3(20), 465.3(10), 283.1(10), 269.1(30), 223.1(10), 213.1(20) 547.4(15), 531.3(10), 490.3(10), 469.3(15), 465.3(100), 227.1(5)
32	25.31	Epoxy-apo-15'- astaxanthinal palmitate ester	[M+H] ⁺ [M+Na] ⁺	569.4 N.D.	551.4(5) N.D.	331.1(100) N.D.	313.1(30) N.D.	295.1(15) N.D.	523.3(10), 407.2(5), 285.1(25), 267.1(20), 239.1(10), 211.1(20) N.D.
33	25.34	Epoxy-apo-15'- astaxanthinoic acid palmitate ester	[M+H] ⁺ [M+Na] ⁺	585.4 607.4	N.D. 589.5(5)	347.1(100) 369.2(25)	329.1(85) 351.1(100)	N.D. N.D.	553.4(70), 315.1(60), 297.1(100), 279.1(15), 269.1(20), 255.1(25) 588.4(5), 575.4(5), 561.3(5), 551.3(10), 465.3(65), 189.1(5)
34	25.43	Apo-14'-astaxanthinal palmitate ester	[M+H] ⁺ [M+Na] ⁺	579.4 601.4	561.4(15) N.D.	341.1(100) 363.2(5)	323.2(55) 345.1(15)	305.1(20) N.D.	457.3(10), 295.2(10), 277.1(10), 249.1(10), 213.0(10), 201.0(10) 573.4(10), 509.3(5), 481.3(10), 465.3(100)
35	25.54	Apo-14'-astaxanthinal palmitate ester	[M+H] ⁺ [M+Na] ⁺	579.4 601.4	Idem 32 ^d Idem 32 ^d				
36	25.56	Epoxy-apo-15'- astaxanthinal palmitate ester	[M+H] ⁺ [M+Na] ⁺	569.4 N.D.	551.4(15) N.D.	331.4(100) N.D.	313.1(50) N.D.	295.1(40) N.D.	523.4(25), 463.3(5), 267.1(50), 249.1(25), 239.1(25), 211.1(25) N.D.
37	25.91	Apo-14'-astaxanthinal palmitate ester	[M+H] ⁺ [M+Na] ⁺	579.4 601.4	561.4(10) 583.4(5)	341.1(100) 363.3(5)	323.2(40) 345.1(10)	305.1(10) N.D.	533.4(10), 502.3(25), 501.3(30), 457.3(5), 231.1(5), 173.1(5) 573.4(15), 569.4(30), 521.3(10), 509.3(5), 481.3(10), 465.3(100)
38	25.91	Epoxy-apo-15'- astaxanthinal palmitate ester	[M+H] ⁺ [M+Na] ⁺	569.4 N.D.	551.3(100) N.D.	331.1(20) N.D.	313.1(20) N.D.	295.1(30) N.D.	277.1(5), 267.1(10) N.D.
39	26.15	Epoxy-apo-12'- astaxanthinal palmitate ester	[M+H] ⁺ [M+Na] ⁺	635.4 N.D.	617.4(35) N.D.	397.2(80) N.D.	379.2(100) N.D.	351.2(55) N.D.	607.4(45), 457.3(40), 333.2(70), 293.1(25), 219.0(25), 201.1(25) N.D.
40	27.01	Apo-12'-astaxanthinal palmitate ester	[M+H] ⁺ [M+Na] ⁺	619.4 641.4	601.4(90) 623.4(10)	381.2(95) 403.1(10)	363.2(100) 385.2(40)	345.2(70) N.D.	527.3(20), 513.3(10), 457.3(35), 289.1(35), 271.1(40), 201.0(35) 549.3(30), 535.3(15), 465.3(100)
41	27.23	Apo-12'-astaxanthinal palmitate ester	[M+H] ⁺ [M+Na] ⁺	619.4 641.4	Idem 38 ^d Idem 38 ^d				
42	27.54	Apo-10'-astaxanthinal palmitate ester	[M+H] ⁺ [M+Na] ⁺	645.4 ^e 667.5	627.4(65) 649.4(20)	407.2(100) N.D.	389.2(80) 411.2(50)	371.2(50) N.D.	601.5(15), 553.4(20), 457.3(25), 361.2(25), 315.1(15), 297.2(15) 610.4(35), 587.4(25), 575.4(85), 561.4(20), 465.3(100), 311.3(25)

Table S2. Continued.

Epoxy-apo-12'-												
		[M+H] ⁺	635.4	617.4(100)	397.2(25)	379.2(35)	361.1(45)	529.3(15), 457.3(25), 333.2(15), 219.1(15), 201.0(10)				
43	28.58	astaxanthinal palmitate ester	[M+Na] ⁺	657.4	N.D.	419.2(5)	401.2(100)	N.D.	613.4(25), 565.4(20), 551.3(10), 465.3(60), 373.2(100), 289.1(5)			
44	28.88	Apo-8'-astaxanthinal palmitate ester	[M+H] ⁺	685.4	667.4(55)	447.2(50)	429.2(100)	411.2(40)	653.4(20), 593.4(15), 579.4(10), 457.3(20), 401.3(20), 316.2(15)			
			[M+Na] ⁺	N.D.	N.D.	N.D.	N.D.	N.D.				
45	29.15	Apo-8'-astaxanthinal palmitate ester	[M+H] ⁺	685.4	667.5(65)	447.2(60)	429.2(100)	411.2(45)	653.5(30), 593.4(15), 590.4(20), 401.2(25), 385.2(30), 316.2(35)			
			[M+Na] ⁺	N.D.	N.D.	N.D.	N.D.	N.D.				
46	29.30- 29.60 ^c	Epoxy-astaxanthin palmitate ester	[M+H] ⁺	851.6	833.4(100)	613.3(30)	595.3(65)	577.3(45)	815.5(25), 559.3(20), 549.3(10)			
			[M+Na] ⁺	873.7	N.D.	N.D.	617.4(40)	N.D.	874.6(100), 845.6(15), 829.6(25), 465.4(15)			
47	29.30- 29.60 ^c	Diepoxy-astaxanthin palmitate ester	[M+H] ⁺	N.D.	N.D.	N.D.	N.D.	N.D.	N.D.			
			[M+Na] ⁺	889.5	N.D.	N.D.	N.D.	N.D.	N.D.			
48	29.30- 29.60 ^c	Triepoxy-astaxanthin palmitate ester	[M+H] ⁺	N.D.	N.D.	N.D.	N.D.	N.D.	N.D.			
			[M+Na] ⁺	905.5	N.D.	N.D.	N.D.	N.D.	N.D.			
49	30.60- 31.10 ^c	Epoxy-astaxanthin dipalmitate ester	[M+H] ⁺	1089.8	1071.8(30)	851.5(60)	833.5(100)	815.5(35)	805.6(15), 613.3(15), 595.3(25), 577.3(30), 559.28(15), 457.3(10)			
			[M+Na] ⁺	N.D.	N.D.	N.D.	N.D.	N.D.	N.D.			
50	30.60- 31.10 ^c	Diepoxy-astaxanthin dipalmitate ester	[M+H] ⁺	1106.7	N.D.	N.D.	N.D.	N.D.	N.D.			
			[M+Na] ⁺	N.D.	N.D.	N.D.	N.D.	N.D.	N.D.			
51	30.60- 31.10 ^c	Triepoxy-astaxanthin dipalmitate ester	[M+H] ⁺	N.D.	N.D.	N.D.	N.D.	N.D.	N.D.			
			[M+Na] ⁺	1143.8	N.D.	N.D.	N.D.	N.D.	N.D.			

N.D., not determined.

^aEpoxides can be either in the 5,6 or 5,8 configuration.^b**I, II, III, IV** are used as diagnostic MS² ions for identification; **I**, loss of water; **II**, loss of palmitate ketene; **III**, loss of palmitate; **IV**, tandem loss of palmitate and water.^cNo accurate retention time could be determined.^dIdem: MS² spectrum, including relative intensities of the fragments, similar as peak number indicated.^eMS² spectrum not detected at Rt. 27.57 min, data from spectrum at Rt. 27.99 min.

Preliminary UHPLC-PDA-ESI-MS screening of light-accelerated autoxidation products of the tetrapyrrole biliverdin

Application of phycobiliproteins, for example the blue C-phycocyanin, as natural water-soluble food colourant is emerging. The chromophore of these proteins comprises a number of tetrapyrroles (or phycocyanobilins), which have an extensive conjugated system, vulnerable to autoxidation. To assess the autoxidation products, a simplified model system was used in which the free tetrapyrrole biliverdin, instead of phycobiliprotein, was subjected to light-accelerated autoxidation. Degradation products of biliverdin were subsequently annotated by reversed-phase ultra-high performance liquid chromatography with photo diode array and positive mode *in-line* electrospray ionization mass spectrometry (RP-UHPLC-PDA-ESI-MS). To facilitate the analysis of degradation products, autoxidation of the three methine bridges in biliverdin was mimicked *in silico*. It was found that both peripheral and the central methine bridge of biliverdin were susceptible to light-accelerated autoxidation. Scission products tentatively annotated with MS² and MS³ were propionic acid-containing pyrroles. From this, it can be speculated that also tetrapyrroles attached to phycobiliproteins are susceptible to autoxidative degradation.

Based on: Weesepeel Y.; Gruppen, H.; Vincken, J.-P. Preliminary UHPLC-PDA-ESI-MS screening of light-accelerated autoxidation products of the tetrapyrrole biliverdin, *Submitted to Food chemistry*.

INTRODUCTION

Besides application of algal carotenoids in foods, also the use of protein-based colourants is increasing. An example is the blue phycobiliprotein C-phycocyanin (CPC) from *Spirulina platensis*, which can be used as a replacer for blue food colourants (1). The blue colour of CPC originates from linearized porphyrin-based chromophores, covalently bound to specific protein subunits, at least when the chromophores are organised in a protein complex (**Figure 1**) (2).

S. platensis CPC consists of two different sub-units, α and β , with molecular masses of 18.2 and 19.2 kDa, respectively (3) (**Figure 1**). The molecular mass of the protein complex depends on its aggregation state which is influenced by pH, temperature, protein concentration, ionic strength, and solvent (4). The subunits spontaneously associate into a heterodimer (also referred to as α,β monomer), which can assemble into $(\alpha\beta)_3$ trimers. These trimers can then interact in a face-to-face manner, forming disc shaped $(\alpha\beta)_6$ hexamers by various types of linker proteins, which make up 15% of the mass of phycobiliproteins (2). Finally, hexamers can arrange into tube-like structures in the phycobilisome.

The chromophore is known as a bilin. Five main types of bilin exist in cyanobacteria and red algae: biliverdin, phycocyanobilin, phycoviolobilin, phycoerythrobilin and phycourobilin. The bilins are all derived biosynthetically from protoheme via biliverdin as is elaborated extensively elsewhere (5). Bilins have an open-chain tetrapyrrolic structure and are attached to the polypeptide chain by a linkage between a cysteine residue and the vinyl substituent on one of the outer pyrrole rings (6). The difference between the five bilins lies in the number of double bonds and side groups participating in the chromophore, which influence their absorption maxima.

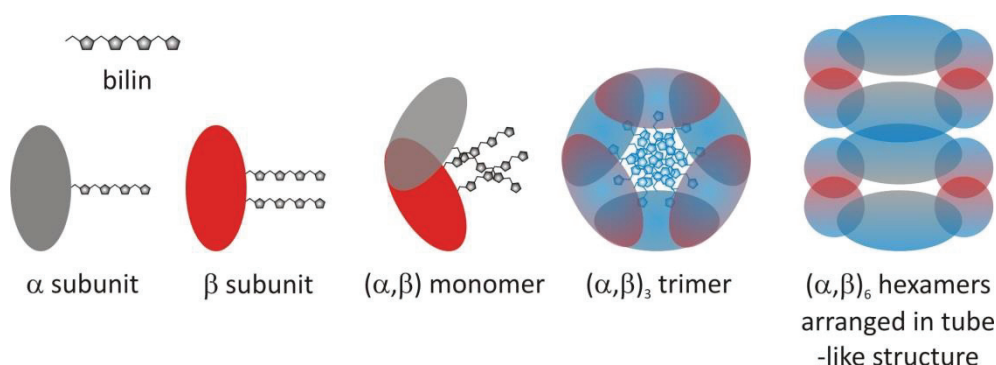


Figure 1. Aggregation of α and β subunits with one and two covalently attached phycocyanobilins in CPC, adapted from (2). Linker peptides connecting $(\alpha,\beta)_3$ trimers are not shown.

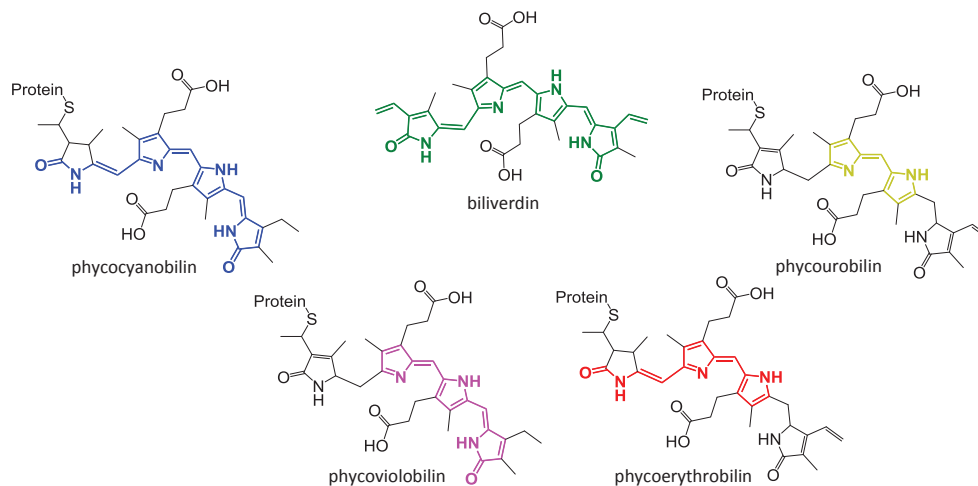


Figure 2. Bilins commonly found bound to phycobiliproteins. Conjugated system is highlighted in its actual colour. Adapted from (7).

In **Chapter 4**, it became clear that all (carbon-carbon) conjugated double bonds (CDB) of astaxanthin could be cleaved or epoxidized resulting in apo-astaxanthin ketones, aldehydes and epoxides. In analogy, the tetrapyrroles present in CPC have an extensive conjugated system (**Figure 2**) and are excellent antioxidants. Three of the phycocyanobilin's pyrrole groups contain so-called 'active hydrogen atoms' (N-H). These hydrogens can be easily transferred to a radical (*e.g.* peroxy radical) and the resulting pyrrole radical is stabilized by electron delocalization (8, 9). Hence, a process like autoxidation is likely to occur. The identification of the phycocyanobilin degradation products resulting from autoxidation is more challenging compared to that of carotenoids, because the protein part of CPC complicates matters. (i) As only 5% w/w of CPC consists of phycocyanobilin, a given amount of CPC will generate relatively low concentrations of intact phycocyanobilin and its degradation products. (ii) Before autoxidation products can be identified, CPC requires proteolysis. Identification of the resulting plethora of peptides released is laborious, as it is unclear which oxidation products are formed from the phycocyanobilin group. As a consequence, it is difficult to predict by which residual pyrrolic structures the peptides are substituted. This makes targeted mass spectrometric analysis, using specific masses or specific UV-VIS wavelengths of detection impossible. (iii) Besides a hypsochromic shift in the absorption spectrum of phycocyanobilin upon autoxidation, it is likely that also a hypochromic shift occurs, as a result of which peptides containing the partially degraded phycocyanobilin might be overlooked.

Hence, in this research, light-accelerated autoxidation was performed on a free tetrapyrrole in order to avoid the complications stated above. Biliverdin was used as a model tetrapyrrole and degradation products were assessed by UHPLC-PDA-ESI-MS. *In silico* predicted degradation products were used to facilitate annotation.

MATERIALS AND METHODS

Materials

All materials were acquired as described elsewhere (10). Biliverdin hydrochloride (>97% w/w) was purchased from Sigma-Aldrich (St. Louis, MO, USA). Acetone (99.9% v/v) was obtained from Biosolve (Valkenswaard, The Netherlands). Millipore water (MQ) was produced by a Milli-Q Integral 5 system equipped with a 0.22 µm Millipak 40 filter unit (Merck Millipore, Darmstadt, Germany).

Light-accelerated autoxidation

Light-accelerated autoxidation by Suntest XLS+ and sample treatment in quartz cuvettes was performed as described elsewhere (10). Biliverdin was dissolved in 90% (v/v) aqueous acetone and had a start A_{650} of 2.54 and A_{376} of 2.45. Colour degradation experiments were performed at T_{exp} 37 °C at a T_{BST} of 47 °C for 3.5 h.

RP-UHPLC-PDA-ESI-MS analysis of biliverdin autoxidation products

RP-UHPLC-PDA-ESI-MS was performed as described elsewhere (10), with the following modifications: The eluents used were the following: 1% (v/v) acetonitrile in millipore water (A) and acetonitrile (B) both containing 0.10% (v/v) formic acid as a mobile phase modifier. The elution program was started from 95% (v/v) A, 5% (v/v) B and followed by a 0-20 min – linear gradient to 100% (v/v) B; 20-22 min – isocratic at 100% (v/v). The eluent was adjusted to its initial composition in 8 min, followed by equilibration for 5 min. Detection wavelengths for UV-Vis were set at 376 ± 0.5 nm and 650 ± 0.5 nm. Mass spectrometric data were recorded in positive ion mode. Nitrogen was used as both sheath (30 arbitrary units) and auxiliary gas (5 arbitrary units). Settings of the mass spectrometer were tuned by 3 µL min⁻¹ direct injection of approximately 10 µg mL⁻¹ biliverdin in 90% (v/v) aqueous acetone. Most settings were optimized via automatic tuning by using LTQ Tune Plus 2.7. Temperature of the ion transfer tube was 250 °C and the source voltage 3.5 kV. Data were recorded over the m/z segment 125-650. CID fragmentation energy was set at 35%.

RESULTS AND DISCUSSION

In order to understand the degradation of bound bilin groups upon autoxidation, free biliverdin was subjected to light-accelerated autoxidation. Biliverdin was selected as

tetrapyrrolic structure, as it closely resembled the phycocyanobilin structure and because it was readily available. After approximately 3.5 h of light-accelerated autoxidation, the maximum absorption at 650 nm decreased has 36 %, as measured spectrophotometrically (**Figure 3**).

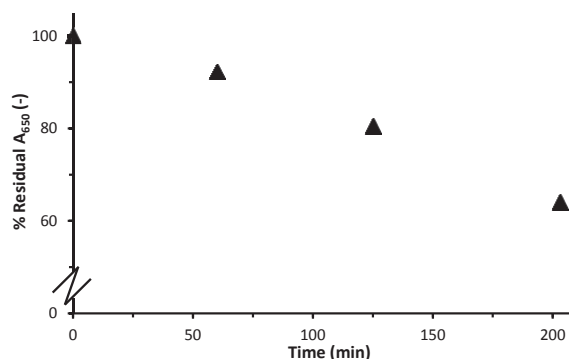


Figure 3. Decrease in visible absorption of biliverdin subjected to light-accelerated autoxidation over time at 650 nm.

Upon examining the RP-UHPLC traces of treated biliverdin, a number of coloured reaction products were found (**Figure 4** and **Table 1**). Two wavelengths were used to cover the set of degradation products formed. Nine degradation products (peaks **3a-b**, **4a-c**, **5a-c** and **8**) could be annotated as will be elaborated later. The parental biliverdin (peaks **1a-c**) eluted at retention times 10.74, 11.27 and 12.83 min. The occurrence of three peaks can be explained by the fact that biliverdin forms geometrical isomers. One or more of the three methine bridges in the molecule are probably responsible for this isomerism. As we were mainly interested in cleavage products of the tetrapyrrole, these isomers were not further characterized. They were annotated with a, b, *etc.*, following their numerical annotation. The absorption spectra of the reaction products, mostly eluting at an earlier stage of the chromatogram, lacked the absorption at 650 nm (**3a-b**, **4a-c**, **5a-c**), and had different absorption maxima at the lower wavelengths compared to biliverdin (**Figure 5**). This indicated that the chromophore of biliverdin was modified and most likely shortened.

In order to interpret the acquired MS^n data for annotation of degradation products **3a-b**, **4a-c**, **5a-c** and **8** (**Table 1**), possible autoxidation products of biliverdin were mapped *in silico* (**Figure 6**). Similar to carotenoids, it was assumed that biliverdin formed carbon-peroxyl *triplet* radicals, which react with a neutral biliverdin molecule (intramolecular homolytic substitution) (11). In this way, by disrupting the CDBs between the pyrrole groups, 11 possible autoxidation products

with additional ketone or aldehyde functionalization were constructed. Exhaustive disruption of the pyrrole-interlinking methine bridges required three autoxidation steps, which resulted in tripyrroles (**3** and **6**), dipyrroles (**4**, **5**, **8** and **11**), individual propionic acid functionalized pyrroles (**7**, **9** and **12**), 3-ethyl-4-methylpyrrole-2,5-dione (**10**) and 3-methyl-4-vinylpyrrole-2,5-dione (**2**). Interestingly, these autoxidation products are not volatile. For example, product **10** has a reported boiling point of 253 °C (12).

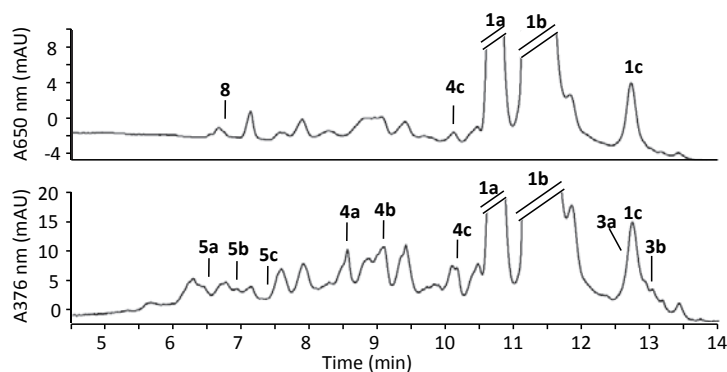


Figure 4. RP-UHPLC traces of light-accelerated autoxidation of biliverdin at 650 nm and 376 nm. Annotation of peaks and accompanying structures in **Figure 6** and **Table 1**.

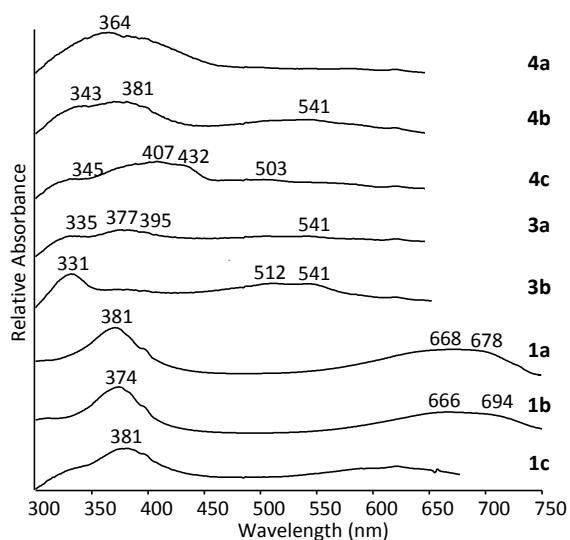


Figure 5. Absorption spectra of biliverdin (**1a-c**) and degradation products **3a-b** and **4a-c**. Structures in **Figure 6**.

Table 1. UHPLC-ESI-MS data of biliverdin and its autoxidation products. Peak numbers refer to figures throughout this chapter.

Peak No.	RT (min)	[M+H] ⁺ (m/z)	MS ² in m/z (rel. intensity)	MS ³ in m/z (rel. intensity)
2 pyrroles				
5a	6.52	301.3	N.D.	N.D.
8	6.64	373.0	N.D.	N.D.
5b	6.87	301.1	N.D.	N.D.
5c	7.35	301.1	N.D.	N.D.
4a	8.54	315.1	297.0(100), 287.1(70), 269.1(5)	269.0(100), 255.0(20), 253.1(30), 227.1(30)
4b	9.08	315.1	N.D.	N.D.
4c	10.17	315.1	297(100), 287(80), 269(5)	269(100), 255(20), 253(40), 227(40)
3 pyrroles				
3a	12.72	478.1	460.1(100), 450.1(40), 297.1(5)	442.1(10), 432.1(80), 416.1(40), 414.1(30), 401.1(50), 400.1(30), 387.1(100), 359.1(30), 328.1(20)
3b	13.01	478.1	460.1(100), 450.1(40), 297(5)	442.1(10), 432.1(80), 416.1(40), 414.1(30), 401.1(50), 400.1(20), 387.1(100), 359.1(30), 328.1(20)
4 pyrroles				
1a	10.74	583.3	565.2(25), 539.2(5), 510.1(5), 299.0(20), 297.1(100), 269.1(10)	297.0(10), 269.0(100), 251.0(10), 237.0(40), 209.0(15)
1b	11.27	583.3	565.1(20), 539.2(10), 510.1(5), 299.0(20), 297.1(100), 269.1(10)	297.0(20), 279.0(10), 269.0(100), 251.0(20), 237.0(40), 209.0(20)
1c	12.83	583.3	565.2(20), 539.2(10), 510.2(10), 299.1(15), 297.1(100), 269.1(10)	297.1(20), 279.1(10), 269.1(100), 251.1(10), 237.1(40), 209.1(25)

N.D., Not determined.

Upon examining the MS data, a number of masses predicted with the *in silico* autoxidation of biliverdin were found by their corresponding [M+H]⁺ values. Interpretation of the MS² and MS³ was greatly aided by first examining the fragmentation of the starting biliverdin parent at *m/z* 583 (**Figure 7**). The most abundant fragment in MS² was *m/z* 297. Furthermore, a less abundant signal at *m/z* 299 was observed. Both fragments represented two different dipyrroles both connected via a methine bridge. Most likely both fragment ions originated from either the single or the double bond of the middle methine bridge. The fragmentation of the methine bridge has been reported before, yielding *m/z* 297 (13). The propionic acid groups exhibited water losses, yielding *m/z* 565, and complete loss of the propionic acid group, yielding *m/z* 510. Finally, the neutral loss of 43 Da, yielding *m/z* 539, was tentatively assigned to pyrrole ring cleavage. In MS³, daughter ions resulting from further water loss (*m/z* 279) and fragmentation of the propionic acid (*m/z* 237 and

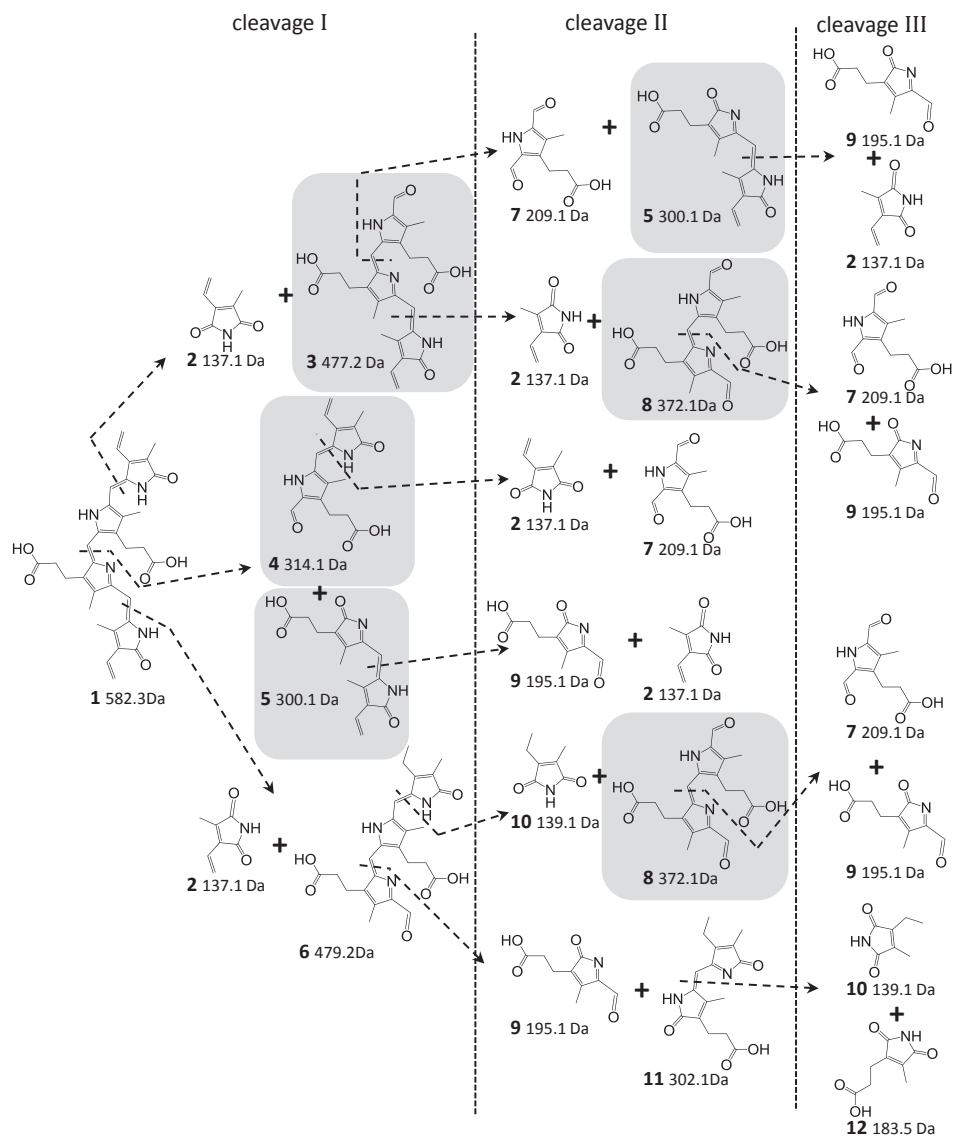
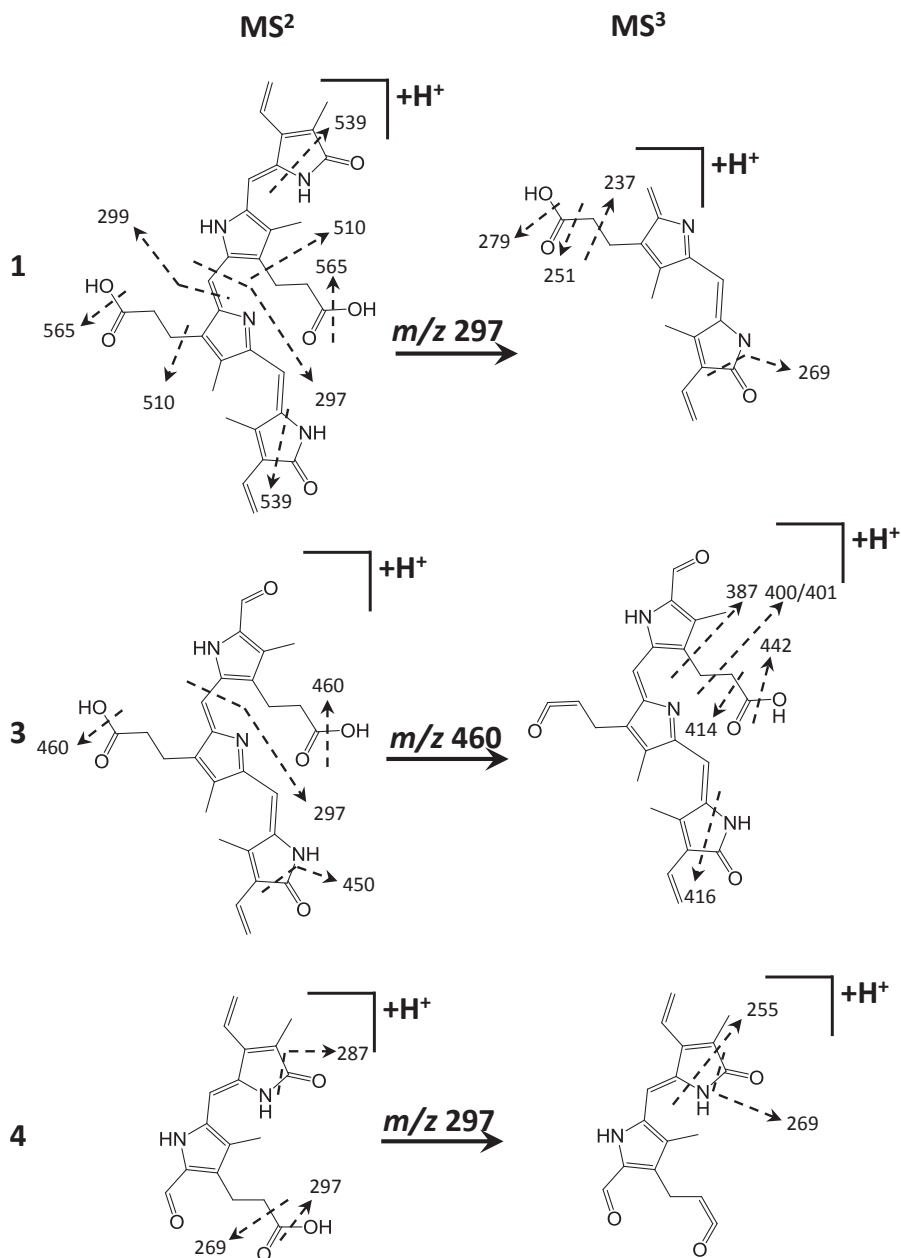


Figure 6. *In silico* autoxidation of biliverdin and autoxidation products via intramolecular homolytic substitution, as for carotenoids (**Chapter 1**). Structure numbers refer to **Figures** and **Table 1**. Structures in grey matched with UHPLC-PDA-ESI-MS data (**Table 1**). Only one of the possible geometrical isomers is depicted here.



251) were tentatively assigned. The most abundant fragment in MS³ was assigned to the loss of CO from the pyrrole ring, yielding m/z 269.

Similarly, fragmentation of autoxidation products **3** and **4** could be interpreted as demonstrated in **Figure 7**. Occurrence of a similar fragmentation with various diagnostic fragments, *i.e.* methine bridge fragmentation, CO loss, pyrrole ring cleavage, water loss and propionic acid loss, strongly suggested that the autoxidation products proposed were formed from biliverdin. For products **5** and **8**, MS² fragmentation was not triggered due to their low abundance. Structures were, therefore, tentatively assigned on the basis of their parent mass. In analogy with biliverdin, the autoxidation products also had multiple geometrical isomers (**3a-b**, **4a-c**, **5a-c**). The methine bridges in these degradation products can obviously result in several geometrical isomers, as has been described for carotenoids elsewhere (10). Large putative products **6** and **11** and the putative small products (**2**, **7**, **9**, **10**, **12**), obtained after CDB cleavage, could not be annotated using this analytical method.

Concluding, the methine bridges in biliverdin were susceptible to autoxidation. It is hypothesized that this reaction also occurs when the bilin is attached to the polypeptide of the phycobiliprotein. Furthermore, RP-UHPLC-PDA-MS was found to be a suitable tool for the assessment of bilin autoxidation products.

REFERENCES

1. Markou, G.; Nerantzis, E., Microalgae for high-value compounds and biofuels production: a review with focus on cultivation under stress conditions. *Biotechnology advances* **2013**, *31*, 1532-42.
2. Shively, J.; Adir, N.; Dines, M.; Klartag, M.; McGregor, A.; Melamed-Frank, M., Assembly and disassembly of phycobilisomes. In: *Complex intracellular structures in prokaryotes*, Vol. 2, Springer, Berlin, Germany **2006**, pp 47-77.
3. Simó, C.; Herrero, M.; Neusüß, C.; Pelzing, M.; Kenndler, E.; Barbas, C.; Ibáñez, E.; Cifuentes, A., Characterization of proteins from *Spirulina platensis* microalga using capillary electrophoresis-ion trap-mass spectrometry and capillary electrophoresis-time of flight-mass spectrometry. *Electrophoresis* **2005**, *26*, 2674-2683.
4. Mishra, S. K.; Shrivastav, A.; Mishra, S., Effect of preservatives for food grade C-PC from *Spirulina platensis*. *Process biochemistry* **2008**, *43*, 339-345.
5. Zhao, K. H.; Porra, R. J.; Scheer, H., Chapter 9: Phycobiliproteins. In: *Phytoplankton pigments: characterization, chemotaxonomy, and applications in oceanography*. Roy, S., Llewellyn C.A., Egeland, E.S., Johnsen, G. Cambridge University Press, New York, NY, USA **2011**, pp 375-411.
6. Beale, S. I.; Cornejo, J., Biosynthesis of phycobilins. Ferredoxin-mediated reduction of biliverdin catalyzed by extracts of *Cyanidium caldarium*. *Journal of biological chemistry* **1991**, *266*, 22328-22332.
7. Blot, N.; Wu, X. J.; Thomas, J. C.; Zhang, J.; Garczarek, L.; Bohm, S.; Tu, J. M.; Zhou, M.; Ploscher, M.; Eichacker, L.; Partensky, F.; Scheer, H.; Zhao, K. H., Phycourobilin in trichromatic phycocyanin from oceanic cyanobacteria is formed post-translationally by a phycoerythrobilin lyase-isomerase. *The Journal of biological chemistry* **2009**, *284*, 9290-9298.

8. MacLean, P. D.; Chapman, E. E.; Dobrowolski, S. L.; Thompson, A.; Barclay, L. R. C., Pyrroles as antioxidants: solvent effects and the nature of the attacking radical on antioxidant activities and mechanisms of pyrroles, dipyrinones, and bile pigments. *Journal of organic chemistry* **2008**, *73*, 6623-6635.
9. Chepelev, L. L.; Beshara, C. S.; MacLean, P. D.; Hatfield, G. L.; Rand, A. A.; Thompson, A.; Wright, J. S.; Barclay, L. R. C., Polypyrroles as antioxidants: kinetic studies on reactions of bilirubin and biliverdin dimethyl esters and synthetic model compounds with peroxy radicals in solution. Chemical calculations on selected typical structures. *Journal of organic chemistry* **2006**, *71*, 22-30.
10. Weesepeel, Y.; Vincken, J. P.; Bruijn, W.; Gruppen, H., Analysis of palmitoyl apo-astaxanthins and -ones, and their epoxides by UHPLC-PDA-ESI-MS, This thesis, **Chapter 4**.
11. Mordt, R. C.; Walton, J. C.; Burton, G. W.; Hughes, L.; Ingold, K. U.; Lindsay, D. A.; Moffatt, D. J., Oxidative-degradation of beta-carotene and beta-apo-8'-carotenal. *Tetrahedron* **1993**, *49*, 911-928.
12. http://www.chemicalbook.com/ChemicalProductProperty_EN_CB81454848.htm. **Last visited 12 April 2014**.
13. Gorchein, A.; Lim, C. K.; Cassey, P., Extraction and analysis of colourful eggshell pigments using HPLC and HPLC/electrospray ionization tandem mass spectrometry. *Biomedical chromatography* **2009**, *23*, 602-606.

Fatty acids attached to all-*trans*-astaxanthin alter its *cis-trans* equilibrium, and consequently its stability, upon light-accelerated autoxidation

Microalgae produce astaxanthin, which occurs mainly esterified to one or two fatty acids. Fatty acid esterification has been suggested to influence both colour stability and all-*trans*-astaxanthin stability. Discolouration can be triggered by autoxidation, that is caused by light exposure and elevated temperatures. Therefore, the influence of esterification with palmitate on astaxanthin stability was studied by exposure to light-accelerated autoxidation at different temperatures, using free all-*trans*-astaxanthin, its monoester, and its diester. An increase in palmitate esterification enhanced stability of all-*trans*-astaxanthin (measured by RP-UHPLC-PDA), whereas it had no influence on colour loss in time (measured spectrophotometrically ($A_{470\text{ nm}}$)). The mismatch in results obtained with the two assays might be explained by the observation that substitution with fatty acids influenced the *cis-trans* equilibrium. Besides many other degradation products, a larger amount of 9-*cis* astaxanthin was obtained with free astaxanthin than with its esterified forms. Furthermore, monopalmitate esterification of astaxanthin resulted in increased 13-*cis* isomer formation. The molar ratios of 9-*cis* : 13-*cis* after 60 min were 1 : 1.7 (free), 1 : 4.8 (monopalmitate) and 1 : 2.6 (dipalmitate). With its higher molar extinction coefficient compared to that of all-*trans*-astaxanthin, the formation of 9-*cis* astaxanthin might partially compensate the colour loss induced by conjugated double bond cleavage in the parent material. The different ratios of *cis-trans* isomers obtained with the three all-*trans*-astaxanthin forms might also underlie the differences in their actual stability.

INTRODUCTION

Synthetic carotenoids are used to correct for natural colour imbalances in raw materials and foods. Recent market demands for natural substitutes have stimulated carotenoid research focusing on production of carotenoids and oxygenated carotenoids (xanthophylls) from natural sources and their application in foods. An emerging source of carotenoids are microalgae (1). Unlike β,β -carotene, the 3-hydroxylated xanthophylls, *e.g.* astaxanthin, produced by microalgae predominantly exist in their fatty acid esterified forms. Hence, by implementing astaxanthin from for example *Haematococcus pluvialis* in foods, one introduces mainly monoesterified (70-90%) and diesterified fatty acid ester astaxanthin (5-25%) instead of 'free' astaxanthin (5-10%) (2, 3).

Conflicting data exists in the literature on the influence of esterification with fatty acids on the colour stability of xanthophylls (4). This is surprising, as the esters do not participate in the conjugated system of the xanthophyll. To investigate stability, purified carotenoids have been dissolved in a solvent and the mixture is subjected to oxygen, light and/or elevated temperatures (5). The degradation kinetics of the esterified xanthophyll are subsequently studied by monitoring the decrease of absorption at the wavelength of maximum absorbance (λ_{max}) or by liquid chromatography analysis. It was shown that (β)cryptoxanthin monoesters were more resistant to heat in tetrahydrofuran and hexane than their free form. Variation of the length of the saturated fatty acid attached did not influence their stability (6, 7). For lutein mono- and diesters, higher stability was reported compared to free lutein when exposed to UV light and heat in benzene (8). No significant difference was found between mono- and diesters. Other reports indicate that esterification does not always influence stability. An important factor in these studies was the choice of solvent in which the degradation was performed. A stability study of astaxanthin esters from *Euphausia superba* (antarctic krill) showed an increased stability of esterified carotenoids when dissolved in benzene or hexane, whereas for other solvents this effect was unclear (9). Capsanthin and its esters did not show any differences in stability when exposed to autoxidation in ethanol (10). Besides, it was shown that free capsanthin had higher stability in aqueous solvents and lower stability in non-polar solvents compared to diester capsanthin. The activation energies were also found to be solvent dependent. Furthermore, zero order kinetics was found in ethanol and cyclohexane, whereas first order kinetics was determined in aqueous emulsions (11). In all these reports, no analysis of degradation products was presented in order to explain the effect of fatty acid esterification on the (colour) stability of the xanthophyll.

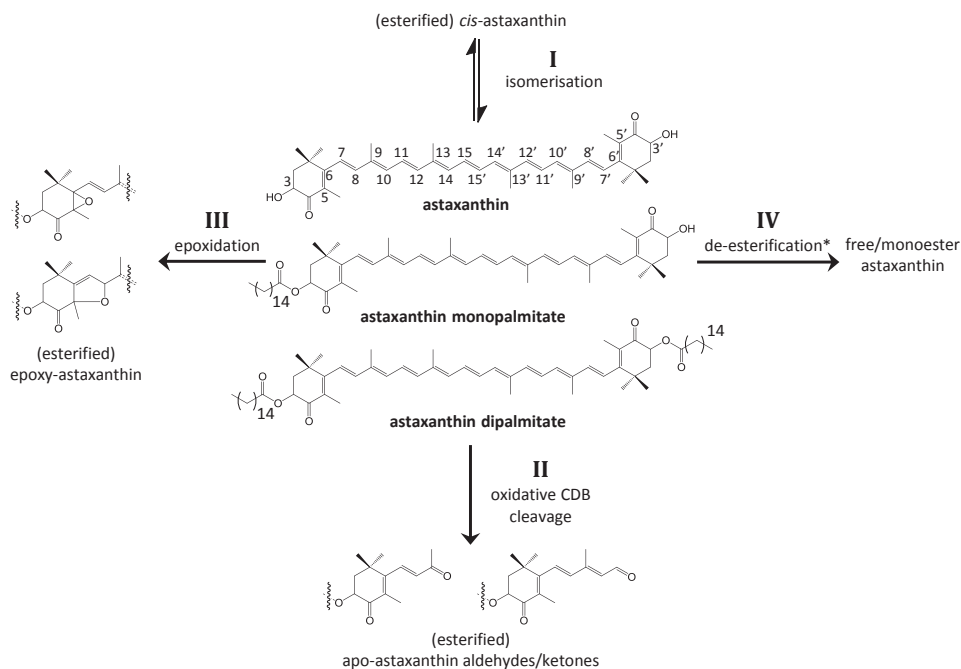


Figure 1. Simplified overview of several reactions occurring during astaxanthin degradation towards colourless products. Reactions can occur consecutively. *All astaxanthins can undergo reactions I – IV, except free astaxanthin cannot undergo reaction IV.

Hence, esterification might influence the stability of xanthophylls, but the parameters governing stability are currently unclear. For β,β -carotene, degradation processes were investigated extensively (5). Four of these degradation processes are schematically projected onto astaxanthin in **Figure 1**, as research on astaxanthin degradation is scarce. Conversion of all-*trans* astaxanthin to its geometrical *cis*-isomer (**I**, **Figure 1**) can cause a hypochromic shift leading to loss in colour intensity (12). For β,β -carotene this is reflected in the significantly lower molar extinction coefficients for the 13-*cis* (19% lower) and 15-*cis* (30% lower) isomer, whereas the 9-*cis* (2% lower) isomer is relatively unaffected (13). The *cis-trans* equilibrium is solvent dependent and is generally believed to proceed via a carotenoid biradical intermediate (14, 15). Disruption of the conjugated double bonds (CDB, **II** and **III**) also leads to colour loss. This process involves mostly autoxidation, which is a carbon-peroxyl *triplet* biradical mediated process consisting of multiple (tandem) reactions (5, 15). It can result in either the formation (**III**) of (5,6)-epoxy- or (5,8)-furanoid functionalized astaxanthins or in the formation (**II**) of apo-astaxanthin ketones and aldehydes (16). Disruption of the fatty acid ester bond (**IV**) does not lead to immediate discolouration of astaxanthin. In previous work (17), we showed that the ester bond was hardly

disrupted by light-accelerated autooxidation resulting in the formation of fatty acid esterified apo-astaxanthins. In addition to this, the different reactions **I-IV** might follow upon each other (not depicted). To conclude, it can be hypothesized that it is unlikely that fatty acid esterification at the 3- and 3'-OH position influences cleavage of the CDBs of the chromophore moiety.

In this study, we report on the effect of fatty acid esterification on the colour and all-*trans*-astaxanthin stability. Light-accelerated autooxidation is employed for degradation of the various types of astaxanthin in hexane. For colour stability, spectrophotometry at the λ_{max} of all-*trans*-astaxanthin is used and the different degradation products were monitored in time by UHPLC-PDA-ESI-MS. Both methods are compared and colour loss is related to the actual composition of the treated samples.

MATERIALS AND METHODS

Materials

All-*trans* retinal ($\geq 98\%$ w/w) was purchased from Sigma-Aldrich (St. Louis, MO, USA), (*rac.*)-apo-12'-astaxanthinal ($> 98\%$ w/w), 3*RS*,3'*RS*-astaxanthin (97% w/w), 3*RS*,3'*RS*-astaxanthin monopalmitate (97% w/w) and 3*RS*,3'*RS*-astaxanthin dipalmitate (98% w/w) were purchased from Carotenature (Lupsingen, Switzerland). ULC/MS grade acetonitrile ($\geq 99.9\%$ w/w), water containing 0.1% (v/v) formic acid (99% w/w), LC/MS grade ethyl acetate (99.8% w/w), LC grade *n*-hexane (95% w/w), and HPLC grade chloroform ($\geq 99.9\%$ v/v, corrected for stabilizer, stabilized by 0.5-1.5% (w/v) ethanol) were purchased from Biosolve (Valkenswaard, The Netherlands).

Preparation of carotenoid stock solutions

Apo-12'-astaxanthinal, retinal, free astaxanthin, astaxanthin monopalmitate and astaxanthin dipalmitate were separately dissolved in chloroform. The concentrations of all stock solutions were determined spectrophotometrically in hexane:chloroform (minimum 98% v/v *n*-hexane). Astaxanthin concentrations were determined at 470 nm using the absorption coefficient $A_{1\text{cm}}^{1\%}$ of 2100 L g⁻¹ cm⁻¹ (18). For astaxanthin monopalmitate and dipalmitate the concentrations determined were subsequently corrected for the difference in molecular weight, yielding values of $A_{1\text{cm}}^{1\%}$ 1501 and 1167 L g⁻¹ cm⁻¹, respectively. It is assumed that the fatty acid moiety had no influence on the molar extinction coefficient. For apo-12'-astaxanthinal and retinal, concentrations were determined at 421 nm and 368 nm, respectively, using absorption coefficients of 2276 (19) and 1690 L g⁻¹ cm⁻¹ (18).

Light-accelerated autoxidation

Astaxanthin (ester) solutions (1.5 mL) were subjected to light-accelerated autoxidation in quartz cuvettes (type 114-QS, Hellma Analytics, Müllheim, Germany). The cuvettes were closed and a headspace of approximately 50 μL containing atmospheric air was left. The cuvettes were incubated with their transparent side facing upwards towards the illumination source of a Suntest XLS+ (Atlas MTS, Chicago, IL, USA) equipped with a 1700 W Xenon Arc lamp and window glass filter. No air was present between the carotenoid liquid and the inner transparent side of the cuvette. The irradiation energy was set to $30 \pm 1.1 \text{ W m}^{-2}$. The black standard temperature (sensor) (T_{BST}) was used to control the liquid temperature in the cuvettes. The T_{BST} could be set in a range of $45 - 80 \text{ }^{\circ}\text{C}$ ($\pm 2 \text{ }^{\circ}\text{C}$) at an irradiation of 30 W m^{-2} . Obviously, the T_{BST} did not reflect the actual experimental temperature (T_{exp}). To measure the T_{exp} precisely, a 10 mL vapour-tight capped reference vial filled with solvent (3 mL) and similar astaxanthin concentration was used to monitor T_{exp} , which was $55.4 \pm 0.7 \text{ }^{\circ}\text{C}$, referred to as $55 \text{ }^{\circ}\text{C}$ throughout this work. The T_{exp} was monitored during the degradation with a digital HI 935005 K-type waterproof thermocouple thermometer (Hanna Instruments, Smithfield, RI, USA) equipped with a HI 776E1 general purpose thermocouple probe (resolution $0.1 \text{ }^{\circ}\text{C}$, $20 \text{ }^{\circ}\text{C} \pm 0.2\%$ deviation).

Colour loss experiments

Monitoring of colour loss by UV-Vis spectrophotometry (470 nm) was performed by diluting stock solutions of free astaxanthin, astaxanthin monopalmitate and astaxanthin dipalmitate in *n*-hexane to 10.1, 9.5, and 8.0 μM , respectively, measured by spectrophotometry. Subsequently, fourteen cuvettes were filled (1.5 mL) with a single type of astaxanthin. Absorbance of the solutions in cuvettes was measured at $t = 0$ after which they were incubated in the Suntest XLS+. Absorbance of all samples was measured at $t = 15$ and subsequently at 60 min intervals ($t = 60 - 420 \text{ min}$). For every time point, two cuvettes were taken from the Suntest XLS+ and subsequently samples from these cuvettes were pooled and evaporated to dryness under a stream of nitrogen prior to UHPLC analysis.

RP-UHPLC-PDA-ESI-IT-MS analysis of astaxanthin (esters) and degradation products

Separation and identification of carotenoid degradation products was carried out using a Thermo Accela UHPLC system (Thermo Scientific, San Jose, CA, USA) equipped with pump, degasser, auto sampler and photo diode array (PDA) detector and coupled *in-line* to a LTQ-Velos double ion trap mass spectrometer equipped with a heated ESI probe (Thermo Scientific). Samples were injected on an Aquity UPLC BEH Shield RP18 column (2.1 x 150 mm, 1.7 μm particle size; Waters, Milford, MA, USA) fitted to a Vanguard pre-column (2.1 x 5 mm, 1.7 μm particle size; Waters). The flow rate was

300 $\mu\text{L min}^{-1}$, operated at 23 °C. The eluents used were: 1% (v/v) acetonitrile in millipore water (A), acetonitrile (B) and ethyl acetate (C), all containing 0.10% (v/v) formic acid. The elution program started from 95% (v/v) A, 5% (v/v) B and followed by 0-20 min – linear gradient to 100% (v/v) B; 20-25 min – isocratic at 100% (v/v) B; 25-32 min – linear gradient to 100% (v/v) C; 32-35 min – isocratic at 100% (v/v) C; The eluent was adjusted to its initial composition in 10 min, followed by equilibration for 5 min. Detection wavelengths for UV-Vis were set at 280 ± 0.5 nm, 370 ± 0.5 nm and 450 ± 0.5 nm. Data were recorded at 10 Hz. The response of the PDA detector was found to be linear in a concentration range of 0.07-6.51 μM for free astaxanthin, 0.07-30.96 μM for astaxanthin monopalmitate, 0.03-13.60 μM for astaxanthin dipalmitate, 0.14-68.65 μM for retinal, and 0.03-17.30 μM for apo-12'-astaxanthinal, with a minimum R^2 of 0.996.

Mass spectrometric data were recorded in positive ion mode. Nitrogen was used as both sheath (30 arbitrary units) and auxiliary gas (10 arbitrary units). Settings of the mass spectrometer were tuned by 3 $\mu\text{L min}^{-1}$ direct injection of retinal in a mixture of ethyl acetate:acetonitrile 1:3 (v/v). Most settings were optimized via automatic tuning by using LTQ Tune Plus 2.7 (Thermo Scientific). Temperature of the ion transfer tube was 450 °C and the source voltage 3.5 kV. Data were recorded over the m/z segments 150-350 (0.50-10.00 min), 250-500 (10.00-15.40 min), 350-500 (15.40-19.00 min), 420-680 (19.00-23.00 min), 400-575 (23.00-24.40 min), 400-590 (24.40-24.95 min), 542-650 (24.95-26.80 min), 615-720 (26.80-29.30 min) and 615-1250 (29.30-37.00 min). Within these segments dynamic data-dependent MS^2 fragmentation was performed on the most intense parent ion ($x = 1$) and subsequently on the second most intense parent ($x = 2$). Dynamic exclusion was used to identify co-eluting apo-astaxanthins. A repeat count of two MS^2 spectra per parent ion and a maximum of $x = 25$ or within a time frame of 5.0 s were used as settings. The collision-induced dissociation was set to 35%. Data acquisition and reprocessing were done with Xcalibur 2.2 (Thermo Scientific).

Quantification by RP-UHPLC-PDA

Based on molar extinction coefficients reported for β,β -carotene and its β -apocarotenoids (18, 20, 21), a linear correlation was established between the number of carbon-carbon CDBs and the molar extinction coefficient at λ_{max} ($R^2 = 0.986$, **Figure S1, Table S1**). For astaxanthin, ϵ_{mol} was assumed to correlate in a similar way to the number (n) of carbon-carbon CDBs ($\epsilon_{\text{mol}} = 12525n - 12021$, $R^2 = 0.998$). This correlation was calculated using the values reported for apo-8'- and apo-12'-astaxanthinal (19) and all-*trans* astaxanthin (18). The molar extinction coefficients for the apo-astaxanthins are shown in **Table 1**. The aldehyde and ketone CDBs of the β -apocarotenoids were not included in this model, because correlation between the calculated ϵ_{mol} values and the reported ϵ_{mol} values for β,β -carotene and β -

apocarotenoids was found to be lower, than when these were accounted for. For astaxanthin, the C4 and C4' carbonyl groups were also omitted. For *cis*- and all-*trans*-astaxanthin an average ϵ_{mol} was determined from all three astaxanthin species used in this study. An average of at least 10 PDA UV-Vis-spectrum scans were used for calculations. The UHPLC calibration of apo-12'-astaxanthinal was used to quantify all apo-astaxanthins at their absorption maximum after correction with their corresponding calculated ϵ_{mol} values at λ_{max} . The wavelengths at which the apo-astaxanthin peak areas were determined are at their respective λ_{max} values. Epoxy-apo-9-astaxanthinone was determined using the ϵ_{mol} of apo-9-astaxanthinone at 270 nm. The *cis*-astaxanthins were quantified with the all-*trans*-astaxanthin calibration curve after correction with their corresponding ϵ_{mol} (19). Finally, the UV-Vis absorption spectra from the UHPLC-PDA of the *cis*- and apo-astaxanthins (not shown) were used to calculate their ϵ_{mol} values at 470 nm (Table 1).

Table 1. Calculated ϵ_{mol} values for apo-astaxanthins based on their number of CDBs and reported ϵ_{mol} values for intact astaxanthins.

Compound	λ_{max} (nm) ^b	Estimated ϵ_{mol} (L mol ⁻¹ cm ⁻¹) at λ_{max} ^d	Estimated ϵ_{mol} (L mol ⁻¹ cm ⁻¹) at 470 nm ^{d,e}
All- <i>trans</i> ^a	470	125100	125100
9- <i>cis</i> ^a	466	158000	157700
13- <i>cis</i> ^a	462	88100	88900
Apo-8'	461	100700	101700
Apo-10'	449	88200	74600
Apo-12'	430	75650	33450
Apo-14'	398	63100	4600
Apo-15	377	50600	0
Apo-13	340	38000	0
Apo-11	314	25550	0
(Epoxy-) Apo-9	270 ^c	13000	0

^aReported values at λ_{max} (19). ^bPreviously determined (17). ^cActual λ_{max} is 260 – 270 nm.

^dValues rounded off. ^eAverage ϵ_{mol} value for apo-astaxanthins determined from the free and the palmitate ester form.

RESULTS

Reactions occurring upon light-accelerated autoxidation by RP-UHPLC-PDA-MS analysis

To understand the influence of the fatty acid ester during degradation upon light-accelerated autoxidation, RP-UHPLC separation in combination with tandem mass spectrometry was applied to assess the reaction products of degradation reactions I – IV (**Figure 1**). Furthermore, the degradation of the three carotenoid species and the accumulation of individual reactions products were quantified, in order to relate the individual and cumulative contribution to the absorption at 470 nm measured spectrophotometrically. The RP-UHPLC method was designed to analyse both non-esterified (or ‘free’) and palmitate esterified degradation products in a single chromatographic run (17). As an example, a selection of chromatograms from the degradation of astaxanthin monopalmitate at 55 °C is depicted in **Figures 2** and **3**. Conversion of the monoester resulted in a mixture of *cis-trans* geometrical isomers (**M1-M3**) (**Figure 2A**, **Table 2**). The two main isomers formed upon astaxanthin degradation were tentatively assigned as 9-*cis*- and 13-*cis*-astaxanthin on the basis of their UV-Vis absorption spectra (**Figure 2B**) and parent masses $[M+H]^+$ (**Table 2**), as reported before (22). Similar findings were obtained with free astaxanthin (**F1-F3**) and astaxanthin dipalmitate (**D1-D3**) (chromatograms not shown). Also other geometrical isomers were formed, most likely 15-*cis* and di-*cis* variants (23). As they were solely found for the monoester and diester and were present in low quantities during the course of the degradation ($<0.1 \mu\text{M}$, max), they were not further considered.

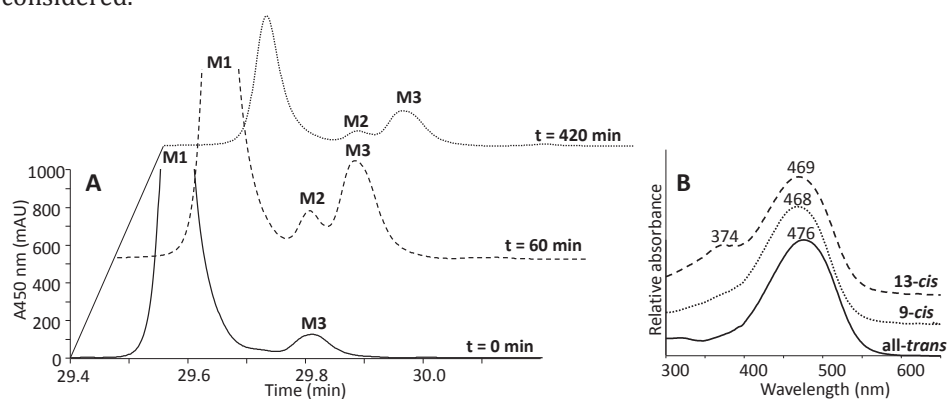


Figure 2. RP-UHPLC chromatograms of astaxanthin monopalmitate degradation at 55 °C in hexane. **A** All-*trans*- and *cis*-astaxanthin monopalmitate at 450 nm. **B** Absorption spectra of all-*trans*- (M1), 9-*cis*- (M2) and 13-*cis*- (M3) astaxanthin monopalmitate. Data for annotation are provided in **Table 2**.

Table 2. Annotation of products from reactions **I – IV** by RP-UHPLC-PDA-ESI-MS. Underlined values for reaction **II** relate to the palmitate ester of apo-astaxanthin.

No.	Rt. (min)	Identification ^a	Found for ^a	λ_{max} (nm)	[M+H] ⁺ (m/z)	No.	Rt. (min)	Identification ^a	Found for ^a	λ_{max} (nm)	[M+H] ⁺ (m/z)
Reaction I <i>cis-trans</i> isomerisation						Reaction II CDB cleavage					
F1	21.04	All- <i>trans</i> -astaxanthin	F	476	597.3	F4/E4	7.34/ <u>23.04</u>	apo-9-astaxanthinone (PE)	F,M/ <u>M,D</u>	260-270/ <u>260-270</u> ^b	223.1/ <u>483.3</u>
F2	21.57	9- <i>cis</i> -astaxanthin	F	468	597.3	F5/E5	9.32/ <u>23.21</u>	apo-11-astaxanthinal (PE)	F,M/ <u>M,D</u>	314/ <u>N.D.</u>	249.1/ <u>509.3</u>
F3	21.82	13- <i>cis</i> -astaxanthin	F	374, 469	597.3	F6/E6	11.21/ <u>23.96</u>	apo-13-astaxanthinone (PE)	F,M/ <u>M,D</u>	340/ <u>342</u>	289.1/ <u>549.3</u>
M1	29.57	all- <i>trans</i> -astaxanthin PE	M	476	835.5	F7/E7	13.09/ <u>24.59</u>	apo-15-astaxanthinal (PE)	F,M/ <u>M,D</u>	377/ <u>N.D.</u>	315.2/ <u>553.4</u>
M2	29.73	9- <i>cis</i> -astaxanthin PE	M	468	835.5	F8/E8	14.69/ <u>24.59</u>	apo-14'-astaxanthinal (PE)	F,M/ <u>M,D</u>	398/ <u>400</u>	341.2/ <u>579.4</u>
M3	29.8	13- <i>cis</i> -astaxanthin PE	M	374, 469	835.5	F9/E9	16.97/ <u>26.94</u>	apo-12'-astaxanthinal (PE)	F,M/ <u>M,D</u>	430/ <u>431</u>	381.2/ <u>619.5</u>
D1	31.15	all- <i>trans</i> -astaxanthin diPE	D	476	1073.7	F10/E10	17.68/ <u>27.37</u>	apo-10'-astaxanthinal (PE)	F,M/ <u>M,D</u>	449/ <u>450</u>	407.2/ <u>645.4</u>
D2	31.24	9- <i>cis</i> -astaxanthin diPE	D	470	1073.7	F11/E11	19.39/ <u>28.81</u>	apo-8'-astaxanthinal (PE)	F,M/ <u>M,D</u>	461/ <u>460</u>	447.2/ <u>685.4</u>
D3	31.32	13- <i>cis</i> -astaxanthin diPE	D	373, 469	1073.7	Reaction IV de-esterification					
EE4	22.78	epoxy-apo-9-astaxanthin PE	M,D	260-270	477.2	F1	21.04	all- <i>trans</i> -astaxanthin	M,D	N.D.	597.3
						M1	29.58/ <u>29.65</u>	all- <i>trans</i> -astaxanthin PE	D	N.D.	N.D.

^aPE, palmitate ester; diPE dipalmitate ester; F, free astaxanthin; M, astaxanthin monopalmitate; D, astaxanthin dipalmitate. ^bNo exact maximum could be determined.

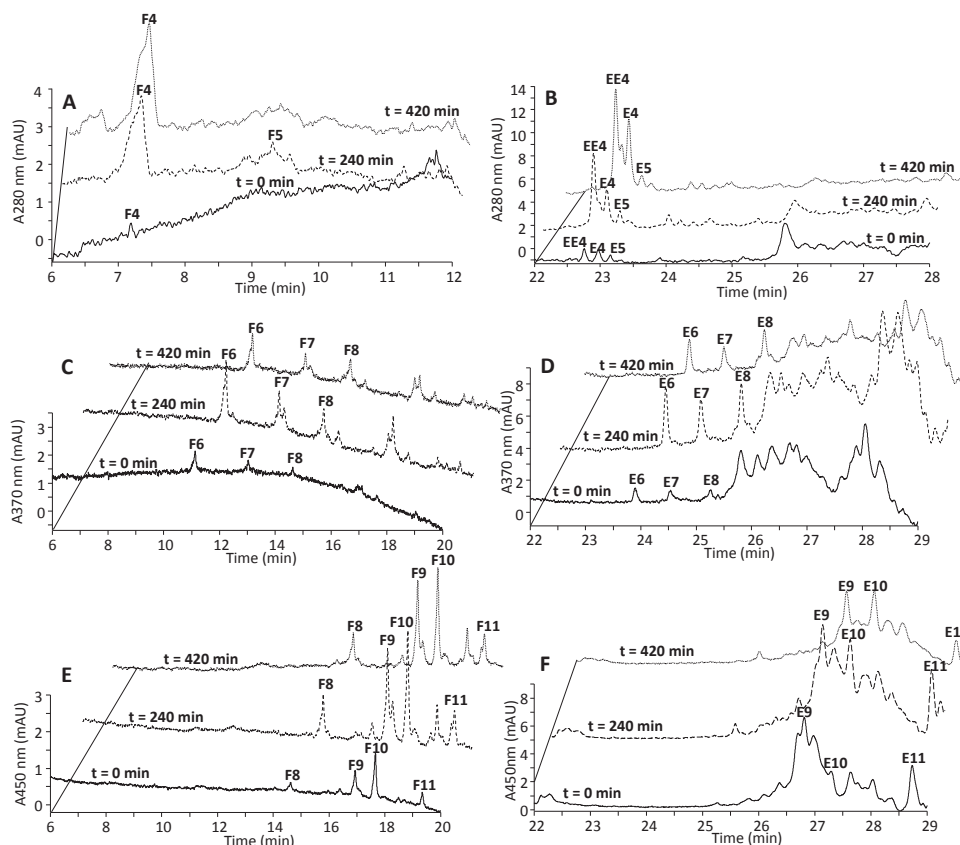


Figure 3. RP-UHPLC chromatograms of astaxanthin monopalmitate degradation at 55 °C in hexane. **A** to **F** Free apo-astaxanthins (annotated with 'F'), apo-astaxanthin palmitate ester (annotated with 'E') and epoxy-apo-astaxanthin palmitate ester (annotated with 'EE'). Apo-astaxanthins at 280 nm (**A-B**), 370 nm (**C-D**), 450 nm (**E-F**). Data for annotation are provided in **Table 2**.

Annotation of the CDB cleavage products resulting from autoxidation was performed following a similar strategy combining retention time, UV-Vis absorption spectra and parent masses. Autoxidation of astaxanthin monoester led to the formation of free apo-astaxanthins (**F4-F11**) and apo-astaxanthin palmitate esters (**E4-E11**) (**Figure 3**, **Table 2**), which were detected at 280, 370 and 450 nm. It should be noted that apo-astaxanthins formed from fatty acid esterified astaxanthins kept their fatty acid moiety upon formation of their respective aldehydes or ketones. The fatty acid moiety was confirmed by MS² fragmentation yielding the typical neutral losses (238 and 256 Da) associated with palmitate esterified apo-astaxanthins, which has been shown previously (17). The apo-astaxanthin backbones found were the ketones apo-9- and apo-13-astaxanthinone and the aldehydes apo-11-, apo-15-, apo-

14', apo-12', apo-10'- and apo-8'-astaxanthinal. The formation of apo-7'-astaxanthinal and its palmitate ester was not detected, probably due to either the volatile properties of the non-esterified form or the lack of a PDA response for the fatty acid esterified form, at the wavelengths set.

Formation of intact astaxanthin epoxides occurred, although quantification was difficult due to co-elution with a plethora of other compounds, similar as reported before (17). Nevertheless, a reaction product resulting from combined CDB cleavage and epoxidation (5,6-epoxy or 5,8-furanoid), epoxy-apo-9'-astaxanthinone palmitate ester (**EE4**, **Figure 3B**), was found. The free epoxy-apo-9'-astaxanthinone was not found. Also the de-esterification reaction occurred, yielding either free astaxanthin or astaxanthin monopalmitate. As the ester bond was hardly affected by the autoxidation process, the formation of free astaxanthin, from both monoester or diester astaxanthin, was found to be below the linear limit of detection over the entire time range (<1% of starting material). This was also the case for monopalmitate astaxanthin formation upon dipalmitate astaxanthin degradation.

All-*trans*-astaxanthin degradation rates and total accumulation of degradation products

The degradation rates (k) of free astaxanthin, astaxanthin mono- and astaxanthin dipalmitate in *n*-hexane were calculated using two methods (**Table 3**). All degradation rates were found to obey zero order kinetics. The k -values found with method 1 represented the rate of astaxanthin colour loss at 470 nm. The A_{470} could be converted to k -values for all-*trans* astaxanthin degradation when the assumption was made that the complete signal at 470 nm belonged to the residual all-*trans*-astaxanthin. Using method 1, no clear effect of esterification on k -values was observed. However, when the composition of the samples after astaxanthin treatment was assessed, it appeared that many degradation products were likely to contribute to the A_{470} (**Table 1** and **Figure 4**). As the amount of all-*trans*-astaxanthin decreased over time, the reaction products resulting from *cis*-isomerization (**I**) (9-*cis*- and 13-*cis*-astaxanthin) increased rapidly after initiation of the reaction, and subsequently decreased upon further degradation. The CDB cleavage reaction products (**II**) remained constant over time (apo-8'- to apo-11'-astaxanthinal and apo-13'-astaxanthinone), with the exception of apo-9'-astaxanthinone, which showed an increase. Also the epoxidized form of palmitoyl apo-9'-astaxanthinone accumulated for astaxanthin monopalmitate and dipalmitate (**II** + **III**). Therefore, it can be concluded that assumptions made with method 1 did not reflect reality. It was unexpected to observe compounds other than all-*trans*-astaxanthin at $t = 0$. This might be explained by observations made by others indicating that *cis* isomerisation can occur spontaneously upon dilution of the astaxanthin stock solutions in *n*-hexane (14). Furthermore, occurrence of CDB

Table 3. Zero order degradation reaction rate constants of all-*trans*-astaxanthin with different degree of fatty acid esterification determined by UV-Vis absorption at 470 nm and RP-UHPLC-PDA.

Type ^a	Method 1 ^b			Method 2 ^c	
	A_{470} $k \pm SD^d \times 10^{-3}$ ($A_{470} \text{ min}^{-1}$)	All- <i>trans</i> $k \pm SD^d \times 10^{-3}$ ($\mu\text{M min}^{-1}$)	R^2	UHPLC All- <i>trans</i> $k \times 10^{-3}$ ($\mu\text{M min}^{-1}$)	R^2
F	1.96 ± 0.09	16.4 ± 0.7	0.99	18.3	0.97
M	1.99 ± 0.03	16.6 ± 0.2	0.99	16.5	0.97
D	1.95 ± 0.01	15.4 ± 0.1	0.98	11.2	0.96

^aF, free astaxanthin; M, astaxanthin monopalmitate; D, astaxanthin dipalmitate. ^bDetermined from $t = 15$ min to $t = 420$ min. ^cDetermined from $t = 60$ min to $t = 420$ min. ^dSD, standard deviation.

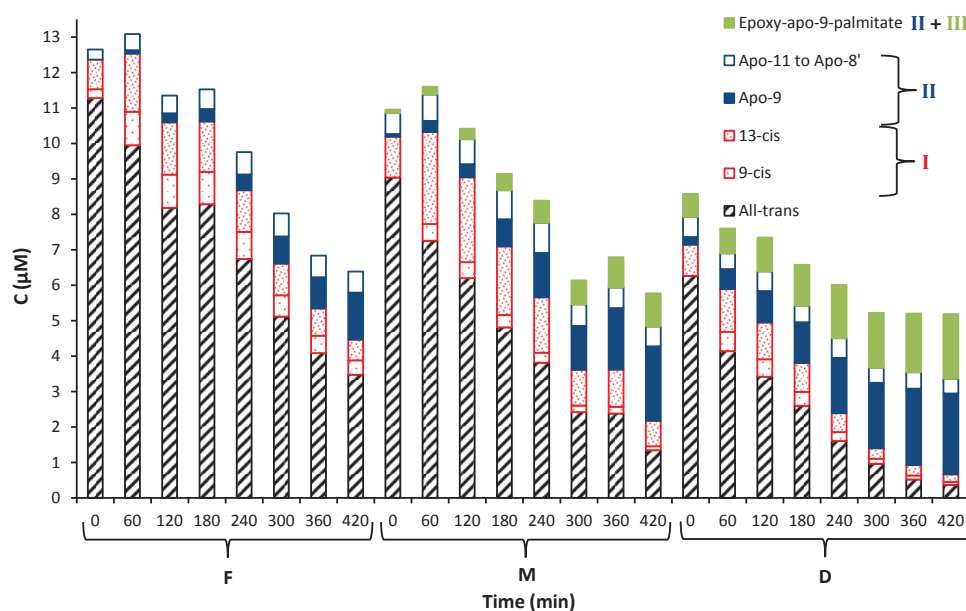


Figure 4. Total all-*trans* astaxanthin, *cis*-astaxanthins (type I reaction), apo-astaxanthin (type II reaction) and epoxy-apo-9-astaxanthin palmitate ester (type II + III reactions) content measured by RP-UHPLC-PDA in time at 55 °C. F, free astaxanthin; M, astaxanthin monopalmitate; D, astaxanthin dipalmitate.

cleavage products at $t = 0$ might be related to minor impurities from astaxanthin synthesis (24), or as a result of sample processing or storage.

As some reaction products had a maximum absorption wavelength and molar extinction coefficient quite similar to that of astaxanthin (Table 1), their contribution

to colour (A_{470}) could be substantial. As a result of this, the actual degradation of all-*trans*-astaxanthin might be underestimated. Calculating the *k*-value of all-*trans*-astaxanthin degradation by assessment of UHPLC peak areas as in **Figure 2A** (method 2) avoided this problem. Now, the *k*-values reflected an increase in all-*trans*-astaxanthin stability with esterification, a trend also reported by others in hydrophobic solvents (6-8). Thus, the A_{470} measured spectrophotometrically did not reflect the actual conversion of all-*trans*-astaxanthin.

Cis-trans isomerisation (I)

An increase of the concentration of *cis*-astaxanthins occurred rapidly, followed by a linear decrease of the *cis*-isomers as they were further degraded (**Figure 5**), obeying zero order degradation kinetics (data not shown). The 13-*cis* isomer formation was clearly more favoured than that of 9-*cis*. Similar observations have been made for free astaxanthin in other organic solvents (14). The levels of 13-*cis* isomer found after 60 min represented 15, 29 and 19 % (w/w) of the all-*trans* free astaxanthin, monopalmitate and dipalmitate starting quantities, respectively. The highest level of the 9-*cis* isomer was found for free astaxanthin and was equivalent to 8% (w/w) of the quantity of the parental all-*trans* form. For astaxanthin monoester and diester 9-*cis*

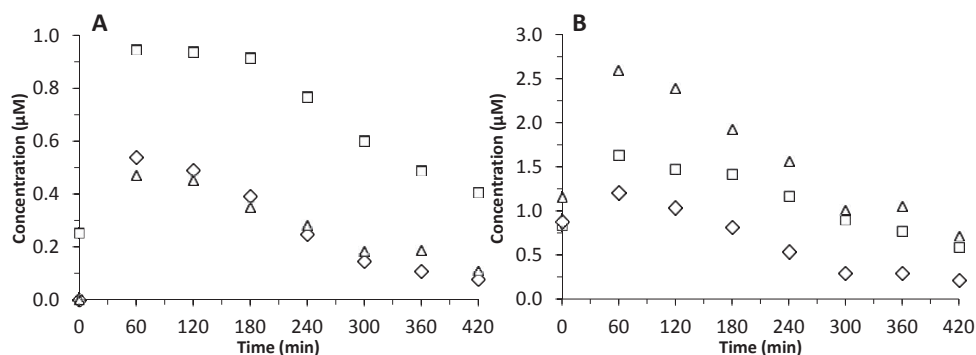


Figure 5. Concentrations of 9-*cis*-astaxanthin (**A**) and 13-*cis*-astaxanthin (**B**) during the course of 420 min of light-accelerated autoxidation in hexane at 55 °C measured by UHPLC. Free *cis*-astaxanthin (□), *cis*-astaxanthin monopalmitate (△), *cis*-astaxanthin dipalmitate (◇).

isomers, these values were 6 and 8 % (w/w), respectively. The molar ratios of 9-*cis* : 13-*cis* after 60 min were 1 : 1.7 (free), 1 : 4.8 (monopalmitate) and 1 : 2.6 (dipalmitate). During the course of degradation, absolute differences in both 9-*cis* and 13-*cis* concentrations became smaller between the different types of astaxanthin. The 13-*cis* isomerisation was especially favoured by the asymmetrical monoester. Due to this asymmetry, both the 9- and 9'-*cis* isomer, as well as the 13- and 13'-*cis* isomer can potentially be formed, but RP-UHPLC analysis did not show separate 9-, 9'-, 13- and

13'-*cis* peaks. So, either co-elution occurred or only one of the two possible *cis* isomers was formed. Remarkably, the extents of both 9-*cis* and 13-*cis* isomer formation were highly dependent on the fatty acid substitution.

CDB cleavage (II) and epoxidation (III)

The oxidation products that showed the most distinct increase in concentration were apo-9-astaxanthinone and epoxy-apo-9-astaxanthinone (**Figures 4 and 6**). The apo-9-astaxanthinone was in its free form, in both free and fatty acid ester form, and in the fatty acid ester form, when derived from free astaxanthin, astaxanthin monopalmitate and astaxanthin dipalmitate, respectively. After 420 min, concentrations reached maximum values of 12 % (free astaxanthin), 23 % (monoester) and 36 % (diester) (*mol/mol*) of its starting all-*trans* astaxanthin parent. This was 5 - 20 fold higher than that of any other apo-astaxanthin detected. Also the epoxy palmitate ester form of apo-9-astaxanthinone was found. The diester formed approximately twice as much of the epoxy-apo-9-astaxanthinone palmitate as the monoester. This might be explained by the fact that degradation of the diester will result in two epoxy-apo-9-astaxanthinone palmitates and the monoester into one. The free form of epoxy-apo-9-astaxanthinone was not observed. The prominent accumulation of apo-9-carotenones, and epoxide forms thereof, were also observed in several studies comprising astaxanthin and β,β -carotene (15, 16, 25).

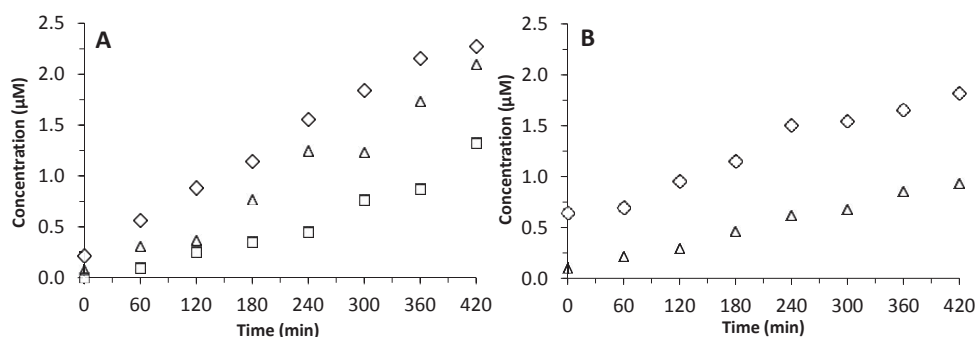


Figure 6. Formation of apo-9-astaxanthinone forms (A) and epoxy-apo-9-astaxanthinone forms (B) during light-accelerated autoxidation in hexane at 55 °C. For the monoester, non-esterified apo-9-astaxanthinone and apo-9-astaxanthinone palmitate were summed. (Epoxy)-Apo-9-astaxanthinone was derived from free astaxanthin (□), astaxanthin monopalmitate (Δ), astaxanthin dipalmitate (◇).

The apo-11, apo-13, apo-15 and apo-14 oxidation products only accumulated until 240 or 300 min (**Table 4**). After that, concentrations were reduced or remained constant probably due to exhaustion of the parent material. The apo-12', apo-10' and apo-8'-astaxanthinals did not show a distinct increase or decrease in concentration

during the course of degradation. Attachment of fatty acids did not influence the CDB cleavage in the polyene backbone. All CDBs were found to be subjected to cleavage as was shown before (16, 17, 26). The constant occurrence of low amounts of apo-11- to apo-8'-astaxanthins indicated that rapid cleavage of the first CDB was followed by further autoxidation to smaller apo-astaxanthins (Figure 4 and Table 4).

Table 4. Changes in concentrations of apo-astaxanthins and –ones during light-accelerated degradation of astaxanthins in hexane at 55 °C from t = 60 min onwards.

Apo-astaxanthin	C _{max} (μM) ^a	F	M	D
Apo-9-astaxanthinone	2.3	+	+	+
Epoxy-apo-9-astaxanthinone	1.8	N.D.	+	+
Apo-11-astaxanthinal	0.2	+ (300, –)	•	+
Apo-13-astaxanthinone	0.2	+ (240, •)	+ (240, •)	• (240, –)
Apo-15-astaxanthinal	Trace ^b	+ (240, •)	+ (240, •)	–
Apo-14'-astaxanthinal	Trace ^b	+ (300, •)	+ (240, •)	–
Apo-12'-astaxanthinal	0.4	–	–	• (420, –)
Apo-10'-astaxanthinal	Trace ^b	+	+ (240, –)	–
Apo-8'-astaxanthinal	Trace ^b	+	–	–

F, free astaxanthin; M, astaxanthin monopalmitate; D, astaxanthin dipalmitate. Symbols indicate increasing (+), decreasing (–), or constant (•) concentration observed over time. Numbers and symbols between brackets indicate changes in trend after a specific time point. Apo-astaxanthins were in their free form, in both free and fatty acid ester form, and in the fatty acid ester form when derived from F, M and D, respectively. ^aC_{max} expresses the maximum concentration of the concerning apo-astaxanthin observed. ^b<LOD, maximum values obtained estimated in the 0.1 μM range.

DISCUSSION

Spectrophotometric monitoring of colour loss and UHPLC analysis of astaxanthins compared

The use of UV-Vis spectrophotometry is a rapid and simple method for determining the colour loss of astaxanthin (esters) upon exposure to light-accelerated autoxidation. Similarly, reports on the degradation of carotenoids monitored by colour loss showed excellent reproducibility by colour determination (Hunter/CIELAB colour *e.g.* (27)) and spectrophotometric measurements (absorbance at a specific wavelength *e.g.* (11)). Cleary (Table 3), the colour loss rates for the three forms of astaxanthins was not influenced by the degree of fatty acid esterification. However, our results indicated that the UV-Vis measurements alone did not reflect the actual conversion of the parental all-*trans*-astaxanthin, as many degradation products with a substantial absorption at 470 nm were formed (Figure 4). By monitoring the actual

conversion of all-*trans*-astaxanthin for the free, the monoester, and the diester type with UHPLC-PDA, it was shown that astaxanthin stability increased with esterification. Conclusions concerning the influence of the fatty acid ester on the stability of the all-*trans*-astaxanthin should, therefore, not be drawn based on UV-Vis spectrophotometry.

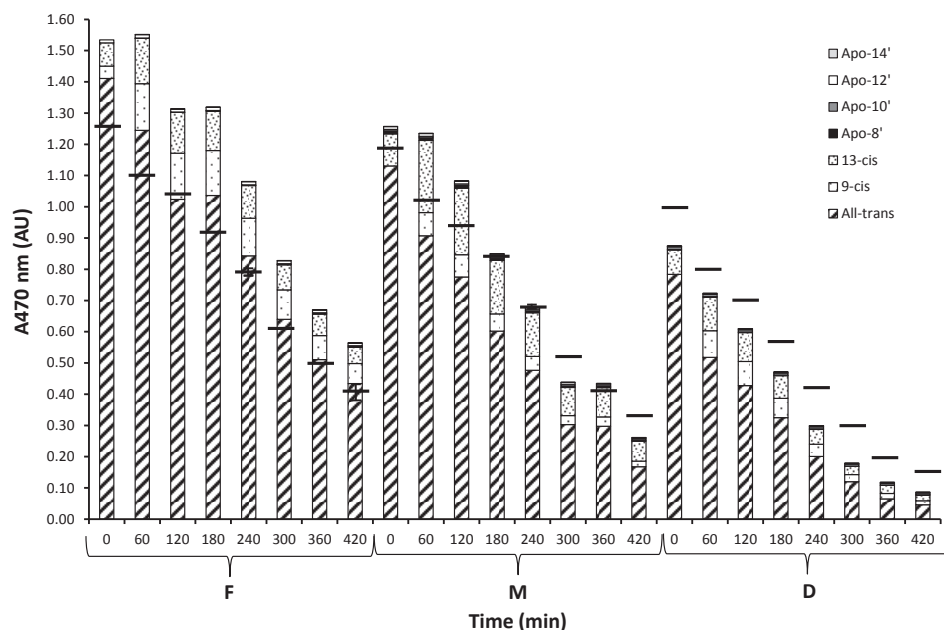


Figure 7. Comparison of the colour loss at 470 nm (55 °C) by spectrophotometry (indicated by —) and the contribution of all-*trans*-, *cis*-, and apo-astaxanthins to the cumulative absorption at 470 nm of the individual peaks, measured by RP-UHPLC-PDA (bars).

To support the above statement, the contribution of all-*trans*- and *cis*-astaxanthins and apo-astaxanthins to the total absorption at 470 nm (55 °C) was calculated (**Figure 7**). By summing the A_{470} signal of various peaks obtained with UHPLC, combined with the calculated ϵ_{mol} of the degradation products at 470 nm (**Table 1**), the A_{470} found by spectrophotometry could be (partially) reconstructed. For the reconstructed A_{470} values, a trend can be observed, *i.e.* for free astaxanthin an overestimation was found compared to the A_{470} spectrophotometric measurements, whereas for monoester and diester the values matched or were an underestimation, respectively. We do not have an explanation for this. Typically, the free astaxanthin yielded relatively more 9-*cis* than 13-*cis*, compared to its esterified forms. The 9-*cis*-astaxanthin ($\epsilon_{466} = 157,700$ and $\epsilon_{470} = 158,250 \text{ L mol}^{-1} \text{ cm}^{-1}$) has a higher molar

extinction coefficient than all-*trans*-astaxanthin ($\epsilon_{470} = 125,100 \text{ L mol}^{-1} \text{ cm}^{-1}$) and 13-*cis*-astaxanthin ($\epsilon_{462} = 88,100$ and $\epsilon_{470} = 88,900 \text{ L mol}^{-1} \text{ cm}^{-1}$). With its higher molar extinction coefficient than that of all-*trans*-astaxanthin, formation of 9-*cis* astaxanthin might partially compensate the colour loss induced by conjugated double bond cleavage in the parental all-*trans*-astaxanthin. This might explain, to some extent, the similarity in k-values for the degradation of the three types of astaxanthin obtained with spectrophotometric measurements. Formation of 13-*cis*-astaxanthin is less favourable in terms of colour (or A_{470}) retention. Larger apo-astaxanthins (**Table 1**, apo-8' to apo-14') also absorb at 470 nm, and will contribute to the A_{470} , albeit minimally due to their low concentrations. Concluding, esterification enhanced the stability of all-*trans*-astaxanthin, but this effect only becomes apparent by detailed compositional analysis of astaxanthin degradation products.

Mechanism behind enhanced stability of esterified astaxanthins

Most striking in the compositional analysis of reaction products derived of all-*trans*-astaxanthin was the observation that the fatty acid ester influenced the formation of the *cis* geometrical isomers. For free astaxanthin after 60 min at 55 °C, 23% (w/w) of the original all-*trans* astaxanthin was converted into the 9- and 13-*cis* geometrical isomers, whereas for the monopalmitate and dipalmitate this was 34 % and 28 % (w/w), respectively. Especially the formation of 13-*cis* from astaxanthin monopalmitate (29% (w/w)) stood out compared to the free and dipalmitate form (15% and 19% (w/w), respectively) (**Figure 5**). The formation of carotenoid *cis* geometrical isomers is generally believed (15) to proceed via a carotenoid *singlet* biradical and involves subsequent rotation on one of the CDBs (**Figure 8**). It remains unclear why esterification with one palmitic acid increased rotation around one of the 13-14 CDBs.

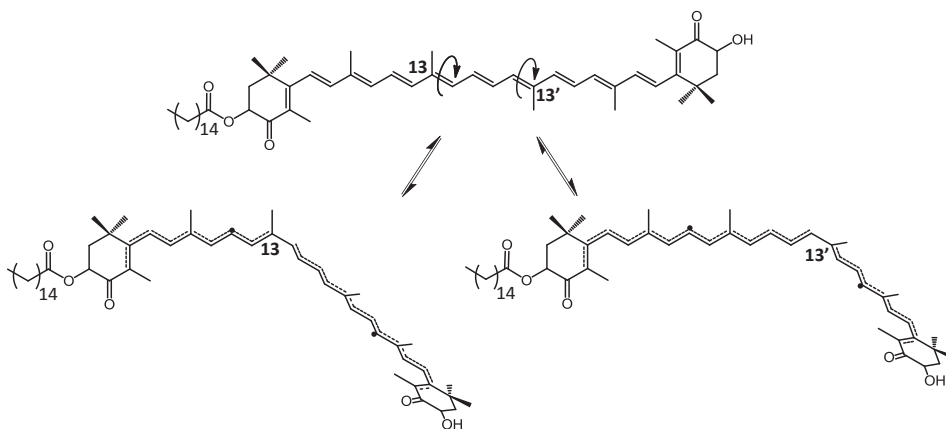


Figure. 8 Formation of the 13-*cis* and 13'-*cis* geometrical isomers of astaxanthin monopalmitate via the carotenoid biradical.

With respect to CDB cleavages, esterification of astaxanthin with fatty acids did not seem to alter the pattern of apo-astaxanthins formed, as evidenced by the similar accumulation of (epoxy-)apo-9-astaxanthinones (**Figure 6**) and that of the other apo-astaxanthins (**Table 4**). Interestingly, the apo-9-astaxanthinone and its epoxide variant were clearly more resistant towards further degradation than the other apo-astaxanthins measured. They probably served as an apo-astaxanthin 'sink' before further autoxidation will degrade them into structures, which are no longer reminiscent of astaxanthin. Due to their keto functionalization, the reactivity of the (epoxy)-apo-9-astaxanthinones was lower compared to that of the aldehydes. Furthermore, larger apo-astaxanthins in general do not accumulate, as they are more rapidly degraded and subsequently result in additional amounts of smaller apo-astaxanthins (15). The question arises if one of the CDBs might be indicated as the weakest link or if CDB scissions were random. Several propositions on the first cleavage site in the polyene tail have been made. It has been proposed that the 7-8 CDB position was cleaved first, followed by subsequent progressive degradation of the backbone (28). A second theory indicated that the 13-14 CDB is most vulnerable to autoxidation in the case of astaxanthin (16). As constant levels of all apo-astaxanthins were found, with the exception of (epoxy)-apo-9-astaxanthinones, both theories are in principle possible. Interestingly, it has been suggested that *cis*-astaxanthins are less stable than all-*trans*-astaxanthin, and that the position of the *cis*-bond affected the stability in a rather unpredictable way (29). Besides affecting colour intensity as a result of different molar extinction coefficients of the various geometrical isomers, *cis-trans* isomerisation also seems to affect the sensitivity to cleavage of certain double bonds in the polyene chain. Thus, it seems as if both reactions **I** and **II** can be influenced by esterification with fatty acids: reaction **I** directly, as esterification affects the ratio between geometrical isomers, reaction **II** indirectly, as cleavage of certain geometrical isomers seems to be preferred.

ACKNOWLEDGEMENTS

This work was supported by FeyeCon D&I and by grants from NL Agency and the Ministry of Education, Culture and Science (Project no. FND09014).

REFERENCES

- Mulders, K. J. M.; Lamers, P. P.; Martens, D. E.; Wijffels, R. H., Phototrophic pigment production with microalgae: biological constraints and opportunities. *Journal of phycology* **2014**, *50*, 229-242.
- Hussein, G.; Sankawa, U.; Goto, H.; Matsumoto, K.; Watanabe, H., Astaxanthin, a carotenoid with potential in human health and nutrition. *Journal of natural products* **2006**, *69*, 443-449.
- Miao, F.; Lu, D.; Li, Y.; Zeng, M., Characterization of astaxanthin esters in *Haematococcus pluvialis* by liquid chromatography-atmospheric pressure chemical ionization mass spectrometry. *Analytical biochemistry* **2006**, *352*, 176-81.
- Pérez-Gálvez, A.; Mínguez-Mosquera, M. I., Esterification of xanthophylls and its effect on chemical behavior and bioavailability of carotenoids in the human. *Nutrition research* **2005**, *25*, 631-640.
- Boon, C. S.; McClements, D. J.; Weiss, J.; Decker, E. A., Factors influencing the chemical stability of carotenoids in foods. *Critical reviews in food science and nutrition* **2010**, *50*, 515-532.
- Fu, H.; Xie, B.; Fan, G.; Ma, S.; Zhu, X.; Pan, S., Effect of esterification with fatty acid of β -cryptoxanthin on its thermal stability and antioxidant activity by chemiluminescence method. *Food chemistry* **2010**, *122*, 602-609.
- Arita, S.; Otsuki, K.; Osaki, K.; Murata, Y.; Shimoishi, Y.; Tada, M., Reduction in photostability by the esterification of beta-cryptoxanthin. *Bioscience biotechnology and biochemistry* **2004**, *68*, 451-453.
- Subagio, A.; Wakaki, H.; Morita, N., Stability of lutein and its myristate esters. *Bioscience biotechnology and biochemistry* **1999**, *63*, 1784-1786.
- Miki W.N.; Kondo Y.; Murakami M.; Yamaguchi K.; Konosu S.; Satake M.; Fujita T., The stability of carotenoids pigments in the antarctic krill *Euphausia superba*. *Bulletin of Japanese society of scientific fisheries* **1983**, *49*, 1417-1420.
- Goda, Y.; Nakamura, H.; Sakamoto, S. S.; Ishikawa, K.; Maitani, T.; Yamada, T., Photo-stability of coloring constituents in paprika color. *Journal of the food hygienic society of Japan* **1997**, *38*, 240-247.
- Mínguez-Mosquera, M. I.; Jaren-Galan, M., Kinetics of the decolouring of carotenoid-pigments. *Journal of the science of food and agriculture* **1995**, *67*, 153-161.
- Schüep, W.; Schierle, J., Example 9: determination of stabilized, added astaxanthin in fish feeds and pre-mixes. In: *Carotenoids Vol. 1A Isolation and analysis*, Edited by Britton G., Liaen-Jensen S., Pfander H., Birkhäuser Verlag, Basel, Switzerland **1995**, pp 273-276.
- Schierle, J.; Härdi, W.; Faccin, N.; Bühler, I.; Schüep, W., Example 8: Geometrical isomers of β , β -carotene. In: *Carotenoids Vol. 1A Isolation and analysis*, Edited by Britton G., Liaen-Jensen S., Pfander H., Birkhäuser Verlag, Basel, Switzerland **1995**, pp 265-272.
- Yuan, J.-P.; Chen, F., Isomerization of *trans*-astaxanthin to *cis*-isomers in organic solvents. *Journal of agricultural and food chemistry* **1999**, *47*, 3656-3660.
- Mordi, R. C.; Walton, J. C.; Burton, G. W.; Hughes, L.; Ingold, K. U.; Lindsay, D. A.; Moffatt, D. J., Oxidative-degradation of beta-carotene and beta-apo-8'-carotenal. *Tetrahedron* **1993**, *49*, 911-928.
- Etoh, H.; Suhara, M.; Tokuyama, S.; Kato, H.; Nakahigashi, R.; Maejima, Y.; Ishikura, M.; Terada, Y.; Maoka, T., Auto-oxidation products of astaxanthin. *Journal of oleo science* **2012**, *61*, 17-21.
- Weesepoel, Y.; Vincken, J. P.; Bruijn, W.; Gruppen, H., Analysis of palmitoyl apo-astaxanthinols and -ones, and their epoxides by UHPLC-PDA-ESI-MS **This thesis, Chapter 4**.
- Britton, G., Chapter 2: UV/Visible spectroscopy. In: *Carotenoids Vol. 1B Spectroscopy*, Edited by Britton G., Liaen-Jensen S., Pfander H., Birkhäuser Verlag, Basel, Switzerland **1995**, pp 13-62.

19. CaroteNature GmbH, Lupsingen, Switzerland, Data Sheets (9Z,*rac./meso*)-astaxanthin, (13Z,*rac./meso*)-astaxanthin, (*rac.*)-8'-apo-astaxanthinal, (*rac.*)-12'-apo-astaxanthinal.
20. Barua, A.B.; Olson, J.A.; Furr, H.C.; van Breemen, R.B., Chapter 1: Vitamin A and carotenoids. In: *Modern chromatographic analysis of vitamins*. Edited by: Leenheer, A. P.; Lambert, W. E.; Van Bocxlaer, J. F., 3rd ed., Marcel Dekker, New York, NY, USA **2000**, pp 13- 86.
21. El-Agamey, A.; McGarvey, D., *Chapter 7 Carotenoid Radicals and Radical Ions*. In: Carotenoids vol. 4: Natural functions. Edited by: Britton, G.; Liaaen-Jensen, S.; Pfander, H., Birkhäuser Verlag, Basel, Switzerland **2008**, pp 119-154.
22. Weesepeel, Y.; Vincken, J.-P.; Pop, R. M.; Liu, K.; Gruppen, H., Sodiation as a tool for enhancing the diagnostic value of MALDI-TOF/TOF-MS spectra of complex astaxanthin ester mixtures from *Haematococcus pluvialis*. *Journal of mass spectrometry* **2013**, *48*, 862-874.
23. Euglert, G.; Vecchi, M., *trans/cis* Isomerization of astaxanthin diacetate/isolation by HPLC and identification by ¹H-NMR. Spectroscopy of three mono-*cis*- and six di-*cis*-isomers. *Helvetica chimica acta* **1980**, *63*, 1711-1718.
24. Rao, R. N.; Alvi, S. N.; Rao, B. N.; Chemis, H. G. A., Preparative isolation and characterization of some minor impurities of astaxanthin by high-performance liquid chromatography. *Journal of chromatography A* **2005**, *1076*, 189-192.
25. Kanasawud, P.; Crouzet, J. C., Mechanism of formation of volatile compounds by thermal degradation of carotenoids in aqueous medium. 1. beta-carotene degradation. *Journal of agricultural and food chemistry* **1990**, *38*, 237-243.
26. Rodriguez, E. B.; Rodriguez-Amaya, D. B., Formation of apocarotenals and epoxycarotenoids from β-carotene by chemical reactions and by autoxidation in model systems and processed foods. *Food chemistry* **2007**, *101*, 563-572.
27. Marty, C.; Berset, C., Factors affecting the thermal degradation of all-*trans*-beta-carotene. *Journal of agricultural and food chemistry* **1990**, *38*, 1063-1067.
28. Ghidouche, S.; Rey, B.; Michel, M.; Galaffu, N., A rapid tool for the stability assessment of natural food colours. *Food chemistry* **2013**, *139*, 978-985.
29. Hernandez-Marin, E.; Galano, A.; Martínez, A., *cis* Carotenoids: colorful molecules and free radical quenchers. *The journal of physical chemistry B* **2013**, *117*, 4050-4061.

SUPPLEMENTARY INFORMATION

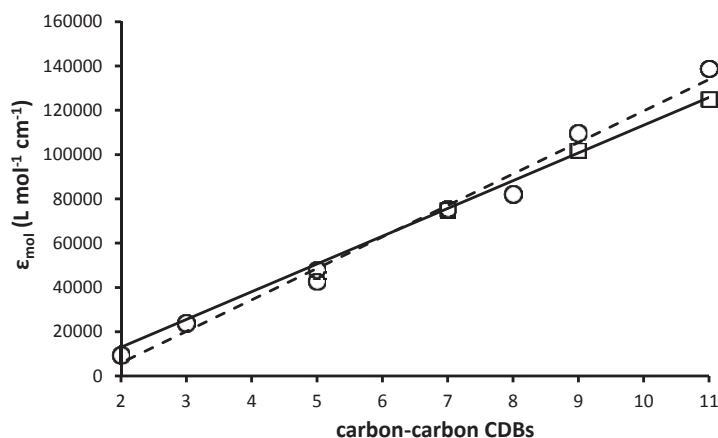


Figure S1. Correlation between the number of carbon-carbon CDBs (conjugated double bonds) and their ϵ_{mol} for β,β -carotene (○, dashed line) and astaxanthin (□, continuous line) with correlation coefficients $R^2=0.986$ and $R^2=0.998$, respectively.

Table S1. Maximum absorption (λ_{max}) with accompanying molar extinction coefficients (ϵ_{mol}) for β -apo-carotenoids and β,β -carotene (18, 20, 21).

	No. c-c-CDB	λ_{max} (nm)	ϵ_{mol} (L mol ⁻¹ cm ⁻¹)
Apo-9	2	295	9450
Apo-11	3	350	24000
Apo-13	4	N.A.	N.A.
Apo-15	5	368	48000
Apo-15	5	383	42800
Apo-14'	6	N.A.	N.A.
Apo-12'	7	414	75600
Apo-10'	8	435	82300
Apo-8'	9	457	109800
β,β -car	11	450	139000

N.A.: not available

Chapter 7

General discussion

As described in **Chapter 1**, the research in this thesis was aimed at understanding the influence of fatty acid esterification on stability of astaxanthin and the kind of degradation products formed. For this, hyphenated analytical methodologies were developed. Two main techniques were in the centre of the analytical arena: (i) MALDI-TOF/TOF-MS, for the analysis of complex astaxanthin ester mixtures in **Chapter 2** and (ii) UHPLC-PDA-ESI-MS, for extensive exploration of the carotenoids (esters) in *Chlorella zofingiensis* in **Chapter 3**, apo-astaxanthins (esters) in **Chapters 4** and **6**, and oxidation products of biliverdin, as an additional microalgal pigment, in **Chapter 5**. This chapter discusses the major findings of this thesis and extrapolates these in order to address the prospects and limitations of the use of hyphenated analysis techniques in carotenoid research. Furthermore, it evaluates the validity of research on the stability of astaxanthin esters in model systems.

HYPHENATED TECHNIQUES IN CAROTENOID AND TETRAPYRROLE ANALYSIS

Sodiation as a tool for mass spectrometry of xanthophylls: curse or cure?

The first main conclusion of this research was that in MALDI-TOF(/TOF)-MS analysis, sodiation simplifies parent mass spectra and fragmentation spectra of astaxanthin fatty acid esters, whereas it also improves the signal to noise (S/N) ratios (**Chapter 2**). For the astaxanthin monopalmitate esters the improvement in S/N ratio was more pronounced than for the dipalmitate esters. The fragmentation spectra in both ion trap (IT) and TOF/TOF fragmentation were simpler and became unambiguous for the identification of astaxanthin and its fatty acid ester forms. This advantage of obtaining simpler mass spectra from sodiated parent masses was also exploited upon ESI-IT-MS analysis in **Chapter 3** to identify ketolutein fatty acid esters. A similar strategy in ESI-IT-MS analysis was employed in **Chapter 4**, where MS² spectra of sodiated parents of fatty acid esterified apo-astaxanthins were used as additional evidence for annotation, besides MS² spectra of the protonated parents. (apo)-Astaxanthins and ketoluteins have keto groups at the C4 position(s) and hydroxyl groups at the C3 position(s) in common. This combination of substituents might, therefore, be very favourable for the formation of the sodiated adducts. Nevertheless, the following question arises: Would other xanthophylls with different end group substitutions also benefit from sodiation in mass spectrometry?

In order to gain additional insight in this matter, as an additional experiment, a number of xanthophyll standards were analysed in a similar way as in **Chapter 2**. The spontaneous formation of [M+Na]⁺ without any pre-treatment (desalting) of (free) astaxanthin is immediately reflected by the high prevalence of *m/z* 619.3 (**Figure 1A**). The xanthophylls echinenone (C4-keto, *m/z* 550.4), canthaxanthin (C4 and C4'-keto, *m/z* 565.4) and lutein (C3 and C3' -hydroxyl, *m/z* 568.4), all lacking the specific keto-hydroxyl configuration at the C3 and C4 positions, had clearly detectable

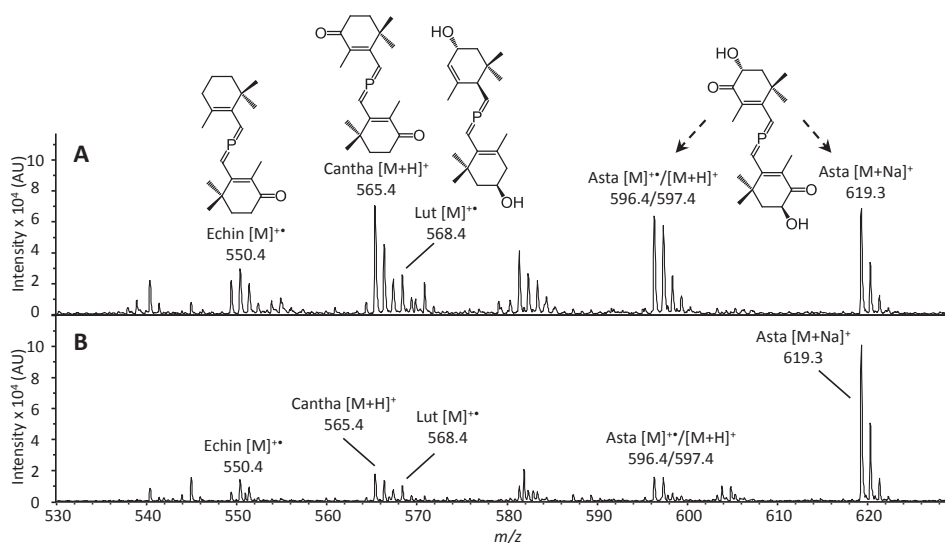


Figure 1. Effect of sodiation on the parent mass formation of different xanthophylls by MALDI-TOF-MS. **A** No pretreatment, **B** Addition of 0.1 mM sodium acetate. *Echin*, echinenone; *Cantha*, canthaxanthin; *Lut*, lutein; *Asta*, astaxanthin; $P = \text{CH}_2 = \text{CH} - \text{CH}(\text{CH}_3) - \text{CH} = \text{CH} - \text{CH}(\text{CH}_3) - \text{CH} = \text{CH} - \text{CH}(\text{CH}_3) - \text{CH} = \text{CH} - \text{CH}(\text{CH}_3) - \text{CH} = \text{CH} - \text{CH}_3$. MALDI-TOF-MS analysis was performed as in **Chapter 2**. Standards were as in **Chapter 3**.

Another extension of this sodiation concept would be the use of full sodiation of astaxanthin ester parents with LC-MS (ESI or APCI spray interfaces). In **Chapters 2, 3 and 4**, sodium adducts were spontaneously formed, besides the more abundant protonated parents. To achieve this parent mass sodiation in LC-MS, either the ion house gasses should be adjusted or a volatile sodium salt should be added to the eluents of the LC apparatus. However, both options have disadvantages. First, the ion house gasses need to be dynamically adjusted, while the solvent composition is changing during elution. For most soft ionization MS devices, adjusting ion house gasses during analysis will disrupt the spray current, resulting in loss of MS signal. Hence, numerous MS tuning settings need to be adjusted during the analysis. The

second option, adding sodium to the eluents, is often undesirable because salt will crystallize on the spray nozzle or at the entrance (ion transfer tube) of the mass spectrometer. Although this second option has been performed before (1) with a volatile sodium salt, long-term effects on the condition of the equipment are not known.

Combining *in-line* and *off-line* MS techniques for rapid profiling of carotenoids

The second main finding (by UHPLC-PDA-ESI-MS analysis) was that *C. zoefingiensis* produced ketolutein and its fatty acid esters upon nitrogen depletion (**Chapter 3**). The combination of LC and *in-line* MS proved to be an essential analytical technique to annotate ketolutein and its fatty acid esters as well as to determine its possible biosynthetic pathway. The combination of visible absorption spectra, parent mass and daughter ions provided sufficient information to exclude possible other carotenoid structures. The lutein *R/S* configuration was probably unchanged upon conversion to ketolutein, making this the 3*S*, 3'*R*, 6'*R* isomer better known as fritschiellaxanthin. Furthermore, UHPLC analysis showed that upon diphenylamine addition, the ketolutein and the primary carotenoids were not affected, whereas the levels of secondary β,β -carotene derivatives decreased. The use of LC-MS techniques to obtain quantitative information is essential for modelling the fluxes through the biosynthetic pathways of the pigments in microalgae. Although daily LC analysis of reactor samples is possible, usually the samples of several days are collected. In this way an efficient LC-MS experiment can be carried out taking into account the set-up of an LC-MS experiment. UV-VIS analysis does not suffice either. Although it is possible to estimate the total pigment accumulation by measuring the ratio of two optical densities at 450 and 660 nm spectrophotometrically, this ratio is often insufficient for microalgae that accumulate a complex set of pigments with overlapping UV-Vis spectra. MALDI-TOF-MS is more suitable for routine daily analysis, as analysis set-up is fast and analysis time is very short. The potential of MALDI-TOF-MS analysis for semi *real-time* monitoring has been enhanced by the development of direct MALDI-TOF-MS analysis of plant and algal cells *in vivo* (2, 3), thereby eliminating solvent-mediated extraction, which decreases total analysis time even more. Sodiation for enhancing the S/N ratios of astaxanthin and ketolutein (esters) might play a crucial role in semi *real-time* measurements. The ratios between carotenoid ester parent masses give an indication of the relative concentrations of the esters in the sample, assuming that ionization efficiencies of the different types of astaxanthin are equal (**Chapter 2**). Hence, MALDI-TOF-MS might be used as a semi *real-time* analysis method for targeting individual carotenoids.

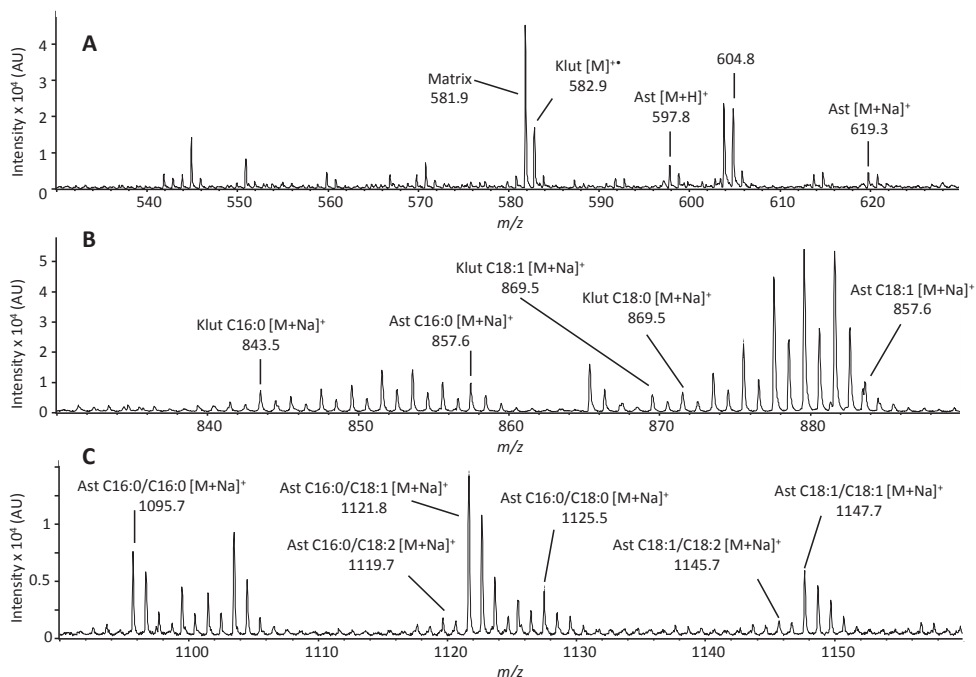


Figure 2. MALDI-TOF-MS analysis (DHB + 0.1 mM sodium acetate) of a crude chloroform extract of nitrogen depleted *C. zoefingensis*. **A** free xanthophyll range, **B** xanthophyll monoester range, **C** xanthophyll diester range. Ast: astaxanthin, Klut: ketolutein. MALDI-TOF-MS analysis was performed as in **Chapter 2**. Disruption and extraction (*in singlo*) of *C. zoefingensis* biomass was performed as in **Chapter 3**.

Therefore, as an additional experiment, we demonstrated the use of MALDI-TOF-MS on a carotenoid chloroform extract (without prior fractionation as in **Chapter 2**) of late stage nitrogen depleted *C. zoefingensis* cells (**Figure 2**). Three analysis windows were chosen for free (m/z 530 – 630), monoesterified (m/z 830 – 890) and diesterified (m/z 1090 – 1160) xanthophylls. The addition of 0.1 mM sodium acetate pushed both astaxanthin and ketolutein into their sodiated parents. In the *C. zoefingensis* extract a plethora of different masses appeared. Masses associated with chlorophylls *a* and *b* were not found. This was probably due to the late stage of nitrogen starvation, which resulted in the complete decay of chlorophylls. Free astaxanthin $[M+H]^+$ and $[M+Na]^+$ and ketolutein $[M]^{+•}$ (**Figure 2A**) could be swiftly annotated based on their parent masses. For ketolutein, no $[M+Na]^+$ was found at m/z 605, solely a slightly smaller m/z value of 604.8, which could be matrix related. The astaxanthin and ketolutein fatty acid esters (**Figures 2B** and **C**) were all annotated on the basis of their sodiated parent masses, with exception of the ketolutein diesters, which were probably present in trace amounts (**Chapter 3**). The other free

xanthophylls were not found upon using sodiation, as we commented in the previous section. Interestingly, the astaxanthin diesters were found without prior concentration. Quantification of carotenoids using MALDI-TOF-MS was demonstrated before (2). The method involved relative quantification of carotenoids by using internal carotenoid standards (*e.g.* isotope labelled or endogenous carotenoids). Although the development of this method requires additional ascertainment, this opens the opportunity for MALDI-TOF-MS to become a tool to monitor pigment accumulation or stress responses in algae semi *real-time* on a day-to-day or, if desirable, an hour-to-hour basis. This enables researchers to adjust experimental settings if necessary before the run-out is completed. Furthermore, it can be envisioned that the knowledge obtained in *off-line* MS techniques can be extended to other applications (*e.g.* food matrices, higher plants). Evidently, when unknown samples are assessed, LC analysis for initial determination of the exact qualitative pigment composition remains a prerequisite prior to MALDI-TOF-MS application.

The use of chemical derivatization for additional ascertainment of functional groups

The third main conclusion is that mild (light-accelerated autoxidation) and harsh (hypochlorite bleaching) oxidation of mono- and dipalmitate astaxanthins resulted in the formation of palmitoyl apo-astaxanthin aldehydes and ketones (**Chapter 4**). The LC-MS technique was crucial to (i) establish the correct apo-astaxanthin and (ii) the fatty acid ester substitution. Non-esterified apo-astaxanthins and -ones were formed upon degradation of free and monopalmitate astaxanthins. For light-accelerated autoxidation, the apo-astaxanthins detected had 3 (apo-9) to 10 (apo-8') conjugated double bonds (CDB), whereas for hypochlorite bleaching this apo-astaxanthin set was more restricted. Furthermore, the fatty acid ester was found to be hardly affected by light-accelerated autoxidation, resulting in trace amounts of free and monopalmitate astaxanthin upon dipalmitate degradation. For hypochlorite bleaching, fatty acid ester scissions were more frequent. This was observed by the formation of free apo-astaxanthins upon astaxanthin dipalmitate degradation.

Additionally, hypochlorite bleaching was of interest because of the relatively high formation of epoxide-apo-9 and 13-astaxanthinones. However, mass spectrometric data could not distinguish between a 5,6-epoxide or 5,8-furanoid configuration. This was in contrast with **Chapter 3**, where MS² fragmentation in combination with UV-Vis spectra was sufficient for ascertainment of ketolutein. To gain additional insight in the epoxide group configuration in **Chapter 4**, chemical derivatization was used (4). It was shown (**Chapter 4**) that this tool was not always a guarantee for an indisputable conclusion on epoxide groups in the case of apo-astaxanthins. In the case of ketolutein, when the hyphenated analytical techniques used would not have provided the diagnostic information, application of chemical

derivatization for end group characterization by sodium borohydride (NaBH_4) could have been a possible strategy. Recently, the occurrence of ketolutein (esters) in other green algal species (*H. pluvialis*, *S. rubescens* and *C. reinhardtii*) was reported (5). In that research the identification of ketolutein was performed by comparing the UV-Vis spectra with literature values. As additional proof, NaBH_4 reduction of the C4 carbonyl was performed, resulting in 4-hydroxylutein, which had an increased spectral fine structure, resembling lutein (**Figure 3**) (6). As a comparison, (incomplete) reduction of astaxanthin containing two carbonyls resulted in idoxanthin and crustaxanthin.

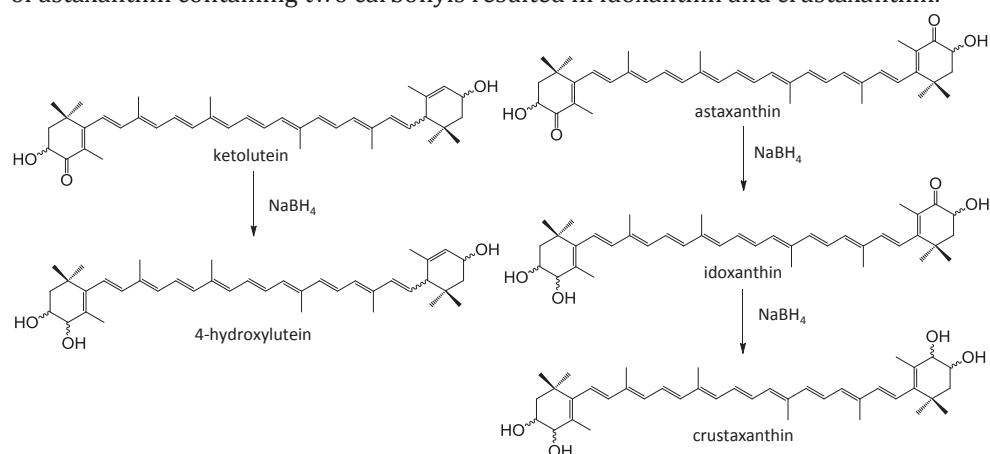


Figure 3. NaBH_4 reduction of ketolutein and astaxanthin to their respective hydroxylated carotenoids. *R/S* configuration was not regarded here. Adapted from (5).

Impact of biliverdin light-accelerated autoxidation on phycobiliproteins

A fourth conclusion is that also tetrapyrrole pigments derived from microalgae were susceptible to light-accelerated autoxidation (**Chapter 5**). Following a similar strategy as in **Chapter 4**, it was shown that the methine bridges in biliverdin were susceptible to scission. By combining UV-Vis, $[\text{M}+\text{H}]^+$, MS^2 and MS^3 data gained from UHPLC-PDA-ESI-MS analysis and *in silico* degradation, propionic acid functionalized pyrroles could be tentatively assigned. This analytical setup was, therefore, also suitable to analyse tetrapyrrole degradation products. Furthermore, it can be hypothesized that similar as for fatty acid esterified astaxanthin (**Chapter 4**), additional esterified decorations of a tetrapyrrole (*e.g.* an esterified phytol tail as in chlorophyll *a*) are probably not disrupted. Additionally, these experiments suggest that autoxidation of the phycocyanobilin group of CPC can also occur when it is attached to the protein backbone. Therefore, as an additional experiment to **Chapter 5**, we exposed a 0.45 mg mL^{-1} CPC^a solution in 50 mM sodium phosphate buffer pH 7.0 to light-accelerated autoxidation for approximately 7.15 h at a sample liquid temperature of 45 °C. A loss in CPC of 48% (*w/w*) was observed over the course of the degradation as analysed by spectrophotometry. Visually, turbidity was observed after approximately 4.5 h,

^aPhycopro C-phycocyanin from *Spirulina platensis* ($A_{620}/A_{280} = 4.68$) was obtained from Prozyme (Hayward, CA, USA). CPC concentration was determined as in (7).

indicating protein denaturation. Summarizing, the phycocyanobilin tetrapyrroles are probably also susceptible to degradation, although it is unclear if this process precedes protein denaturation.

COLOUR STABILITY OF ASTAXANTHIN IN MODEL SYSTEMS

In **Chapter 6**, it was shown that the degree of esterification with palmitate positively influenced the all-*trans*-astaxanthin stability and modified its *cis-trans* equilibrium. It was demonstrated that spectrophotometric monitoring at 470 nm was not representative for the actual conversion of all-*trans*-astaxanthin to its degradation products as indicated by UHPLC-PDA.

Light-accelerated autoxidation

The method used for triggering and accelerating the autoxidation reactions throughout **Chapters 4, 5 and 6**, was light-accelerated degradation. Although only used at one temperature and one solvent in the experimental chapters, this equipment can be employed in a temperature range and with different solvents in order to assess temperature and solvent dependency of astaxanthin (or biliverdin) colour stability. In order to do so, a number of parameters of the equipment need to be adjusted, prior to measurements. Controlling the liquid temperature in the cuvettes requires three temperature parameters, the black standard temperature (T_{BST}), the target temperature (T_{target}) and the actual liquid temperature at which the experiment is performed (T_{exp}). The T_{exp} of the liquid in the cuvettes is controlled by T_{BST} . The T_{BST} can be set in a range of 45 – 80 °C ($\pm 2^\circ\text{C}$) at an irradiation of 30 W m⁻². Obviously, the T_{BST} does not reflect the actual T_{exp} . To measure the T_{exp} precisely, a 10 mL vapour-tight capped reference vial is filled with solvent (3 mL) and a similar astaxanthin concentration has to be used to obtain a relationship between T_{BST} and T_{target} . The T_{exp} can be monitored during the degradation with a digital waterproof thermocouple thermometer with a thermocouple probe as in **Chapter 6**. When doing so, it is shown that the T_{BST} and the T_{target} had a linear relationship ($R^2 = 0.987$) (**Figure 4**). The T_{target} can subsequently be used for every solvent to set the appropriate T_{BST} , which resulted in the desired T_{exp} . In conclusion, the T_{exp} was solvent dependent and, therefore, for each solvent a slightly different equilibrium value was reached (**Table 1**).

Impact of solvents and temperature on colour loss

As discussed in **Chapter 1**, stability measurements of astaxanthins have been performed in a different solvents. In the previous chapters no comparison of the effect of solvents was made. As an additional experiment, we here report on the effect of solvents on the colour stability of astaxanthin and its palmitate fatty acid esters, in hexane, iso-propanol, ethanol, 75% (v/v) aqueous ethanol and glyceryl trioleate by

monitoring colour loss at 470 nm^a. The kinetic experiments were based on the following considerations. A relatively large difference in absorbance was found between $t = 0$ min to $t = 15$ min, which was attributed to equilibration and warming up of the solvent. Linear regression was, therefore, performed using $t = 15$ min as the start. Absorbance values lower than 0.100, the lower limit of the linear range of the spectrophotometer, were excluded. For regression an equation of $y = ax + b$ was used. A comparison of $y = ax + b$ and $y = ax$ showed that the former correlated better to the measured data (data not shown). Correlation coefficients (R^2) for 0th and 1st order kinetics were found to be very similar in most cases (*e.g.* 0th order R^2 ranges:

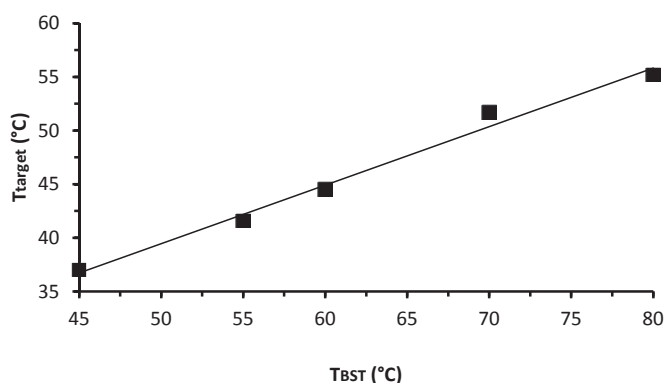


Figure 4. Relation between black standard temperature ($T_{BS\text{T}}$) of the Suntest XLS+ and temperature of a reference (T_{target}) of free astaxanthin in ethanol at an irradiation energy of 30 W m^{-2} with a correlation coefficient of $R^2 = 0.987$.

Table 1. Targeted temperatures and actual liquid temperatures measured in the reference vial after $t = 15$ min, minimal amount of temperature measurements is $n = 8$.

T_{target} (°C)	T_{exp} Hexane ± SE (°C)	T_{exp} Ethanol ± SE (°C)	T_{exp} Iso- propanol ± SE (°C)	T_{exp} 75% (v/v) Ethanol ± SE (°C)	T_{exp} Glyceryl trioleate ± SE (°C)
38.0	37.0 ± 0.1	36.6 ± 0.1	37.6 ± 0.1	37.7 ± 0.1	40.7 ± 0.1
45.0	45.2 ± 0.1	46.2 ± 0.2	46.3 ± 0.2	46.4 ± 0.2	49.0 ± 0.1
50.0	52.1 ± 0.2	52.6 ± 0.2	52.9 ± 0.2	52.7 ± 0.2	54.1 ± 0.1
55.0	54.2 ± 0.4	56.7 ± 0.3	55.1 ± 0.1	55.9 ± 0.3	59.2 ± 0.5

SE: standard error.

^aMonitoring of colour degradation by UV-Vis spectrophotometry was done by diluting free astaxanthin, astaxanthin monopalmitate and astaxanthin dipalmitate to 11.5-15.4 μM from their stock solutions as in **Chapter 4** and **6** into the desired solvent (*n*-hexane, ethanol, iso-propanol, 75% (v/v) aqueous ethanol and glyceryl trioleate). Triplicate cuvettes were filled with solutions and irradiated in the Suntest XLS+. Sample temperatures were monitored for each experiment using a reference vial (**Table 1**). Absorbance at 470 nm was measured at the start ($t=0$ min), after 15 min ($t=15$), and subsequently at 30 min intervals ($t=30, 60$, etc., until 270 to 300 min). This experiment was performed at four values of T_{target} : 38, 45, 50 and 55 °C.

hexane 0.99 – 1.00; ethanol 0.90 – 1.00; iso-propanol 0.83 – 0.98; 75% (v/v) ethanol 0.99 – 1.00. 1st order R² ranges: glyceryl trioleate 0.97 – 0.99). Therefore, the lowest possible reaction order was chosen with which the data showed conformity (*i.e.* a linear relationship).

Reaction rate constants (*k*) were determined at four different temperatures for each sample (**Table 2**). The five solvents were all food grade and provided a polarity range from 0.009 (hexane) to 0.741 (75% (v/v) aqueous ethanol) (8). Astaxanthin dipalmitate was found to be insoluble in 75% (v/v) aqueous ethanol, the most polar solvent. Differences in colour loss rates between the various types of astaxanthin were mostly statistically significant ($p \leq 0.05$) in hexane, 75% (v/v) aqueous ethanol and glyceryl trioleate. In hexane, ethanol, iso-propanol and ethanol 75%, all three types of astaxanthin were found to obey 0th order kinetics. In glyceryl trioleate, colour loss was found to obey 1st order kinetics. Differences in reaction order caused by solvents for carotenoids (*e.g.* β , β -carotene) have been reported before and degradation in oil was reported to obey first order kinetics (9, 10). It should be noted that the rate constants for astaxanthin mono- and dipalmitate at 55 °C reported here differed from those reported in **Chapter 6**. Although the intra-day variations in both independent experiments were small, the inter-day variation was apparently higher. No clear explanation can be provided for this observation. For ethanol and iso-propanol, no significant difference between the three types of astaxanthin was found. The highest colour loss rates were found for iso-propanol, followed by ethanol. Hexane and 75% (v/v) aqueous ethanol showed relatively low colour loss rates. In conclusion, the colour loss rates for free, monopalmitate and dipalmitate astaxanthins were solvent dependent.

Table 2 showed that no clear temperature dependence of astaxanthin colour loss was found. Actually, temperature dependence was only observed for ethanol and isopropanol. This, together with the fact that no clear trends with respect to stability of free, monopalmitoyl, and dipalmitoyl all-*trans*-astaxanthin were found, underlines once more the importance of our conclusions in **Chapter 6**. In order to understand astaxanthin stability in different solvents, the colour loss experiments measured spectrophotometrically should be backed up by compositional analysis of the mixtures of astaxanthin degradation products (by UHPLC-PDA-ESI-MS). This will give more detailed information on the conversions **I - IV**, as specified in **Chapter 6**. It has been suggested that *cis-trans* equilibria are solvent-dependent (11). Together with our findings that the isomerisation reaction plays a key role in astaxanthin stability, and that stability of all-*trans*-astaxanthin increases with esterification (**Chapter 6**), it is suggested that the observed differences in (esterified) all-*trans*-astaxanthin stability in various solvents might find their origin in tuning of the *cis-trans* equilibrium. Future investigations should address these relationships in a more systematic way.

Table 2. Rate constants (k) and correlation coefficients (R^2) of the colour loss (470 nm) of free astaxanthin (F), astaxanthin monopalmitate (M), and astaxanthin dipalmitate (D) followed at 470 nm in different solvents.

Solvent	Reaction order	DE	38 °C ^b			45 °C ^b			50 °C ^b			55 °C ^b		
			(k ± SE) × 10 ³ (A ₄₇₀ ·min ⁻¹)			(k ± SE) × 10 ³ (A ₄₇₀ ·min ⁻¹)			(k ± SE) × 10 ³ (A ₄₇₀ ·min ⁻¹)			(k ± SE) × 10 ³ (A ₄₇₀ ·min ⁻¹)		
				R^2			R^2			R^2			R^2	
Hexane		F	1.37 ± 0.03 ‡	0.96	1.39 ± 0.01 ‡	1.00	1.43 ± 0.08 ‡	1.00	1.89 ± 0.13 ‡	1.00	1.89 ± 0.13 ‡	0.99		
	0	M	1.93 ± 0.02 ‡	1.00	1.58 ± 0.04 ‡	1.00	1.89 ± 0.05 ‡	1.00	2.49 ± 0.00 §†	1.00	2.49 ± 0.00 §†	1.00		
		D	1.46 ± 0.02 ‡	1.00	2.41 ± 0.06 ‡	1.00	2.62 ± 0.05 ‡	1.00	1.66 ± 0.08 §	1.00	1.66 ± 0.08 §	1.00		
Ethanol		F	0.45 ± 0.21 ‡	1.00	0.62 ± 0.26 ‡	1.00	1.06 ± 0.33 ‡	0.99	3.37 ± 0.61 ‡	0.99	3.37 ± 0.61 ‡	0.96		
	0	M	0.50 ± 0.03 §	1.00	2.86 ± 0.38 §†	0.98	3.50 ± 0.59 §	0.97	6.32 ± 0.10 §†	1.00	6.32 ± 0.10 §†	1.00		
		D	0.44 ± 0.02 *	1.00	0.70 ± 0.06 §	1.00	3.45 ± 0.71 *	0.99	3.67 ± 0.93 §	1.00	3.67 ± 0.93 §	1.00		
Iso-propanol		F	2.34 ± 0.49 ‡	0.99	2.83 ± 0.29 ‡	0.98	4.73 ± 0.26 *†	1.00	5.78 ± 0.37 ‡	1.00	5.78 ± 0.37 ‡	1.00		
	0	M	3.00 ± 0.31 §	1.00	3.92 ± 0.02 §	1.00	5.16 ± 0.13 ‡	1.00	6.25 ± 0.21 §	1.00	6.25 ± 0.21 §	1.00		
		D	2.07 ± 0.21 *	1.00	2.50 ± 0.42 §	0.99	5.15 ± 0.03 *	1.00	4.37 ± 0.24 ‡§	1.00	4.37 ± 0.24 ‡§	1.00		
75% (v/v) Ethanol		F	0.99 ± 0.16 ‡	1.00	0.78 ± 0.02 ‡	1.00	0.66 ± 0.03 ‡	0.99	1.01 ± 0.02 ‡	0.99	1.01 ± 0.02 ‡	0.99		
	0	M	1.02 ± 0.18 §	1.00	0.86 ± 0.03 ‡	1.00	0.76 ± 0.02 ‡	1.00	1.29 ± 0.11 ‡	1.00	1.29 ± 0.11 ‡	1.00		
		D	N.D.	N.D.	N.D.	N.D.	N.D.	N.D.	N.D.	N.D.	N.D.	N.D.		
Glycerol trioleate		F	2.33 ± 0.05 ‡	1.00	2.19 ± 0.05 ‡	1.00	2.30 ± 0.05 ‡	0.99	2.45 ± 0.20 ‡	0.99	2.45 ± 0.20 ‡	0.99		
	1 ^a	M	3.56 ± 0.04 ‡	1.00	3.40 ± 0.02 ‡	1.00	3.47 ± 0.05 ‡	1.00	3.76 ± 0.05 ‡	1.00	3.76 ± 0.05 ‡	1.00		
		D	5.10 ± 0.12 ‡	1.00	4.79 ± 0.23 ‡	1.00	4.47 ± 0.18 ‡	1.00	5.14 ± 0.12 ‡	1.00	5.14 ± 0.12 ‡	1.00		

DE, Degree of esterification; SE, standard error; N.D., not determined. Reaction rates were expressed as the decrease in absorbance at 470 nm and are means of triplicate measurements. ^a Units of reaction rates of first order reaction are min⁻¹; ^b Target temperatures, actual temperatures in **Table 1**; §, *, ‡, at each temperature and solvent combination, astaxanthins with the same symbol are significantly (p<0.05) different according to One-Way ANOVA Post-Hoc LSD analysis with SPSS Statistics 20.0.0 (IBM, Armonk, NY, USA). All materials were acquired as in **Chapter 6**, with the exception of: glycerol trioleate (~65% w/w) obtained from Sigma-Aldrich (St. Louis, MO, USA). ULC/MS grade iso-propanol (99.95%) was purchased from Biosolve (Valkenswaard, The Netherlands). Ethanol absolute was obtained from Merck Millipore (Darmstadt, Germany). Changes in the absorbance values of astaxanthin dissolved in different solvents were used to calculate reaction rate constants by linear regression: zero order ($c = c_0 - kt$) and first order $c = c_0 * e^{-kt}$.

REFERENCES

1. Airs, R. L.; Llewellyn, C. A., Improved detection and characterization of fucoxanthin-type carotenoids: novel pigments in *Emiliana huxleyi* (Prymnesiophyceae). *Journal of phycology* **2006**, *42*, 391-399.
2. Fraser, P. D.; Enfissi, E. M.; Goodfellow, M.; Eguchi, T.; Bramley, P. M., Metabolite profiling of plant carotenoids using the matrix-assisted laser desorption ionization time-of-flight mass spectrometry. *The plant journal* **2007**, *49*, 552-564.
3. Fagerer, S. R.; Schmid, T.; Ibanez, A. J.; Pabst, M.; Steinhoff, R.; Jefimovs, K.; Urban, P. L.; Zenobi, R., Analysis of single algal cells by combining mass spectrometry with raman and fluorescence mapping. *The analyst* **2013**, *138*, 6732-6736.
4. Rivera, S. M.; Canela-Garayoa, R., Analytical tools for the analysis of carotenoids in diverse materials. *Journal of chromatography. A* **2012**, *1224*, 1-10.
5. Bauch, M. E., Identifizierung und quantifizierung der Ketocarotinoide in Dauerstadien von Grünalgen und Ketocarotinoidbiosynthese im Modellorganismus *Chlamydomonas reinhardtii*. *PhD-thesis* Johannes Gutenberg-Universität, Mainz, Germany, **2011**.
6. Eugster, C. H., Chapter 4: Chemical derivatization: microscale tests for the presence of common functional groups in carotenoids. In: *Carotenoids Vol. 1A Isolation and analysis*, Edited by Britton G., Liaaen-Jensen S., Pfander H., Birkhäuser Verlag, Basel, Switzerland **1995**, 71-80.
7. Bennett, A.; Bogorad, L., Complementary chromatic adaptation in a filamentous blue-green alga. *Journal of cell biology* **1973**, *58*, 419-435.
8. Reichart, C.; Welton, T., Appendix A: Properties, purification and use of organic solvents. In: *Solvents and solvent effects in organic chemistry*, Wiley-VCH Verlag GmbH & Co. KGaA., Weinheim, Germany **2010**, p. 549-586.
9. Minguez-Mosquera, M. I.; Jaren-Galan, M., Kinetics of the decolouring of carotenoid-pigments. *Journal of the science of food and agriculture* **1995**, *67*, 153-161.
10. Henry, L. K.; Catignani, G.; Schwartz, S., Oxidative degradation kinetics of lycopene, lutein, and 9-*cis* and all-*trans* beta-carotene. *Journal of the American oil chemists' society* **1998**, *75*, 823-829.
11. Yuan, J.-P.; Chen, F., Isomerization of *trans*-astaxanthin to *cis*-isomers in organic solvents. *Journal of agricultural and food chemistry* **1999**, *47*, 3656-3660.

Summary

Carotenoids produced by microalgae are an interesting new source of food colourants, especially as consumers' interest shifts from synthetic colourants to more natural alternatives. Astaxanthin is well-known for its superior antioxidant qualities compared to other carotenoids. Carotenogenic microalgae like, *Haematococcus pluvialis*, are already regarded as potent sources for the red xanthophyll astaxanthin, and is produced on kiloton scale annually. There are only a limited number of carotenogenic microalgal strains known nowadays. A potent, but unexplored, astaxanthin- and lutein-overproducing microalga is *Chlorella zofingiensis*, which can be an alternative to *H. pluvialis*. Both algae are known to accumulate esterified carotenoids, but little is known on the stability of such carotenoids. It has been reported that fatty acid esterification influences the colour stability of astaxanthin, although no plausible explanation for this has been provided so far.

Hence, this thesis focuses on (i) application of novel analytical techniques for determining the diversity of *H. pluvialis* and *C. zofingiensis* carotenoids, and their degradation products, in model systems, and (ii) the influence of esterification on astaxanthin colour stability.

Chapter 1 provides background information about algal pigments, the classes of carotenoids and xanthophylls, especially astaxanthin, and the microalgal strains used in this work. The degradation of carotenoids by autoxidation and oxidative bleaching is discussed and an overview on the effect of esterification with fatty acid(s) on xanthophyll stability is provided.

In **Chapter 2** the development of a MALDI-TOF-MS application for the rapid fingerprinting of astaxanthin fatty acid esters is described. The ionization behavior of the astaxanthin monopalmitate and astaxanthin dipalmitate standards employed showed formation of radical/protonated ($[M]^{\bullet+}/[M+H]^+$) parents and sodium ($[M+Na]^+$) and potassium ($[M+K]^+$) adduct parents. In order to obtain solely one ionization state, desalting and supplementation with various concentrations of sodium acetate were tested. It was shown that addition of 0.1 to 1.0 mM sodium acetate led to the highest signal to noise ratios, whereas for desalting this effect was either absent or led to only a slight improvement. Furthermore, upon TOF/TOF fragmentation of astaxanthin monopalmitate and dipalmitate, $[M+Na]^+$ parents yielded diagnostic polyene-specific eliminations and fatty acid neutral losses. A fatty acid ester benzonium fragment was used to identify the second fatty acid esterified to the carotenoid, as in astaxanthin dipalmitate. In sharp contrast, the TOF/TOF spectra of $[M]^{\bullet+}/[M+H]^+$ showed a multitude of non-diagnostic ions. This application of sodium acetate was subsequently tested on complex astaxanthin ester fractions from *H. pluvialis* and the results were compared to conventional LC analysis. All 12 main all-*trans* astaxanthin fatty acid esters were found, while only 2 minor esters could not be identified.

In **Chapter 3** the pigment accumulation of *C. zoofingiensis* upon nitrogen depletion is described. Also, the effect of diphenylamine (DPA), inhibiting cytosolic carotenoid biosynthesis, was addressed to gain additional insight in the biosynthetic pathways. First, by means of RP-UHPLC-PDA-MS analysis, all pigments were characterized and quantified. By UV-Vis and MS² spectra, it was found that *C. zoofingiensis* accumulated ketolutein and its fatty acid esters upon nitrogen depletion. Nitrogen depletion (without DPA) resulted in degradation of chlorophylls and plastidial carotenoids and accumulation of cytosolic astaxanthin, ketolutein, canthaxanthin, adonixanthin, and β,β -carotene. With DPA, lower levels of cytosolic β,β -carotene derivatives were detected. The ketolutein production was unaffected. This suggests that the regulatory mechanisms controlling the flux towards ketolutein and plastidial carotenoids were not affected by the lower levels of cytosolic β,β -carotene derivatives.

Chapter 4 addresses the analysis of oxidative degradation products resulting from (free) astaxanthin, astaxanthin monopalmitate and astaxanthin dipalmitate by means of UHPLC-PDA-ESI-MS. To obtain such degradation products, light-accelerated autoxidation was used as a relatively mild oxidation method and hypochlorite bleaching (HOCl/OCl⁻) as a relatively harsh method. Light-accelerated autoxidation yielded a series of apo-astaxanthins and apo-astaxanthinones containing 3 (apo-9) to 10 (apo-8') conjugated double bonds. Upon MS² analysis, it was found that these apo-astaxanthins were either non-esterified (derived from free or monopalmitoyl astaxanthin) or esterified with a palmitate ester (derived from monopalmitoyl or dipalmitoyl astaxanthin). Again, the palmitoyl esters showed formation of [M+Na]⁺, yielding different diagnostic ions, which could be used for additional ascertainment. HOCl/OCl⁻ converted the three astaxanthins into their epoxy-apo-9- and epoxy-apo-13-astaxanthinone, besides other apo-astaxanthins which were also obtained with light-accelerated degradation. Blue shifts compared to their non-epoxidized form indicated that the epoxy-apo-13 species was probably in the 5,6 position. The fatty acid ester bond appeared to be hardly affected by light-accelerated autoxidation, as astaxanthin dipalmitate degradation showed only trace amounts of free and monopalmitate astaxanthin. With HOCl/OCl⁻, the ester bond of the apo-astaxanthin palmitoyl esters was degraded as was observed for the diesters.

In **Chapter 5** the light-accelerated autoxidation process was extrapolated to phycobiliproteins. These tetrapyrrole-containing proteins are blue colourants, which can be obtained *Spirulina platensis*. As autoxidation of tetrapyrroles attached to phycobiliproteins was expected to yield low quantities of pyrrole reaction products, which might be obscured by the protein bulk, the free tetrapyrrole biliverdin was chosen as a preliminary model. By matching UHPLC-PDA-ESI-MS analysis with *in silico* predicted autoxidation products, it was shown that the three methine bridges of the

biliverdin were susceptible to autoxidation, resulting in propionic acids functionalized pyrroles and small heterofuranoids.

In **Chapter 6**, the influence of esterification with palmitate on astaxanthin stability was studied by exposure to light-accelerated autoxidation, using free all-*trans*-astaxanthin, its monoester, and its diester dissolved in *n*-hexane. An increase in palmitate esterification enhanced the stability of all-*trans*-astaxanthin, as measured by RP-UHPLC-PDA, whereas it had no influence on colour loss in time, as measured spectrophotometrically ($A_{470\text{ nm}}$). The mismatch in results obtained with the two assays might be explained by the observation that substitution with fatty acids influenced the *cis-trans* equilibrium. Besides many other degradation products, a larger amount of 9-*cis* astaxanthin was obtained with free astaxanthin than with its esterified forms. Furthermore, monopalmitate esterification of astaxanthin resulted in increased 13-*cis* isomer formation. The molar ratios of 9-*cis* : 13-*cis* after 60 min were 1 : 1.7 (free), 1 : 4.8 (monopalmitate) and 1 : 2.6 (dipalmitate). With its higher molar extinction coefficient than that of all-*trans*-astaxanthin, the formation of 9-*cis* astaxanthin might partially compensate the colour loss induced by conjugated double bond cleavage in the parent material. The different ratios of *cis-trans* isomers obtained with the three all-*trans*-astaxanthin forms might also underlie the differences in their actual stability.

Chapter 7 discusses the implications of our findings. First, the use of hyphenated analytical techniques in carotenoid analysis is discussed. It was further shown that the presence of the configuration with the C4 keto and C3 hydroxy group of astaxanthin and ketolutein is essential for the formation of sodium adducts. Therefore, upon xanthophyll screening by MALDI-TOF-MS, both sodiated and untreated samples should be used. Furthermore, the use of sodiation and MALDI-TOF-MS for the carotenoid analysis of a crude chloroform extract of *C. zoofingiensis* was demonstrated. Finally, the colour stability of astaxanthin, monopalmitate and dipalmitate was described in different solvents at four temperatures by light-accelerated autoxidation. It was found that both esterification and type of solvent influenced colour stability. The findings that the isomerisation reaction plays a key role in astaxanthin stability and that stability of all-*trans*-astaxanthin increases with esterification, together with the known solvent-dependence of *cis-trans* equilibria, suggests that the observed differences in (esterified) all-*trans*-astaxanthin stability in various solvents might find their origin in tuning of the *cis-trans* equilibrium.

Samenvatting

Carotenoïden, geproduceerd door microalgen, zijn een interessante nieuwe bron van voedselkleurstoffen, vooral omdat de interesse van consumenten verschuift van synthetische kleurstoffen naar natuurlijkere alternatieven. Astaxanthine is bekend om zijn superieure kwaliteiten als antioxidant, in vergelijking met andere carotenoïden. Carotenogene microalgen, zoals *Haematococcus pluvialis*, worden nu al beschouwd als belangrijke bronnen voor de roodgekleurde xanthofiel astaxanthine en worden jaarlijks geproduceerd op een schaal van kilotonnen. Op dit moment is slechts een beperkt aantal stammen van carotenogene microalgen bekend. Een potente, maar relatief onbekende, astaxanthine- en luteïne-overproducerende microalg is *Chlorella zofingiensis*, die een alternatief voor *H. pluvialis* kan zijn. Beide algen staan bekend om hun accumulatie van vetzuur veresterde carotenoïden, maar er is weinig bekend over de stabiliteit van deze carotenoïden. Er wordt gerapporteerd dat verestering van vetzuren de kleurstabiliteit van astaxanthine beïnvloedt, maar tot nu toe is hier geen plausibele uitleg voor.

Dit proefschrift vestigt daarom de aandacht op (i) toepassing van nieuwe analytische technieken om de diversiteit te bepalen van carotenoïden afkomstig van *H. pluvialis* en *C. zofingiensis* en hun afbraakproducten in modelsystemen, en (ii) de invloed van verestering op de kleurstabiliteit van astaxanthine.

Hoofdstuk 1 levert achtergrondinformatie over algenpigmenten, carotenoïden en xanthofielen, met name astaxanthine, en de verschillende stammen van microalgen die worden gebruikt in dit werk. De afbraak van carotenoïden door auto-oxidatie en oxidatief bleken wordt bediscussieerd en een overzicht van het effect van verestering van vetzuren op de stabiliteit van xanthofielen wordt gegeven.

In **hoofdstuk 2** wordt de ontwikkeling van een MALDI-TOF-MS-toepassing beschreven, bestemd voor snelle karakterisatie van vetzuurveresterde astaxanthines. Het ioniseren van astaxanthine-monopalmitaat- en astaxanthine-dipalmitaatstandaarden resulteerde in radicale/geprotoneerde ($[M]^{+•}/[M+H]^+$) ouders en natrium ($[M+Na]^+$) en kalium ($[M+K]^+$) adduct-ouders. Om een enkele ionisatietoestand te verkrijgen, werd het effect getest van ontzouten en suppletie van verschillende concentraties natriumacetaat. Toevoegen van 0,1 tot 1,0 mM natriumacetaat leidde tot de sterkste signaal-ruisverhouding. Ontzouten leidde niet tot signaalgvorming of zorgde slechts voor een geringe verbetering. TOF/TOF-fragmentatie van astaxanthine-monopalmitaat- en dipalmitaat van $[M+Na]^+$ ouders resulteerde in diagnostische polyeenspecifieke eliminaties en neutrale vetzuurverliezen. Een vetzuurester-benzoniumfragment werd gebruikt om het tweede vetzuur te identificeren dat veresterd was aan het carotenoïd, zoals in astaxanthine-dipalmitaat. In scherp contrast stonden de TOF/TOF-spectra van $[M]^{+•}/[M+H]^+$ ouders. Deze resulteerden in een woud van niet-diagnostieke ionen. Vervolgens werd deze toepassing van natriumacetaat getest op complexe astaxanthine-esterfracties van *H. pluvialis*. De resultaten werden vergeleken met

conventionele LC-analyse; de 12 belangrijkste all-*trans* astaxanthine-vetzuuresters werden gevonden en slechts 2 minder voorkomende esters konden niet worden getraceerd.

Hoofdstuk 3 beschrijft de pigmentophoping van *C. zofingiensis* na stikstofdepletie. Om inzicht te verkrijgen in de verschillende biosynthetische pathways, is ook het effect van difenylamine (DPA) beschreven. Deze stof inhibeert de biosynthese van carotenoïden in het cytosol. Door middel van RP-UHPLC-PDA-MS-analyse werden eerst alle pigmenten gekarakteriseerd en gekwantificeerd. Door het bestuderen van UV-Vis en MS²-spectra werd ontdekt dat *C. zofingiensis* na stikstofdepletie ketoluteïne en zijn vetzuuresters ophoopt. Stikstofdepletie zonder toevoeging van DPA resulteerde in degradatie van chlorofyl en plastidiale carotenoïden, en ophoping van astaxanthine, ketoluteïne, canthaxanthine, adonixanthine en β,β -caroteen in het cytosol. Lagere concentraties cytosole β,β -caroteenderivaten werden gevonden als DPA werd toegevoegd. Echter, de productie van ketoluteïne werd niet beïnvloed. Dit doet vermoeden dat de regulatoire mechanismen, die de flux naar ketoluteïne en plastidiale carotenoïden besturen, niet beïnvloedt worden door de lagere concentraties cytosole β,β -caroteenderivaten.

Hoofdstuk 4 belicht de analyse van oxidatieve degradatieproducten van (vrije) astaxanthine, astaxanthine-monopalmitaat en astaxanthine-dipalmitaat door middel van UHPLC-PDA-ESI-MS. Om deze afbraakproducten te verkrijgen werd lichtversnelde auto-oxidatie gebruikt als een betrekkelijk milde oxidatiemethode. Bleken met hypochloriet (HOCl/OCl⁻) werd gebruikt als een betrekkelijk ruwe methode voor oxidatie. Lichtversnelde auto-oxidatie resulteerde in een reeks apo-astaxanthinalen en apo-astaxanthinonen die 3 (apo-9) tot 10 (apo-8') geconjugeerde dubbele bindingen bezaten. MS²-analyse wees uit dat deze apo-astaxanthines niet veresterd waren (wanneer afkomstig van vrije of monopalmitoyl-astaxanthine) of veresterd waren met een palmitaatester (wanneer afkomstig van monopalmitoyl- of dipalmitoyl-astaxanthine). Wederom vormden de palmitoyl-esters [M+Na]⁺ ouders, na fragmentatie, verschillende diagnostieke ionen, die vervolgens zouden kunnen worden gebruikt voor aanvullende karakterisatie. Bleken met HOCl/OCl⁻ resulteerde in de conversie van de drie astaxanthinen tot epoxy-apo-9- en epoxy-apo-13-astaxanthinon en de andere apo-astaxanthines die ook werden verkregen met lichtversnelde degradatie. De geobserveerde blauwverschuiving van de epoxy-apo-13-astaxanthinon vergeleken met de niet-geëpoxideerde vorm wijzen op het feit dat de epoxidegroep waarschijnlijk in de 5,6-positie stond. De vetzure esterbinding bleek nauwelijks te worden afgebroken door lichtversnelde auto-oxidatie: de afbraak van astaxanthine-dipalmitaat liet slechts minuscule hoeveelheden zien van vrije en monopalmitaat-astaxanthine. Met HOCl/OCl⁻ werd de esterverbinding van de apo-astaxanthine-palmitoylesters wel afgebroken, zoals aangetoond met de analyse van dipalmitoyl-astaxanthine afbraakproducten.

In **hoofdstuk 5** wordt het lichtversnelde auto-oxidatieproces geëxtrapoleerd naar fycobiliproteïnen. Deze tetrapyrrol-bevattende eiwitten zijn blauwe kleurstoffen, die gewonnen kunnen worden uit *Spirulina platensis*. Verwacht werd dat auto-oxidatie van tetrapyrrolen, gehecht aan fycobiliproteïnen, een lage hoeveelheid pyrrol-reactieproducten zou opleveren. Bovendien zouden deze kunnen worden overschaduwd door de eiwitbulk. Daarom werd het niet-gebonden tetrapyrrol biliverdine gekozen als een voorbereidend model. Door middel van het vergelijken van UHPLC-PDA-ESI-MS-analyse met *in-silico* voorspelde auto-oxidatieproducten werd aangetoond dat de drie methinebruggen van biliverdine gevoelig zijn voor auto-oxidatie, resulterend in de productie van kleine heterofuranoïden en pyrrolen met propionzuurgroepen.

In **hoofdstuk 6** wordt beschreven wat de invloed is van esterificatie met palmitaat op de stabiliteit van astaxanthine. Dit werd bewerkstelligd door vrije all-*trans*-astaxanthine, en de mono- en di-ester, opgelost in *n*-hexaan, bloot te stellen aan lichtversnelde auto-oxidatie. Met RP-UHPLC-PDA werd gemeten dat een grotere mate van palmitaat-esterificatie de stabiliteit van all-*trans*-astaxanthine liet toenemen. Met spectrofotometrie (A_{470} nm) werd geen invloed gemeten op kleurverlies in de tijd. De discrepantie in de resultaten die met de beide methoden werden gemeten kan worden verklaard door de observatie dat het *cis-trans*-evenwicht wordt beïnvloed door de aangehechte vetzuren. Naast veel andere afbraakproducten werd met vrije astaxanthine een grotere hoeveelheid 9-*cis*-astaxanthine gevormd dan met andere veresterde vormen. Verder resulteerde monopalmitaat-esterificatie van astaxanthine in een verhoogde vorming van 13-*cis*-isomeren. De molaire ratio's van 9-*cis* : 13-*cis* waren 1 : 1,7 (vrij), 1 : 4,8 (monopalmitaat) en 1 : 2,6 (dipalmitaat). Met een hogere molaire extinctiecoëfficiënt dan die van all-*trans*-astaxanthine zou de vorming van 9-*cis*-astaxanthine deels kunnen compenseren voor het kleurverlies dat wordt geïnduceerd door het verbreken van dubbele bindingen van het startmateriaal. De verschillende ratio's van *cis-trans*-isomeren, verkregen met de drie all-*trans*-astaxanthinevormen, kunnen ook ten grondslag liggen aan de verschillen in hun eigenlijke stabiliteit.

Hoofdstuk 7 bediscussieert de implicaties van onze bevindingen. Ten eerste wordt het gebruik bediscussieerd van gekoppelde analytische technieken in carotenoid-analyse. Er wordt aangetoond dat de C4-keto- en C3-hydroxygroep van astaxanthine en ketoluteïne een essentiële configuratie zijn voor de vorming van natriumadducten. Daarom zouden zowel genatrieerde als onbehandelde monsters moeten worden gebruikt tijdens screening van xanthofielen met MALDI-TOF-MS. Ook werd het gebruik van natriëring en MALDI-TOF-MS gedemonstreerd voor carotenoid-analyse van een ruw chloroformextract van *C. Zofingiensis*. Ten laatste werd de kleurstabiliteit beschreven van astaxanthine, monopalmitaat en dipalmitaat in verschillende oplosmiddelen bij vier temperaturen, bij gebruik van lichtversnelde

auto-oxidatie. Zowel esterificatie als het soort oplosmiddel beïnvloedden de kleurstabiliteit. De bevindingen dat de isomerisatiereactie een sleutelrol speelt in de stabiliteit van astaxanthine, en dat de stabiliteit van all-*trans*-astaxanthine toeneemt met esterificatie, samen met de al bekende afhankelijkheid van het oplosmiddel bij het onderzoeken van *cis-trans*-evenwichten, duiden erop dat de geobserveerde verschillen in de stabiliteit van (veresterd) all-*trans*-astaxanthine in verschillende oplosmiddelen hun oorsprong vinden in het afstemmen van het *cis-trans*-evenwicht.

Acknowledgements

Acknowledgements

In this section, the most important part of this work will be described: the people that helped me in *any* way to complete this booklet. Unfortunately, this is also the shortest chapter ☺. At least another 166 pages could've been written about these people, but fortunately that amount of words is not necessary. In contrast to the scientific work that has to be written down in order to remember, all friendships and fun stuff from the last four years do not need this. Therefore, **Thank You (!!!)** in a fairly random order:

(Co-)Promoters: Jean-Paul & Harry

Bioprocess engineering: Kim, Packo, Dirk & René

Paranymphs: Koen & Wouter / *FCHnymph:* Annewieke

Students: Kun, Caroline, Bart, Evert, Sally, Iris, Kristina & Wouter

Held in bange dagen: Peter W.

Food Chemistry: Jolanda, Roy, Christiane, Lingmin, Aisyah, Tomas, Maxime, Milou, Carla, Anne, Wibke, Renske, Anne, Rudy, Carlos, Ya, Marijn, Stephanie, Connie, Raluca, Julia, Lia, Maaïke, Mirjam, Henk, Stefano, Koos, Katharina, Hugo, Yuxi, Fang-Jie, Claire, Elisabetta, Surender, Abhishek, Frederik, Alexandra, Martijn, Patricia, Emma, Red, Klaus, Thibaut, Matthias, Suzanne, Melliana, Marit, René, Jesse, Mark, Edwin, Peter G., Margaret, Rianne, Arjen, de Smaaklessen dames and many many other former PhD students and employees.

Feyecon: Andreas, Raquel, David, Gerard, Hayley, Christina, Cynthia & Annet.

Inspiratie buiten dienst: De Trompetsectie der Ontzetting (Maarten Fungeson, Sybren, Roger, Robert, Lucie, Paul, Jeroen, Margo, Maarten Zilverberg, Jelle, Paul, Jochem), De Ontzetting (Jeroen S., Ewert, Aad, KT, Xavier, Willeke, Alie, Raymond, Yorick, Rutger, e.v.v.v.v.a.), Jean-Pierre Gabriël, Moleculairen (Tineke, Sjoerd, Evan, Niels & Marjolein), Fanfare Heikant, Etienne Ferket, (H)ulst (Koen+, Arjan+, Broek+, Sander+, Niels+, Annemiek, Carolien+, Terry+, Sytze+, Wouter+, Rodin+, Tuk+), Haarweg 9 (Esther, Casper, Maike, Richi), Fanfare St. Jan, De Notekrakers, Kicks & Ko, Coverband Thunk & Henk Kraus.

Pa, Ma & Do

Boobles 🐾 & Edita ♡

Yannick
Z

The Author

CURRICULUM VITAE

Yannick Joseph Angeline Weesepeel was born the 8th of October 1984 in Hulst, The Netherlands. After graduating gymnasium high school (Reynaertcollege, Hulst) in 2003, he studied a free programme in Molecular Sciences in Wageningen starting in the same year. His BSc degree was completed with a thesis on the covalent coupling of enzymes to magnetic particles at the Agrotechnology and Food Innovations institute. His MSc degree in Food Technology, with a specialization in Food Bioprocess Engineering, was completed with a thesis on the extraction and profiling of triterpenoids and polyphenols in two medicinal Chinese mushrooms at the Laboratory of Food Chemistry. Yannick spent his final six months of his study in München, Germany, where he studied flavor and aroma chemistry at Kraft Foods R&D.



Yannick started his PhD work described in this thesis with Dr. Jean-Paul Vincken and Prof. Harry Gruppen in April 2010 at the Laboratory of Food Chemistry, before graduation in June 2010. After completion of this in May 2014, he started in June 2014 as a Scientist in Food Authenticity with the group of Prof. Saskia van Ruth at RIKILT, institute for food safety at Wageningen University.

Contact information

E-mail: Yannick.weesepeel@wur.nl

LinkedIn: www.linkedin.com/in/yannickweesepeel

LIST OF PUBLICATIONS**This thesis**

Weeseipoel, Y.; Vincken, J.-P.; Pop, R.M.; Liu, K.; Gruppen, H. Sodiation as a tool for enhancing the diagnostic value of MALDI-TOF/TOF-MS spectra of complex astaxanthin ester mixtures from *Haematococcus pluvialis*. *Journal of mass spectrometry*, **2013**, 48, 862-874.

Mulders, K.J.M.; **Weeseipoel, Y.**; Bodenes, P.; Lamers, P.P.; Vincken, J.-P.; Martens, D.E.; Gruppen, H.; Wijffels, R.H. Nitrogen-depleted *Chlorella zofingiensis* produces astaxanthin, ketolutein and their fatty acid esters: a carotenoid metabolism study. *Journal of applied phycology*, DOI 10.1007/s10811-014-0333-3

Weeseipoel, Y.; Gruppen, H.; de Bruijn, W.; Vincken, J.-P. Analysis of palmitoyl apo-astaxanthinals, apo-astaxanthinones, and their epoxides by UHPLC-PDA-ESI-MS, *Submitted to Journal of agricultural and food chemistry*.

Weeseipoel Y.; Gruppen, H.; Vincken, J.-P. Preliminary UHPLC-PDA-ESI-MS screening of light-accelerated autoxidation products of the tetrapyrrole biliverdin, *Submitted to Food chemistry*.

Weeseipoel Y.; Vincken, J.-P.; Gruppen, H. Fatty acids attached to all-*trans*-astaxanthin alter its *cis-trans* equilibrium, and consequently its stability, upon light-accelerated autoxidation, *To be submitted*.

Other work

Mulders, K.J.M.; **Weeseipoel, Y.**; Lamers, P.P.; Vincken, J.-P.; Martens, D.E.; Wijffels, R.H. Growth and pigment accumulation in nutrient-depleted *Isochrysis* aff. *galbana* T-ISO, *Journal of applied phycology*, **2013**, 25-5, 1421-1430.

Pop, R.M.; **Weeseipoel, Y.**; Socaciu, C.; Pintea, A.; Vincken, J.-P.; Gruppen, H. Carotenoid composition of berries and leaves from six Romanian sea buckthorn (*Hippophae rhamnoides* L.) varieties, *Food chemistry*, **2014**, 147, 1-9.

OVERVIEW OF COMPLETED TRAINING ACTIVITIES

Discipline specific activities

Courses

- Advanced Food Analysis (VLAG), Wageningen, NL, 2010^a
- Ion Trap operations (Thermo), London, UK, 2011
- Structure and Reactivity (ORC-30806, WUR), Wageningen, NL, 2013

Conferences

- 16th International symposium on carotenoids, Krakow, PL, 2011^a
- Young Algaeneers Symposium, Wageningen, NL, 2012^a

General courses

- VLAG PhD Introduction Week (VLAG), 2011
- Techniques for writing and presenting a scientific paper (WGS), 2011
- Project and Time management (WGS), 2011
- Mobilizing your Scientific network (WGS), 2012
- Scientific Writing, (WUR In'to Languages), 2013
- Career Orientation (WGS), 2013

Additional activities

- Preparation PhD research proposal
- PhD trip FCH to Switzerland/Italy, 2010^{a,b}
- Organization of PhD trip FCH to Singapore/Malaysia, 2012
- PhD trip FCH to Singapore/Malaysia, 2012^{a,b}
- BSc/MSc thesis student presentations and colloquia, 2010-2014
- PhD presentations Food Chemistry, 2010-2014

^aPoster; ^bOral presentation

VLAG: Graduate School for Nutrition, Food Technology, Agrobiotechnology and Health Sciences

WGS: Wageningen Graduate School

FCH: Food Chemistry

ORC: Organic Chemistry

WUR: Wageningen University

The work in this thesis was performed at the Laboratory of Food Chemistry, Wageningen University, The Netherlands. This research was financially supported by FeyeCon D&I and by grants from NL Agency and the Ministry of Education, Culture and Science (Project no. FND09014).

This thesis was printed by Gildeprint Drukkerijen, Enschede, The Netherlands
Edition: 350 copies

Cover design: Sander Blommaert

Yannick Weesepeel, 2014